THE EFFECTS OF VARIOUS LEVELS OF COMPRESSIVE STRESS FIELDS ON THE DETERIORATION RATE AND MICROCRACKING OF PLAIN CONCRETE SUBJECTED TO FREEZING AND THAWING

by

Lemuel Bembry Battle, Jr.

Thesis submitted to the Graduate Faculty of the
Virginia Polytechnic Institute and State University
in partial fulfillment of the requirements for the degree of

MASTER OF SCIENCE

in

Civil Engineering

APPROVED:

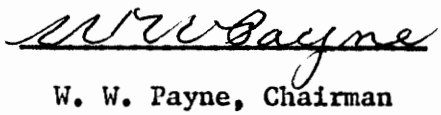

W. W. Payne, Chairman

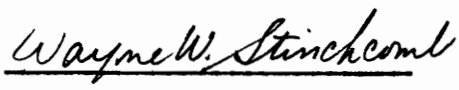

W. W. Stinchcomb

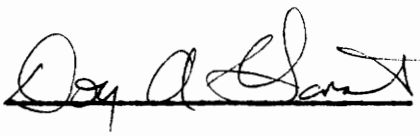

D. A. Garst

March, 1975

Blacksburg, Virginia

ACKNOWLEDGEMENTS

The author wishes to express his sincerest appreciation and gratitude to Dr. William W. Payne whose guidance, encouragement, and invaluable knowledge made this thesis possible.

Appreciation is also extended to the other members of the author's advisory committee, Dr. Wayne W. Stinchcomb and Professor Don A. Garst, for their advice and suggestions.

Finally, my most humble and sincere thanks goes to my mother and father for their love, support, patience, and financial aid, and to Betsy for her time and patience.

TABLE OF CONTENTS

LIST OF FIGURES

LIST OF TABLES

LIST OF PLATES

CHAPTER I

INTRODUCTION

Research tests conducted throughout the world have indicated significant improvement in the durability of portland cement concrete under a constant compressive stress (prestress). Prestressed specimens have shown better durability than unstressed concrete made of the same concrete mixture in a large number of cases [1,2,3]*. Hence, it is concluded that the durability of concrete is generally enhanced by prestressing, and that concrete under compression is believed to exhibit greater resistance to weathering action.

Due to the rapid pace of modern construction, new technological advances, and the high cost of labor and other economic concerns, the use of prestressed concrete as a competitive construction material has reached a stage of paramount importance within the last decade. The material is now being used extensively in Europe and in parts of the United States where the effect of freezing and thawing action is an important factor. This undoubtedly raises a question regarding the performance and usefulness of prestressed concrete as a construction material.

Another question of concern is an economical construction method for prestressed concrete. For example, while it appears that the performance of prestressed concrete pavements has been quite good, the complex problems of design and the present methods of construction are more complex than those of conventional pavements. Therefore, it is apparent that simple design and economical construction methods need

---

*Numerals in brackets refer to references given in the Bibliography.

to be developed to take full advantage of this material.

With further research and improvement of present methods of construction, prestressed concrete will become a competitive material in the construction industry. Already, prestressing offers many distinct advantages in the construction world. Lighter and stronger bridges are being constructed; economical prestressed piles have grown in use; and the construction of prestressed highway and airport pavements is becoming more and more evident.

The advantages of a prestressed concrete pavement over a conventional rigid one are as follows [4]:

1. Prestressing of pavement slabs upwards of 800 feet long is a promising method of controlling cracks in concrete. Therefore, extended pavement life and reduced maintenance costs under normal conditions are evident.

2. A prestressed pavement of a given thickness has a greater load-carrying capacity than one without prestressing. This is due to the permanent compressive stresses induced in the concrete which increases its effective flexural strength.

3. For a given design load, the depth of a prestressed pavement is less than that of a conventional rigid pavement.

4. The price of one square yard of prestressed pavement could be less than that of unstressed pavement.

5. Prestressed pavements can be designed with fewer contraction-expansion joints.

The effect of freezing and thawing action on prestressed concrete has not been investigated as extensively as that of ordinary concrete. Natural weathering of prestressed concrete bridges and the freezing and thawing of prestressed pavements have brought about the necessity for further research in this area.

Of increasing concern is the availability of the coarse aggregates

used in prestressed concrete. Sources of known sound aggregate are being rapidly depleted in many areas of the United States, and this shortage is the most serious problem facing the concrete industry today [5]. Many known deposits of excellent aggregate are being zoned out for residential and commercial areas and for environmental concerns. It becomes expensive to obtain sound aggregate when it must be transported over long distances.

Studies of the frost durability of aggregates in concrete have been increased by the growing scarcity of "good" aggregates and the necessity to use materials that would have been bypassed in former days. In the near future, it may become necessary to utilize coarse aggregates which are known to perform poorly when subjected to adverse weathering conditions. In addition, if an aggregate is mixed into the concrete while in a quarry-wet or stream-wet condition, the probability of high saturation and, therefore, of some kind of failure in freezing is high. With highway and airport pavements and highway bridges being the most vulnerable to natural freezing and thawing action, the performance of prestressed concrete containing poor performing aggregates should be known.

Problem Statement

With regard to the above discussion, it is the intent of this thesis to determine the effects of various levels of compressive stress fields on the deterioration rate and microcracking of plain concrete subjected to freezing and thawing. The concrete used in this research contained aggregates with little resistance to freezing and thawing action. Since air entrainment was used, it was assumed that the primary damage to the

concrete was due to the deep-seated type of destruction caused by the coarse aggregate particles. The disintegration to the mortar matrix was practically eliminated by the entrained air.

Scope of Investigation

A typical prestressed concrete mixture was designed for this research. Beams, 3" x 3" x 14", were used as the test specimens. They were uniaxially prestressed by the post-tensioning method to 500, 1000, and 1500 psi, respectively. These beams were subjected to alternating cycles of freezing and thawing. The directional disintegration (permanent change of length in any one direction) of the prestressed beams were compared for the three different levels of prestress. Results were then analyzed and conclusions drawn. A theory was also presented to explain the results obtained from the investigation.

CHAPTER II

LITERATURE REVIEW

The effect of freezing and thawing action on the durability of prestressed concrete has not been investigated quite as extensively as that of ordinary concrete. Much research has been done on the behavior of concrete under a compressive stress field (prestressing). Other extensive research has been done on the behavior of concrete during freezing and thawing. However, research involving the combination of these two effects is limited. This chapter is divided into two sections: a brief review of research on the freezing and thawing of concrete, and a review of research on the freezing and thawing of concrete under a compressive stress field.

Review of Freezing and Thawing of Concrete

Before 1900, most of the work on the behavior of concrete exposed to freezing and thawing was basically concerned with the various sizes of building stones and aggregates used in the concrete, and the behavior of concrete placed in freezing weather [6]. It was not until after the turn of the century that the effect of the repetition of freezing and thawing cycles was considered.

In the late 1920's and early 1930's, the durability of plain concrete was researched considerably. This continued until the early 1940's when the beneficial effects of air entrainment in concrete were discovered.

Reagel [7], in 1940, investigated many unanswered questions of that time. Such questions were:

1. What kind of weather conditions are the major factors causing

deterioration of concrete?

2. To what cycles of freezing and thawing may concrete be subjected during service?

3. How shall freezing and thawing deterioration be measured?

4. What cycle of freezing and thawing should be used for laboratory testing?

5. Can a freezing and thawing test predict the effect of aggregates on the durability of concrete?

6. What are the effects of various curing treatments prior to freezing?

Reagel concluded that these questions and many others were far from being answered, and that there were many years of work ahead in this field of research.

Research on the freeze-thaw durability of concrete continued throughout the years. In 1966, William A. Cordon [6] published an article concerning the mechanisms and control of freezing and thawing of concrete. This article gave a thorough and complete treatment of this subject.

Lin [8], in 1974, explored the effects of freezing rates on the durability of plain concrete. Concrete specimens made from aggregates having various levels of saturation were subjected to alternate cycles of freezing and thawing at three different freezing rates. Various factors such as relative dynamic modulus, cumulative change in length, and durability factor were investigated. It was concluded that for concrete made from vacuum saturated aggregates, the rate of freezing did not produce any different effect on the durability of concrete. Also, for concrete made from soaked or air-dried aggregates, the faster rate of freezing resulted in higher concrete durability. Lin also showed that the slower the rate of freezing, the faster the rate for the aggregates to become critically

saturated.

Review of Freezing and Thawing of Prestressed Concrete

Of most interest in this investigation is the past research on the freezing and thawing of concrete under a compressive stress field. Pendley [2], in 1949, investigated the behavior of beams which were restrained against elongation and subjected to freezing and thawing. The beams tested were not exactly prestressed in the sense we think of today, and the level of this restraint was unknown. The dimensions were 4" x 4" x 16" and contained aggregates of varied performance records. The durability of the concrete was measured by the fundamental transverse frequency method. It was noticed that cracks developed in the restrained beams parallel to the longitudinal axis, and those in the unrestrained beam were in a random pattern. Pendley concluded that the restrained beams were more durable against freezing and thawing than the unrestrained beams.

Rieb [9], in 1959, used 3" x 4" x 32" pre-tensioned beams containing sound aggregate in his research. The levels of stress in these specimens ranged in increments of 500 psi from 0 to 2000 psi, respectively. It was hoped that such a range of stress would provide an indication of what effect different levels of stress have on the durability of concrete. Durability was measured by the fundamental transverse frequency, weight change, and change in length. The beams were programmed to include three variables which were level of prestress, type of cement, and method of curing. The conclusions drawn were that prestressing did not improve the durability of prestressed concrete over non-prestressed concrete, and that the use of Type III cement as a means of obtaining high early strength

concrete had no detrimental effect on the durability of the concrete.

Klieger [10], in 1960, used 2 1/2" x 2 1/2" x 16 1/4" post-tensioned beams containing sound aggregates to investigate the effects of prestressing on the durability of concrete. The level of prestress was between 350 to 400 psi, and the durability was measured by the fundamental transverse frequency method. The conclusion reached was that prestressing had no significant influence on the resistance of the concrete to freezing and thawing.

Gutzwiller and Musleh [1], in 1960, used 3" x 4" x 16" beams which contained various qualities of coarse aggregates. Prestressing was performed by the post-tensioning method to a level of 2000 psi. The durability was measured by the fundamental transverse frequency method. The conclusion drawn was that prestressed concrete specimens showed better durability than the unstressed concrete made from the same mix.

Roshore [11,12], in 1961 and 1966, used 4 1/2" x 9" x 81" pre-tensioned and post-tensioned concrete beams containing durable aggregates in his research. The level of prestress was varied, and the durability was measured by the pulse velocity method. The conclusion was that the prestressed concrete was no more durable than the same unstressed concrete.

Jamil [3], in 1964, also explored the effects of prestressing on the freeze-thaw durability of concrete. The concrete beams used for this study were 3" x 3" x 14" and made of aggregates having a low resistance to freezing and thawing action. Prestressing was performed by the post-tensioning method to a level of 600 psi. The durability was measured by the fundamental transverse frequency method. The conclusions drawn from this study were that prestressing of concrete made of these aggregates

improved the freeze-thaw durability of this concrete by an appreciable amount, and that the magnitude of improvement in the durability tends to diminish with the increasing proportion of sound aggregates.

Finally, Payne [13], in 1972, made an extensive and time-consuming investigation into this area of research. The beams used were 3" x 3" x 14", and contained aggregates known to produce the deep-seated type of damage when subjected to freezing and thawing. The method of prestressing was post-tensioning, and the level of prestress was 1000 psi only. The durability was measured by the change in length of the concrete. The conclusions drawn from the investigation were as follows:

1. Uniaxial prestressing improved the freeze-thaw resistance of the concrete in the direction of the prestressing force only.

2. The non-prestressed direction of the prestressed beam disintegrated at the same or greater rate than the same direction of the non-prestressed beam.

3. For concrete members uniaxially prestressed at 1000 psi, disintegration (due to frost damage) continued at approximately the same rate, in the non-prestressed direction, as non-prestressed concrete.

Payne also presented a theory, "THE PLANE OF LEAST RESISTANCE THEORY," that offered an explanation of this physical phenomenon. He determined where cracks in the concrete would originate, and the direction in which they would propagate.

CHAPTER III

TWO THEORIES

This chapter presents two theories on the behavior of concrete under a compressive stress field and subjected to freezing and thawing. The first is a theory presented by Payne [13], and the second is a theory presented by the author.

Appendices A through D are invaluable sections concerning the previous theories and knowledge about cracking and deterioration in concrete not subjected to any external load, subjected to an applied compressive load, and subjected to freezing and thawing. It may first be necessary to read these appendices in order to understand the following material; however, it is suggested that the reader digest the following material through the final chapter, then proceed to Appendices A through D.

Payne's Theory

The theory stated by Payne [13] is the following:

> Linear prestressing is a structural physical phenomenon. The applied compressive stress in the concrete, produced by concentric prestressing, changes the engineering properties of concrete, especially the ability of this concrete to sustain subsequently applied tensile stresses before fracturing.
>
> An important engineering property of non-prestressed (non-restrained) concrete is its relative weakness in tension and its inclination to fail in tension. Under a critical (damaging) fluid pressure, the coarse aggregate particle would fracture (microcrack) and then by repeated dilation, propagate this fracture through the matrix and the concrete, destroying the structural integrity of the concrete.
>
> The fluid pressure in a capillary of the aggregate varies and is a maximum at the freezing front. Also, this pressure moves through the aggregate with the freezing front. At any instant, in one of the capillaries, a maximum value of fluid pressure exists and it is equal in all directions. If the tensile stresses pro-

duced by this pressure exceed the strength of the confining material, a microcrack or minute fracture occurs. This microcrack reduces this pressure. This phenomenon may be repeated at another point in a capillary.

A mental picture of the capillary system of these aggregate particles may be obtained from assuming that the 20 percent or more void space, of the average particle in this investigation, is an interconnected uniformly distributed capillary system. It is also assumed that these capillaries run in all directions. The remaining 80 percent of this particle is an elastic, brittle material.

Therefore, it is conjectured by Payne that this physical phenomenon is analogous to the thick-wall cylinder problem and may be treated so.

The next freezing cycle propagates the microcracks or develops new microcracks or both. Repeated freezing cycles propagate these fractures through the coarse aggregate particle, through the matrix (assuming that the bond at the interface does not fail), or through the concrete to the surface. Eventually these microcracks become visible fractures on the surface of the concrete. Propagation of these microcracks is by a stress-concentration-fatigue function as cyclic freezing occurs, and the direction of crack propagation will be in the plane offering the least resistance to crack propagation. For a non-prestressed or non-restrained member, this plane could be in any direction.

Although this physical phenomenon does not meet the exact criterion of the elastic thick-wall cylinder problem, it does approach this criterion. This material can be assumed to be approximately isotropic in tensile strength and linear-elastic in compression and tension up to the point of tensile failure. Then this phenomenon can account for the frost damage that occurs in non-prestressed members. (Definition: Frost damage is defined as permanent deformation.)

The stresses created by a transient fluid pressure on infinitesimal elements at a capillary boundary are illustrated in Figure 3.1a. This is a two-dimensional illustration, assuming a unit thickness. For an internal pressure of "p", the stresses on the elements are as indicated in Figure 3.1a. The calculations of these values are shown in Appendix E.

A pre-applied uniaxially prestressing force in the Z-direction could produce a stress concentration on the boundary of a capillary as indicated by Wang. These stresses are indicated in Figure 3.1b. Here again, these stresses act at the boundary, and if this conjecture is true, these stresses are an upper bound to this stress-concentration problem. The calculations of these values are shown in Appendix E.

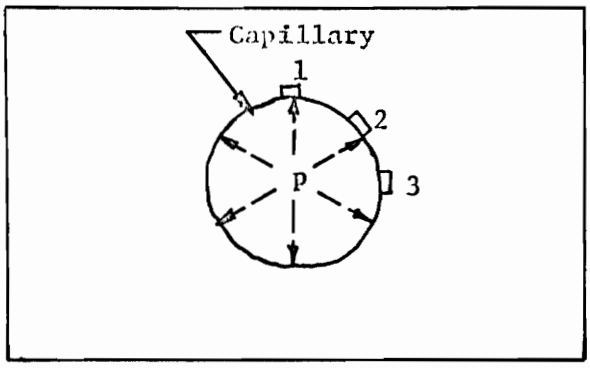

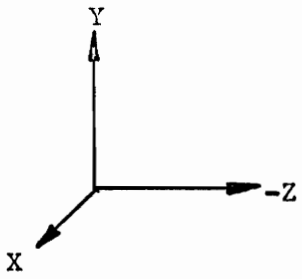

Note:

Potential Microcrack

Transient Stress

Element 1 at $\theta = 90^{o}$

Element 2 at $\theta = 45^{o}$

Element 3 at $\theta = 0^{o}$

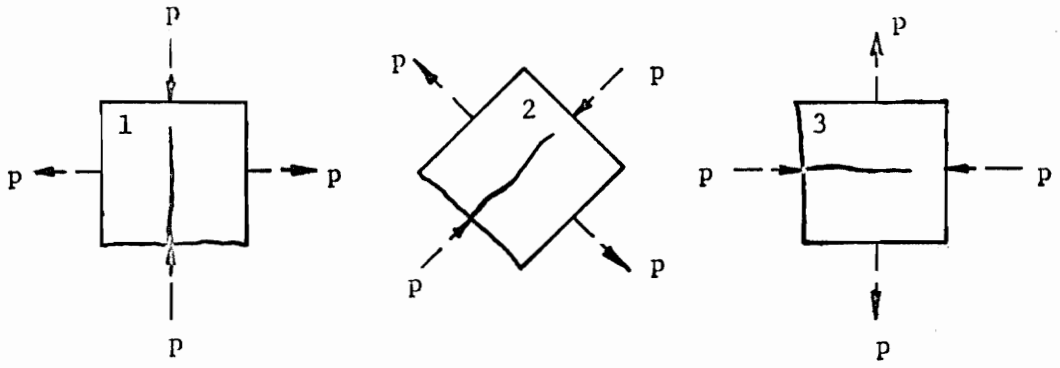

FIGURE 3.1a STRESSES ON INFINITESIMAL ELEMENTS AT THE CAPILLARY BOUNDARY DUE TO A TRANSIENT FLUID PRESSURE (FROM PAYNE)

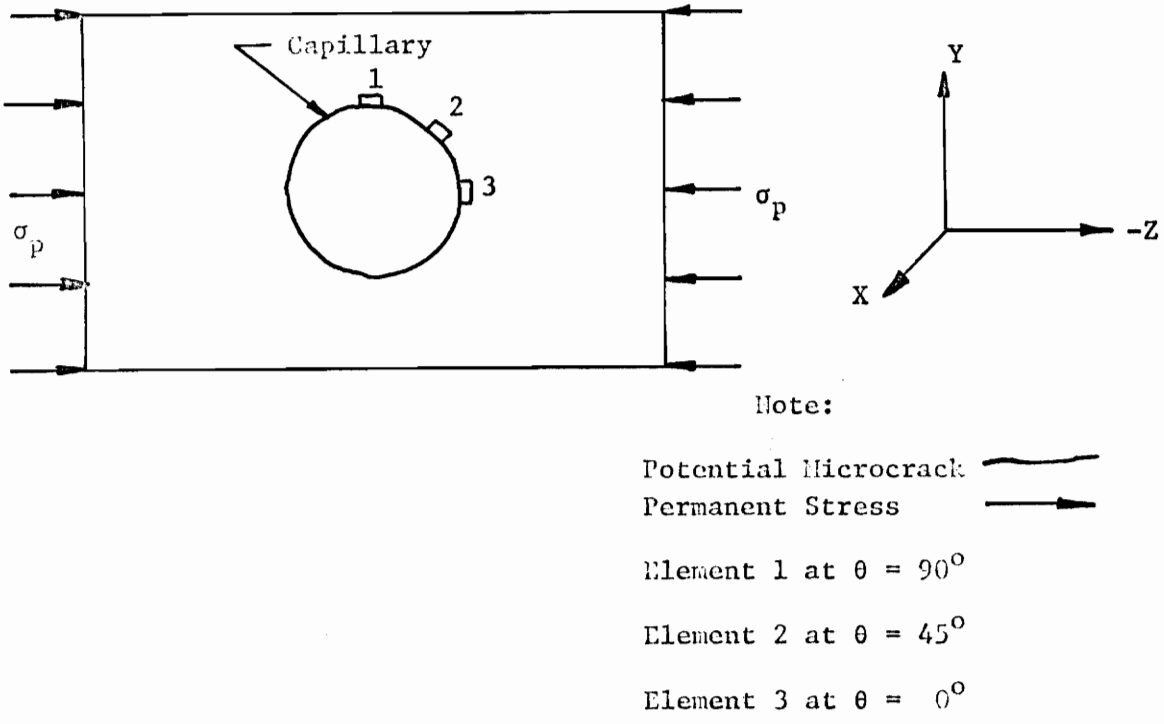

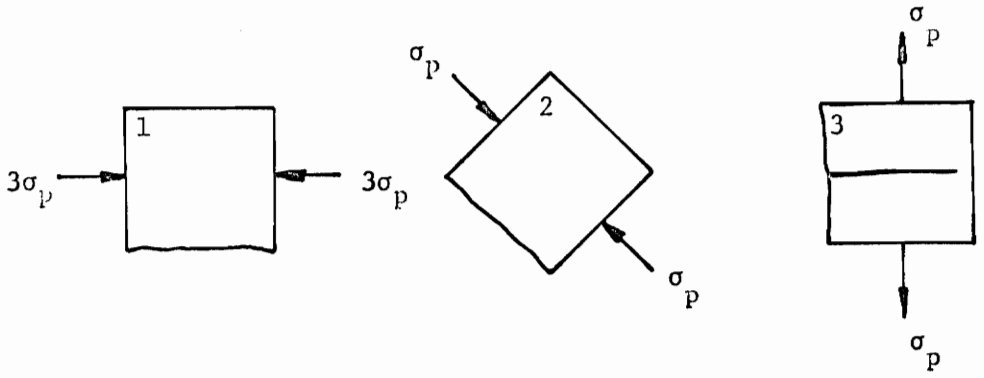

FIGURE 3.1b STRESSES ON INFINITESIMAL ELEMENTS AT THE CAPILLARY BOUNDARY DUE TO UNIAXIAL PRESTRESSING (FROM PAYNE)

The pre-applied compressive stress from a uniaxially applied prestressing force can be calculated by the formula

$$\sigma_p = \frac{P}{A_c} \tag{3.1}$$

where σ_p = unit compressive stress in the concrete

P = initial uniaxially applied prestressing force

A_c = the net cross-sectional concrete area

The actual (absolute) value of the stresses at point 1 and at point 3 must be somewhat less than the values indicated by the theory of elasticity and shown on Figure 3.1b. If these indicated values were true, the material would probably fail at both points. The sense of these stresses is correct and may be used to indicate what could happen.

Since the stresses shown in Figure 3.1a and Figure 3.1b act in homologous directions (radial and tangential) and in the limit (at the boundary of the capillary) on like areas, these stresses will be treated as forces and manipulated as vectors.

By superimposing the stresses of Figure 3.1b on the stresses of Figure 3.1a, the stresses shown in Figure 3.1c are produced.

Analyzing this complex problem indicated that prestressing could mitigate frost-damage on planes perpendicular to the direction of the prestressing force. Also, that this effect should attenuate as this plane is rotated (about a center) and that this effect should vanish when this rotating plane is orthogonal to its original position. That is, the planes of least resistance to tensile microcracks and the planes of microcrack propagation should be parallel to the direction of the applied prestressing force. This will be true even if the stresses in Figure 3.1b are greatly reduced.

The above statements should be valid regardless of the orientation or direction of the capillary. Likewise, this theory applies regardless whether the aggregate fractures first or dilates and fractures the matrix first. In other words, the microcracks and fractures are directionalized by the prestressing force.

This study also indicated there is a possibility that prestressing could accelerate disintegration of this concrete in a direction orthogonal to the direction of the prestressing force. First, the concentrated tensile stresses produced by prestressing are additive to the tensile stresses produced by fluid pressure. This is hypothesized to be an initial effect, i.e., assist in initiating the microcrack. Second, the fractures that occur are being forced into pre-determined directions or planes. Therefore, the measured permanent deformation (change in length) orthogonal to the plane containing the prestressing force, the sum of these fractures, could be accelerated.

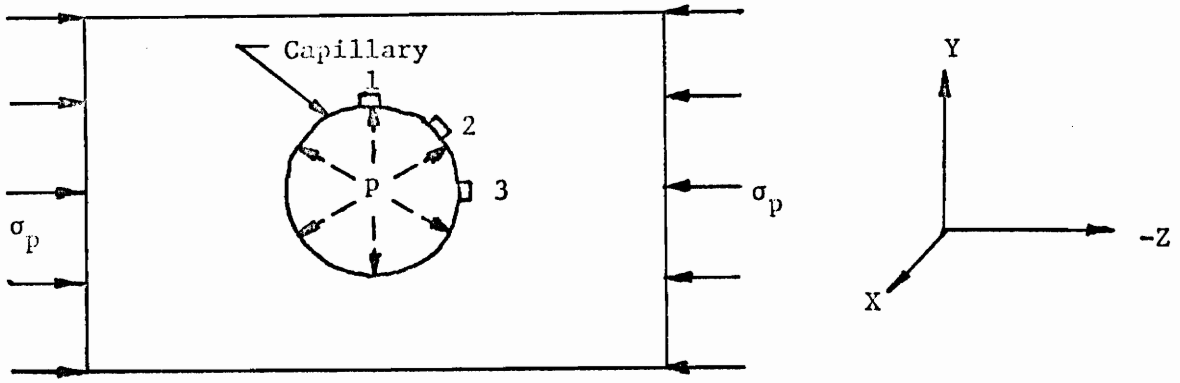

Note:

Potential Microcrack
Transient Stress
Permanent Stress

Element 1 at $\theta = 90^o$

Element 2 at $\theta = 45^o$

Element 3 at $\theta = 0^o$

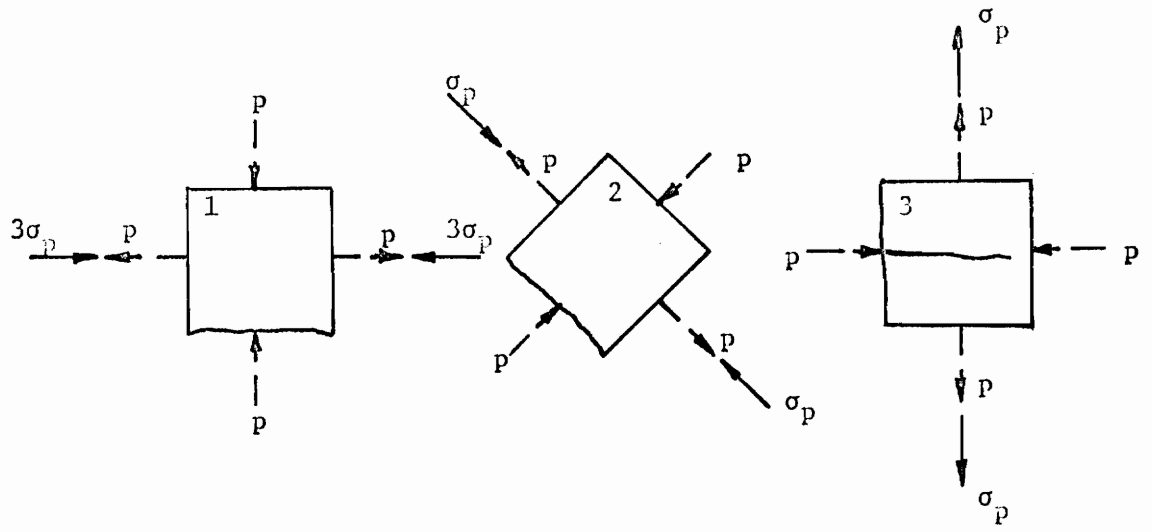

FIGURE 3.1c STRESSES OF FIGURE 3.1b SUPERIMPOSED ON THE STRESSES OF FIGURE 3.1a (FROM PAYNE)

Author's Theory

Development of Equations of Equilibrium

Continuing from Payne's work, the equations of equilibrium in polar coordinates can be derived. Since the primary damage of the concrete system is thought to originate in the capillaries of the various aggregate particles, a model is needed to develop a criterion for this damage.

The model used by Payne to represent the stresses around an aggregate capillary due to an internal fluid (hydraulic) pressure is a thick-walled circular cylinder subjected to an internal pressure only. This model is shown in Figure 3.2a. The model used by Payne to represent the stresses around an aggregate capillary due to a uniaxial compressive stress field (uniaxial prestress) is a plate of unit thickness with a circular hole subjected to a uniaxial compressive stress. This model is shown in Figure 3.2b. It can be seen from these two figures that a polar-coordinate reference frame is used in both cases to determine the location of any point P outside the capillary boundary. The model representing the actual conditions inside the aggregate particle in this research is shown in Figure 3.2c as the superposition of Figures 3.2a and 3.2b.

Since point P on the superimposed model represents any point outside the capillary boundary, the stresses at this point can be determined from a differential element. From the free-body diagram of the polar element shown in Figure 3.3, the stress equations of equilibrium in polar coordinates can be derived. The element is assumed to be very small. In Figure 3.3, the stresses are assumed to represent the superposition of stresses due to the fluid pressure and the prestressing force and are designated by the following:

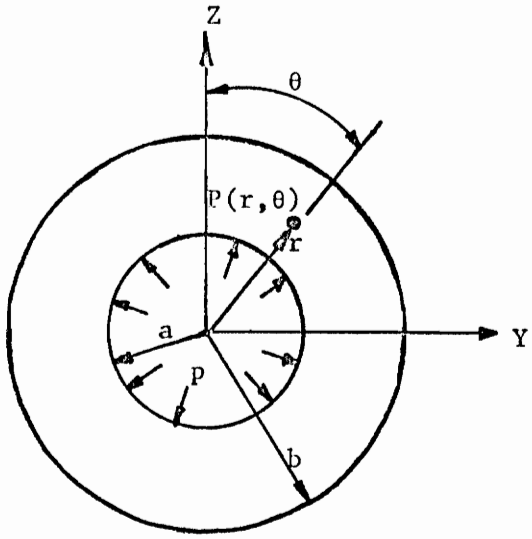

FIGURE 3.2a THICK-WALLED CIRCULAR CYLINDER SUBJECTED TO INTERNAL PRESSURE

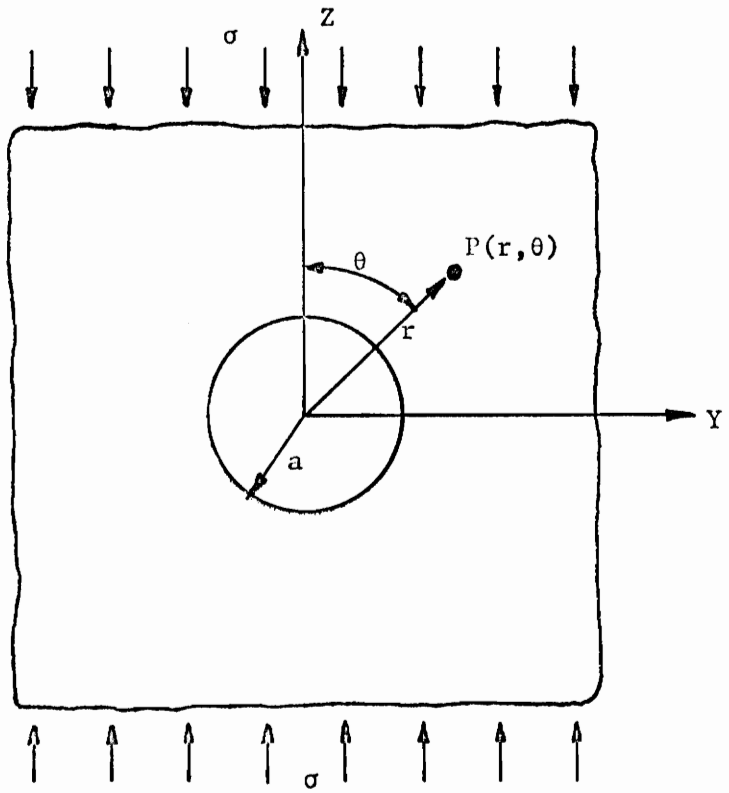

FIGURE 3.2b PLATE OF UNIT THICKNESS WITH A CIRCULAR HOLE SUBJECTED TO A UNIAXIAL COMPRESSIVE STRESS

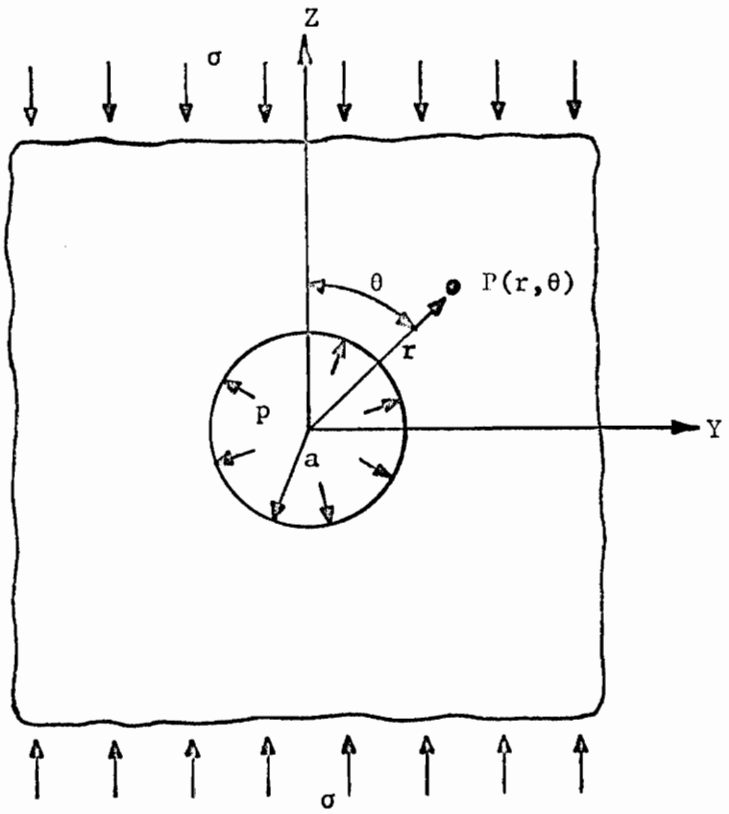

FIGURE 3.2c SUPERPOSITION OF FIGURES 3.2a AND 3.2b TO FORM THE MODEL

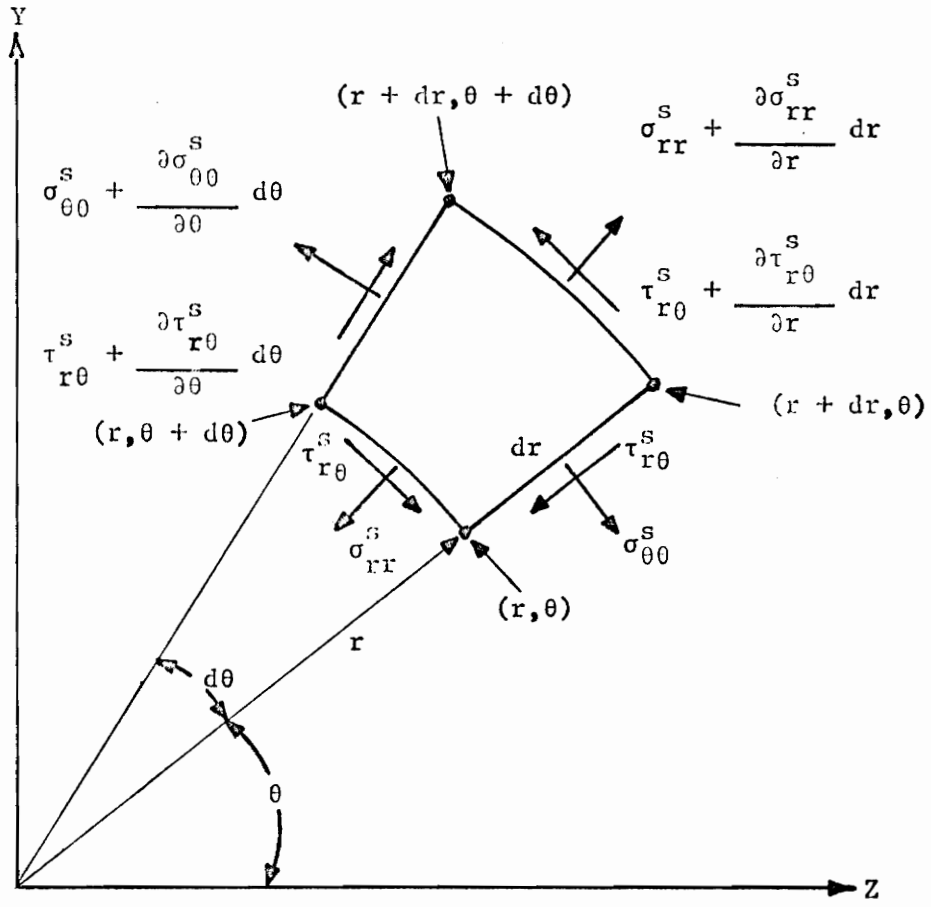

FIGURE 3.3 POLAR ELEMENT OF UNIT DEPTH SHOWING THE STRESSES ACTING ON THE FREE FACE

$\sigma^s_{rr} = \sigma^f_{rr} + \sigma^p_{rr}$ = superimposed radial (normal) stresses

σ^f_{rr} = the radial stress due to the fluid pressure

σ^p_{rr} = the radial stress due to the prestressing force

$\sigma^s_{\theta\theta} = \sigma^f_{\theta\theta} + \sigma^p_{\theta\theta}$ = superimposed tangential stresses

$\sigma^f_{\theta\theta}$ = the tangential stress due to the fluid pressure

$\sigma^p_{\theta\theta}$ = the tangential stress due to the prestressing force

$\tau^s_{r\theta} = \tau^f_{r\theta} + \tau^p_{r\theta}$ = superimposed shearing stresses

$\tau^f_{r\theta}$ = the shearing stress due to the fluid pressure

$\tau^p_{r\theta}$ = the shearing stress due to the prestressing force

For a polar element of unit thickness to be in a state of equilibrium, the sum of all forces in the radial (r) and tangential (θ) directions must equal zero. By summing forces first in the radial direction, the equation of equilibrium shown below is obtained. Therefore, from Dally and Riley [14] we have

$$\left(\sigma^s_{rr} + \frac{\partial \sigma^s_{rr}}{\partial r}\, dr\right)(r + dr)\, d\theta - \sigma^s_{rr} r\, d\theta - \left[\sigma^s_{\theta\theta}\, dr + \left(\sigma^s_{\theta\theta} + \frac{\partial \sigma^s_{\theta\theta}}{\partial \theta}\, d\theta\right) dr\right] \frac{d\theta}{2} + \left(\tau^s_{r\theta} + \frac{\partial \tau^s_{r\theta}}{\partial \theta}\, d\theta - \tau^s_{r\theta}\right) dr = 0 \qquad (3.2)$$

Dividing this equation by dr dθ and simplifying gives

$$\frac{\partial \sigma^s_{rr}}{\partial r}\, dr - \frac{\partial \sigma^s_{\theta\theta}}{\partial \theta}\, \frac{d\theta}{2} + \sigma^s_{rr} + \frac{\partial \sigma^s_{rr}}{\partial r}\, r - \sigma^s_{\theta\theta} + \frac{\partial \tau^s_{r\theta}}{\partial \theta} = 0 \qquad (3.3)$$

If the element is made infinitely small by permitting dr and dθ each to approach zero, the first two terms in Equation 3.3 also approach zero

and the expression may be rewritten as

$$\frac{\partial \sigma^s_{rr}}{\partial r} + \frac{1}{r}\frac{\partial \tau^s_{r\theta}}{\partial \theta} + \frac{1}{r}(\sigma^s_{rr} - \sigma^s_{\theta\theta}) = 0 \qquad (3.4)$$

The equation of equilibrium in the tangential direction may be derived in the same manner if the forces acting in the θ direction on the polar element are summed and set equal to zero. Therefore,

$$\frac{1}{r}\frac{\partial \sigma^s_{\theta\theta}}{\partial \theta} + \frac{\partial \tau^s_{r\theta}}{\partial r} + \frac{2\tau^s_{r\theta}}{r} = 0 \qquad (3.5)$$

Equations 3.4 and 3.5 represent the equations of equilibrium in polar coordinates for any aggregate capillary perpendicular to the prestressing force (these are the critical capillaries). Any solution for stresses to this elasticity problem must satisfy these equilibrium equations.

The stresses along the boundary of the capillary are vital in determining when and where fracture of the capillary will occur. Payne has determined where these cracks originate and the direction they will propagate, and he has predicted that the propagation of the cracks is a function of the stress field. This theory and analytical results are presented in the beginning of this chapter and in Appendix E, respectively.

Now, the author will present a theory to show that for the given conditions of this research, the rate of deterioration of plain concrete is a function of the level of compressive stress field; that is, as the level of stress increases the rate of deterioration increases. This theory will now be presented in a five-step procedure.

Development and Propagation of Primary Cracks

Step 1: Development of critical stress for fracture

The primary cracks are assumed to originate from the capillaries within the aggregate particles. From the discussion and calculations by Payne, the cracks begin at the boundary of a capillary. Assuming this theory to be valid, it can be applied to various levels of compressive stress. Considering element 3 of Figure 3.1c, there exists a state of stress at the capillary boundary due to the prestressing force and fluid pressure. At this point, the concentrated tensile stress produced by prestressing is additive to the tensile stress produced by fluid pressure. If it is assumed that the tensile stress produced by the fluid pressure remains constant for increasing levels of stress, then only the tensile stress produced by prestressing will increase for increasing levels of stress. As a result, cracks will originate sooner for increasing levels of stress since the tensile strength of the aggregate will be exceeded sooner. The author defines the combined stress which initiates the microcrack at the aggregate capillary boundary as the "critical fracturing stress." Thus, the rate of deterioration for the concrete member as a whole will increase for increasing stress. This deterioration begins in the early freeze-thaw cycles and applies to every capillary which generates a critical hydraulic pressure.

This phenomenon is shown in Figure 3.4. A linear analysis can be used for determining when and where the primary cracks will originate. However, after the first crack has formed in the capillary boundary, a non-linear analysis (inelastic theory) is needed to determine further crack propagation.

The author also believes (from unpublished data by Payne and the author) that the initiation of microcracks at the capillary boundary

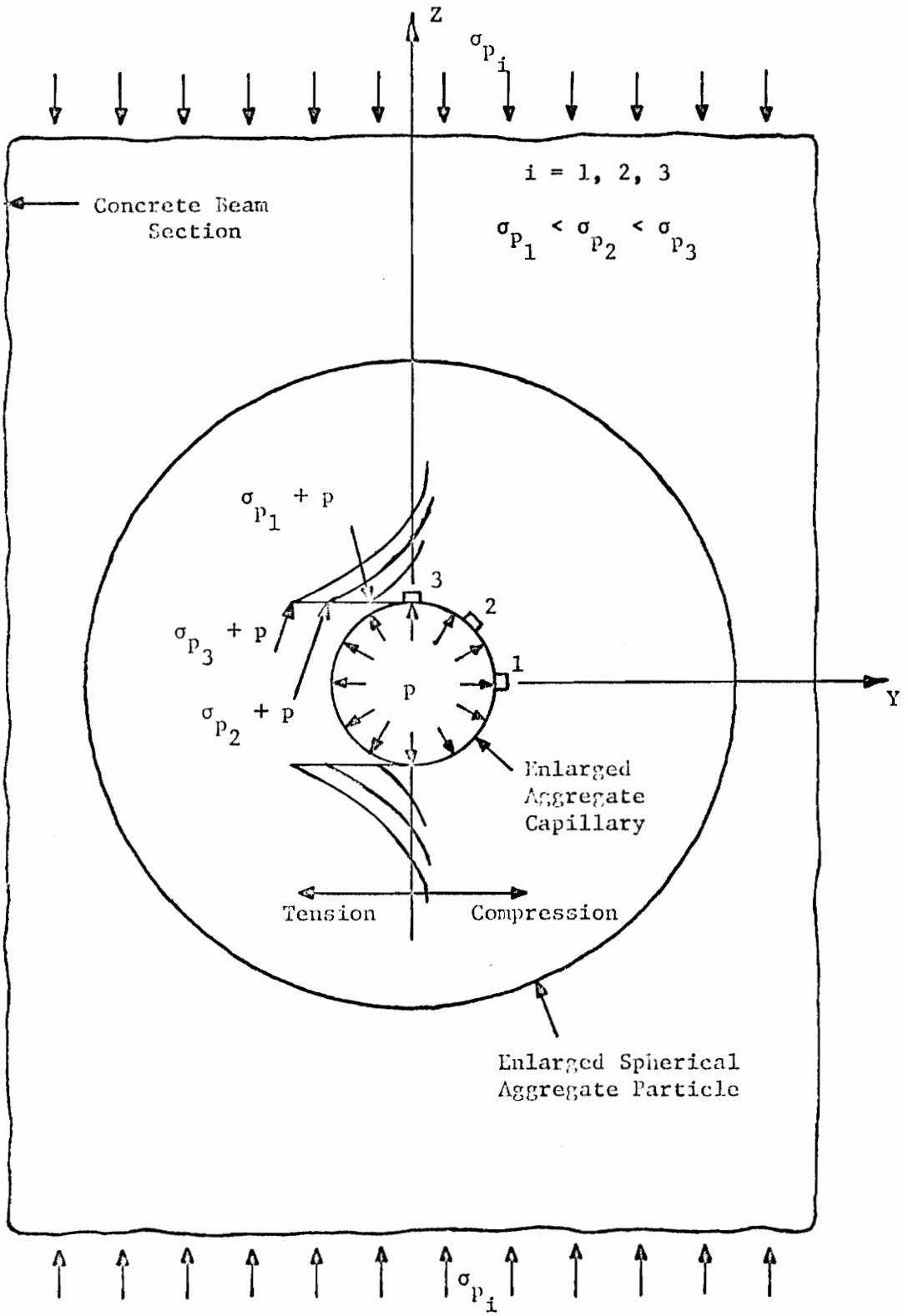

FIGURE 3.4 STEP 1: DEVELOPMENT OF CRITICAL STRESS FOR FRACTURE

depends on the rate of freezing of the concrete. The rate of freezing is considered to be a function of distance. That is, as the freezing rate increases, the water within the capillaries travels a constant distance in a shorter length of time. This creates a greater pressure on the capillary walls causing them to fracture sooner than at a slower freezing rate.

Step 2: Stresses at crack tip after capillary fracture

Now, assuming cracks have developed in a capillary boundary after continued freezing and thawing action, the ideas developed by Glucklich in Appendix C can be applied. The cracks thus formed will carry a tension zone at the tip. This tensile stress will be smaller than the singly applied compressive stress as shown in Figure C.8b. However, for increasing compressive stress, the tension zone at the crack tip will be increasingly larger even though it is not exactly equal to the applied stress. This relationship is shown in Figure 3.5.

Step 3: Crack propagation through the aggregate

The cracks produced in Step 2 conveniently fit Griffith's criteria for an elliptical crack. This is seen by considering the region AB in Figure 3.5. Thus, Griffith's theory can now be applied for crack propagation in the author's case. Griffith's theory and its development for concrete under compression was discussed in Appendix C. However, in applications of Griffith's theory, propagation of cracks was due to stress concentrations at the crack tip due to increasing load. For the situation in the author's case, crack propagation was due to the stress concentrations at the crack tip due to the formation of hydraulic (fluid) pressure in this region during each freezing cycle. This hydraulic pressure

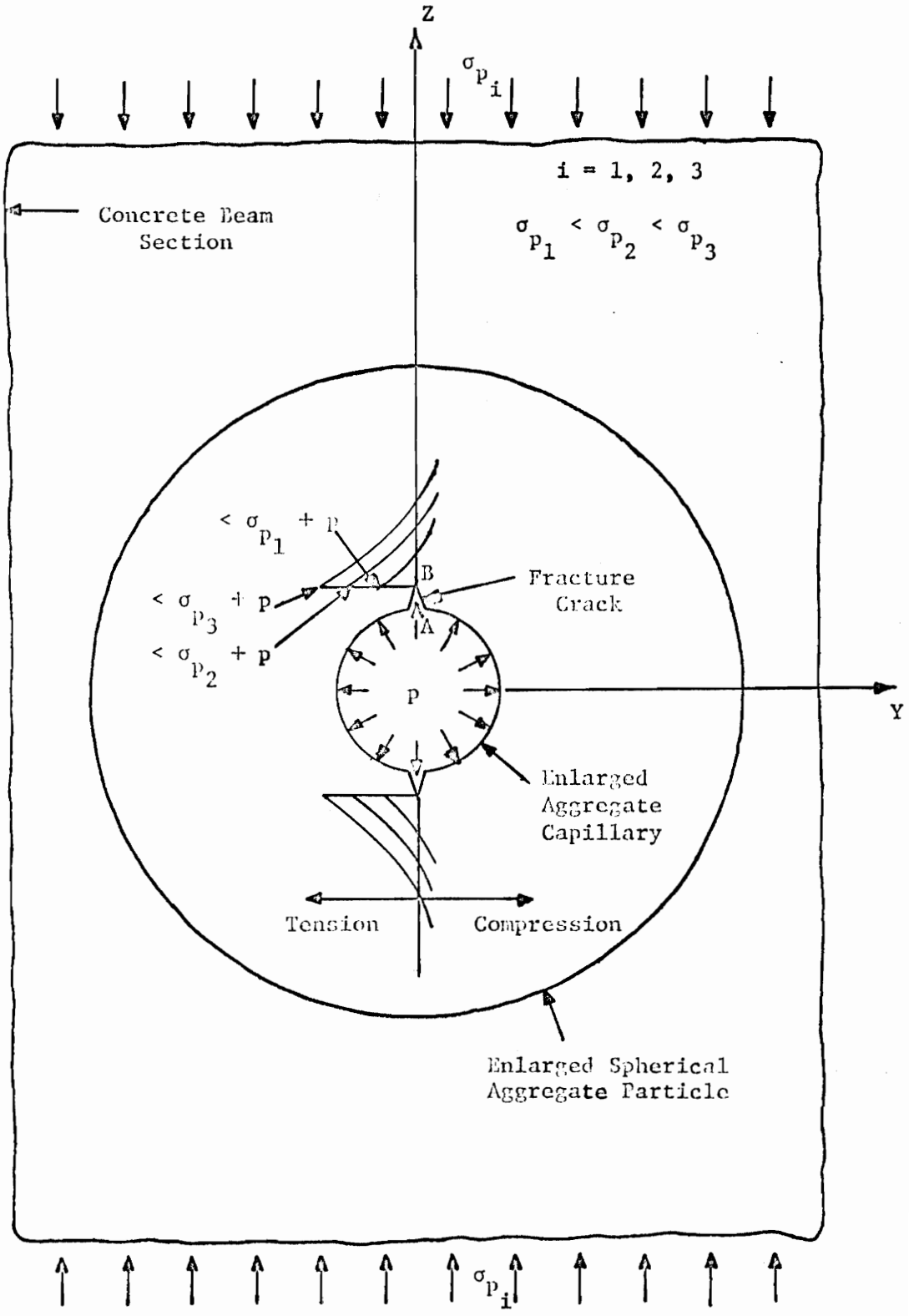

FIGURE 3.5 STEP 2: STRESSES AT CRACK TIP AFTER CAPILLARY FRACTURE

was constant for each level of increasing stress and created a stress, when superimposed with the compressive stress, to propagate the crack. The author defines the total combined stress which initiates crack propagation as the "critical propagation stress." Thus, it is believed that the stress concentration factor at a crack tip increases as the level of compressive stress increases.

From Step 2, the tension zone is carried forward by the tips of the expanding cracks. This tension zone will increase in magnitude for increasing stress. Thus, it is obvious that the rate of deterioration and crack propagation is greater for increasing stress. From this development, it is assumed that the stress concentrations at the crack tip region are larger for increasing stress levels and constant hydraulic pressure. This condition is shown in Figure 3.6. In this figure, the cracks have propagated from the capillary boundary, through the aggregate particle, and almost to the outer boundary of the aggregate particle itself. Due to the effect of the applied stress field, crack propagation will always be in planes parallel to the applied stress.

Step 4: Superimposed stress conditions at aggregate boundary

Goodier's equations, discussed in Appendix C, can now be applied to concrete under a compressive load to determine the stress distribution around an aggregate particle located in the cement mortar matrix. In using these equations, various material properties of the author's concrete mixture had to be determined.

From the equations by Hansen in Appendix C, the modulus of elasticity, E, of the cement mortar matrix was determined. First, Equation C.2 was

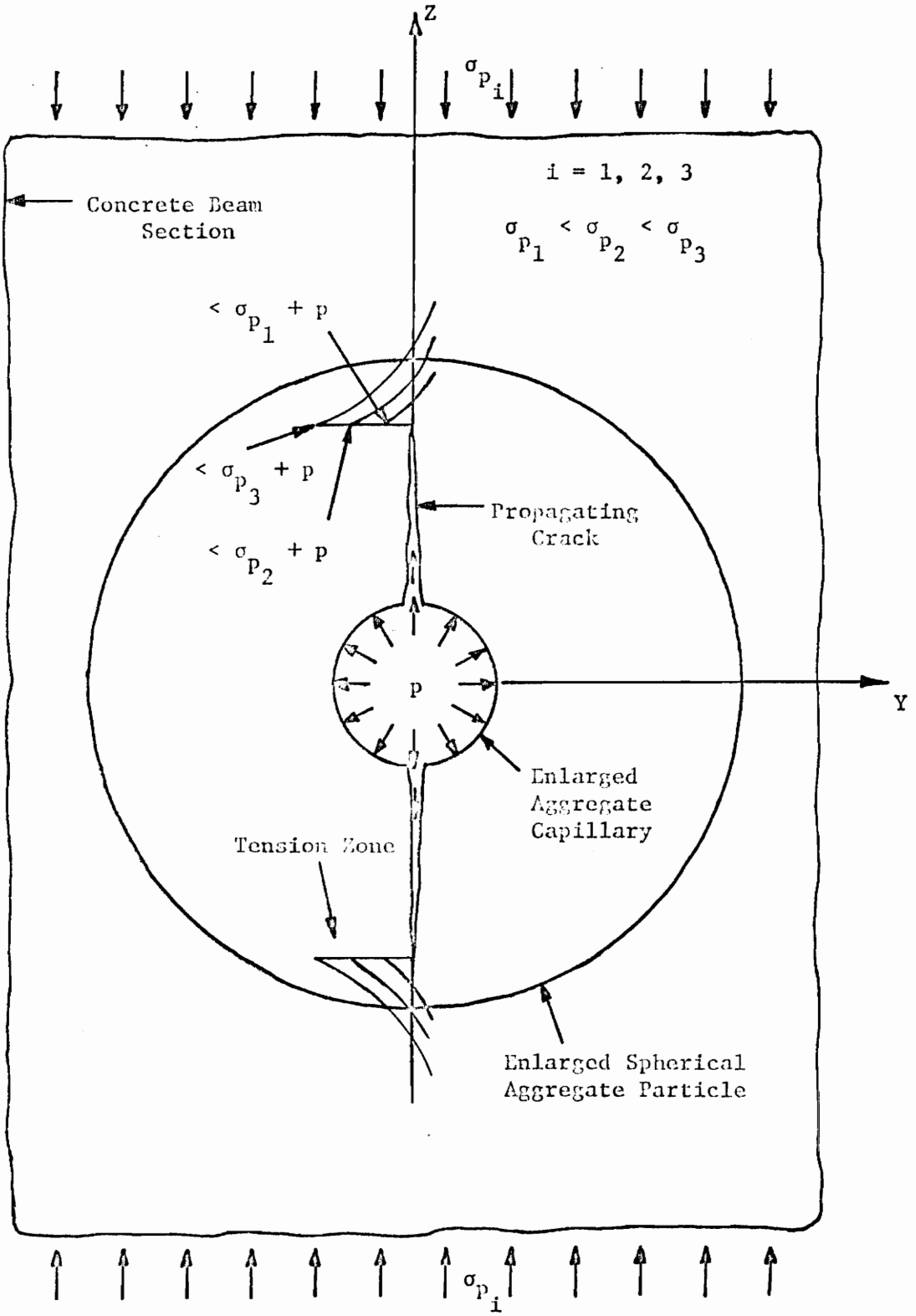

FIGURE 3.6 STEP 3: CRACK PROPAGATION THROUGH THE AGGREGATE

used to determine E of the cement paste with air-entrained pores. This value was then used in Equation C.3 to determine E of the cement mortar matrix. In using Equation C.2, E of plain cement paste was assumed to be 3.51×10^6 psi, and the fractional volume of air-entrained pores was determined to be 0.04. The value obtained for E of the cement paste with pores was 3.1×10^6 psi. In using Equation C.3, E of the author's fine aggregate (Petersburg quartz sand) was assumed to be 5.5×10^6 psi (this is one-half the E value of pure quartz sand since the sand in this research was not completely pure). The fractional volume of each material was taken from Table 6.4. Thus, the value obtained for the cement mortar matrix was 3.50×10^6 psi. As an additional calculation, E of the author's concrete as a whole was determined from Equation C.1. Again, the fractional volume of each component was taken from Table 6.4, and the E of the mortar was taken as 3.50×10^6 psi as determined from Equation C.3. The modulus of elasticity of the coarse aggregate as a whole was determined from Table 6.1 by considering E of each aggregate type individually on a percentage basis. This value was assumed to be 4.0×10^6 psi. Thus, E of the author's concrete was calculated to be 3.8×10^6 psi, a typical, average value for plain structural concrete.

Other material properties had to be determined for use in Goodier's equations. Since the coarse aggregate particles were sieved into 1/4" to 1/2" and 1/2" to 3/4" sizes and combined on a 50 percent to 50 percent basis, an aggregate particle diameter of 0.5 inches was assumed. Thus, r and a in Goodier's equations were 0.25 inches. Poisson's ratio of the coarse aggregate was assumed to be 0.20 (by considering Table 6.1) and of the cement mortar matrix to be 0.17. Using all these values and the mod-

ulus of elasticity of the mortar and coarse aggregate to be 3.5×10^6 and 4.0×10^6 psi respectively, Goodier's equations were used to determine the stresses around an aggregate particle. These values are shown in Table 3.1 for the three levels of compressive stress used in this research. It should be noted that these stresses are for aggregate particles which are assumed to be spherical. Non-spherical particles, as in regular concrete, could produce a somewhat different stress distribution around the particle. Thus, the stress distribution around an aggregate particle is a function of particle geometry and also, indirectly, as a function of surface texture. The geometry, stiffness, and volume content of aggregate particles all influence the stress distribution characteristics throughout the concrete; and, hence, directly influence the energy requirements for crack propagation and fracture toughness.

In the discussion about Goodier's equations in Appendix C, an example was shown in which the aggregate particle is assumed to be perfectly rigid (that is, $E_2 = \infty$). However, in the author's calculations the particles are assumed to have an elastic property since rocks are not completely rigid.

Three orientations on the aggregate particle are considered, 0^o, 45^o, and 90^o. These orientations can be determined from Figure C.4. From the values in Table 3.1, a tensile stress exists around the particle in the tangential direction for a spherical particle. It is obvious that for the increasing levels of compressive stress, the tensile stresses around the particle increase. The author conjectures that these tensile stresses will have an effect on the approaching crack from within the aggregate particle which was described in Step 3.

In Step 3, it was shown that a tensile stress exists at the tip of

TABLE 3.1 CALCULATED STRESSES AROUND A SPHERICAL AGGREGATE PARTICLE

	Applied Compressive Stress 500 psi			Applied Compressive Stress 1000 psi			Applied Compressive Stress 1500 psi		
Stress (psi)	Angle 0^{o}	Angle 45^{o}	Angle 90^{o}	Angle 0^{o}	Angle 45^{o}	Angle 90^{o}	Angle 0^{o}	Angle 45^{o}	Angle 90^{o}
σ_{rr}	-1865	-1848	-1831	-3730	-3700	-3660	-5601	-5552	-5501
$\sigma_{\theta\theta}$	900	924	948	1802	1849	1897	2703	2774	2845
$\sigma_{\psi\psi}$	903	910	917	1799	1813	1827	2703	2723	2743

Positive sign indicates tension.

the propagating, internal crack; and it has just been shown that a tensile stress exists in the mortar matrix around the coarse aggregate particle. Thus, the author believes that if the bond has not been broken at the aggregate-mortar interface, then, when the internal aggregate crack reaches this boundary, the tensile stresses at the crack tip will superimpose with the tensile stresses around the particle and possibly accelerate crack propagation. This propagation will occur if the stresses caused by this superposition exceed the strength of the mortar matrix. Since the tensile stress at the crack tip and around the aggregate are correspondingly larger for increasing compressive stress and constant hydraulic pressure, it is obvious that the rate of deterioration is greater for the higher compressive stress levels. This situation is shown in Figure 3.7.

There is also the possibility of the superposition of four tensile stress components when an internal aggregate crack approaches the aggregate-mortar interface. As discussed in Appendix B, stresses may exist at the aggregate-mortar interface which are generated by the volume shrinkage of the mortar. It is generally thought that such volume shrinkage produces radial compression in the aggregate and circumferential tension in the mortar. These stresses are independent of the external load. They may also be large enough to create mortar cracks when the strength of the material is exceeded.

Step 5: Crack propagation possibilities

If a bond or mortar crack (secondary cracks) already exists at the aggregate-mortar interface, the approaching internal aggregate crack will possibly connect with it. When this occurs, the tension at the crack tip

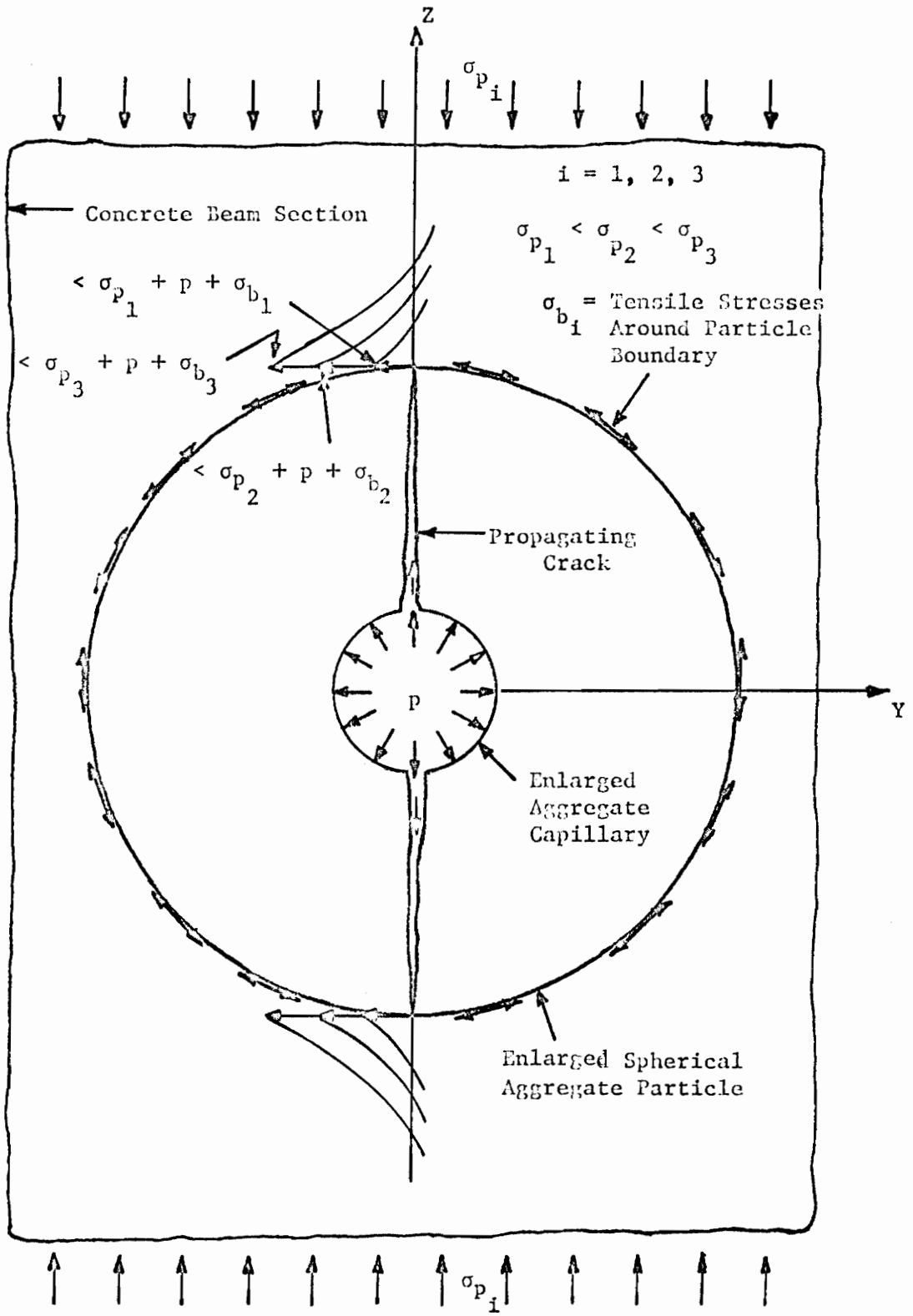

FIGURE 3.7 STEP 4: SUPERIMPOSED STRESS CONDITIONS AT AGGREGATE BOUNDARY

of the internal crack is relieved. Also, when there is a bond or mortar crack at the interface, tensile stresses at the boundary of the aggregate will not exist at this point. Propagation of the crack as a whole will continue when tensile stresses at the crack tip produced by hydraulic pressure superimposed with tensile stresses caused by the external stress exceed the strength of the cement mortar matrix.

Goodier's equations can be used with the approporiate material values to determine the stresses which will cause bond cracks to form around the aggregate particle. If these stresses exceed the strength of the aggregate-mortar bond at the interface, then bond cracks will form. These and other secondary cracks will be discussed in the next section of this chapter.

When primary cracks propagate out of the aggregate particle into the mortar matrix or join secondary cracks and propagate through the mortar matrix, Griffith's fracture theory can still be applied. This complex mathematical analysis applied to the freezing and thawing of concrete under a constant load is too involved to be undertaken here. Thus, it is only implied.

As the cracks propagate through the mortar during each alternating freeze-thaw cycle, they will seek the planes of least resistance as described by Payne. These planes will also be the planes of minimum energy required for propagation. This may mean that the cracks can deviate around certain obstacles (containing planes of high resistance) or pass through others (containing planes of low resistance). In either case, crack propagation will be in planes parallel to the direction of the applied load. If Goodier's equations are applied to a spherical air void,

tensile stresses above and below the void are shown to exist as with an aggregate particle. Thus, as cracks propagate through the mortar, they may pass through the top or bottom of an air void.

When a crack approaches an isolated mortar matrix crack, the two may connect due to the influence of tensile stresses at the tips of both. Also, when a crack approaches another aggregate particle, the tensile stresses at the tip may be influenced by the tensile stresses around the particle, and the crack may deviate around it. In addition, if the same fracturing process has taken place in another aggregate particle and the internal crack has reached or passed the aggregate-mortar interface, the tension at the tip of an approaching crack may superimpose with the tension at the tip of the aggregate crack. Usually, the crack will pass completely through the aggregate particle and continue its journey with each alternating freeze-thaw cycle. Figure 3.8 gives a brief illustration of these situations.

Creep in the concrete also accounts for a very small amount of deterioration. However, this was not measured in the author's research. As discussed in Appendix C, the author believes that creep is caused by a two stage phenomenon. The first stage is due to Poisson's elastic shortening after the application of load, and the second stage to the slow formation and propagation of internal microcracks caused by an external load.

Development and Propagation of Secondary Cracks

Cracks due to no external load and cracks due to an external load exist in concrete. These are called secondary cracks and are discussed

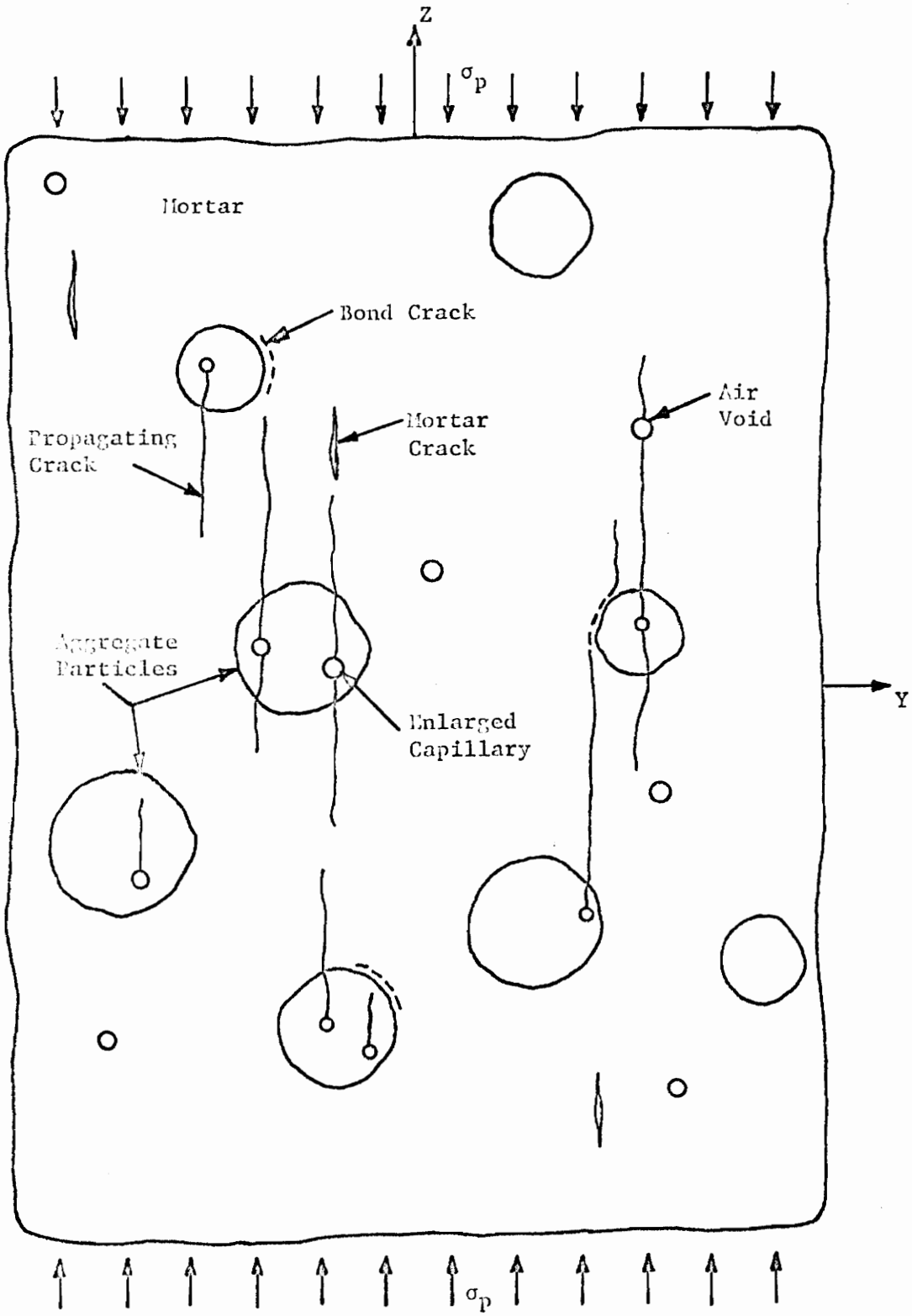

FIGURE 3.8 STEP 5: CRACK PROPAGATION POSSIBILITIES

in Appendices B and C, respectively. Not all of those discussed are involved in the author's concrete. However, those that do apply are thought to be responsible for concrete deterioration also. If a hydraulic pressure can be developed inside of the cracks, they will propagate through the concrete according to the theory thus presented.

Secondary cracks, such as bond and mortar cracks, are assumed to exist in the concrete from the discussion in Appendices B and C. It was shown that bond cracks exist in the concrete at loads as low as 30 percent of the ultimate strength. Since the ultimate strength of the author's concrete was 4188 psi, the percentages of the ultimate strength of the three levels of prestress used in this research can be determined. These are as follows: 500 psi is 12 percent of the ultimate strength, 1000 psi is 24 percent, and 1500 psi is 36 percent. Thus, it is assumed that the beams of 1500 psi prestress contain bond cracks, those of 1000 psi contain only a few, and those of 500 psi zero. The bond and mortar cracks due to no external load (due to volume changes) are assumed to exist in the members before the application of the prestressing force. It is also assumed that the same number of cracks exist in each member.

Since the members with the highest level of stress contain the greatest number of bond cracks, internal disintegration is greater, and there is a greater chance for these to propagate through the matrix. Since at lower levels of stress, cracks have to be first formed before they can propagate, bond cracks already formed at higher levels of stress can propagate initially if the "critical propagation stress" is reached. It is assumed that there is no water originally in the bond cracks. However, after the first few freeze-thaw cycles, water may be forced into these

cracks and be available to create a hydraulic pressure. Thus, this discussion supports the theory that the rate of deterioration increases as the level of compressive stress increases.

It should also be noted that if entrained air was not used to reduce matrix deterioration, then the same theory of crack initiation and propagation can be applied to the critical capillaries or pores in the cement mortar matrix. However, once a crack has formed, it will propagate as previously described.

Recommendations to Author's Theory

It would be interesting to develop a yield and fracture criteria for the area around an aggregate capillary and the aggregate particle itself. A widely accepted criteria for the fracture of brittle materials is the maximum normal stress theory (or maximum stress theory). This theory asserts that failure or fracture of a material occurs when the maximum normal stress at a point reaches a critical value regardless of the other stresses. Only the largest principal stress must be determined.

Experimental evidence indicates that this theory applies well to brittle materials (concrete) in all ranges of stress, provided a tensile principal stress exists. Failure is characterized by a separation or cleavage type of fracture.

Thus, in applying this theory to the author's case, the planes on which the maximum principal stresses exist as θ is rotated 360^{o} around the capillary or aggregate particle is required. Failure will occur when the maximum principal stress exceeds the confined tensile strength of the aggregate or the tensile strength of the cement mortar matrix.

CHAPTER IV

DESIGN OF THE EXPERIMENTAL INVESTIGATION

This chapter consists of four main sections, namely, programming of test specimens, prestressing of specimens, testing procedures, and non-linear transformation of restrained directions.

Programming of Test Specimens

Variables

As mentioned earlier, the purpose of this thesis was to study the effects of various levels of compressive stress fields on the deterioration rate (deep-seated) and microcracking of concrete subjected to freezing and thawing. Therefore, the only variable in this research was the level of stress in the concrete. Variables which could not be controlled were eliminated by subjecting each member to the same set of conditions each time. For example, the rate of freezing was not the same for all directions, but was controlled by placing each member in the exact same position and orientation after a strain reading was taken.

Levels of stress in the concrete

A summary of the levels of stress used by other researchers are as follows:

1. Pendley used an unknown restraint.
2. Rieb used 500, 1000, 1500, and 2000 psi.
3. Klieger used 350-400 psi.
4. Gutzwiller and Musleh used 2000 psi.
5. Roshore used varied stresses.

6. Jamil used 600 psi.

7. Payne used 1000 psi.

Therefore, the initial stresses in the concrete beam specimens chosen by the author were 500, 1000, and 1500 psi. Such a range of stresses should provide an indication of what effect different levels of stress have on the freeze-thaw durability of this concrete. The beams were prestressed by the post-tensioning method with a concentric force which produced a symmetric compressive stress intensity on the net cross sectional area of the concrete. This prestressing force was maintained until the freeze-thaw investigation was terminated. It should also be noted that the beams were not subjected to any eccentric loading conditions which could produce flexure and thus possible flexural cracking while undergoing prestressing and testing.

Constants

The factors which were held as constant as possible throughout the research are listed as follows:

1. Type of cement.
2. Air-entrainment.
3. Type of aggregate and saturation.
4. Mixture design.
5. Method and period of curing.
6. Dimensions of specimens.
7. Dimensions of containers.
8. Freezing rate and direction of freezing.

Type of cement

Type IIIA cement was used. This is an air-entrained portland cement which provides high strength at an early period, usually a week or less.

Specifications for Type IIIA, air-entrained cement are given in ASTM Designation: C150 [15]*. This corresponds in composition to Type III; however, it has small amounts of air-entraining materials mixed with the clinker during processing [16]. This cement produces a concrete with a greater resistance to freeze-thaw action and scaling caused by de-icing salts or harsh chemicals. Such concrete contains small, well-distributed air bubbles. A more detailed description of this cement is given in Chapter VI.

Air-entrainment

The disintegration of the matrix (fine aggregate plus cement plus water) and the deep-seated type of destruction of certain kinds of coarse aggregate particles are the two general types of frost damage to portland cement concrete [17]. The frost damage to concrete resulting from the disintegration of the matrix can generally be controlled by intentionally entraining microscopic air bubbles in the matrix [6]. Thus, air-entrainment held the matrix disintegration in all members constant. The purpose of air-entrainment and how it works are discussed in Appendix D.

Type of aggregate and saturation

As a research technique, the coarse aggregate used was a material very susceptible to freezing and thawing. Ample quantities of the same types of aggregates were heavily distributed throughout the concrete mixture to produce a uniform concrete and to ensure concrete deterioration

*All succeeding ASTM Designations refer to this reference.

from freezing and thawing action. Thus, it was hoped the effects of frost damage from the aggregate would be constant for all members.

Verbeck and Landgren [18] have demonstrated the principle of critical size of coarse aggregates. It states that for a given coarse aggregate, the smaller the size of the aggregate, the smaller the developed hydraulic pressures, providing everything else remains constant. This means that if the pores or capillaries of the aggregate are not long enough, the developed hydraulic pressure will not be high enough to damage the concrete by producing microcracks and macrocracks. Therefore, a coarse aggregate with a maximum size of 1/2 inch or larger should be used to ensure aggregate damage. For this research, 50 percent of the coarse aggregates ranged from 1/4" to 1/2" and the other 50 percent ranged from 1/2" to 3/4".

Also as a research technique to ensure concrete deterioration, all aggregate particles were vacuum saturated to a constant pressure to fill every capillary or pore as full as possible with water.

A description of this coarse aggregate is given in Chapter VI.

Physical and mechanical properties of a material

For the materials or components used in this research, such as rock, concrete, sand, cement paste, and cement mortar, there are certain physical and mechanical properties which may be helpful in evaluating the performance of the material under various conditions. Such properties, especially for rock, are described as follows:

Modulus of Elasticity, E (Young's Modulus): If the stress-strain curve is straight, when loaded in uniaxial compression, the ratio of

stress to strain may be taken as the value of the modulus of elasticity over the range of stress for which the relationship is linear. The value is expressed in terms of stress. The modulus of elasticity is a measure of stiffness or of the resistance of a material (rock or concrete) to deformation. The amount, type, and grading of aggregate has an important effect on E. The value of E is greater for lower water-cement ratios, richer mixtures, lower air contents, and longer curing periods [19]. Generally, the higher the compressive strength of the material, the higher its E value, though there are exceptions. The value of E for the same material also varies according to its moisture content. Observations have also shown that the E value of a rock apparently increases after the rock has been loaded for a long period of time [20].

Poisson's Ratio: When compressed in one direction, most materials expand in the direction transverse to that of the applied stress. The ratio of the transverse or lateral strain to the longitudinal strain, within the elastic range for axially loaded specimens, is known as Poisson's ratio. The value of Poisson's ratio for solid rock in general is taken normally to be in the range of 0.2 to 0.3. In any work involving elastic analysis of rocks, there is sufficient evidence available to suggest that a value of 0.25 for Poisson's ratio should be assumed unless there is ample evidence to the contrary [21].

Uniaxial Compressive Strength: The uniaxial compressive strength of a material, such as rock, is the stress required to break a loaded sample that is unconfined at the sides. Compressive stresses tend to decrease the volume of the material. Rocks are considerably stronger than the concrete of which they are a part. Therefore, the compressive

strength of rock is greater than the compressive strength of concrete. The compressive strength of rocks is influenced by their texture, particularly by the coarseness of their grains. Saturation by water decreases the compressive strength of a rock. It is known that the higher the porosity--and thus the greater the chance for saturation--the lower will be the strength of the rock when saturated. Thus, it has also been shown that as the percent absorption increases, the compressive strength decreases. The compressive strength of a rock also increases as the lateral restraint increases.

Uniaxial Tensile Strength: The tensile strength of rocks and concrete is practically negligible. Tensile stresses tend to produce cracks and fissures in the material. However, the concept of tensile strength in rocks is of paramount importance in the Griffith criterion of failure. It is a property of brittle materials that their tensile strength is considerably less than their compressive strength. The tensile strength of concrete is relatively low, about 10 to 15 percent of the compressive strength.

Porosity: The porosity of a rock is the ratio of the volume of voids (pores) to the over-all volume of the rock specimen. Aggregates make up from 70 to 75 percent of the total concrete volume and have porosities that range from nearly 0 to about 20 percent by solid volume. The porosity of rocks and concrete is discussed in more detail in Appendix D.

Absorption: Absorption refers to the process by which a rock or concrete draws water into its pores and capillaries. This process is also discussed in more detail in Appendix D.

Coefficient of Permeability: The permeability of rock or concrete

to water or vapor is the property which permits the passage of the fluid or vapor through the material. This property for concrete is discussed in Appendix D.

Coefficient of Thermal Expansion (thermal coefficient): The coefficient of thermal expansion is a length change in a unit length per degree of temperature change. Variations in temperature cause a material to expand when the temperature rises and contract when the temperature falls. The value is expressed in inches per inch per degree Fahrenheit, or more commonly as millionths per degree Fahrenheit (10^{-6} in/^{o}F). For aggregates in general, the value ranges between 3 to 7 x 10^{-6} in/^{o}F, with an average value taken as 5 x 10^{-6} [22]. The coefficient of thermal expansion for concrete depends largely on the coefficient of the aggregate particles themselves. It also depends on the type and amount of aggregate, method of storage of the concrete, and the hydration state of the concrete mixture at the time of the temperature change. The thermal coefficient of the aggregate material in concrete will not be the same as that of the cement mortar matrix. The coefficients of dry and saturated concretes are the same, but they are lower than those of partially dried concrete. Thus, concrete cured in air has a higher thermal expansion than concrete kept in water. The curing history has little effect on the coefficient, and age appears to have only a minor effect. Different types of cement have little effect upon the coefficient except when the concrete has been stored in water.

Numerical values for the seven properties just discussed are given in Chapter VI for the different geological types of aggregates used in this research.

Mixture design

The concrete mixture design used in this investigation involved the application of the aggregate-void concept given by Goldbeck and Gray [23], the so-called b/b_o method.

The mixture was designed for 0.793 cubic feet or 0.0294 cubic yards of concrete. This included enough concrete to mold the required number of test beams and test cylinders, plus a 5 percent waste. The concrete was also designed for a compressive strength of 4000 psi and a slump of 6 inches.

The cement content of this mixture was hoped to be maintained at 7 bags per cubic yard. This figure is comparable with that used in prestressed concrete construction practice [9].

The design of the mixture used for all the test specimens and other pertinent information concerning the mixture may be found in Chapter VI.

Method and period of curing

There are two common methods of curing prestressed concrete members, namely, moist and steam curing. Steam curing is one means used to attain a reasonably high strength concrete in a short period of time. In moist curing, the members are continuously subjected to moist water which prevents the beams from drying out and cracking.

For this research, a moist curing room of 70^{o}F and 100 percent relative humidity was used. After the forms were removed, the beams were submerged in a container of lime-saturated water inside the curing room. The limewater helped to maintain a constant rate of hydration of the concrete and prevented any water loss from the members. Hopefully, extra

water was absorbed to ensure disintegration from freezing and thawing. The lime content of the water remained constant for all members.

All specimens were accorded the same curing period before the freezing and thawing tests began. Of course, the concrete need not attain its full design strength, but must be strong enough to transfer the force in the steel to the concrete and to carry any stresses caused by handling.

Dimensions of specimens

Since studying the effects of prestressing on the freeze-thaw durability of concrete would be almost impossible on a full-scale member or a prototype, a small-scale model was designed for use in this research. The dimensions of this model were chosen to be 3" x 3" x 14". Since the post-tensioning method of prestress was utilized, the beams with this rigging, had to be of a size to accomodate the freeze-thaw cabinet and light enough in weight to be easily handled by hand. Also, since the post-tensioning method of prestress was used, the specimens had to have sufficient length to exclude the triaxial prestressing effect developed on the ends of the members. This effect and its solution are discussed in the section entitled Prestressing of Specimens.

Brass inserts, with a 3/8" hexagonal cross section and 3/8" long, serving as carriers for stainless steel gage points, had to be positioned throughout the beams. Having only a 2 inch and 10 inch Whittemore strain gage, the spacing of these inserts had to be chosen utilizing these dimensions. It was decided that for each beam, the disintegration in the X and Y-directions together would be averaged over 12 inches, and the disintegration in the Z-direction would be averaged over 10 inches. This

was done to mitigate the particle effect and to give a true perspective of the phenomenon within the concrete. The 10 inch center region of each beam was used to locate the brass inserts.

The specimens prepared for compressive strength studies were 3 inch diameter by 6 inch long cylinders.

Dimensions of the beams and locations of the gage points are shown in Figure 4.1.

Dimensions of containers

The dimensions of the containers were 1/4 inches larger than the actual dimensions of the beams, thus leaving an 1/8 inch zone of liquid of constant thickness around each member. The reason for this was to ensure that the rate of temperature change and, hence, the severity of exposure would be the same for all members.

Freezing rate and direction of freezing

The general freezing rate used in this research was approximately 27°F/hr and was constant for all members. However, the freezing rate for the length of the freezer and the length of the beams varied by a small amount. This was attenuated by placing the members in the freezer in alternating order of level of prestress, i.e., 500, 1000, 1500 ..., and averaging the results for each level.

The differences in the direction of freezing was eliminated from the investigation by placing each member in the exact same orientation and position after a strain reading was taken.

Number of Specimens

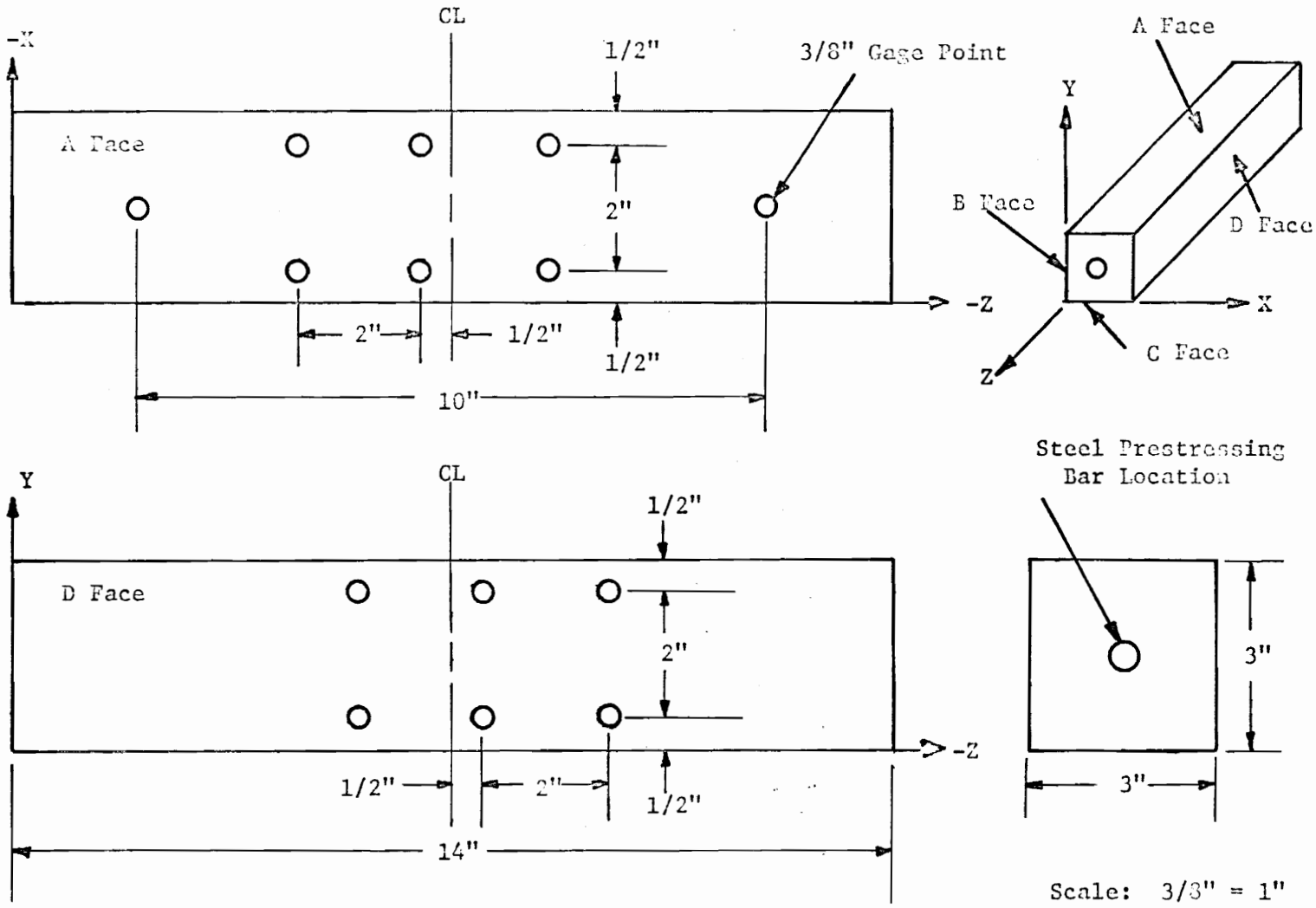

FIGURE 4.1 BEAM DIMENSIONS AND GAGE POINT LOCATIONS

For statistical purposes, 3 beams of each level of prestress were chosen. They were as follows:

1. Three beams prestressed to 500 psi (B1, B2, and B3).
2. Three beams prestressed to 1000 psi (B4, B5, and B6).
3. Three beams prestressed to 1500 psi (B7, B8, and B9).

This provided a total of 30 inches over which the disintegration in the Z-direction would be averaged, and a total of 36 inches over which the disintegration in the X and Y-directions together would be averaged for each level of prestress. As mentioned before, this should give a true value of the strains in the concrete per inch and should eliminate any discrepancies from the particle effect.

A thermocouple was also placed in one beam of each level of stress.

In the actual prestressing procedure, beam B5 was destroyed due to an overload. Thus, only 2 beams of the 1000 psi level of prestress were used throughout the investigation.

Prestressing of Specimens

Choosing the Method

The two types of linear prestressing systems are pre-tensioning and post-tensioning [24]. In the pre-tensioning method, tendons are pulled between two bulkheads anchored against the ends of a prestressing bed. After the concrete hardens, the tendons are loosened and removed from the bulkheads. Then the prestressing force is transferred to the concrete through the bond between the tensioning strand and the concrete. For this system, both the bulkheads and the bed must be designed to resist the prestressing force and its eccentricity if any.

The other type of prestressing, post-tensioning, was selected as the method of prestress in this research because of the following advantages:

1. No prestressing bed and bulkheads had to be designed and made.
2. The transmission or transfer length to develop the required stress through bond between the concrete and steel was to long to accommodate specimens in the freezing and thawing cabinet.
3. Post-tensioning produced a more uniform compressive stress throughout most of the beam.
4. Post-tensioning permitted the removal of the prestressing steel so that all members could be tested in flexure as plain concrete members.
5. For the nine beams made, it was uneconomical to use pre-tensioning.
6. By using pre-tensioning, there was no way to ensure that the proper levels of stress would be developed in the member.

However, using this method produced a triaxial stress on the ends of the member. The next section explains this phenomenon and its solution.

Triaxial Effect

In applying the prestressing force, steel bearing plates at the end boundaries of the concrete members created a complicated triaxial state of stress on the ends of the members. The friction between the steel plate and the concrete face leads to restrained lateral deformations, including forces in the concrete specimens added to the nominal test load [25]. This quasi, multiaxial state of stress is not well defined, and the frictional forces in the contact zone between the steel plate and concrete end-face are unknown.

Payne [13], using a finite element analysis on his model-size prestressed beams, found that the triaxial effect attenuated rapidly from the ends of the beam. The analysis indicated the middle 10 inches of the

beam were relatively free of the end-plate effect and were under a relatively uniform compressive stress. This analysis was made to select controlled stress areas for location of the brass inserts and gage points. Since the exact same model and prestressing procedures were used by the author, the results from Payne's analysis will be used in this research. Therefore, all strain measurements were taken in the middle 10-inch region of the beams.

To permit elongation in the X and Y-directions of the ends of the beams, the frictional forces in the contact zone between the plate and concrete should be reduced as much as possible. Some methods of reducing the end face friction are as follows [25]:

1. Teflon sheets.
2. Lubricated packs of thin aluminum sheets.
3. Brush bearing plates.
4. Deformable piston plates.

Due to the complexity of most of the above devices and the prestressing arrangement used, a teflon sheet was chosen to reduce the end face friction and permit relatively load-free movements in the transverse direction. This sheet was 0.01 inches in thickness and was placed between the steel bearing plates and the concrete face at each end. The ends were also ground smooth and perpendicular to the longitudinal axis of the beam to help reduce friction.

Figures 4.2a and 4.2b show the state of stress at the ends of the beams without and with the teflon sheets.

Method of Prestressing

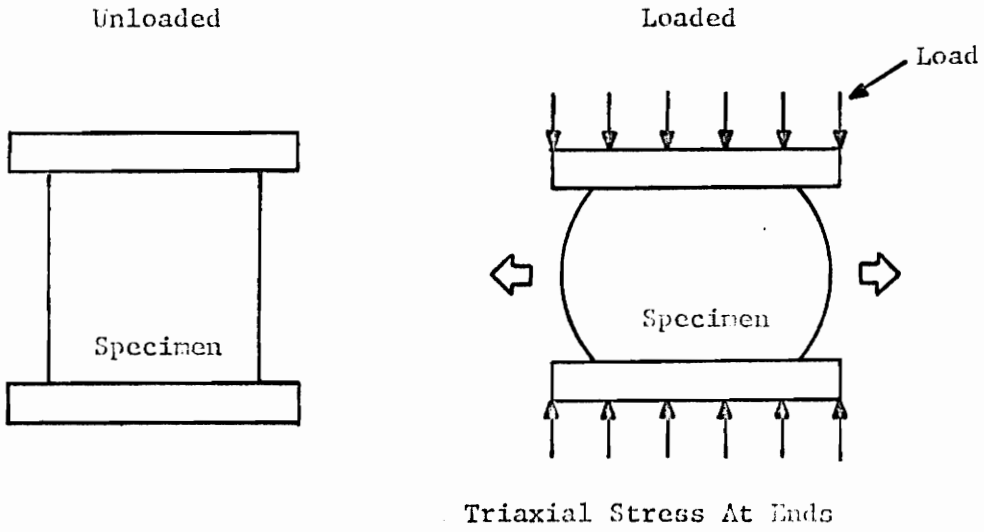

FIGURE 4.2a STATE OF STRESS AT ENDS WITHOUT TEFLON SHEETS

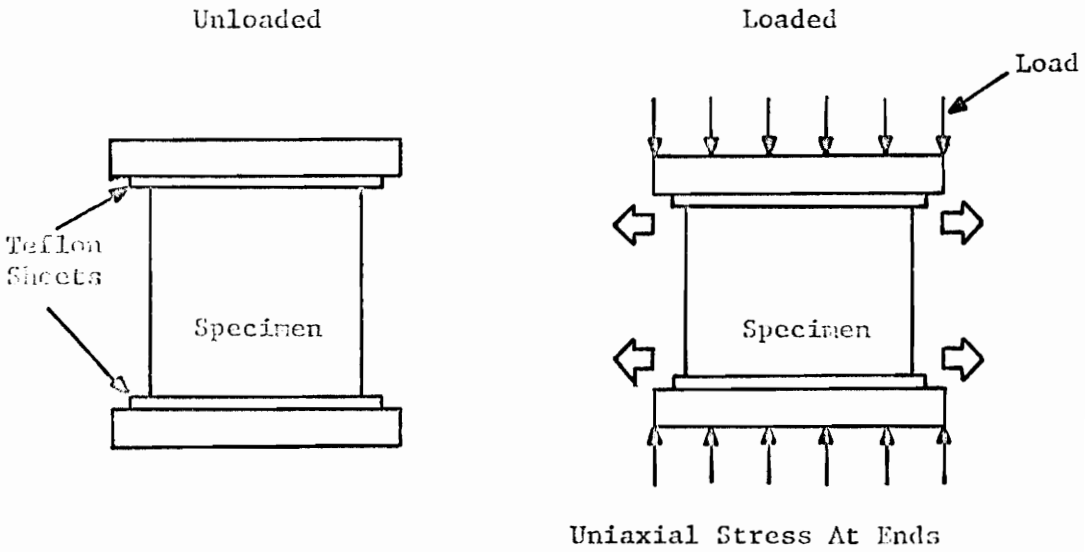

FIGURE 4.2b STATE OF STRESS AT ENDS WITH TEFLON SHEETS

Electrical resistance strain gages were first attached to the prestressing bars at one end. When the members were ready, prestressing was done by a Tinius Olsen testing machine. The beam with the prestressing apparatus was attached, with the aid of couplers, to the machine and the bar tensioned. The bearing plates were tightened and the load from the bar removed. This process continued until the proper strain was read on the strain indicator which indirectly indicates the required level of stress in the member.

Testing Procedures

Laboratory Freeze-Thaw Tests

Accelerated freezing and thawing tests have been conducted by many laboratories for years to evaluate the durability of concrete and aggregates. They have also been conducted to study the effect on durability of various materials, treatments (such as prestressing), curing conditions, etc. It is very hard to predict the actual durability of concrete in the field from laboratory tests because simulating actual load conditions, temperature changes, and weather conditions upon the structure in service is almost impossible. The main purpose of laboratory freezing and thawing tests is to detect differences in resistance to freezing and thawing of various concretes which may be related to the field performance of similar concretes.

Scholer, Lang, and Withey were forerunners in developing freeze-thaw tests. Later the Portland Cement Association, the Bureau of Public Roads, and others developed methods concerned with this area. Equipment and procedures are as numerous as the organizations and laboratories

making the tests.

ASTM standard methods

For many years, researchers have tried to determine a single standard freeze-thaw test which will yield information regarding the evaluation of the durability of concrete and aggregates. The variables associated with different laboratory procedures are as follows [8]:

1. A medium in which the specimens were frozen and thawed.
2. Freezing rate of the cycle.
3. Length and number of cycles the specimen was subjected to.
4. Amount of air-entrainment used.
5. The shape and size of specimens.
6. Methods of fabricating and curing specimens.
7. Method of measuring deterioration.

In 1952 and 1953, four standardized tentative methods of test were adopted by ASTM. These methods were:

1. ASTM Designation: C290--Rapid Freezing and Thawing in Water.
2. ASTM Designation: C291--Rapid Freezing in Air and Thawing in Water.
3. ASTM Designation: C292--Slow Freezing and Thawing in Water or Brine.
4. ASTM Designation: C310--Slow Freezing in Air and Thawing in Water.

Currently, the slow freezing tests, C292 and C310, are not in the ASTM standards. The rapid freezing tests, C290 and C291, have been replaced and combined into ASTM Designation: C666.

Although the standard ASTM method of testing is not applicable to this investigation concerning the behavior of prestressed concrete, many

methods and suggested operating procedures are similar to the ones used in this investigation, for example [15]:

> The freezing and thawing apparatus shall consist of a suitable chamber or chambers in which the specimens may be subjected to the specified freezing and thawing cycles, together with the necessary refrigerating and heating equipment and controls to produce continuously and automatically, reproducible cycles within the specified temperature requirements. Each specimen shall be completely surrounded by approximately 1/8 inches of water at all times while it is being subjected to freezing and thawing cycles. The temperature of the heat-exchanging medium shall be uniform within 6°F throughout the specimen cabinet when measured at any given time. The temperature-measuring equipment shall be capable of measuring the temperature at various points within the specimens to within 2°F.
>
> The nominal freezing and thawing cycle shall consist of alternately lowering the temperature of the specimens from 40°F to 0°F and raising it from 0°F to 40°F in not less than 2 nor more than 4 hours. The difference between the temperature at the center of a specimen and the temperature at its surface shall at no time exceed 50°F.
>
> For this test the specimens shall be stored in saturated limewater from the time of their removal from the molds until the time freezing and thawing tests are started. All specimens to be compared with each other initially shall be of the same nominal dimensions.
>
> Protect the specimens against loss of moisture between the time of removal from curing and the start of the freezing and thawing cycles.

It is essential that care be taken to maintain the same conditions throughout the duration of test so that results obtained can give a true indication of differences in behavior of the concrete.

Powers' slow-freeze method

Powers [26] proposed a freezing and thawing test method to evaluate the effect of frost action in concrete. He believed that the ASTM rapid freeze-thaw tests, C290 and C291, would overestimate the susceptibility of concrete to frost damage. This would be due to the high freezing rates

which would produce excessive hydraulic pressures and to the absence of an extended period of low temperature which would cause frost destruction from the growth of ice lenses to be underestimated.

In Power's method, the specimens would be cooled from room temperature to 0^{o}F at approximately 5^{o}F per hour. This temperature would be held overnight to permit growth of ice bodies, and then the specimens would be thawed in water at room temperature for two weeks between freezing cycles. Expansion would be measured continuously with a suitable strain-measuring device. Entrained air would be used to inhibit destruction of the matrix.

VPI&SU method (not the One-Cycle Slow-Freeze method)

Due to the uniqueness of this research, many techniques and operating procedures were developed specially for this investigation. Whenever applicable, the procedures in ASTM Designation: C666 were followed as closely as possible.

The freezing apparatus which is regulated by an upper and lower temperature switch consists of a freezing chamber with heaters. The upper and lower temperature limits are controlled by a thermometer located in the center of a control beam. The temperature of the concrete members was monitored throughout each freeze-thaw cycle with thermocouples and a continuous recorder.

To have all members free from other external forces, water-saturated kerosene was used as the temperature transfer medium. Payne [13] found in his research that if the changes in length of the specimens were to be measured and used as a means of determining concrete disintegration, then

these directions must be free to elongate. This means that the concrete must be free from all external forces except the prestressing force. He also found that freezing in water produced very high strain readings because of the resulting pressure produced by ice between the copper container and the concrete and by the space between the prestressing bar and the concrete.

The number of cycles which would cause excessive deterioration was unknown at the beginning. It was thought that between 20 and 50 cycles would produce sufficient damage. The range of cycle used consisted of alternately lowering the temperature of the specimens from 40°F to 0°F and then raising it from 0°F to 40°F in about 2 to 3 hours.

A Whittemore strain gage was used for measuring changes in length of the members. This gage reads to 0.0001 inches; and when used in conjunction with properly installed stainless-steel gage points, is accurate to $\pm$ 0.00005 inches or better. Stainless-steel gage points were required to maintain the necessary degree of accuracy in the measurement of change in length.

A complete description of the freeze-thaw testing apparatus and procedures are given in Chapters V and VIII, respectively.

Methods of Measuring Freeze-Thaw Damage

Many methods and test procedures have been developed for evaluating and determining the changes in concrete properties caused by freezing and thawing action in concrete. Some test methods are of more value than others, and some cannot be applied to this specific type of research.

Weight change

The use of weight change by itself as a measure of freeze-thaw deterioration is somewhat questionable because of the general lack of correlation between weight change and concrete durability [8]. Concrete specimens may be seriously damaged without any indication of weight loss. Conversely, damage may be so severe that scaling and pop-outs cause a reduction in specimen weight. There is also the possibility of absorption of the temperature transfer medium which may cause an increase in specimen weight.

In this research, weight readings were taken even if useless data was produced.

Flexure or compressive strength change

The deterioration of concrete due to freezing and thawing is caused by the formation of cracks in the aggregate and matrix. Since cracks reduce the strength of the material, it is possible to evaluate the frost damage by making flexure or compressive strength tests after a certain number of freeze-thaw cycles. These tests are performed on the test specimens which had been frozen and then compared to the results obtained from unfrozen companion specimens maintained under the same curing conditions. However, this test always destroys the test specimen.

In this investigation, three beams corresponding to the same concrete mixture design and unfrozen, were tested in flexure exactly as the frozen specimens.

For a complete description of the flexure testing apparatus and procedures, see Chapters V and VII, respectively.

Change in ultrasonic pulse velocity

An important and useful nondestructive test for measuring and detect-

ing cracks and deterioration in concrete is the ultrasonic pulse velocity method. This is a dynamic method which has gained considerable popularity. In this technique, pulses of ultrasonic sound are developed in the material; and the velocity of their transmission through it are measured. This technique has the unique advantage of being independent of the size or shape of the body under test. Measurements can be made with equal ease in mass concrete, slabs, or laboratory specimens.

Malhotra [27], describes the basic principle of operation as follows: The ultrasonic pulse velocity method consists of measuring the time of travel of an ultrasonic wave (longitudinal vibrations) through the concrete to be tested. An electrical impulse from a central unit is transmitted to a sending transducer (electro-acoustical), held in contact with one surface of the concrete member under test, where it excites a block of crystals. The transducer, through the block, emits an ultrasonic pulse which travels a known path length, L, through the concrete under test to the receiving transducer (electro-acoustical). Here the ultrasonic pulse is converted back into an electric impulse which is then displayed on the face of a cathode-ray oscilloscope. The time of travel, T, between the initial onset and the reception of the pulse is measured electronically. The path length between transducers, divided by the time of travel, gives the average velocity of wave propagation or the pulse velocity, V. This can be given by the formula, $V = L/T$.

Difficulties with the pulse velocity method involve the accurate measurement of the short time intervals required for the usually small test models, the high signal attenuation with deteriorated specimens, and the location of proper contact points.

The method of test is defined under ASTM Designation: C597 and has not been as widely used in the laboratory as it has in the field.

Elastic properties

It is known that the relative dynamic modulus of elasticity, E_D, measured from the fundamental transverse frequency of the specimens, is a nondestructive test of determining deterioration of concrete subjected to freezing and thawing. There is a direct relation between the fundamental frequency and E_D: as the fundamental frequency decreases, E_D decreases; and as E_D decreases, there is disintegration of the concrete due to microcracking. This change of the dynamic modulus of elasticity indicates a loss in the flexural strength of the concrete.

Another criterion, the durability factor, is also used to measure deterioration by determining the relative dynamic modulus of elasticity from the fundamental transverse frequency.

As described in ASTM Designation: C215, the method basically consists of measuring the natural frequency of the specimen. This is done by inducing controlled frequency vibrations in the specimen with a driving unit at various frequencies produced by a variable frequency oscillator. There are a crystal pick-up and a voltmeter for measuring the magnitude of the voltage output produced by the current flowing from the pick-up. When the induced vibration is the same as the natural frequency of the specimen, resonance occurs and is indicated by a sudden increase in the voltmeter reading. Thus, the maximum voltage occurs at the fundamental frequency of vibration of the specimen, and this fundamental frequency is read directly from the oscillator dial.

Payne [13], after a two-month theoretical and experimental investigation of the fundamental frequency method of measuring concrete deterioration, realized that this method was not very sensitive to directional disintegration which is prevalent in this investigation. Since the beams were post-tensioned, the steel bearing plates on the ends of the beam created an extra mass which made determination of the fundamental frequency difficult. Therefore, this method of measuring concrete deterioration was not applicable for this investigation.

Length change

Since the concrete is changing in volume or in dimensions during freezing and thawing, a measurement of this change will be helpful in determining the disintegration and durability of concrete. This is accomplished by measuring the distance between two gage points embedded in the concrete beam and located at different regions. First, an initial measurement was made before any freezing and thawing. Then after different freeze-thaw intervals, measurements were taken and changes in length were determined. These changes in length can be designated as ΔX, ΔY, and ΔZ which are defined as the directional disintegration of the concrete in the X, Y, and Z-directions, respectively. This directional disintegration is also a microscopic and macroscopic measurement of permanent deformation expressed in inches per inch.

The permanent change in length of the X, Y, and Z-directions was measured for each beam and plotted against the number of freeze-thaw cycles. These curves represented the directional disintegration due to the various levels of compressive stress fields which can be compared to

one another. By taking the slopes of these curves, the rate of change of disintegration can be found for each level of prestress.

This method is one of the most reliable for indicating deterioration in concrete. Thus, it was the basic method used in this research.

Non-Linear Transformation of Restrained Directions

The concrete was free to expand or elongate in all directions during testing, except in the direction of the applied prestressing force. The homologus directions of the three different levels of prestress were compared by permanent changes in length. Thus, to have a similar basis for comparison, it was necessary to convert the change in length of the prestressed direction of each level of stress into an equivalent change in length. This was accomplished by a non-linear transformation using Reagel's graph [7]. This graph correlates the loss in flexural strength of a beam to the equivalent permanent change in length due to freezing and thawing. Payne [13], verified Reagel's graph by using beams that were free to elongate in all directions during the freeze-thaw cycles. This graph is shown in Figure 4.3. The author assumes this graph correct and applicable to the purpose mentioned above.

A sensitive flexure testing apparatus to obtain the flexural strength of the beams was required for the above transformation. The author used the same specially made device as Payne in his work. This apparatus is shown in Figure 4.4. As previously mentioned, this test was an excellent measure of frost damage in the longitudinal direction of the beam. The flexure testing necessitated the removal of the prestressing steel. Thus, the advantages of post-tensioning are apparent.

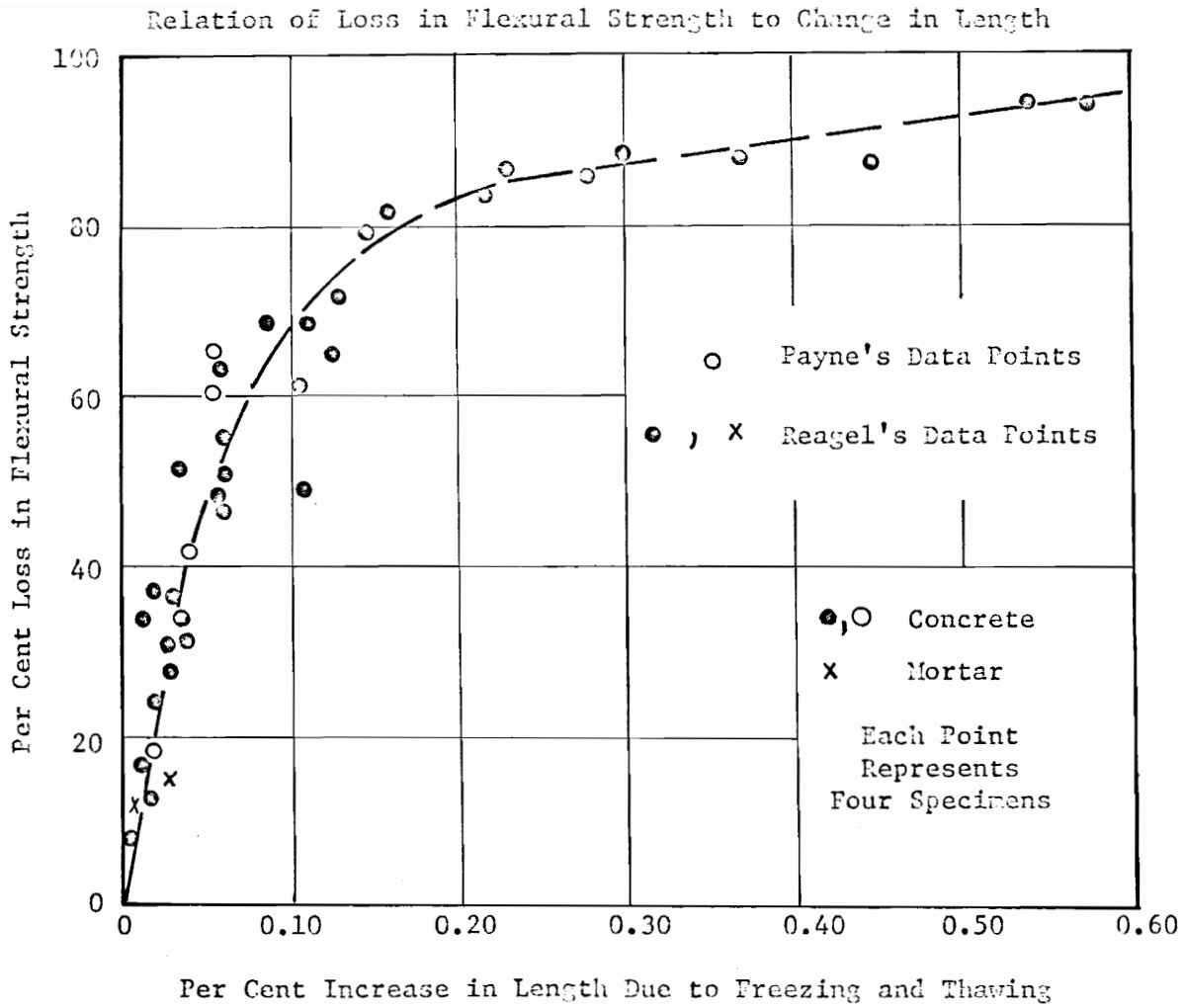

FIGURE 4.3 REAGEL'S GRAPH (FROM REAGEL AND PAYNE)

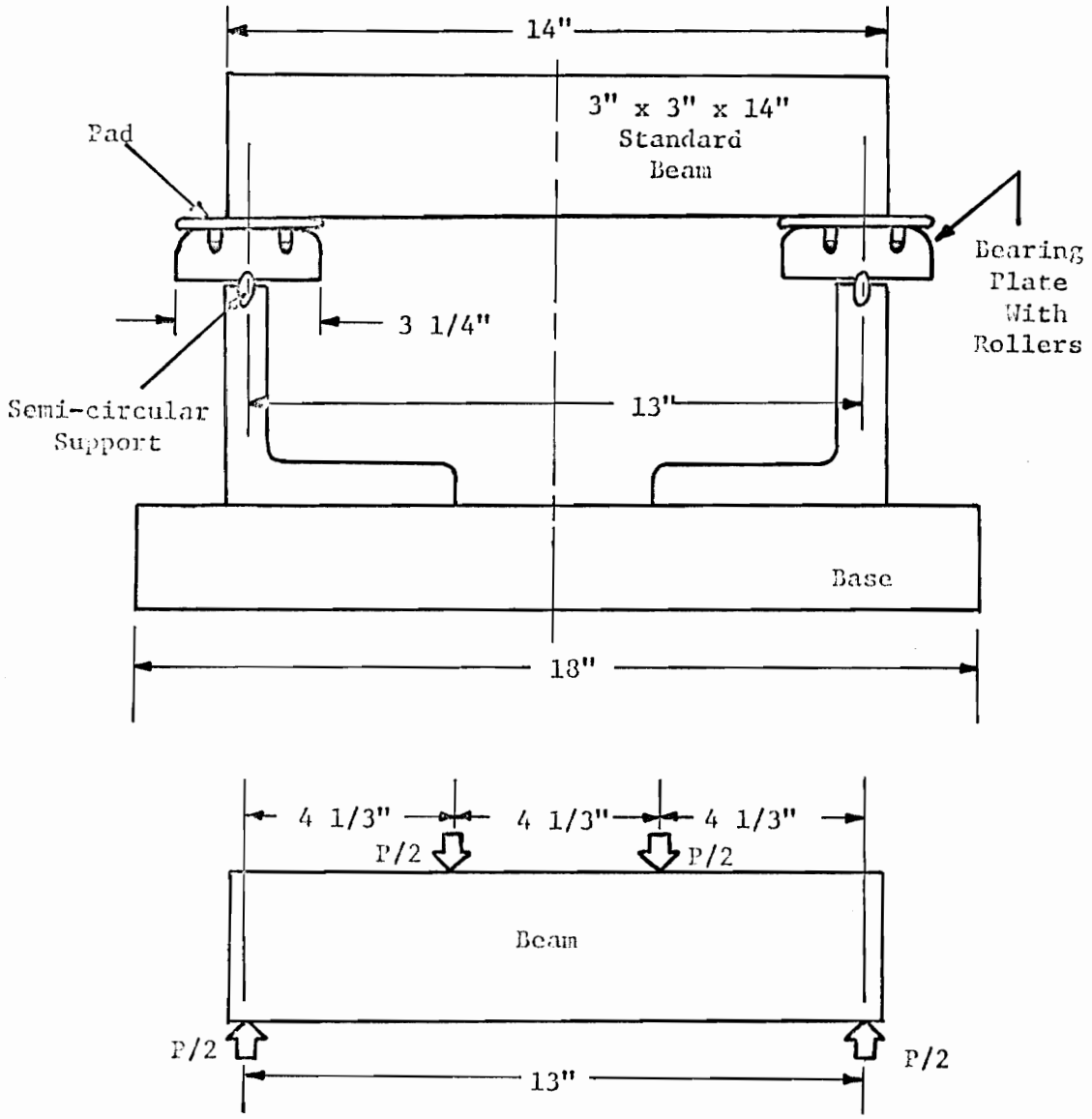

Load Distribution During Testing

FIGURE 4.4 FLEXURE TESTING APPARATUS

CHAPTER V

EXPERIMENTAL EQUIPMENT

This chapter contains information on the pertinent equipment used in the experimental investigation. The design features and the operation of this equipment are described individually. The experimental equipment includes the freezing and thawing apparatus, the prestressing system, the flexure testing apparatus, the Whittemore strain gages, and the supporting equipment. The supporting equipment consists of the vacuum tank and vacuum pump, the mercury manometer, the concrete mixer, the loading machine, the steel forms, the plexiglass spacers, the brass inserts and stainless steel gage points, the copper containers, the thermocouples and continuous recorder, and the SR-4 strain gages and accessories.

Freezing and Thawing Apparatus

The freezing and thawing apparatus used in this research was one used by other researchers at VPI&SU. It is an automatic type of machine designed and developed by the Engineering Experiment Station of Utah State University and manufactured by the Logan Refrigeration Company of Logan, Utah.

The apparatus consists mainly of a stainless steel cabinet, a cooling or evaporating plate, a one-half horsepower compressor, a condenser, a fan, a micro-valve adjustment, and electric resistance strip heaters. The cabinet is 6'-6" long, 2'-2" wide, and 7" deep with 3" of insulation on all sides. The cooling plate is 6' long, 2' wide, and is supported within the cabinet. Resting on the cooling plate are copper containers which hold the concrete specimens and the temperature transferring liquid

(water-saturated kerosene). Electric resistance heaters are placed in direct contact along the sides of the copper containers.

During the freezing phase of operation, the compressor pumps liquid freon into the cooling plate where it absorbs heat from inside the cabinet and from the concrete specimens by conduction and convection through the liquid transfer medium. The freon then vaporizes so that the cooling plate and, consequently, the concrete specimens are cooled. During the thawing phase, heat from the electric resistance heaters is transferred through the water-saturated kerosene by conduction and convection. The upper and lower temperature limits of the cycle are controlled by means of a control specimen in the center of the cabinet. A thermostat located in the center of this control specimen is connected to an upper-and-lower limit temperature switch located outside the cabinet. The switch controls the starting of the compressor at a preset temperature and the activation of the electric heaters at a preset temperature. When this last temperature is reached, the compressor will start and the cycle will begin again. The freezing rate of the cycle can be controlled by the micro-valve adjustment which regulates the amount of freon going into the cooling plate. Also, a continuous record of the temperature at the center of the control specimen is kept by a recording thermometer located on the side of the cabinet. This operation exposed the specimens to 30 cycles of freezing and thawing, and it was designed to meet the American Society for Testing and Materials requirements prescribed by ASTM Designation: C666 (formerly designated as C290 and discontinued in 1971). The freezing and thawing cabinet containing the beam specimens, control beam, and copper containers are shown in Plate 5.1.

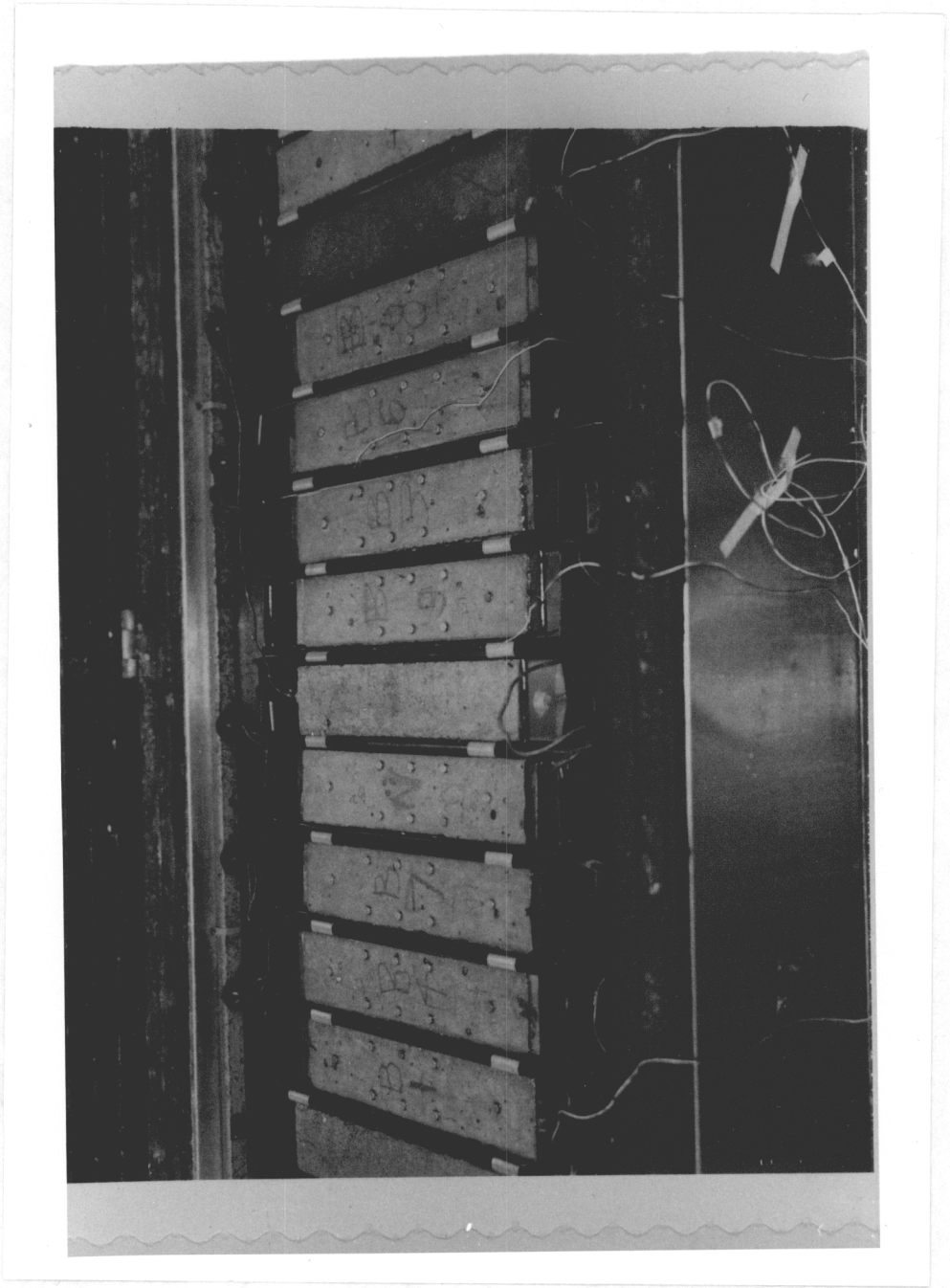

PLATE 5.1 THE FREEZE-THAW CABINET CONTAINING THE PRESTRESSED BEAMS

Prestressing System

The post-tensioning prestressing system used in this research for each beam consisted of a steel bar, 2 steel end plates, 2 nuts, and 2 teflon sheets. The high strength prestressing steel bars were 1/2" in diameter and were manufactured by the Stressteel Corporation of Wilkes-Barre, Pennsylvania. The engineering properties of these steel bars are as follows: a yield strength of 135,000 psi, ultimate tensile strength of 170,000 psi, and a modulus of elasticity of 31,000,000 psi. The bars were 18" in length with special threads 2 1/2" at each end. The two steel end plates were 2 7/8" x 2 7/8" x 1/2" with a 9/16" diameter hole drilled in the center. On one surface of one plate for each beam system there was milled across the center, a 1/16" deep by 1/8" wide groove to run the SR-4 strain gage lead wires. Corresponding hexagonal nuts, also made by the Stressteel Corporation, of 1/2" diameter, were used at each end of the post-tensioning system. During the prestressing operation, in order to avoid damage to the threads at the ends of the bars, couplers were used.

The teflon sheets used to prevent friction and the triaxial prestressing effect between the prestressing steel plates and the concrete end surfaces were made by the Cadillac Plastic and Chemical Company, Charlotte, North Carolina. The sheet was 0.01 inches thick and was coated with teflon on one side only. The engineering properties of a teflon sheet are listed as follows: a compressive strength of 1700 psi, a tensile strength of 2500 psi, a modulus of elasticity of 58,000 psi, and a thermal coefficient of 0.0001 inches per inch per degree Centigrade ("/"/^{o}C).

The individual prestressing parts are shown in Plate 5.2, parts A, B, C, and D.

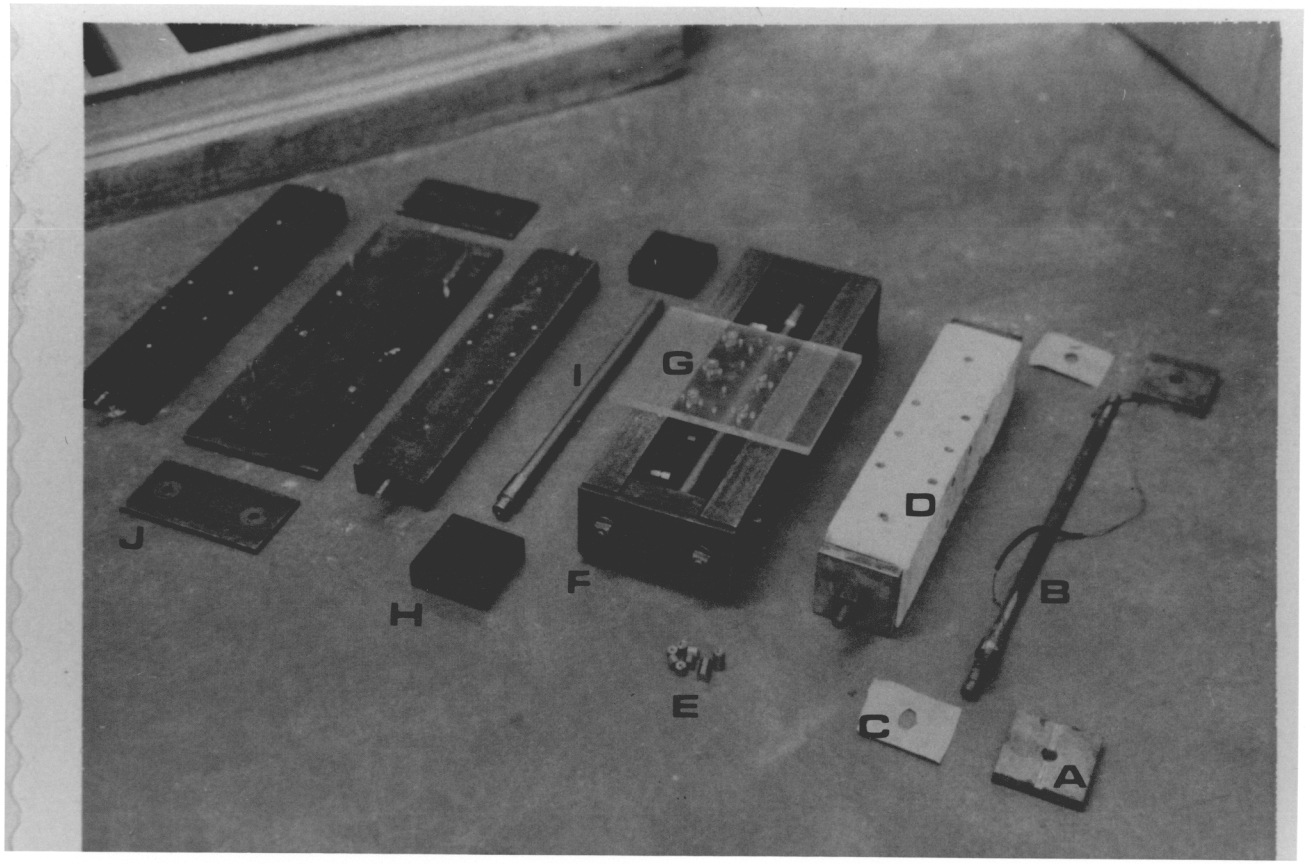

PLATE 5.2 VARIOUS EXPERIMENTAL EQUIPMENT (A. Steel End Plate, B. Steel Prestressing Bar, C. Teflon Sheet, D. Beam After Prestressing, E. Brass Inserts, F. Assembled Steel Form, G. Plexiglass Spacer, H. Wooden Block, I. Bar to Form Center Duct, J. Unassembled Steel Form)

Flexure Testing Apparatus

The flexure testing apparatus used to test the flexural strength of the beams was made at a machine shop out of steel. The device is similar to that used in ASTM Designation: C78. The dimensions of the apparatus are shown in Figure 4.4, and it can be seen during the flexure test in Plate 5.3.

Whittemore Strain Gages

Two Whittemore strain gages were used during the experiment: a 2 inch gage and a 10 inch gage. Both were made by Baldwin Testing Equipment and contained a spring balanced dial indicator made by the Standard Gage Co., Inc., Poughkeepsie, N. Y., which reads in 0.0001 inch divisions.

The Whittemore strain gage is a direct-reading mechanical extensometer. It uses no magnification of motion but depends directly upon the sensitivity of a dial indicator. In the instrument, two bars are connected by flexible plates. A dial indicator is attached to one bar, and the indicator spindle bears against the second bar. One gage point is attached to each bar. The relative motion of the bars is indicated by the dial reading.

For this research, these gages measured the directional disintegration (change in length) of the concrete beams in the X, Y, and Z-directions. The 2 inch gage measured the X and Y-directions, and the 10 inch gage measured the Z-direction. A general sketch is shown in Figure 5.1 [28].

Supporting Equipment

Vacuum Tank and Vacuum Pump

The vacuum tank used in this research had an inside diameter of 13

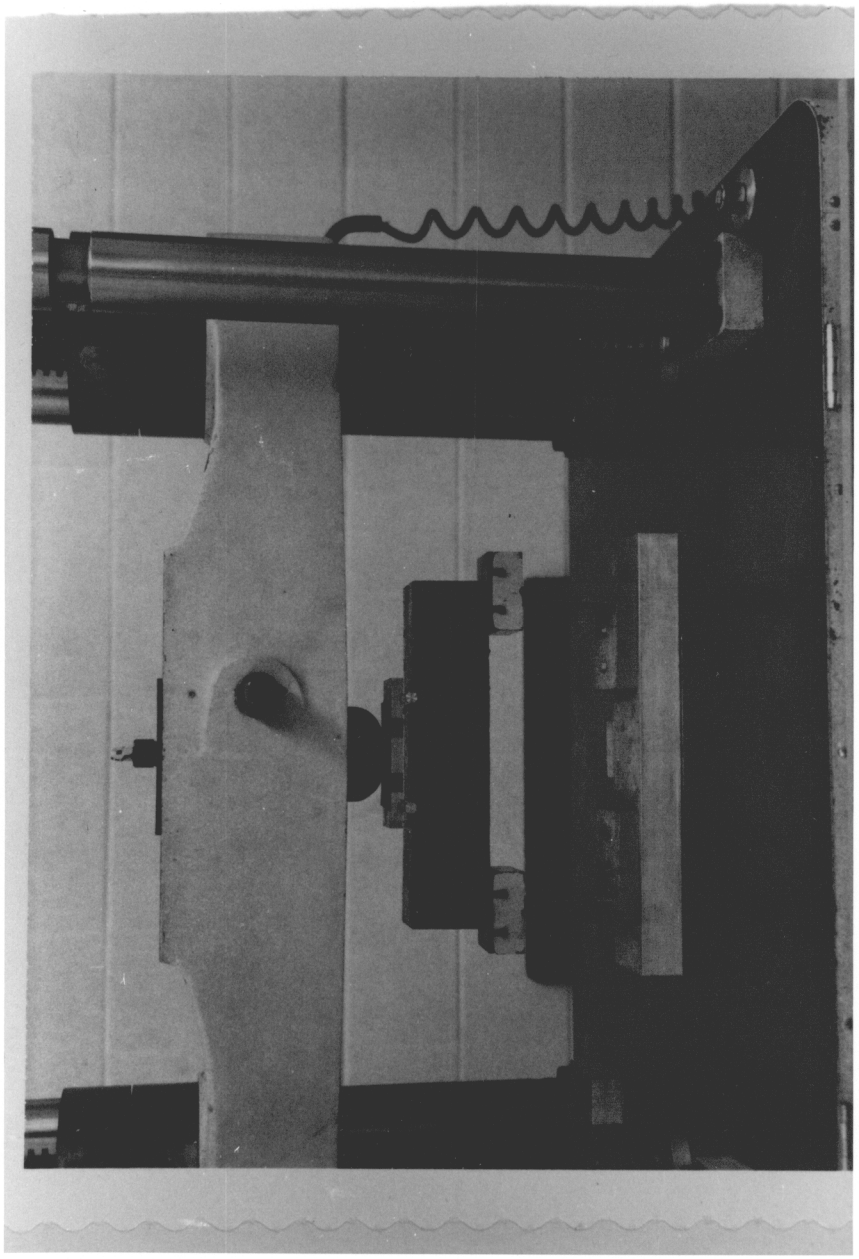

PLATE 5.3 ACTUAL FLEXURE TEST

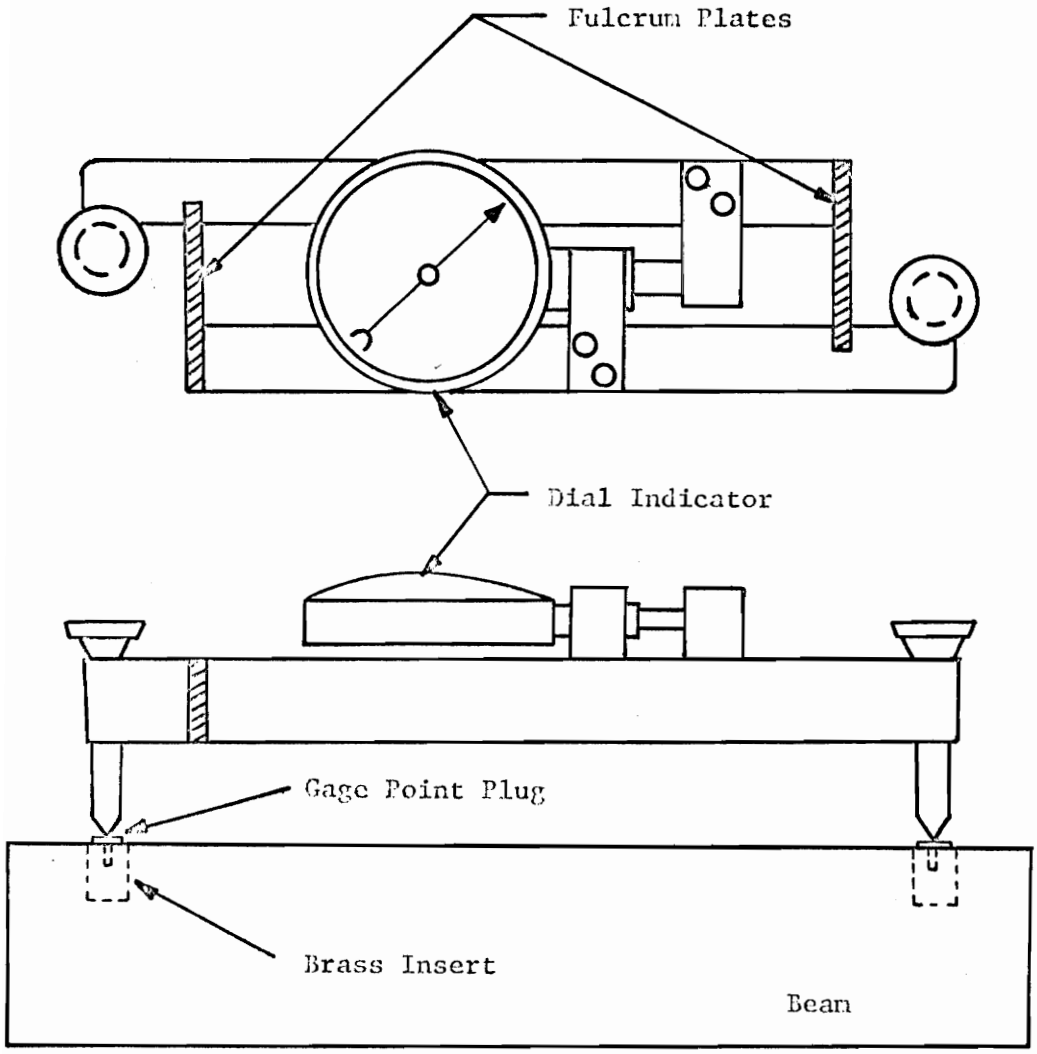

FIGURE 5.1 TYPICAL WHITTEMORE STRAIN GAGE

inches and a height of 25 inches and was made from 1/2 inch steel plate. The removable air-tight lid had 6 screw-type clamps and 3 external valves. These valves connected rubber tubes to the water container, the mercury manometer, and the vacuum pump.

The vacuum pump used was driven by a General Electric motor and was a "Duo-Seal" vacuum pump, model 1400, manufactured by the Welch Scientific Company, Skokie, Illinois. These two devices are shown in Plate 5.4, parts A and D.

Mercury Manometer

The mercury manometer used to measure the vacuum inside the vacuum tank was an open-tube, "U" type, model 10AA25WM, with a 36 inch range. It was manufactured by the Meriam Instrument Company, Cleveland, Ohio. This is also shown in Plate 5.4, part C.

Concrete Mixer

The concrete mixer used in this research was a 1 1/2 cubic foot, tub-type, Lancaster counter current batch mixer, type 30 DH. It was manufactured by Posey Iron Works, Inc., Lancaster, Pennsylvania. The mixing drum of this mixer rotates at 11 rpm in a clockwise direction while two blades, one near the rim of the drum and the other near the center, rotate at 40 rpm in a counterclockwise direction. This type of arrangement produces a well-mixed concrete.

Loading Machine

A screw driven testing machine manufactured by Tinius Olsen Testing Machine Company, Willow Grove, Pennsylvania, was used to prestress the

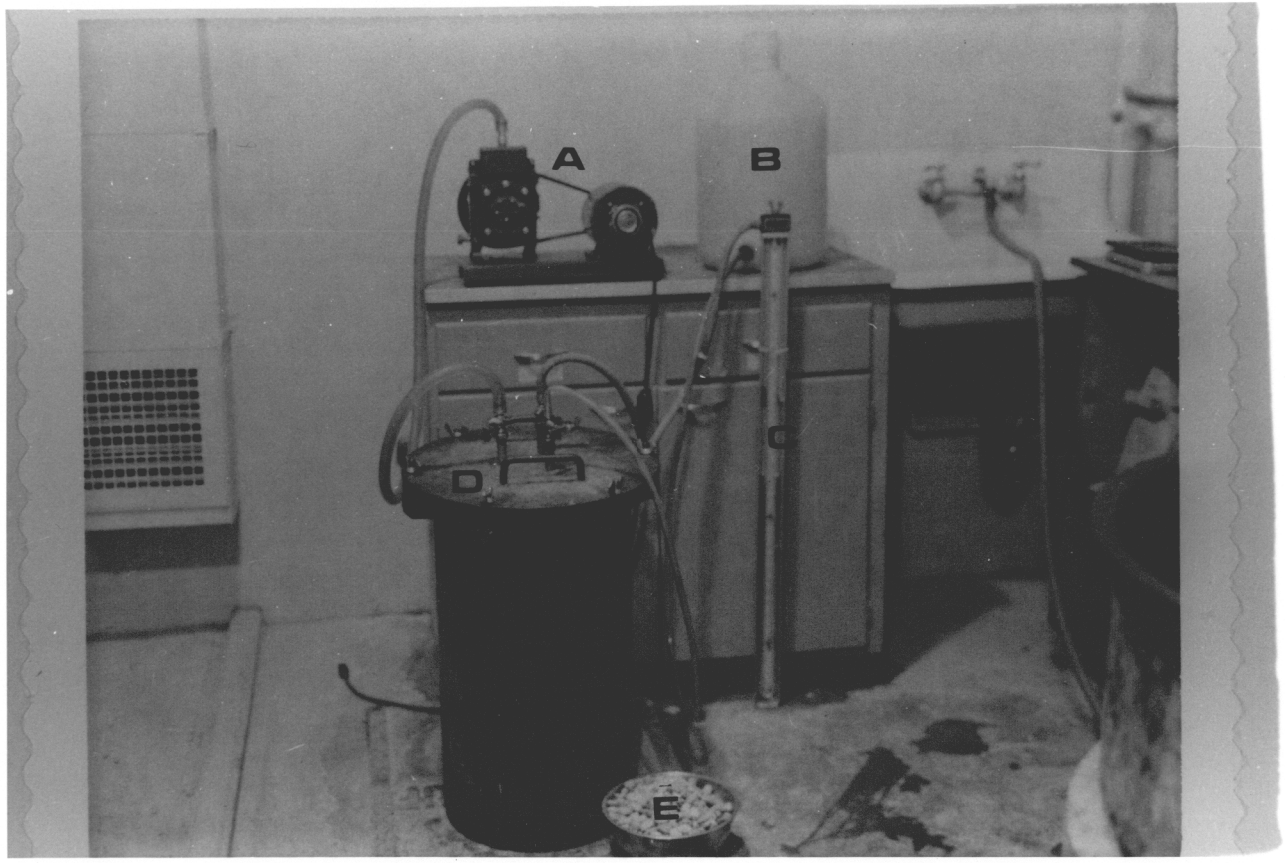

PLATE 5.4 VACUUM SATURATION EQUIPMENT (A. Vacuum Pump, B. Water Container, C. Mercury Manometer, D. Vacuum Tank, E. Coarse Aggregate)

the beams, to load the beams during the flexure test, and to load the test cylinders during the compression test. The machine had a maximum range of 120,000 pounds and is shown in Plates 5.3 and 7.1.

Steel Forms

Reusable, detachable steel forms were made by a machine shop. They had been used by previous researchers and were suitable for this research as well. They were made with inside dimensions to produce concrete beams according to Figure 4.1. Also, in order to provide a duct of sufficient diameter to accommodate the 1/2 inch diameter prestressing bar, a 5/8 inch diameter rod of steel was used. One end was slightly larger than the other to provide room inside the concrete for the strain gages attached to the prestressing rod. This bar is shown in Plate 5.2, part I. The 5/8 inch rod was positioned lengthwise in the center of the steel forms by 2 wooden blocks with holes drilled in the centers. These blocks were 3" x 3" x 1". They are shown in Plate 5.2, part H. The steel forms can be seen assembled and disassembled in Plate 5.2, parts F and J.

Plexiglass Spacers

The plexiglass spacers used were 8" x 6" x 3/8". They were used to space the brass inserts at proper intervals along one face of the concrete beam. This device is shown in Plate 5.2, part G.

Brass Inserts and Stainless Steel Gage Points

Brass inserts, serving as carriers for stainless steel gage points, were 7/8 inches long and were hexagonal shaped.

The stainless steel gage points were made to screw into the brass

inserts. They had a 3/8 inch hexagonal head and a small hole drilled in the center to hold the points of the Whittemore strain gage.

Soiltest, Inc., of Evanston, Illinois, furnished both of these items. The brass inserts are shown in Plate 5.2, part E.

Copper Containers

The copper containers, used previously by other researchers, were manufactured by the H. B. Smith Company, Christiansburg, Virginia, out of 16 ounce weight copper. They were used as freeze-thaw containers for the concrete beams and were 1/4 inches larger than the actual dimensions of the beams, thus leaving a 1/8 inch layer of water-saturated kerosene on all four sides and top and bottom of the specimens. The beams rested on wire spacers which left the bottom space. These copper containers are shown in Plate 5.1.

Thermocouples and Recorder

Iron-constantan thermocouples were placed in the center of the beams to monitor the internal temperature. They were connected to the continuous recorder which kept a record throughout the experiment.

The continuous recorder was a Bristol dynamaster recorder manufactured by the Bristol Company, Waterbury, Connecticut, model 6PG 560-21, with a temperature range from $0^{o}C$ to $150^{o}C$.

SR-4 Strain Gages and Accessories

All of the SR-4 strain gages and accessories were supplied by the Baldwin-Lima-Hamilton (BLH) Electronics Corporation of Waltham, Massachusetts. The strain gages were the electrical-resistance type and were

BLH type FAE-25-1256-ET. The adhesive cement used to attach the strain gages to the prestressing bars and to waterproof all strain gages was BLH EPY-150 and BLH EPY-600. All lead wires used were BLH type STC-26V-1R. A BLH switching and balancing unit, model 225, and a BLH strain indicator, model 120, were used during the prestressing operation. These last two pieces of equipment are shown in Plate 7.1, parts A and B.

CHAPTER VI

EXPERIMENTAL MATERIALS

This chapter contains information regarding the experimental materials used in this investigation. They include the following: the concrete mixture materials consisting of coarse aggregate, fine aggregate, and portland cement; the concrete mixture; and the supporting materials which are lime, kerosene, motor oil, and petroleum jelly.

Concrete Mixture Materials

Coarse Aggregate

The coarse aggregate used in the concrete made for this research was a heavy media float material of glacial origin from Michigan. It was obtained from the Whittaker and Gooding Co., Ypsilanti, Michigan. The particles were subangular to subrounded and had a smooth outer surface or one which was rough and irregular. The geological types of aggregate in this coarse aggregate mixture include the following: sandstone, quartzite, chert, claystone, limestone, granite, shale, dolomite, miscellaneous igneous, and conglomerate. Table 6.1 lists the important physical and mechanical properties of these aggregates. The values in the table were determined from averaging the different values obtained from various sources. Since the values for each property will vary for each specific rock type and conditions of testing, these values are just an estimate of the actual values for the rock types.

This poor performing aggregate, as previously described, was used as a research technique to ensure that the deep-seated type of frost damage would be generated. The material was separated on a 1/2 inch sieve into

TABLE 6.1a PHYSICAL AND MECHANICAL PROPERTIES OF AGGREGATES USED

Family	Class	Percent*	Young's Modulus ($\times 10^6$ psi)	Poisson's Ratio	Compressive Strength (psi)
Granite	Igneous	1	6.5	0.23	24295
Claystone	Sedimentary	2	5.5	0.26	11200
Dolomite	Sedimentary	2	8.0	0.24	25832
Limestone	Sedimentary	4	4.4	0.24	18577
Quartzite	Metamorphic	4	7.0	0.14	34082
Conglomerate	Sedimentary	5	--	--	24000
Sandstone	Sedimentary	56	4.3	0.17	13354
Chert	Sedimentary	16	--	--	--
Shale	Sedimentary	9	2.2	0.10	6704
Miscellaneous	Igneous	1	--	--	--

*Percent by weight of the geological types of coarse aggregates. Taken from Payne and assumed to represent an average estimate of quantities used in the author's concrete mixture.

The symbol -- designates that this value could not be found.

TABLE 6.1b CONTINUATION OF PHYSICAL AND MECHANICAL PROPERTIES OF AGGREGATES USED

Family	Tensile Strength (psi)	Porosity %	Absorption %	Coefficient Of Permeability (ft/sec)	Thermal Coefficient ($\times 10^{-6}$ in/°F**)
Granite	2275	1.06	0.37	5.0×10^{-12}	4.4
Claystone	--	--	--	--	--
Dolomite	2844	3.0	1.10	3.1×10^{-10}	4.3
Limestone	2133	13.2	0.78	1.3×10^{-6}	3.5
Quartzite	2844	0.35	0.24	3.8×10^{-12}	6.4
Conglomerate	--	--	1.20	--	--
Sandstone	2062	10.2	2.96	2.3×10^{-7}	5.4
Chert	--	4.1	1.65	--	6.2
Shale	1196	20.0	--	--	--
Miscellaneous	--	--	--	--	--

**Multiply by 1.8 to obtain 10^{-6} in. per degree Centigrade.

The symbol -- designates that this value could not be found.

two different sizes: 1/4" to 1/2" and 1/2" to 3/4". Then they were recombined by weight on a 50 percent to 50 percent basis.

The physical properties of the coarse aggregates as a whole were determined according to ASTM Designations: C127 and C29. Listed in Table 6.2 are the physical properties used in designing the concrete mixture for the beams used in the experiment. The values obtained are for the material in a vacuum-saturated condition.

Fine Aggregate

The fine aggregate used in this research was a "Petersburg" quartz sand from Richmond, Virginia. The physical properties of the fine aggregate were determined according to ASTM Designations: C136 and C128. Listed in Table 6.3 are the sieve analysis and the physical properties used in designing the concrete mixture.

It should be noted here that an average value for the modulus of elasticity of a pure quartz sand is approximately 11 x 10^6 psi.

Portland Cement

The portland cement used in this research was Incor, air-entraining, high early strength, Type IIIA cement. It was manufactured by the Lone Star Cement Corporation of Roanoke, Virginia.

It is also interesting to note that for a cement paste, an average value for the modulus of elasticity is approximately 3.51 x 10^6 psi [29]. Also, the coefficient of thermal expansion for a mature, hardened cement paste is normally in the range of 6 to 11 x 10^{-6} in/^{o}F [22], whether the paste is in either a dry or saturated condition.

TABLE 6.2 PHYSICAL PROPERTIES OF THE COMBINED COARSE AGGREGATE

Property	Value
Specific Gravity (Bulk Dry)	2.21
Specific Gravity (B.S.S.D.)	2.40
Specific Gravity (Apparent)	2.74
Percent Absorption	8.81 %
Unit Weight (Dry Rodded)	101 pcf

TABLE 6.3 PHYSICAL PROPERTIES OF THE FINE AGGREGATE

Sieve Analysis:

Sieve Number	Accumulative % Retained
4	1.2
8	15.0
16	36.5
30	71.5
50	92.2
100	98.0

Properties:

Property	Value
Fineness Modulus	3.14
Specific Gravity (Bulk Dry)	2.49
Specific Gravity (B.S.S.D.)	2.53
Specific Gravity (Apparent)	2.57
Percent Absorption	1.21 %

Concrete Mixture

The portland cement concrete mixture used in this research was designed by the b/b_o method for 4000 psi concrete and batched on a weight basis. A description of this concrete mixture design is in Chapters IV and VII.

The air content was determined by a Chase Air Meter. The 3-day compressive strength on two 3" x 6" test cylinders was averaged to be 4188 psi.

Table 6.4 shows the materials, by weight, required to produce one cubic yard of concrete and the physical properties of the mixture. The material weights are based on the coarse aggregate in a vacuum-saturated surface dry condition and the fine aggregate in a saturated surface dry condition.

Various physical and mechanical properties of an average concrete should also be mentioned here. For average weight structural concrete, the modulus of elasticity normally varies between 2 and 6 million psi, with 4 million psi as an average value [19].

Poisson's ratio for most average concretes falls within the limits of 0.15 to 0.20. In the absence of experimental data, Poisson's ratio is frequently assumed to be 0.17 [30]. This static value is essentially constant for stresses below 40 percent of the ultimate strength. The compressive strength of concrete ranges from 2000 to 6000 psi with 4000 psi taken as an average value. The tensile strength of concrete can be assumed to be negligible. For concrete and mortar with a water-cement ratio of 0.5 to 0.6, the coefficient of permeability is approximately equal to 1.5×10^{-10} ft/sec [19]. The coefficient of thermal expansion

TABLE 6.4 PHYSICAL PROPERTIES OF THE CONCRETE MIXTURE

Materials Required to Produce One Cubic Yard of Concrete:

Material	Amount (pounds)	Fractional Volume (%)
Cement	695.9	13
Water	357.4	21
Fine Aggregate	1071.8	25
Coarse Aggregate	1481.6	37
Entrained Air	--	4

Properties:

Property	Value
Air Content (Chase Air Meter)	4.0 %
Water-Cement Ratio	0.51 or 5.78 gal/sack
Slump	6.25 in
Unit Weight	131 pcf
Compressive Strength	4188 psi
Workability	Good

for hardened concrete is normally assumed to be about 5.5×10^{-6} in/°F [19].

Supporting Materials

Lime

As previously mentioned, lime-saturated water was used to soak the concrete beams in to prevent hydration and water loss. The brand of lime was Gold Bond, hydrated lime, manufactured at Kimballton, Virginia by the National Gypsum Company of Buffalo, New York. It was comprised of 71.5 percent calcium oxide, 1 percent magnesium oxide, and 2 percent oxides contained as carbonates. It had a fineness of 100 percent through a #20 mesh, 98 percent through a #60 mesh, and 95 percent through a #100 mesh.

Kerosene

Each concrete specimen was completely submerged in the kerosene, which was used as a heat transfer medium in the copper containers. This kerosene was obtained from the Radford Brothers Amoco Station, Blacksburg, Virginia.

Motor Oil

Motor oil was used to coat the inside of the steel forms to ensure easy removal from the concrete after it had hardened. The oil was Phillips 66, SAE 40, manufactured by Phillips Petroleum Company, Bartlesville, Oklahoma.

Petroleum Jelly

White petroleum jelly, a Golden T product distributed by T. G. and

Y. Company, Oklahoma City, Oklahoma, was used to coat the center rod to ensure easy removal from the surrounding concrete.

CHAPTER VII

EXPERIMENTAL PROCEDURES

This chapter contains the experimental procedures used in this investigation. It is divided into four main sections as follows: preparation of beams which includes concrete mixture design, preparation of the coarse and fine aggregate, mixing and molding, and curing; prestressing of the beams which includes method of attaching strain gages to bar, and procedure of prestressing; freeze-thaw testing of beams which includes testing procedures and measurement of specimen deterioration; and flexure testing of beams.

Preparation of Beams

Concrete Mixture Design

The portland cement concrete mixture was designed by the b/b_o method [23] and batched on a weight basis. First, the design proportions were obtained based on the laboratory established values of the volume of coarse aggregate, fine aggregate, cement, and water required per unit volume of concrete for the desired water-cement ratio, consistency, and workability. The mixture was then modified for this research. The size effect of the model made this a necessary procedure. The materials required to make one cubic yard of concrete and other properties are shown in Chapter VI.

Preparation of the Coarse and Fine Aggregate

The calculated proportion of air-dried coarse aggregate was placed in the vacuum tank and the vacuum lowered to 27.2 inches of mercury

(open-tube manometer). This value was held for one hour; after which, the vacuum was broken and the aggregate was saturated with water at atmospheric pressure for 24 hours prior to mixing. At the end of this time, the aggregate was drained, weighed, and used in the concrete mixture.

After the properties of the fine aggregate were determined, the designated proportion was placed in a pan and a small amount of water added to saturate the sand particles. This mixture was left 24 hours under a damp paper towel prior to mixing.

Mixing and Molding

To begin the mixing process, the 1 1/2 cubic foot Lancaster tub mixer was "buttered" for two minutes. The coarse aggregate and the fine aggregate were placed into the mixing tub and dry-mixed for two additional minutes. The portland cement was added and the mixer allowed to run for another minute before adding any water. First, only about 50 percent of the mixing water required from the mixture design was added to the contents in the tub. The mixer ran for three more minutes and additional water was added until the desired slump was obtained. Two air content measurements were made with a Chase Air Meter. The slump test was performed according to ASTM Designation: C143 and the unit weight test according to ASTM Designation: C138.

Since the specimens were to be post-tensioned, the 5/8 inch steel rods, used to form conduits for the 1/2 inch prestressing bars were coated with petroleum jelly to ensure easy removal after the concrete hardened. These were placed lengthwise at the center of the forms, and

the forms were coated inside with a thin layer of oil. Next, the concrete was placed into the steel forms and vibrated lightly. They were prepared essentially according to ASTM Designation: C192. Using the plexiglass spacer plate, the brass inserts, serving as carriers for the stainless steel gage plugs, were inserted in the open face of the concrete beams. These inserts were cleaned with acetone beforehand so that no foreign matter would interfere with the concrete-insert bond. Iron-constantan thermocouples were also cast in three different specimens (one in each different level of prestress).

Curing

The steel forms containing the concrete were placed in the curing room of 70°F and 100 percent relative humidity for 48 hours. After curing for two days, the steel forms and the 5/8 inch steel center rods were gently removed. The members were then returned to the curing room and placed in lime-saturated water having a temperature of approximately 70°F until they were ready to be prestressed six days later. After prestressing, they were carefully identified using a red lumber crayon and returned to the lime-saturated water until freezing and thawing testing began the next day.

Prestressing of Beams

Method of Attaching Strain Gages to Bar

All nine steel prestressing bars were instrumented with two SR-4 strain gages, placed 180 degrees apart and approximately three inches from one end of the bar. The author used bars which already had the gages attached and had been previously used. These gages were visibly

checked and tested in flexure for damage.

A step by step procedure for applying the electrical-resistance strain gages on the 1/2 inch round steel prestressing bars is as follows:

1. Clean the surface of the steel bar with a fine emery cloth and then with acetone. Wipe dry with clean cotton.

2. Air dry the bar surface for several minutes and then apply a thin coat of adhesive on the bar and on the back surface of the strain gage. This adhesive was BLH EPY-600. Place the gages (BLH FAE-25-1256-ET) 180 degrees apart on one end of the bar. Cover gages with a teflon sheet, rubber sponge, and clamp in place with a spring-loaded (10 psi) clamp.

3. Place the bar in an oven and cure (raise temperature gradually) at 225^{o}F for one hour.

4. Remove the system from the oven and let it cool. Solder lead wires to the leads coming out from the gage. Clean the top surface of the gages, leads, a short length of lead wire, and the surrounding area with acetone and dry with cotton.

5. As soon as the surrounding area is dry, waterproof the gages, leads, and lead wires with the above adhesive.

6. Place the system back in the oven and perform the same curing procedure as described in Step 3.

7. Remove the system from the oven; cool and check the system. The system was checked by connecting the gages to the BLH, model 225, switching and balancing unit and the BLH, model 125, strain indicator and straining the bars in flexure. Then the bars were placed in water and checked again (this may be optional).

Procedure of Prestressing

The specimens were post-tensioned when they were eight days old by using the Tinius Olsen testing machine. First, the steel prestressing bar was placed through the duct in the center of the beam, making sure the end with the strain gages was in the larger portion of the duct. The teflon sheets, steel bearing plates, and nuts were then assembled in that order. The whole system was centered and nuts tightened snugly. Care had to be taken so that the lead wires from the strain gages followed the groove in the bearing plate. This was required so that the wires would not be crushed between the concrete and steel when prestressing began. With the aid of couplers, the beam was attached in the testing machine. The lead wires from the SR-4 strain gages were attached to the strain indicator which was used in conjunction with the switching and balancing unit. This monitoring system employed a temperature-compensating dummy gage (another SR-4 gage fixed on a prestressing bar) to eliminate the effect due to temperature on the two attached gages. All levels of prestressing forces were applied according to the strain gage readings. These readings were shown on the strain indicator.

In continuing the prestressing operation, the bar was pulled until the gage dial of the testing machine indicated more load than was actually needed on the bar. The nut was tightened on one end of the bar with a wrench to an arbitrary tightness. The member was released of the load in the steel at which time part of this load was transferred to the concrete. Thus, the steel was in tension while the concrete was in compression. The reading of the strain in the steel was then checked using the strain indicator for the specified value. The discrepancy, if any, was made as

small as possible by reloading the machine and readjusting the nut on the bar. This process continued until the desired strain in the concrete was reached. The prestressing force remained on the beams throughout the duration of the freeze-thaw testing. After prestressing, the beams were returned to the curing room in the lime-saturated water until ready for testing.

Plate 7.1 shows a beam undergoing the actual prestressing operation.

Freeze-Thaw Testing

Testing Procedure

The beams were removed from the curing room and placed in the copper containers in the freeze-thaw cabinet. They were arranged in the center portion of the cabinet in alternating order of level of prestress. Each was returned after a strain reading to this same position and orientation. The thermometer was inserted in the control beam which was located in the center of the freezing cabinet. Next, all beams and the control beam were completely covered with water-saturated kerosene. If the specimen contained a thermocouple, it was connected to the continuous temperature recorder so that the temperature of that test member could be monitored throughout the test.

All beams were approximately at 70°F when first placed in the cabinet. To obtain the initial reading, the temperature was lowered to 40°F within the specimen. With all specimens approximately at this constant 40°F temperature, readings of specimen weight and initial gage lengths in the X, Y, and Z-directions were taken. After these initial readings, the beams were cycled from 40 degrees to 0 degrees and back to 40 degrees

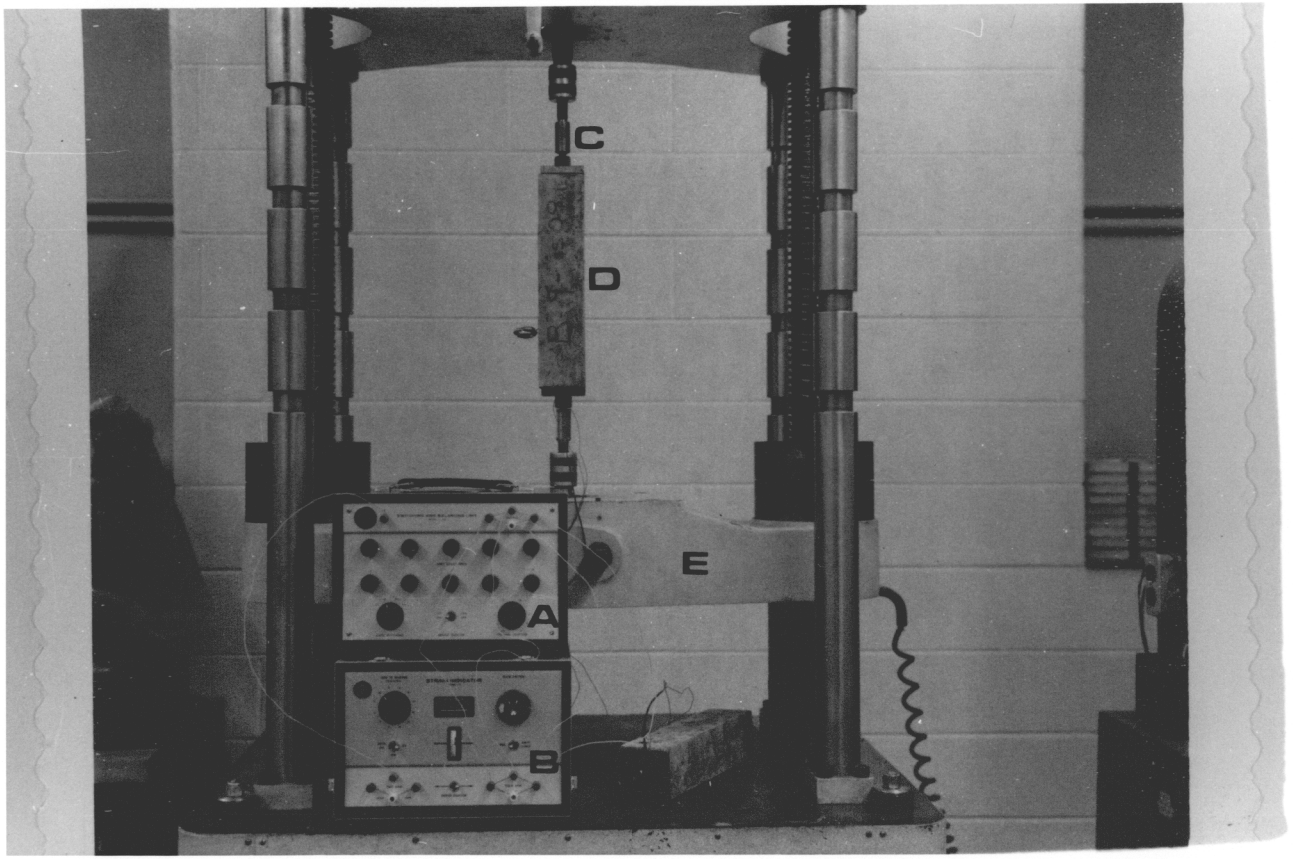

PLATE 7.1 ACTUAL PROCESS OF PRESTRESSING BEAMS (A. Switching and Balancing Unit, B. Strain Indicator, C. Couplers, D. Beam, E. Loading Machine)

in approximately 2 hours and 20 minutes.

For all readings, each specimen was taken out of the cabinet individually, placed on a sheet of newspaper, measured for strains in the respective directions, weighed to the nearest gram, returned to the cabinet, and recovered with water-saturated kerosene. Each reading was made twice; and if the values varied more than 0.0001 of an inch, that value was read again. This procedure continued for all eight beams and took approximately 45 minutes each time. After this, the machine was reactivated and another freeze-thaw cycle obtained.

The readings were taken after various freeze-thaw cycles, and the test was terminated at the end of 30 freeze-thaw cycles. Readings each time were taken with the temperature in the concrete specimens at a constant 40°F. At the end of cyclic freezing, the prestressing bars were removed and all beams were tested in flexure.

Plate 5.1 shows all members in the freezing cabinet undergoing testing.

Measurement of Specimen Deterioration

Measurement of specimen deterioration was determined by the changes in length of the concrete. When readings were taken, these changes in length were measured using a Whittemore strain gage. Both points of the gage were inserted into the stainless steel gage points located throughout the beam. The dial was then read and the readings recorded on a form for analysis later.

Flexure Testing of Beams

The final test for evaluating and determining the changes in concrete

properties caused by freezing and thawing action was the flexure test. This test is similar to the ASTM Designation: C78 method. The beams which had undergone freezing and thawing were tested four hours after undergoing their final cycle.

Each beam was mounted on the flexure testing apparatus and centered in the Tinius Olsen testing machine. The load was then applied in the center of the beam until the specimen failed. This load was recorded and used for later analysis. The three beams, which were unfrozen, were tested in the exact same manner.

Plate 5.3 shows the actual flexural testing of the beams.

CHAPTER VIII

RESULTS

This chapter contains the results of this investigation. These results are divided into the following seven sections: general surface observations and notation, lateral change in length results, comparison of X and Y-face disintegration, longitudinal change in length results, flexure results, equivalent change in length results, and weight results. Each section contains the numerical data in tabular form, followed by the same data represented graphically when appropriate.

General Surface Observations and Notation

All eight prestressed beams were subjected to the same freezing and thawing conditions for 30 cycles, at the end of which the testing was terminated. Minute surface cracks or fractures, visible to the naked eye, were first noticed developing mostly on the A (top) and C (bottom) faces of all beams at the end of the third freeze-thaw cycle. No one set of beams (all beams of a certain prestress level) showed any progressive cracking over the others. After the completion of the ninth freeze-thaw cycle, surface cracking progressed freely on all faces of the beams (the A and C faces containing the greater number). Extensive cracking developed after the fifteenth cycle and continued until the end of testing. All cracks which were observed on the faces of the beams were always parallel to the direction of the prestressing force. These longitudinal, surface cracks followed the paths of the cracks shown in Plate 8.1 (the prestress level for this beam was 1000 psi).

A photograph of the internal, lateral cross section (sawed and

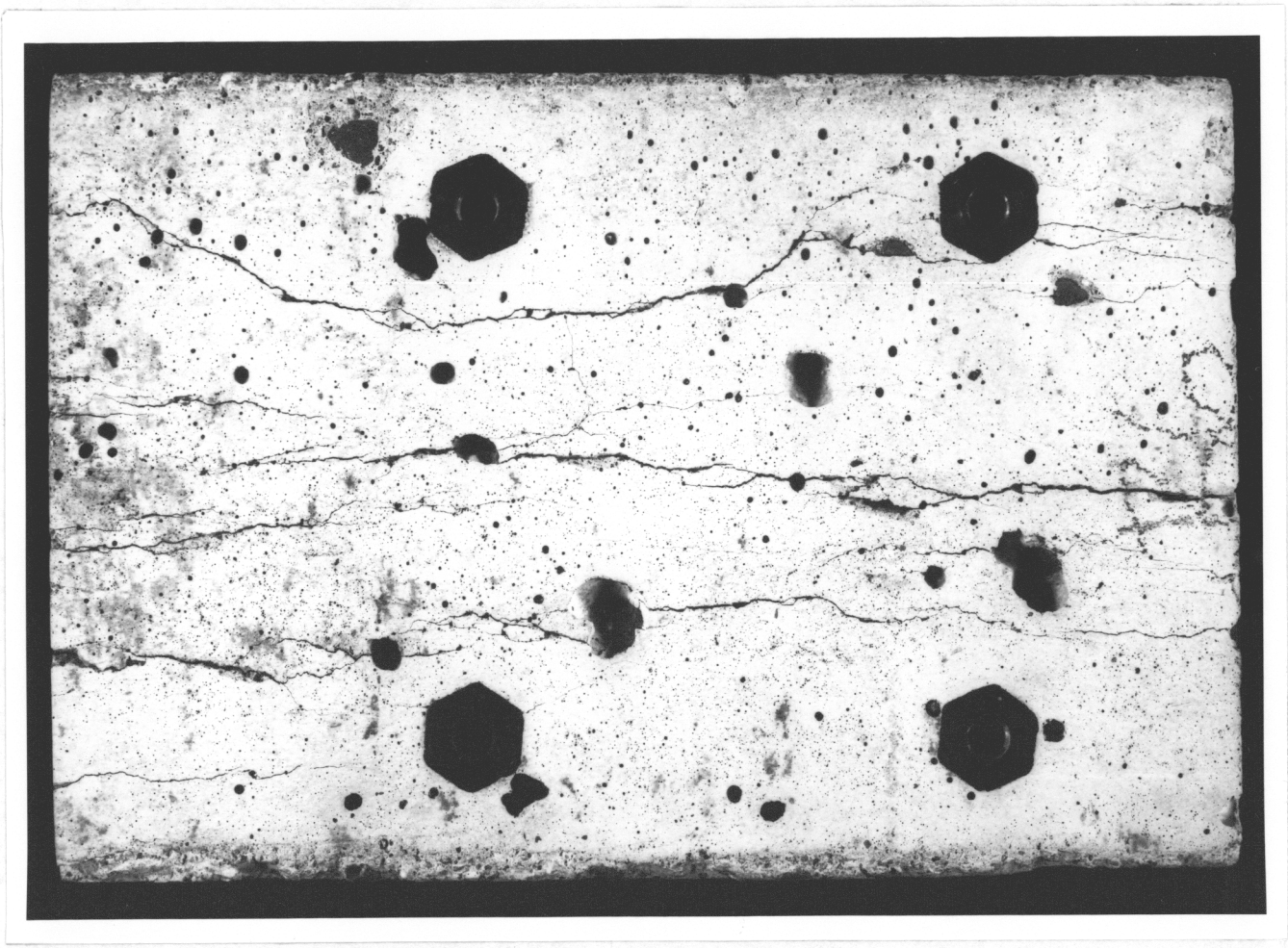

PLATE 8.1 PHOTOGRAPH OF AN EXTERNAL, LONGITUDINAL SURFACE OF A PRESTRESSED BEAM

polished) of the prestressed beam in Plate 8.1 is shown in Plate 8.2 at the end of 30 freeze-thaw cycles. All cracks run in planes perpendicular to this cross section. The destruction to the cement paste matrix and aggregate particles is dramatically shown in this photograph. It was observed that chert particles deteriorated the most, followed by shale, then sandstone. Granite seemed to deteriorate the least.

A few popouts, small pieces of concrete split from the surface, developed on the surfaces of various members. These occured mostly after the fourth or fifth cycle. Again, no one set of beams showed any larger number of popouts over the others. No other matrix damage, such as surface scaling or pattern cracking, was visible on the surfaces of the members. However, there was slight crumbling of the ends on a few beams.

Throughout the discussion of this investigation and in the tables and figures that follow, the following notation is used:

ΔX, ΔY, and ΔZ = the directional disintegration of the concrete in the X, Y, and Z-directions, respectively. They represent a change in length in units of inches per inch.

$\Delta Z'$ = the equivalent change in length in the Z-direction, the direction of prestressing, in units of inches per inch, and calculated from Reagel's graph.

ΔW = the change in weight of a beam measured in grams.

Lateral Change in Length Results

The original data from the prestressed beams that were exposed to freeze-thaw testing are shown in Appendix F. From this data, the total

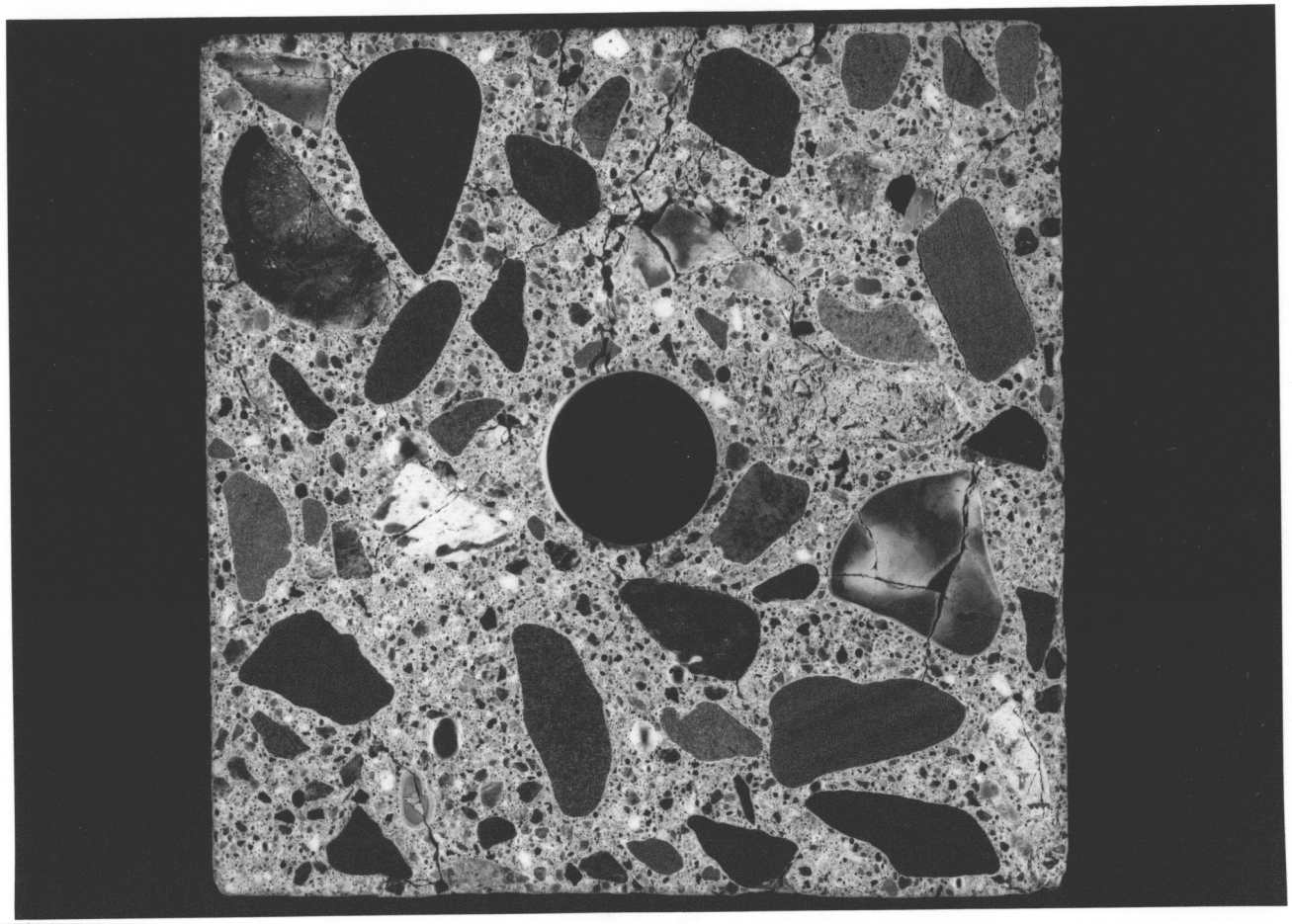

PLATE 8.2 PHOTOGRAPH OF AN INTERNAL, LATERAL CROSS SECTION OF THE BEAM IN PLATE 8.1

change in length per inch of gage length was calculated for each freeze-thaw cycle for each beam. The process of calculating this data is also described in Appendix F.

To determine the directional disintegration in the lateral direction only, the data for the change in length in the X and Y-directions were used. To eliminate the direction of freezing effect, which was constant for the members as a whole, since homologous directions were compared, but variable with respect to the X and Y-directions, the data for the change in length per inch of the two directions were averaged together, i.e., $\Delta X + \Delta Y$, for each beam. Thus, these values are averaged over 12 inches for each beam. For statistical purposes, three beams of the 500 and 1500 psi levels of prestress were used and two of the 1000 psi (there were three of these originally but one was destroyed). Thus, the average of $\Delta X + \Delta Y$ was determined over 36 inches for the 500 and 1500 psi levels and over 24 inches for the 1000 psi level. It is conjectured that averaging over 24 inches reduced the particle effect just as well as averaging over 36 inches. The calculated data for $\Delta X + \Delta Y$ are shown in Table 8.1. Plots of the data from this table are shown in Figure 8.1 as lateral directional disintegration vs. freeze-thaw cycles for each level of prestress.

Comparison of X and Y-Face Disintegration

A comparison of the X and Y-face disintegration for each level of prestress was made due to the corresponding dissimilar data obtained. The X and Y-faces on which this data was obtained was the A and D faces, respectively, shown in Figure 4.1. The A face is parallel to the top

TABLE 8.1 LATERAL DIRECTIONAL DISINTEGRATION DATA

Freeze-Thaw Cycles	Lateral Directional Disintegration, $\Delta X + \Delta Y$ (in/in x 10^{-4})		
	500 psi*	1000 psi**	1500 psi*
0	0.0	0.0	0.0
1	5.4	5.9	6.4
2	10.1	11.3	12.1
3	12.7	14.6	15.6
4	15.1	18.4	19.2
5	18.3	21.4	23.0
9	25.4	29.3	34.1
10	30.1	32.6	38.2
11	32.1	35.5	40.7
15	40.0	42.6	51.2
16	43.8	47.3	55.7
20	52.9	59.7	69.1
25	59.7	73.5	83.0
30	64.0	84.9	94.2

*Each value was averaged over 36 inches.

**Each value was averaged over 24 inches.

LATERAL DIRECTIONAL DISINTEGRATION vs. FREEZE-THAW CYCLES
FOR 500, 1000, AND 1500 PSI

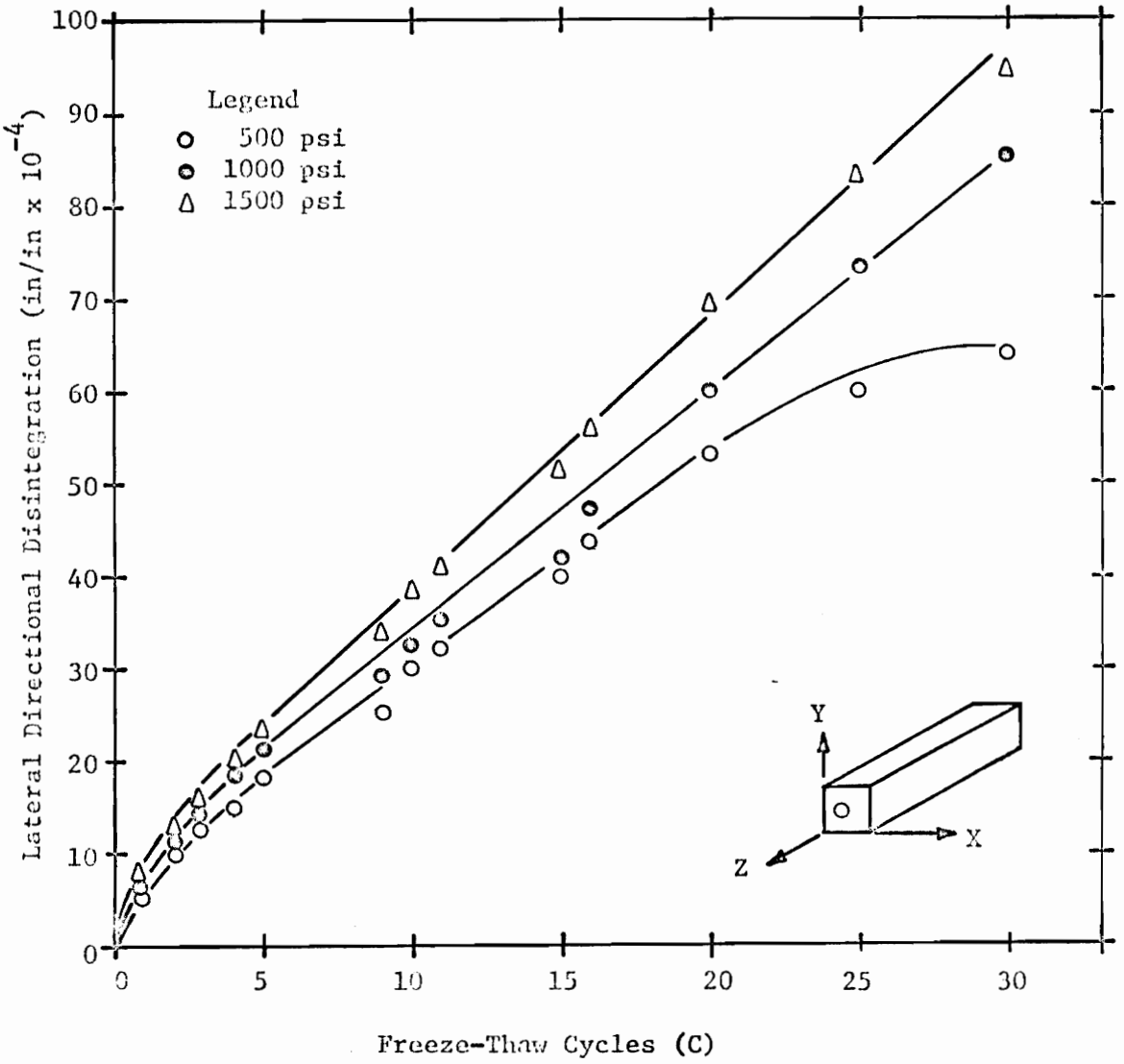

FIGURE 8.1 LATERAL CHANGE IN LENGTH RESULTS (PRESTRESSING IN Z-DIRECTION)

surface of the kerosene, and the D face is perpendicular to this surface. All members were placed in the exact same orientation and position after each designated cycle reading. This is the same data used for plotting the graph of the lateral directional disintegration in the previous section except the values ΔX and ΔY are not averaged together. Thus, both ΔX and ΔY separately are averaged over 18 inches for the 500 and 1500 psi levels and over 12 inches for the 1000 psi level. The calculated data are shown in Table 8.2. Plots of the data from this table are shown in Figure 8.2 as X and Y-face disintegration vs. freeze-thaw cycles for each level of prestress.

Longitudinal Change in Length Results

All beams used in this investigation were prestressed and, therefore, restrained in the longitudinal direction (Z-direction). This prestressing force will cause a strain in the material. Creep (a stress-time function) of the uniaxially prestressed concrete beams also occurred in the prestressed direction. This will cause a small change in length of the member (a contraction) and, thus, a small loss in prestress.

The original data for determining the change in length in the longitudinal direction and the process of calculating this data can be found in Appendix F. For the total change in length per inch in the Z-direction, the values obtained are averaged over 10 inches per beam. Thus, the average of ΔZ was determined over 30 inches for the 500 and 1500 psi levels of prestress and over 20 inches for the 1000 psi level. Again, it is conjectured that 20 inches was enough to reduce the particle effect within the concrete beams. The calculated data for these results are shown in Table

TABLE 8.2 X AND Y-FACE DISINTEGRATION DATA

Freeze-Thaw Cycles	X and Y-Face Disintegration, (in/in x 10^{-4})					
	500 psi*		1000 psi**		1500 psi*	
	ΔX	ΔY	ΔX	ΔY	ΔX	ΔY
0	0.0	0.0	0.0	0.0	0.0	0.0
1	7.0	3.7	7.3	4.5	8.4	4.4
2	13.0	7.1	14.4	8.2	15.4	8.8
3	16.7	8.6	19.7	9.4	20.7	10.5
4	21.1	9.2	25.6	11.1	26.1	12.2
5	25.8	10.8	30.2	12.5	31.9	14.0
9	40.9	13.3	44.7	13.7	49.7	18.4
10	45.7	14.5	50.1	15.0	55.4	20.9
11	48.9	15.2	55.3	15.8	59.3	22.0
15	62.0	17.9	67.0	18.1	74.0	28.4
16	67.0	20.7	73.8	20.7	79.7	31.6
20	80.1	25.6	93.5	25.8	94.9	33.1+
25	89.1	30.1	114.9	32.1	107.2	38.0+
30	95.0	33.0	133.5	36.3	116.0	40.7+

*Each value was averaged over 18 inches.

**Each value was averaged over 12 inches.

+Averaged over 12 inches because values at this point were in error.

X AND Y-FACE DISINTEGRATION vs. FREEZE-THAW CYCLES
FOR 500, 1000, AND 1500 PSI

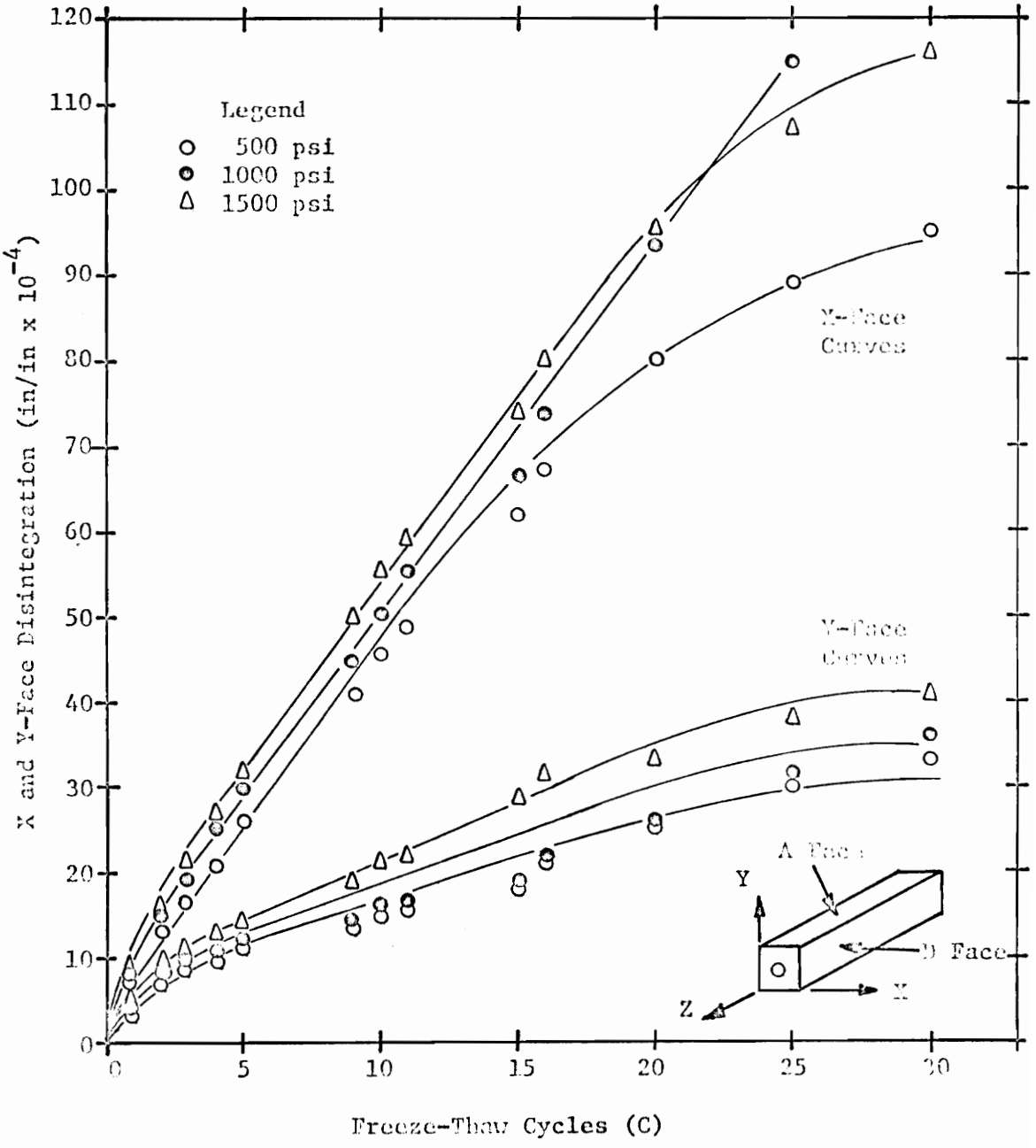

FIGURE 8.2 COMPARISON OF X AND Y-FACE DISINTEGRATION (PRE-STRESSING IN X-DIRECTION)

8.3. Plots of the data from this table are shown in Figure 8.3 as longitudinal change in length vs. freeze-thaw cycles for each level of prestress.

It should be noted that the change in length data in Table 8.3 has the restriction of the prestressing force at each level of prestress incorporated into it. The members are restrained in this direction as compared to the non-restrained X and Y-directions. However, since homologous Z-directions of each level of prestress are compared by permanent changes in length, Figure 8.3 is valid for the given prestressing conditions. It will be shown, in a later section, how the change in length in the Z-directions can be compared on a similar basis (a basis of unrestricted expansion or contraction) as the X and Y-directions by an equivalent change in length.

Flexure Results

After the termination of freeze-thaw testing, all eight prestressed beams were tested in flexure. Three additional beams were also made, following the same mixture proportions and design, and tested in flexure. These non-prestressed, non-frozen beams gave the true (non-frozen) flexural strength of the members.

To obtain the flexural strength of the beams, a sensitive flexure testing apparatus was used (the same as that used by Payne). This apparatus minimized the effect of shear and maximized the effect of fiber continuity in the longitudinal direction and, thus, was an excellent measure of frost damage in this direction [13].

A physical examination of the failure sections of the flexure test

TABLE 8.3 LONGITUDINAL CHANGE IN LENGTH DATA

Freeze-Thaw Cycles	Longitudinal Change in Length, ΔZ (in/in x 10^{-4})*		
	500 psi**	1000 psi***	1500 psi**
0	0.00	0.00	0.00
1	-0.12	-0.88	-0.75
2	0.00	-1.20	-1.00
3	0.13	-1.33	-1.23
4	0.27	-1.28	-1.28
5	0.20	-1.55	-1.50
9	0.43	-2.00	-1.87
10	0.52	-2.00	-1.92
11	0.52	-2.23	-2.07
15	0.73	-2.35	-2.23
16	0.60	-2.45	-2.27
20	0.65	-2.65	-2.43
25	0.88	-2.83	-2.38
30	0.92	-2.93	-2.17

*Positive sign indicates an expansion.

**Each value was averaged over 30 inches.

***Each value was averaged over 20 inches.

LONGITUDINAL CHANGE IN LENGTH vs. FREEZE-THAW CYCLES
FOR 500, 1000, AND 1500 PSI

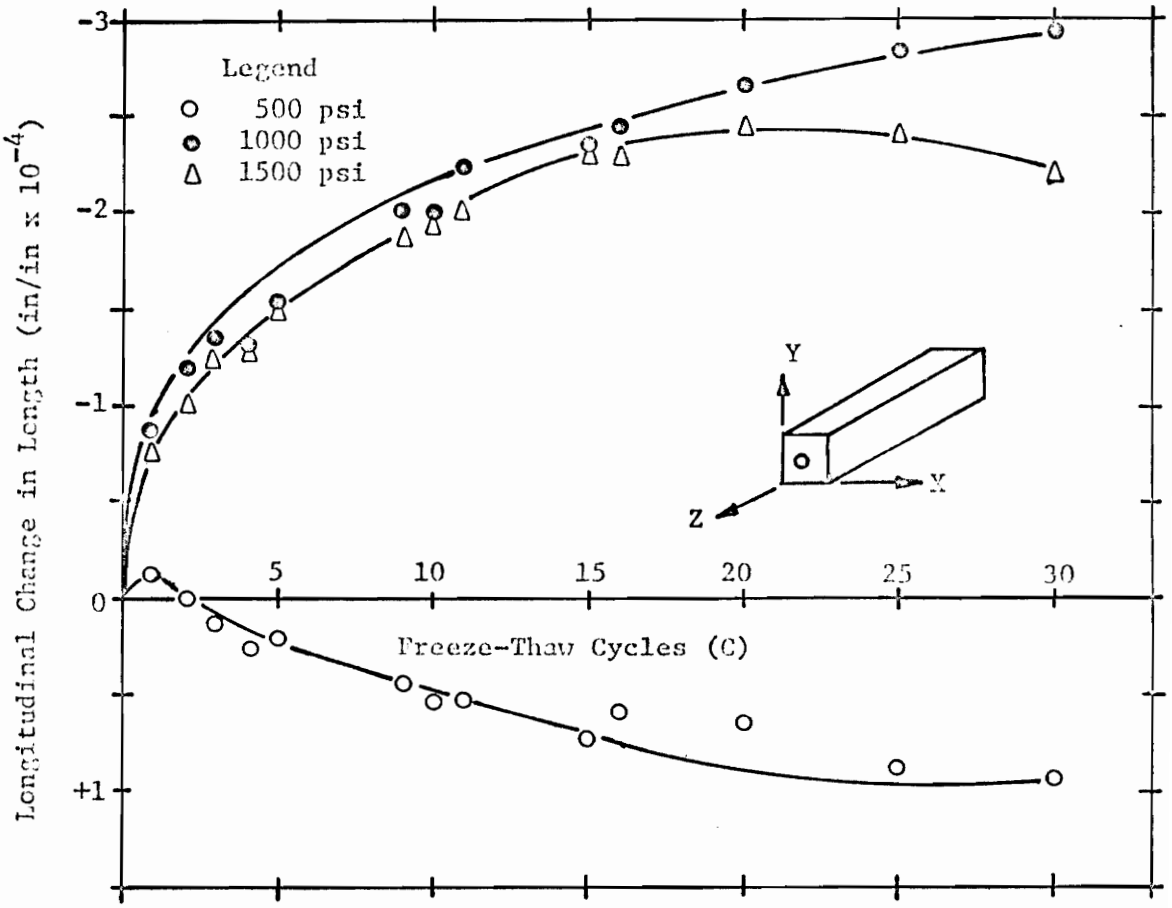

Note: Positive value equals an expansion

FIGURE 8.3 LONGITUDINAL CHANGE IN LENGTH RESULTS (PRESTRESSING IN Z-DIRECTION)

members indicated that a larger percentage of the coarse aggregates failed by fracturing than in bond. This was truer for the prestressed, frozen members than for the non-prestressed, non-frozen ones.

The flexural strengths, σ_f, of the beams and the percent loss in flexural strength for each level of prestress are shown in Table 8.4. The percent loss in flexural strength is 100 minus the ratio of the deteriorated flexure strength divided by the non-deteriorated strength multiplied by 100; i.e., 100 - [(X/Y) x 100].

Equivalent Change in Length Results

The concrete was free to move without restriction in all directions except in the direction of the applied prestressing force. Since the change in lengths for the unrestricted X and Y-directions have been compared and used as a measure of disintegration, it is interesting to compare the change in length in the Z-direction as if it was free to elongate. The values determined represent the elongation of the beam due to freeze-thaw effects as if the beam was totally unrestrained in the prestressed direction. However, these values, as well as the values for the X and Y-directions, are a function of the applied prestressing force. Thus, it was necessary to convert the change in length of the prestressed direction of the prestressed beam into an equivalent change in length, $\Delta Z'$ [13]. This was accomplished by a non-linear transformation by the use of Reagel's graph [7]. This graph gives the relationship between the loss in flexural strength of a beam and the equivalent permanent change in length due to freezing and thawing.

As mentioned in Chapter IV, Payne [13] verified Reagel's graph

TABLE 8.4 FLEXURAL STRENGTH DATA

Flexural Strength, σ_f:

Beam Number	Prestress Level	$\sigma_f = Mc/I$	Average σ_f
	Prestressed and Frozen Beams		
B1	500 psi	247 psi	260 psi
B2	500	250	
B3	500	284	
B4	1000	307	283
B6	1000	259	
B7	1500	232	228
B8	1500	243	
B9	1500	210	
	Non-Prestressed and Non-Frozen Beams		
BI	0 psi	524 psi	504 psi
BII	0	515	
BIII	0	473	

Percent Loss in Flexural Strength:

Prestress Level	Percent Loss
500 psi	48.4 %
1000	43.8
1500	54.8
	49.0 = Average

before using it for his non-linear transformations of the prestressed directions. Figure 4.3 shows Reagel's original graph with Payne's data points superimposed and, thus, will be used to obtain the equivalent change in length for the author's prestressed beams.

The percent loss in flexural strength for each level of prestress was determined in the previous section. Using Reagel's graph, the equivalent percent increase in length due to freezing and thawing can be obtained and, thus, the equivalent change in length for each level of prestress. This data is shown in Table 8.5. Plots of the data are shown in Figure 8.4 as equivalent directional disintegration vs. freeze-thaw cycles for each level of prestress. It is interesting to compare this figure with Figure 8.3.

Weight Results

The weight of each beam was recorded after each designated cycle reading. The original data for these weights are shown in Appendix F. For the 500 and 1500 psi levels of prestress, the values are an average of three beams, and, for the 1000 psi level, an average of two beams. The data for the total change in weight, ΔW, per freeze-thaw cycle are shown in Table 8.6. These values are plotted in Figure 8.5 as change in weight vs. freeze-thaw cycles for each level of prestress.

TABLE 8.5 EQUIVALENT DIRECTIONAL DISINTEGRATION DATA

Prestress Level	Equivalent Percent Increase in Length*	Equivalent Change in Length, $\Delta Z'$
500 psi	0.050 %	5.0×10^{-4} in/in
1000	0.040	4.0×10^{-4}
1500	0.070	7.0×10^{-4}

*Positive values indicate an expansion.

EQUIVALENT DIRECTIONAL DISINTEGRATION vs. FREEZE-THAW CYCLES
FOR 500, 1000, AND 1500 PSI

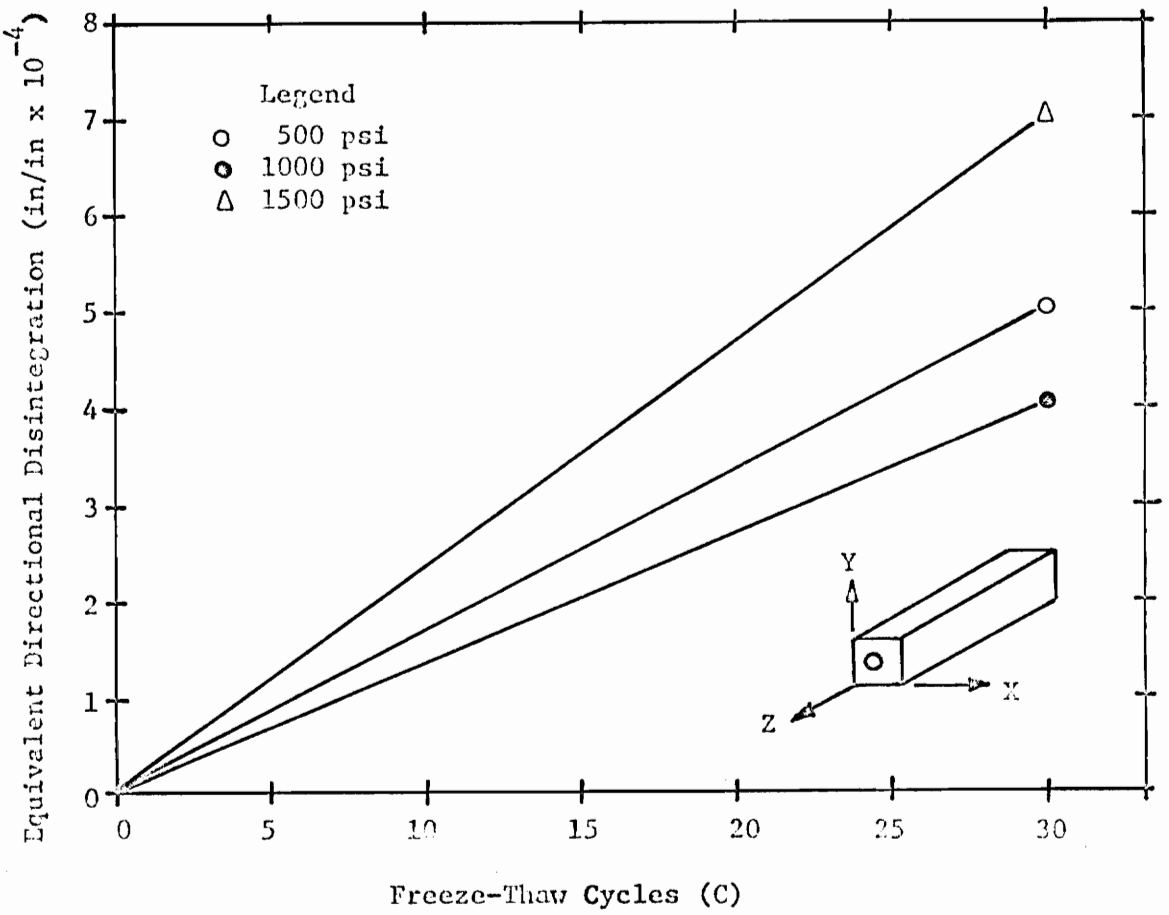

FIGURE 8.4 EQUIVALENT CHANGE IN LENGTH RESULTS (PRESTRESSING IN Z-DIRECTION)

TABLE 8.6 CHANGE IN WEIGHT DATA

Freeze-Thaw Cycles	Change in Weight, ΔW (grams)		
	500 psi*	1000 psi**	1500 psi*
0	0.0	0.0	0.0
1	1.7	4.0	3.3
2	0.0	5.0	7.0
3	1.7	8.0	7.7
4	4.3	9.5	8.0
5	5.7	11.5	7.0
9	9.3	13.5	9.0
10	9.7	14.5	11.0
11	11.7	16.0	12.7
15	13.0	16.5	12.7
16	13.3	18.0	13.7
20	16.0	21.5	16.0
25	18.0	23.0	19.3
30	20.3	27.0	21.3

*Each value was averaged over 3 beams.

**Each value was averaged over 2 beams.

CHANGE IN WEIGHT vs. FREEZE-THAW CYCLES
FOR 500, 1000, AND 1500 PSI

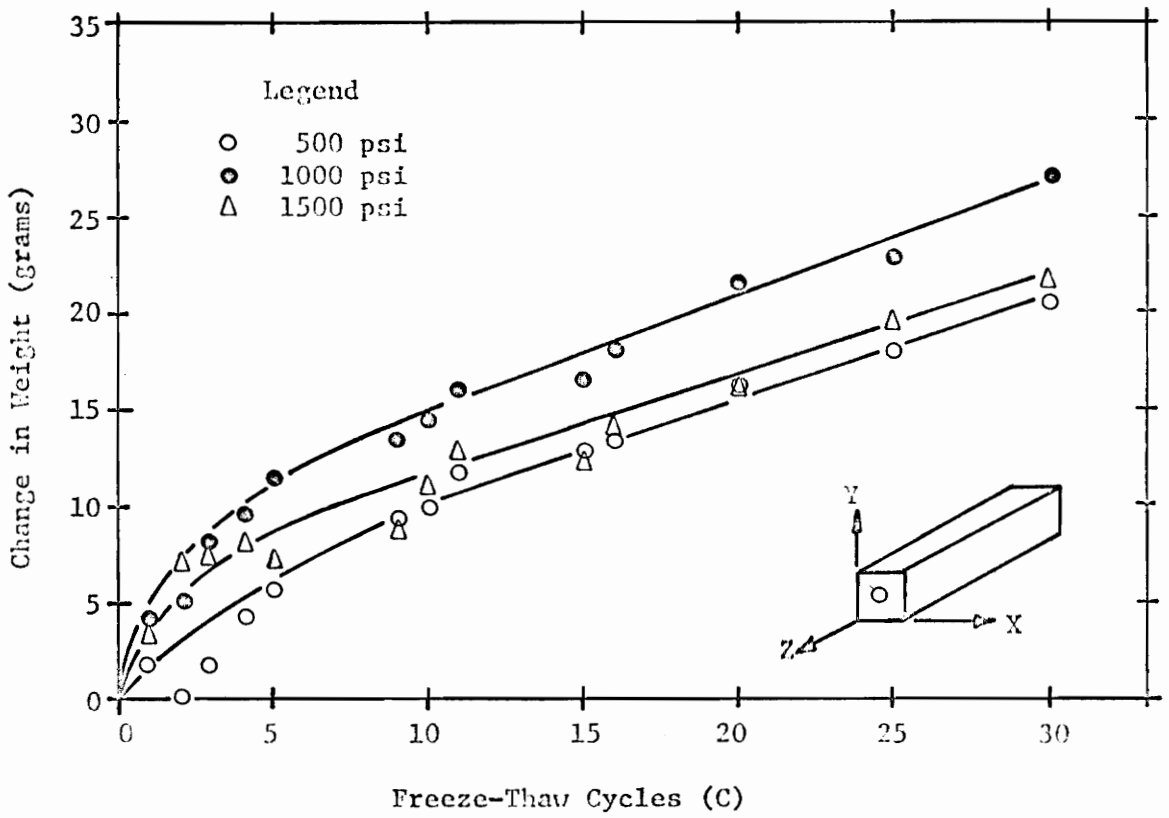

FIGURE 8.5 CHANGE IN WEIGHT RESULTS

CHAPTER IX

DISCUSSION OF THE RESULTS AND PROPOSED THEORY

This chapter contains a discussion of the results of this investigation and a discussion of the proposed theory involved in this phenomenon. The chapter will be divided into the following three sections: discussion of the results, discussion of the proposed theory, and engineering applications of the results.

Discussion of the Results

From Plate 8.1 of the external, longitudinal surface of a deteriorated beam, the following observations were made:

1. In general, the surface cracks are parallel to the direction of the prestressing force. Slight angular deviations may occur, due to internal aggregate particles deflecting the crack around its body, instead of the crack propagating directly through it. In the photograph, this deflection mechanism is shown by a crack being deflected around a brass insert.

2. Small surface air voids can be seen in the photograph. Once an advanced stage of deterioration has started, these surface voids do not arrest the cracks which propagate along the surface. This can be seen by cracks splitting the voids and continuing their propagation.

3. Many cracks which start at opposite ends of the beam from each other, eventually connect themselves as deterioration progresses. This was noted on a number of beams, and some beams had surface cracks connected throughout their longitudinal length.

From Plate 8.2 of the internal, lateral cross section of a deterio-

rated beam, the following observations were made:

1. Bond cracks can be seen at the paste-aggregate interface in various regions of the cross section. These are probably caused by differential volume changes which occur between the cement mortar matrix and/or the aggregate particles.

2. Fracturing and disintegration of the aggregate particles and cement matrix are quite visible throughout the cross section.

3. Fractures seem to originate from inside the aggregate particles and propagate outward toward the surface in planes perpendicular to the cross section.

The following observations were obtained from Figure 8.1, lateral directional disintegration vs. freeze-thaw cycles:

1. Comparing the three $\Delta X + \Delta Y$ curves for each level of prestress indicated that the rate of deterioration of the concrete members increased as the level of the uniaxial prestress increased.

2. Comparing the slopes of the curves through the first few cycles indicated that lateral directional disintegration was accelerated in the early freeze-thaw cycles. This was due to the initial surge of microcrack development which exceeded the strength of the material, afterwhich, cracks still formed and grew, but to a smaller degree.

The following observations were obtained from Figure 8.2, X and Y-face disintegration vs. freeze-thaw cycles:

1. Comparing the ΔX curves, in general, with the ΔY curves indicated that the rate of deterioration in the X-direction is much greater than that in the Y-direction. For example, X-face disintegration is approximately 300 percent greater than the Y-face disintegration for the 1500

psi level of prestress. This phenomenon is probably due to the direction of freezing variable for each direction. The freezing unit used in this investigation, because of the horizontal position of the cooling plate, froze the beams in a vertical direction (the direction of freezing). Thus, the freezing front moved from the bottom (face C) toward the top (face A) of the beam and caused the X-direction to disintegrate more than the Y.

2. Comparing the ΔX and ΔY curves separately for each level of prestress indicated that the rate of deterioration increased as the level of prestress increased.

The following observations were obtained from Figure 8.3, longitudinal change in length vs. freeze-thaw cycles:

1. Comparing the three ΔZ curves indicated that the change in length in the longitudinal direction is greater for the higher levels of prestress. It cannot be explained why the change in length for the 1000 psi level is greater than the 1500 psi level.

2. Comparing these curves with the curves of Figure 8.1 indicated that prestressing reduced the change in length in the direction of the prestressing force. If this direction had not been restrained, the change in length in all three directions would have been approximately the same.

3. It can be seen that the beams with the 1000 and 1500 psi levels of prestress contracted, while the beam with the 500 psi level initially contracted then expanded continuously. This phenomenon was interesting to note. From the 500 psi level curve, there was a point at a certain time (at the end of the second freeze-thaw cycle) at which the total change in length of the beam is equal to zero. At this "equilibrium point" the change in length in the longitudinal direction due to the sum-

mation of the prestressing and creep effects equals the change in length due to freeze-thaw damage. After this point, the beam begins to expand, indicating that the change in length due to the freeze-thaw damage exceeds the change in length due to the opposing effects. Conversely, for the other two prestress levels, the change in length due to prestressing and creep exceeds the change in length due to freeze-thaw damage.

The following observations were obtained from Table 8.4, flexural strength data for the different levels of prestress:

1. Comparing the flexural strength and the percent loss in flexural strength data for each level of prestress after 30 freeze-thaw cycles indicated that the highest level of prestress caused the greatest reduction in flexural strength and, thus, the percent loss. It cannot be explained why the flexural strength for the 1000 psi level is greater than the 500 psi level.

2. There was an average percent loss in flexural strength of 49 percent for all levels of prestress. This indicated that the flexural strength of the beam was a function of the permanent deformation (frost damage) in the longitudinal direction. This deformation was caused by the formation and propagation of microcracks which destroyed the continuity of the beam and reduced its strength.

The following observations were obtained from Figure 8.4, equivalent directional disintegration vs. freeze-thaw cycles:

1. Comparing the three $\Delta Z'$ curves for each level of prestress indicated that the rate of equivalent directional disintegration was greatest for the highest level of prestress. Even though the 500 psi level was greater than the 1000 psi level, both being very close however, there was

the indication of increasing disintegration with increasing stress.

2. Comparing the $\Delta Z'$ curves with the ΔZ curves indicated a linear change in length function for the former, non-restrained condition and a non-linear type function for the latter, restrained condition. The linear change in length was to be expected since the linear region of Reagel's graph was used to obtain the equivalent percent increase in length.

The following observations were obtained from Figure 8.5, change in weight vs. freeze-thaw cycles:

1. Comparing the ΔW curves, in general, indicated that there was a definite, continuous increase in weight of the members for increasing freeze-thaw cycles. This also implies that weight gain increases for increasing change in length (directional disintegration).

2. Weight gain can be attributed to the movement of kerosene into the widening cracks that have propagated to the surface of the members. If this had been actual water, destruction would have been much greater (since water freezes at $32^{\circ}F$ and kerosene does not), and weight gain would have increased as well.

3. Comparing the ΔW curves for each level of prestress indicated that a correspondence between weight gain and increasing stress level cannot be determined. It should be noted that this data was subject to errors such as popouts, nonuniform surface drying, and nonuniform drainage of entrapped kerosene in the center conduit region of the beam each time a weight reading was taken. The same orientation of the beams was maintained for each reading to provide a similar basis for obtaining the data.

Discussion of the Proposed Theory

In advancing the theory in Chapter III to be applied to the results of this investigation, a few ideas from Payne's research should be mentioned [13]:

> This theory, "THE PLANE OF LEAST RESISTANCE THEORY," states that the microcracks originate in the planes of least resistance and propagate in these planes. If this theory is true, then the level of prestress is not a primary factor in this phenomenon. Regardless of the level of prestress, the beneficial effect of prestressing vanishes on planes parallel to the direction of the prestressing force or forces and these planes are the planes of least resistance.
>
> The level of prestress would be a primary factor in initiating the microcracks (stress-concentration effect) in the early freeze-thaw cycles.
>
> The "layered effect" is the effect that occurs when the microcracks, that later become fracture planes, are concentrated from a random direction to two directions. . . .
>
> In the early freeze-thaw cycles, the "stress-concentration effect" and the "layered effect" occur simultaneously. In the latter freeze-thaw cycles, the "layered effect" should be the dominating factor.

The author basically agrees with these ideas except it is believed that the level of prestress is a primary factor in both crack initiation and propagation. The level of stress and internal hydraulic pressure create these planes of least resistance throughout the concrete. Surely a plane containing tensile stresses would respond to an approaching crack more than one containing compressive stresses. Accordingly, a plane containing a tensile stress greater than another would encourage propagation into it first.

The theory presented by the author in Chapter III explains the physical phenomenon that originated in the saturated aggregate particles. Non-saturated aggregates would first have to absorb water to be able to

create hydraulic pressure. Since, in nature or in the laboratory, concrete freezes from the outside inward and thaws from the outside inward, the movement of water in non-saturated concrete is inward. This phenomenon is due to the change in volume that occurs when water is converted to ice or ice is converted to water. During freezing and thawing, aggregate capillaries act as small pumps. Freezing forces water deeper into the capillaries while thawing creates a vacuum which draws water from outside of the particle into the capillary. After partial saturation, the same physical phenomenon will occur, but at a much later time in the course of the freeze-thaw cycles.

The theory explains why concrete subjected to freezing and thawing and external compressive stress deteriorates at a faster rate as the level of stress increases. The same theory will be true no matter what the rate of freezing. However, as the rate of freezing increases, cracks will form and propagate sooner. The same tensile stresses will exist at the crack tip. Repeated freezing and thawing will cause the cracks to propagate as usual.

Engineering Applications

The results obtained from this investigation have numerous important engineering applications. Knowledge of these results and their effects on prestressed concrete subjected to alternating cycles of freezing and thawing will be helpful in predicting the performance of concrete subjected to these conditions.

If the deep-seated type of frost damage occurs in manually prestressed or self-prestressed (structurally loaded) members, then from a know-

ledge of the distribution of compressive stresses throughout the member, the direction and rate of fracturing may be predicted.

For example, the relative performance of highway or airport pavements, subjected to loading conditions which produce compressive stresses in their upper layers, can be predicted when they undergo freezing and thawing action.

The same theory can be applied to the concrete bridge deck deterioration problem. Different regions throughout the bridge deck contain different levels of compressive stresses. Superimposing the applied structural stress-distributions with those generated by freezing temperatures produces a physical explanation of the relative rates and directions of this type of deterioration. Thus, regions containing the higher levels of compressive stress should deteriorate at a faster rate.

Another example is that of externally exposed (to adverse weathering conditions) concrete columns. Since all concrete columns prestress themselves under a large dead load and perhaps live load, freeze-thaw disintegration to the concrete could occur and be accelerated (especially near the ground line or water table) orthogonal to this compressive stress. For higher levels of compressive stress, the deterioration should be greater.

CHAPTER X

CONCLUSIONS AND RECOMMENDATIONS

Conclusions

The results of this investigation indicate:

1. The deterioration rate in the lateral direction of the uniaxially prestressed members subjected to the deep-seated type of freeze-thaw damage increased as the level of the compressive stress field increased.

2. Under all levels of uniaxial compression, cracks formed parallel to the direction of the applied stress field and in any plane parallel to this direction when the members were subjected to freeze-thaw damage.

3. The cracks are assumed to start at the boundary of a capillary within the aggregate and propagate through the aggregate to the aggregate-mortar interface.

4. Due to previous investigations, bond and mortar cracks are assumed to exist in the concrete. These cracks increase for increasing stress levels.

5. For the prestressed direction of any uniaxially prestressed member, there was a certain prestress level for which the change in length due to internal freeze-thaw damage equaled the change in length due to the applied prestressing force plus any longitudinal creep effects. This resulted in a total zero change in length. This zero change in length condition is called the "stress equilibrium condition" and the level of prestress which causes this condition is called the "prestress stability level." However, this condition can only last a short while before equilibrium is destroyed, since freeze-thaw damage and creep are

continuously changing.

6. The increasing lateral strain with each freeze-thaw cycle was due to the increase in new crack development and the increase in the width of old cracks.

7. There was a weight gain as freeze-thaw deterioration progressed.

8. The rate of deterioration in the X-direction is greater than that in the Y-direction and correspondingly greater in each direction as the level of prestress is increased.

9. The failure process can be based on the theory presented by the author in Chapter III.

Recommendations

Due to the results of this investigation and a need for continued research, it is suggested that:

1. A standard method for prestressing laboratory size specimens of plain concrete be developed by the approporite subcommittee of ASTM Committee C-9 on Concrete and Concrete Aggregates.

2. A standard method for the freeze-thaw testing of nonreinforced prestressed concrete be developed by the same subcommittee of ASTM.

3. Experimental techniques be devised for freeze-thaw testing of reinforced prestressed concrete. These should provide for a standard method of prestressing and measuring deterioration.

4. Continued research be encouraged to:

   A. Ascertain the relationship for creep of nonreinforced concrete under uniaxial stress subjected to freezing and thawing.

B. Perform similar freeze-thaw tests on biaxial and triaxial stressed concrete.

C. Perform similar freeze-thaw tests on prestressed concrete in an environment such as salt water.

D. Establish a failure criteria, other than the authors, for uniaxial prestressed concrete and for biaxial and triaxial stressed concrete.

E. Develop further the Griffith theory of crack propagation for this research situation.

F. Learn how uniaxially prestressed concrete subjected to freezing and thawing behaves for different freezing rates, moisture contents, orientations during freezing, and types of aggregates.

CHAPTER XI

SUMMARY

The effects of various levels of compressive stress fields on the deterioration rate and microcracking of plain concrete subjected to freezing and thawing was investigated. The deep-seated (aggregate generated) type of frost damage was investigated since the cement mortar matrix was protected by entrained air.

A typical prestressed concrete mixture was designed for this research. Beams, 3" x 3" x 14", were used as the test specimens. They were uniaxially prestressed by the post-tensioning method to 500, 1000, and 1500 psi, respectively. These beams were subjected to alternating cycles of freezing and thawing. The directional disintegration of the prestressed beams were compared for the three different levels of stress. Results were then analyzed and conclusions drawn.

It was found that the deterioration rate in the lateral direction of the members increased as the level of the compressive stress field increased. The compressive stress directionalized the disintegration in planes parallel to the direction of the applied external load. It was also found that the rate of deterioration in the X-direction was greater than that in the Y-direction and correspondingly greater in each direction as the level of prestress increased.

A five step theory was presented to explain the involved physical phenomenon. The theory is based on tensile stresses existing at the crack tip and around the aggregate particles.

BIBLIOGRAPHY

1. Gutzwiller, M. J., and Musleh, F. E., "Freezing and Thawing Effects on Prestressed Concrete," Journal of the Structural Division, Proc. of ASCE, Oct. 1960, Vol. 86, No. ST10, pp. 109-124.

2. Pendley, S. C., "The Effect of Restraint on the Durability of Concrete Aggregates," M. S. Thesis, Purdue University, June 1949.

3. Jamil, K. S., "Effect of Pre-Stressing on the Durability of Portland Cement Concrete," M. S. Thesis, Virginia Polytechnic Institute and State University, Dec. 1964.

4. Causes, Mechanism, and Control of Cracking in Concrete, ACI Publication SP-20, 1968.

5. Walker, R. D.; Larson, T. D.; and Cady, P. D., Research Needs Relating to Performance of Aggregates in Highway Construction, NCHRP Report 100, Highway Research Board, 1970.

6. Cordon, W. A., Freezing and Thawing of Concrete--Mechanisms and Control, American Concrete Institute Monograph No. 3, 1966.

7. Reagel, F. V., "Freezing and Thawing Tests of Concrete," Proceedings, Highway Research Board, Vol. 20, 1940, pp. 587-598.

8. Lin, C. H., "The Effects of Freezing Rates on the Durability of Concrete," Ph. D. Thesis, Virginia Polytechnic Institute and State University, June 1974.

9. Rieb, S. L., "Preparation and Durability Testing of Pretensioned Prestressed Concrete," Journal of the Prestressed Concrete Institute, Vol. 4, No. 3, Dec. 1959, pp. 102-146.

10. Klieger, P., "Some Aspects of Durability and Volume Change of Concrete for Prestressing," Portland Cement Association, Journal of Research and Development Laboratories, Vol. 2, No. 2, Sept. 1960, pp. 2-12.

11. Roshore, E. C., Durability and Behavior of Prestressed Concrete Beams, Pretensioned Concrete Investigation, Technical Report No. 6-570, Report 1, June 1961, U. S. Army Engineer Waterways Experiment Station, Corps of Engineers.

12. Roshore, E. C., Durability and Behavior of Prestressed Concrete Beams, Post-tensioned Concrete Investigation, Technical Report No. 6-570, Report 2, July 1966, U. S. Army Engineer Waterways Experiment Station, Corps of Engineers.

13. Payne, W. W., "The Effects of Prestressing on the Freeze-Thaw Durability

of Some Concretes," Ph. D. Thesis, University of Virginia, August 1972.

14. Dally, J. W., and Riley, W. F., Experimental Stress Analysis, McGraw-Hill, Inc., 1965.

15. "Manual of Concrete Testing," 1973 Annual Book of ASTM Standards, Part 10, ASTM, Concrete and Mineral Aggregates.

16. Design and Control of Concrete Mixtures, Eleventh Edition, Portland Cement Association, Chicago, Illinois, July 1968.

17. Powers, T. C., The Mechanism of Frost Action in Concrete, Stanton Walker Lecture Series on the Materials Sciences, Lecture No. 3, National Ready Mixed Concrete Association, 1965.

18. Verbeck, G., and Landgren, R., "Influence of Physical Characteristics of Aggregates on the Frost Resistance of Concrete," Proceedings, ASTM, Vol. 60, 1960, pp. 1063-1079.

19. Waddell, J. J., Concrete Construction Handbook, McGraw-Hill, Inc., 1968.

20. Krynine, D. P., and Judd, W. R., Principles of Engineering Geology and Geotechnics, McGraw-Hill, Inc., 1957.

21. Farmer, I. W., Engineering Properties of Rocks, E. and F. N. SPON Ltd., 1968.

22. Neville, A. M., Hardened Concrete: Physical and Mechanical Aspects, American Concrete Institute Monograph No. 6, 1971.

23. Goldbeck, A. T., and Gray, J. E., "A Method of Proportioning Concrete for Strength, Workability, and Durability, Natl. Crushed Stone Assoc. Bull. 11, December 1942, revised 1953, revised 1965.

24. Lin, T. Y., Design of Prestressed Concrete Structures, John Wiley and Sons, Inc., 1963.

25. Schickert, G., "On the Influence of Different Load Application Techniques on the Lateral Strain and Fracture of Concrete Specimens," Cement and Concrete Research, Vol. 3, No. 4, July 1973, pp. 487-494.

26. Powers, T. C., "Basic Considerations Pertaining to Freezing-and-Thawing Tests," Proceedings ASTM, 1955.

27. Malhotra, V. M., Nondestructive Methods for Testing Concrete, Mines Branch Monograph 875, 1968.

28. Manual on Experimental Stress Analysis, Second Edition, SESA Educational Committee, 1965.

29. Hansen, T. C., "Influence of Aggregates and Voids on Modulus of Elasticity of Concrete, Cement Mortar, and Cement Paste," ACI Journal, Proceedings Vol. 62, No. 2, Feb. 1965, pp. 193-216.

30. Significance of Tests and Properties of Concrete and Concrete-Making Materials, ASTM Special Technical Publication No. 169-A, 1966.

31. Hsu, T. T. C.; Slate, F. O.; Sturman, G. M.; and Winter, G., "Microcracking of Plain Concrete and the Shape of the Stress-Strain Curve," ACI Journal, Proceedings Vol. 60, No. 2, Feb. 1963, pp. 209-224.

32. Theocaris, P. S., and Koufopoulos, T., "Photo-Elastic Analysis of Shrinkage Microcracking in Concrete," Magazine of Concrete Research, Vol. 21, No. 66, March 1969, pp. 15-22.

33. Slate, F. O., and Olsefski, S., "X-Rays for Study of Internal Structure and Microcracking of Concrete," ACI Journal, Proceedings Vol. 60, No. 3, May 1963, pp. 575-587.

34. Sturman, G. M., "Microcracking and the Structural Behavior of Plain Concrete," Ph. D. Thesis, Cornell University, Sept. 1963.

35. Hsu, T. T. C., "Mathematical Analysis of Shrinkage Stresses in a Model of Hardened Concrete," ACI Journal, Proceedings Vol. 60, No. 3, March 1963, pp. 371-390.

36. Hsu, T. T. C., and Slate, F. O., "Tensile Bond Strength Between Aggregate and Cement Paste or Mortar," ACI Journal, Proceedings Vol. 60, No. 4, April 1963, pp. 465-486.

37. Slate, F. O., and Matheus, R. E., "Volume Changes Upon Setting and Curing of Cement Paste and Concrete From Time Zero to Seven Days," ACI Journal, Proceedings Vol. 64, January 1967, pp. 34-39.

38. Richart, F. E.; Brandtzaeg, A.; and Brown, L., "A Study of the Failure of Concrete Under Combined Compressive Stresses," Bulletin No. 185, University of Illinois Engineering Experiment Station, Urbana, Ill., April 1929.

39. Jones, R., "A Method of Studying the Formation of Cracks in a Material Subjected to Stresses," British Journal of Applied Physics, (London), Vol. 3, No. 7, July 1952, pp. 229-232.

40. L'Hermite, R., "Present Day Ideas on Concrete Technology, 3rd Part, The Failure of Concrete," Bulletin No. 18, Union of Testing and Research Laboratories for Materials and Structures (RILEM), June 1954, pp. 27-38.

41. Rüsh, H., "Physikalische Fragen der Betonprüfring," (Physical Problems

in the Testing of Concrete), Zement-Kalk-Gips, Vol. 12, No. 1, 1959, pp. 1-9.

42. Shah, S. P., and Winter, G., "Inelastic Behavior and Fracture of Concrete," ACI Journal, Proceedings Vol. 63, No. 9, Sept. 1966, pp. 925-930.

43. Kaplan, M. F., "Strains and Stresses of Concrete at Initiation of Cracking and Near Failure," ACI Journal, Proceedings Vol. 60, No. 2, July 1963, pp. 853-879.

44. Taylor, M. A., and Broms, B. B., "Shear Bond Strength Between Coarse Aggregate and Cement Paste or Mortar," ACI Journal, Proceedings Vol. 61, No. 8, August 1964, pp. 939-958.

45. Goodier, J. N., "Concentration of Stress Around Spherical and Cylindrical Inclusions and Flaws," Journal of Applied Mechanics, Vol. 55, 1933, pp. 39-44.

46. Nielsen, K. E. C., "Internal Stresses in Concrete," RILEM Bulletin (Paris), New Series, Vol. 1, No. 1, March 1956, pp. 11-20.

47. Hast, N., "Measuring Stresses and Deformations in Solid Materials," Handlingar 178, Ingeniors Vetenskaps Akademiet, Stockholm, 1943.

48. Zaitsen, J. W., and Wittmann, F. H., "Fracture of Porous Visoelastic Materials Under Multiaxial State of Stress," Cement and Concrete Research, Vol. 3, No. 4, July 1973, pp. 389-395.

49. Naus, D. J., and Lott, J. L., "Fracture Toughness of Portland Cement Concretes," ACI Journal, Proceedings Vol. 66, No. 6, June 1969, pp. 481-489.

50. Kaplan, M. F., "Crack Propagation and the Fracture of Concrete," ACI Journal, Proceedings Vol. 58, No. 5, Nov. 1961, pp. 591-609.

51. Glucklich, J., "Fracture of Plain Concrete," Journal of the Engineering Mechanics Division, ASCE, Vol. 89, No. EM6, Paper 3715, Dec. 1963, pp. 127-138.

52. Glucklich, J., "On the Compression Failure of Plain Concrete," Dept. of Theoretical and Applied Mechanics--T. and A. M. Report No. 215, March 1962, University of Illinois, p. 31.

53. Glucklich, J., "Rheological Behavior of Hardened Cement Paste Under Low Stresses," ACI Journal, Proceedings Vol. 56, No. 4, Oct. 1959, pp. 327-338.

54. Lott, J. L., "Crack Propagation in Plain Concrete," Ph. D. Thesis, University of Illinois, August 1964.

55. Powers, T. C., The Properties of Fresh Concrete, John Wiley and Sons, Inc., 1968.

56. Griffith, A. A., "The Phenomena of Rupture and Flow in Solids," Philosophical Transactions of the Royal Society of London, Series A, Vol. 221, 1920, pp. 163-198.

57. Irwin, G. R., "Fracture Dynamics," Fracturing of Metals, American Society of Metals, Cleveland, Ohio, 1948.

58. Orowan, E., "Fundamentals of Brittle Behavior in Metals," Fatigue and Fracture of Metals (MIT Symposium, June 1952), John Wiley and Sons, Inc., New York, 1952, p. 154.

59. Jones, R., "A Method of Studying the Formation of Cracks in a Material Subjected to Stress," British Journal of Applied Physics, Vol. 3, No. 7, July 1952, pp. 229-232.

60. Brunauer, S.; Kantro, D. L.; and Weise, C. H., "The Surface Energy of Tobermorite," Canadian Journal of Chemistry, Vol. 37, 1959, p. 714.

61. Walker, R. D., Identification of Aggregates Causing Poor Concrete Performance When Frozen, NCHRP Report 12, Highway Research Board, 1965.

62. Krebs, R. D., and Walker, R. D., Highway Materials, McGraw-Hill, Inc., 1971.

63. Czernin, W., Cement Chemistry and Physics for Civil Engineers, Chemical Publishing Co., Inc., 1962.

64. Timoshenko, S., Strength of Materials Part II Advanced Theory and Problems, D. Van Nostrand Co., Inc., 1930.

65. Wang, C. T., Applied Elasticity, McGraw-Hill, Inc., 1953.

APPENDICES

APPENDIX A

PREVIOUS STUDIES OF CRACKING AND FREEZE-THAW DETERIORATION

Introduction

The purpose of this and the next three appendices is to acquaint the reader with the previously established theories and knowledge of cracking and deterioration in plain concrete. The next three appendices (B, C, and D) deal respectively with the subjects of cracking in plain concrete without external load, cracking in plain concrete due to a uniaxial compressive load, and cracking and deterioration in plain concrete due to freezing and thawing. The author has tried to present a thorough treatment of each subject and does not take credit for any material presented therein.

The processes of elastic and inelastic deformations, yielding, fracture, and freeze-thaw deterioration in concrete are slowly being studied. This is due to the complexity of the material which is caused chiefly by its large-scale heterogeneity. Concrete is not a homogeneous, linear, elastic, or isotropic material during any stage of its formation. However, research directed towards clarifying the nature, origin, and effects of the microcracking phenomenon caused by a compressive load and freeze-thaw action is now underway.

Although it is standard to consider coarse aggregates and mortar (cement plus water plus fine aggregate) to be the two phases of concrete, a different interpretation will be considered here. It has been observed by Hsu [31] and others that for concrete loaded in compression, microcracks

occur first in the bond between the coarse aggregate and the cement paste. This is followed by microcracks forming at the bond between the fine aggregate and cement paste. Thus, the size of the aggregate affects the ultimate strength of the concrete. Therefore, it is more reasonable to consider that the two phases of concrete are the cement paste (cement plus water) and all the aggregate, irrespective of size [32].

It has also been observed by Payne [13] that for concrete loaded in compression and subjected to alternating cycles of freezing and thawing, microcracks occur first in the coarse aggregate, at the capillary, provided the matrix has been properly air entrained.

Cracking can be classified into two general types: one form appears before the concrete hardens and the other form appears after the concrete hardens. The former cracks originate before any external load is applied, and the latter cracks usually develop as a result of an external compressive load or freeze-thaw action. Cracks occurring after the concrete hardens can also be attributed to thermal stresses at elevated temperatures, reversible fatigue loadings, long-term deflections, camber in prestressed concrete, oxidation of reinforcing bars, flexural stress due to bending, and differential movement in the structure. These last seven causes of cracking are not specifically related to this research and will not be discussed. It can be noted, however, that these surface cracks or any type of surface crack will allow water to enter the concrete and be available for freeze-thaw action.

APPENDIX B

CRACKING IN PLAIN CONCRETE WITHOUT EXTERNAL LOAD

Types of Cracks and Voids

This section is concerned with cracks produced by volume changes which occur in concrete independently of externally imposed stresses and freezing temperature changes. Additional cracks and voids may also be present in the material due to other independent influences. The majority of microcracking occurs during the first five or six hours after the concrete has been placed. This is the period during which the largest volume change takes place.

Bond Cracks

Bond cracks are cracks which occur at the interface between aggregate particles and the surrounding mortar matrix. They exist to a sizeable degree in plain concrete before any external load is applied [31]. Orientation of these cracks indicate that some of them are caused by mortar settlement or segregation [33]; however, the majority are evidently not due to settlement, but must be caused by other influences. Such influences may cause tensile or shear cracks or a combination of both to develop from internal stresses caused by volume changes (shrinkage or expansion) of the mortar during setting and hardening.

In 1963, Hsu, Slate, Sturman, and Winter [31] were the first to directly observe the internal microscopic cracks or flaws in unstrained hardened concrete specimens by radiographic and microscopic techniques. They suggested that the microcracks developing from volume changes inside the concrete may be formed by a variety of processes. These processes included

drying shrinkage, carbonation shrinkage, hydration shrinkage, hygrothermal volume change, and segregation due to settlement.

Surface Cracks

Surface cracks, as the name implies, are cracks which occur on the surface of the member. They can be caused by drying shrinkage or by swelling (negative shrinkage) of the member.

Internal Matrix Cracks

Internal matrix cracks (also called mortar cracks) are cracks which develop specifically within the cement matrix (mortar). They are also caused by various shrinkage and volume change mechanisms.

Natural Cracks in Aggregate Particles

These cracks exist in aggregate particles before the aggregate is combined into the concrete mixture. They are caused by weathering processes or by quarrying and handling practices.

Natural Voids

Natural voids exist in the form of entrapped water or air voids of various sizes scattered throughout the concrete, on and beneath the surface. The greatest majority of them, except for some of the largest, have circular cross sections and, thus, are sections of spheres. Some voids may also resemble an irregular honeycomb shape. Natural voids are caused by improper mixing, molding and vibrating techniques.

Air Entrained Voids

Air entrained voids are intentionally impregnated into the concrete

mixture. Too much entrained air can give the concrete a swiss cheese-like appearance. This results in the concrete exhibiting a low strength and a poor resistance to weathering--the very reason for incorporating air.

Shrinkage and Volume Change Mechanisms

Drying Shrinkage

The most common flaw appearing in freshly placed concrete is plastic cracking due to drying shrinkage. This type of cracking takes place before the concrete hardens. The cracks begin to form soon after the concrete is placed and while it is still plastic. Plastic cracking appears most frequently on horizontal surfaces. The cracks take no particular shape, direction, or pattern. The external surface of the member is affected more than internal regions.

The cracks are produced when the surface of newly placed concrete dries too rapidly. Drying, in turn, occurs too quickly when the evaporation rate of water from the surface of fresh concrete exceeds the bleeding rate. Thus, the rate of evaporation is an important factor in determining whether or not cracks will form.

As the concrete begins to set, water rises from within the mixture to its surface. This process is known as bleeding. It keeps the surface damp, even though evaporation is continuously taking water away. Under ideal conditions, bleeding replaces the water that evaporates. Fewer shrinkage cracks will develop if bleeding and evaporation are consistent with one another. Bleeding may also cause water channels to form around some aggregate particles. These channels encourage the infiltration of water and aggressive fluids into the concrete which will lead to swift

deterioration.

The loss of free water, which takes place first, causes little or no shrinkage. As drying continues, adsorbed water from bleeding is removed and the change in the volume of unrestrained cement paste at that stage is equal approximately to the loss of a water layer one molecule thick from the surface of all gel particles [22].

The factors affecting drying shrinkage are numerous. As mentioned, the rate of evaporation is a major factor which depends on wind, air temperature, relative humidity, and the temperature of the concrete. Another important factor is the influence of aggregate, which restrains the amount of shrinkage that can actually occur. The properties of cement have little influence on the drying shrinkage of concrete. The water content of concrete affects drying shrinkage in so far as it reduces the volume of restraining aggregate. Thus, in general, the water content of a mix would indicate the order of shrinkage to be expected.

Hydration Shrinkage and Hygrothermal Volume Change

The volume changes due to hydration and hygrothermal variation may take place simultaneously; in fact, it is difficult to separate the effects of these two phenomena. Both hydration and hygrothermal changes may cause either contraction or expansion of the mortar volume.

During the setting and hardening of most cements, hydration shrinkage takes place because the volume of materials decreases due to the change in the structure of the water-cement combination. In other words, the hydrated gel is more dense than cement grains plus free water [34]. Most normal cements decrease in volume during hydration; however, some cements of

special composition expand during hydration. These are referred to as expanding or non-shrinking cements.

Shrinkage or expansion of cement pastes due to the migration of water to and from the paste is known as hygrothermal volume change [34]. There are many theories on this phenomenon, but none as yet have been accepted.

Since the volume changes taking place in the cement during the early stages of hydration have not yet been fully ascertained, it is difficult to reach a conclusion regarding the effect of volume variations on the initiation of cracks during curing. It has been recently suggested that cement starts of expand during the first few hours of hardening and then begins to shrink.

It can be concluded, however, that a stress field is spread over part of the aggregate-mortar interface which has been proven to create exclusively bond cracks. After these bond cracks are developed, the stress is relaxed in this area of the interface. The volume change due to drying shrinkage is smaller during the first 28 days after placing than that produced by hydration shrinkage during the first few hours after placing [34].

Carbonation Shrinkage

In addition to shrinkage upon drying, concrete also undergoes shrinkage due to carbonation.

When any cement product is exposed to air, the carbon dioxide present in the atmosphere reacts, in the presence of moisture, with hydrated cement minerals to be converted into calcium carbonate, hydrated silica, alumina, and ferric oxide. This action, under ordinary conditions, is limited to the

exposed surface of mortars or concretes; and carbonation penetrates extremely slowly beyond the exposed surface of concrete only. It rarely penetrates into the inner mass. Thus, carbonation of large concrete members will simply be limited to the surface layer representing a small proportion of the total mass. It does not appear that carbonation shrinkage causes internal microcracking.

Carbonation is accompanied by an increase in the weight of the concrete and by shrinkage. Carbonation shrinkage is probably caused by the dissolving of crystals of $Ca(OH)_2$ while under a compressive stress (imposed by the drying shrinkage) and the depositing of $CaCO_3$ in spaces free from stress; the compressibility of the cement paste is thus temporarily increased [22].

Segregation Due to Settlement

Sturman [34] explained segregation due to settlement in the following manner. Mortar, consisting of cement paste, sand, and water, undergoes a dormant period lasting from 40 to 120 minutes after the components are mixed. Since the mixture normally remains plastic during this period, the suspended particles are free to settle. In 1939, Powers hypothesized that bleeding, which is revealed by the appearance of almost clear water at the surface of freshly placed concrete, is essentially a sedimentation phenomenon, or the solids settling in the plastic mass. He also stated at that time that the laws of liquid flow in a capillary system were comparable to those governing the bleeding phenomenon. However, in 1960, Powers indicated that simple settlement due to gravity was the cause of sedimentation and bleeding in cement pastes.

Slate [33] has investigated the influence of segregation due to settle-

ment on the formation of microcracks by testing the hypothesis that sedimentation leads to microscopic voids at the bottom surface (as placed) of large aggregate particles. These discontinuities have the characteristics of a crack in that they are thin and elongated. This is in contrast to other flaws in concrete, such as spherically entrained air bubbles. It was found that cracks at the bottom surface of the aggregate were larger and more numerous than at any other location. In addition, these cracks seem to occur particularly where the aggregate particles form "bridges" supported by other aggregate particles below. Thus, it was possible to distinguish the cracks due to sedimentation only by their location at the bottom surface of the aggregate.

This sedimentation phenomenon does not account for all of the observed preload microcracks. The remaining cracks, while less numerous, are present in sufficient quantity and size to be of major importance. The main cause of these cracks appears to be shrinkage due to hydration and drying [34].

Swelling

Swelling of the concrete which is a negative shrinkage, can occur when it is cured continuously in water from the time of molding. This concrete exhibits a net increase in volume and an increase in weight. Moist-cured concrete has an ultimate expansion which is usually less than 0.025 percent [19]. The swelling is due to the adsorption of water by the cement gel: the water molecules act against the cohesive forces and tend to force the gel particles further apart, with a resultant swelling pressure. In addition, the ingress of water decreases the surface tension of

the gel, and further expansion takes place [22]. Swelling is also responsible for bond cracks and internal matrix cracks.

Autogenous Volume Change

Volume changes without a loss of moisture from the body of the concrete also occur after setting has taken place and may be in the form of shrinkage or swelling. Continued hydration, when a supply of water is present, leads to expansion of the concrete. However, when no moisture movement to or from the paste is permitted, and the temperature is constant, some shrinkage may occur. Shrinkage of such a conservative system is known as autogenous volume change or autogenous shrinkage [22]. For practical purposes, autogenous shrinkage need not be distinguished from drying shrinkage, which normally includes that contraction which is due to autogenous changes.

Effects of Volume Change on Cracking

Hsu's Hypothesis

Even if concrete has been kept wet continuously from the time it was molded, tensile stresses develop at the interface between coarse aggregate particles and the cement mortar. These stresses cause the development of microcracks at the interface during the curing period of concrete and before any application of load. The fact that significant random bond cracking, other than from settlement, exists in hardened concrete prior to loading, Hsu [35] believed that these no-load bond cracks are probably coresponsible for the low tensile strength of concrete and certainly have some bearing on other physical properties of concrete. The appearance of

no-load bond cracks can be explained only [35]:

1. If the tensile-bond strength at the interface between aggregate and mortar is weaker than the strength of the mortar itself.

2. If tensile and/or shear stresses of sufficient magnitude exist to cause this interface bond to fail.

Many tests reported by Hsu and Slate [36] show Proposition 1 to be true. Proposition 2 seems to be contradicted by the prevailing opinion concerning the stresses at the aggregate-mortar interface, which are generated by the volume shrinkage of the mortar. It is generally thought that such shrinkage produces compression on the interface. That is, volume shrinkage in the mortar produces radial compression in the aggregate and circumferential tension in the mortar, a situation which should lead to mortar cracks and should prevent the presence of bond cracks [35]. This is contrary to the observations made by Hsu.

To investigate the stresses which may be responsible for no-load cracks, Hsu [35] constructed a mathematical model of hardened concrete consisting of rigid circular discs arranged in a square array and surrounded by a medium subjected to volume change. The rigid circular discs represent the aggregate particles and the surrounding medium represents the mortar. A numerical, elastic stress analysis of this model by a point matching method showed that large tensile, compressive, and shear stresses at the aggregate-mortar interface are caused by changes in the volume of mortar when the clear distance between the aggregates is less than about 0.2 of the aggregate radius. Volume changes in the mortar can be produced by hydration, wetting and drying, temperature changes, or any of the other mechanisms previously discussed. It was conjectured by Hsu that these interfacial tensile stresses cause bond cracks to appear and that these

stresses are caused chiefly by volume changes in the mortar due to setting.

The model proposed by Hsu [35] can also be related to the mechanism which is operative when concrete disintegrates due to alternating cycles of wetting and drying. Since each cycle results in volume changes, corresponding stresses are produced in each cycle. Thus, the model showed that concrete can disintegrate when subjected to cycles of wetting and drying. In the same manner, concrete can disintegrate due to temperature changes, i.e., due to the stresses produced by differential volume changes between the mortar and aggregate in each temperature cycle.

Information on volume change during hydration and on tensile bond strength at an early age before the concrete sets was not available to Hsu. Thus, it was difficult to give a conclusive statement about the effect of volume change during hydration on the existence of bond cracks. Whether the cement mortar shrinks or expands during hydration is still controversial.

The important conclusions drawn by Hsu in investigating the stresses which may be responsible for no-load cracks were as follows [35]:

1. An extensive investigation of microcracking in concrete showed that significant microcracking existed in hardened concrete before application of any load. Examination showed that most of these cracks were at the interface between mortar and coarse aggregate particles, rather than in the mortar.

2. It was conjectured that these interface tensile stresses cause the described microcracks to appear, chiefly due to volume change during hydration. If the cement mortar expands during hydration, bond cracks should occur without any possibility of mortar cracks. If the cement mortar shrinks during hydration, bond cracks should occur with possible simultaneous mortar cracks.

3. Similar stresses will also be caused by volume changes due to wetting and drying or temperature changes and are believed to be responsible for the observed disintegration of concrete when subjected to cycles of such changes.

Check on Hsu's Hypothesis

In order to check the hypothesis given by Hsu that no-load cracks were formed by volume changes of mortar (or paste) during setting and hardening, an investigation was conducted by Slate and Matheus [37]. Unrestrained bulk volume changes of portland cement paste and concrete from the time of molding (time zero) to an age of seven days were determined by measuring the volumes of displaced liquids. Two extreme conditions were examined: under water where an unlimited amount of free water was available, and under oil where no free water was available.

The conclusions drawn from this investigation were as follows [37]:

1. Cement paste and concrete have autogenous, isothermal volume changes (shrinkage or expansion) of up to one percent within the first 24 hours, depending on the curing conditions.

2. Both cement paste and concrete expand during setting if they are completely submerged under water from the time of molding. The volume increase was from 0.1 to 1.5 percent, with almost the entire change completed within 24 hours for small specimens.

3. When submerged in oil to prevent a gain or loss of water, concrete from time zero, and cement paste from about six hours (after a small initial expansion), shrank continuously with a decreasing rate of change throughout the seven-day period.

4. The volume changes that occur on setting and curing of concrete that is not immersed in water should, and probably do, cause appreciable microcracking.

It was shown in the work of Hsu [35] that a linear shrinkage coefficient of about 0.001 corresponding to a volume change of about 0.3 percent is enough to create interface tensile stresses of the order of 1800 psi. Since the work of Slate and Matheus shows that volume changes even larger than 0.3 percent do occur at an early age, it seems likely that no-load bond cracking may be caused, at least in part, by volume changes during setting and hardening.

Studies of Tensile Bond Strength

To determine whether the tensile stresses produced by the volume changes were sufficient to cause forcible separation of the paste-aggregate or mortar-aggregate bond, Hsu and Slate [36] studied the tensile bond strength between the paste-aggregate and mortar-aggregate interface and related it to the tensile strength of the paste or mortar itself.

Direct tensile bond strength between aggregate and paste or mortar was found to be significantly less than the tensile strength of the paste or mortar itself. It was also found to be dependent on rock type, water-cement ratio, and the surface roughness of the aggregate.

The strength of bond between mortar and aggregate seems to be the weakest link in the strength of concrete [36]. However, little information about bond strength, especially direct tensile bond strength, was available until the work done by Hsu.

Hsu [36], in studying the tensile bond strength at the interface between aggregates and cement paste (or mortar), listed many factors which may affect this strength, such as:

1. Mineralogical characteristics of the aggregates.
2. Water-cement ratio of the cement paste (or mortar).
3. Surface roughness of the aggregates.
4. Age of the cement paste and therefore of the bond.
5. Moisture content of the specimens at the time when they were tested under load.
6. Moisture content of the aggregates at the time when the specimens were poured.
7. Type of cement.
8. Size of the aggregates.

The conclusions drawn by Hsu and Slate were as follows [36]:

For the paste-aggregate tensile bond strength and strength of cement paste:

1. In general, the paste-aggregate tensile bond strength varies from 41 to 91 percent of the tensile strength of paste depending on the rock type, the surface roughness of the aggregate, and the water-cement ratio.

2. Surface roughness of aggregate influences the bond strength. The extent of influence depends on rock type.

3. Paste-aggregate tensile bond strength decreases rapidly with increasing water-cement ratio (ratios from 0.265 to 0.360).

For the mortar-aggregate tensile bond strength and strength of mortar:

1. In general, the mortar-aggregate tensile bond strength varies from 33 to 67 percent of the tensile strength of mortar depending on the rock type and the water-cement ratio.

2. Both the mortar-aggregate tensile bond strength and the tensile strength of mortar decreases quite slowly with increasing water-cement ratio (ratios from 0.360 to 0.750), much more slowly than does the compressive strength of mortar or concrete.

3. When tensile specimens were air-dried (after full moist curing) before being tested, the strength was less than for specimens tested wet.

4. The mathematical analysis by Hsu indicated that for a drying shrinkage of about 0.001, the elastic tensile bond stress in his two-dimensional model may be as high as 1800 psi. In actual three-dimensional concrete, tensile stresses are probably of the same order of magnitude and thus may be 5 to 15 times the mortar-aggregate tensile bond strength. Consequently, they appear to be large enough to result in failure of the interface bond and to cause bond cracks to appear.

APPENDIX C

CRACKING IN PLAIN CONCRETE DUE TO A UNIAXIAL COMPRESSIVE LOAD

Existence of Microcracks

There is considerable evidence to show that microcracks occur in concrete when loaded. It has long been known that microcracking occurs at loads and strains well below the ultimate. The details of the process of microcracking seem to be related to the stress-strain curve of the material and other relevant properties [31].

In 1929, Brandtzaeg [38] first suspected the presence of microcracks and the progressing of internal cracking in concrete specimens under a compressive load. He observed the volumetric changes of plain concrete cylinders in uniaxial compression. He also found that at a "critical load" (the load at which the volume of concrete under increasing compressive load begins to increase rather than continue to decrease) of 75 to 85 percent of the ultimate load, the volume started increasing rather than decreasing. Brandtzaeg made the fundamental assumption, in developing a failure theory for concrete, that the critical load signals the beginning of progressive internal cracking in microscopic regions distributed throughout the concrete. In the same work, it was conjectured that the shape of the stress-strain curve was related to this internal cracking; and that the curvature was due to the rapid expansion of the material.

In 1952, Jones [39] found a change in the sonic velocity through concrete loaded to 25 to 30 percent of the ultimate load. This indicated

that at a relatively low level of stress, there was formation of internal microscopic flaws or cracks.

In 1954, L'Hermite [40] found similar results using the sonic velocity method. By means of a microphone, he observed a "crackling noise" at 50 to 75 percent of the ultimate load.

In 1959, Rüsch [41], using sonic methods, gave an indication of the initiation of microcracks when crackling noises began to increase rapidly at almost 75 percent of the ultimate load. He also noted that this load corresponded to the long-time sustained strength of plain concrete.

Several researchers have implied that the shape of the stress-strain curve is related to irreversible microcracking, but none of them have actually observed this phenomenon. However, in 1963, Hsu, Slate, Sturman, and Winter [31] used direct observation to observe this microcracking and identify its nature. Direct observation was desired since it gave precise information pertinent to the mechanism of cracking, of inelastic deformation, and of eventual failure. Hsu et al. observed that there was a noticeable increase in bond cracks at 30 percent of the ultimate load, and that mortar cracks began to increase at 70 to 90 percent of the ultimate load.

Other researchers have made similar observations which indicate the presence of cracks at a load very much less than that required to cause ultimate failure of the concrete. The initiation and propagation of these small cracks are considered to have an important influence on the fracture strength of concrete.

Listed in Table C.1 [31] are the loads where microcracking begins and the critical loads observed by various investigators.

TABLE C.1 INDIRECT CRACK OBSERVATIONS BY VARIOUS INVESTIGATORS

Investigator	Load Where Microcracks Start	Critical Load
Brandtzaeg	--	0.75 to 0.85 P_{ult}
Berg	Cracks first observed on the surface of concrete specimens at 0.55 to 0.60 P_{ult}	--
Jones (sonic)	0.25 to 0.30 P_{ult}	--
L'Hermite (sonic)	"Crackling noise" at 0.50 to 0.75 P_{ult}	--
Hognestad	--	0.71 to 0.96 P_{ult}
Rüsch	Noise begins at 0.50 P_{ult}	Noise increases at 0.75 P_{ult}
Hsu et al.	Bond Cracks at 0.30 P_{ult}	0.70 to 0.90 P_{ult}

The author believes that these cracks are of some importance in the initiation of deterioration in concrete subjected to freezing and thawing.

Types of Cracks

Bond Cracks

As previously mentioned, these microcracks which originate during setting and hardening and even at low stress levels develop along the interface between the coarse aggregate and surrounding mortar matrix. The length and number of these bond cracks increase as the stress level increases due to the application of an externally applied load.

The bond cracks at the aggregate-matrix interfaces can be caused either by tensile or shear stresses. The tension type of bond crack occurs when the maximun tensile stress at the aggregate-matrix interface reaches the tensile bond strength of the interface. This mechanism of microcracking causes partial separation of the aggregate from the surrounding matrix. The tensile bond strength of aggregate-matrix interfaces has been investigated by Hsu and Slate [36] and discussed in the previous appendix (Appendix B, under the section entitled Studies of Tensile Bond Strength). The shear type of bond crack tends to develop when the maximum shear stress along the aggregate-matrix interface reaches the shear strength of the interface. This mechanism of microcracking is concerned with sliding at the interface rather than separation. The shear bond strength between coarse aggregate and mortar will be discussed in a later portion of this appendix (under the section entitled Strength of an Unconfined Interface).

The bond cracks which develop during setting and hardening are

probably a result of the high normal and shearing stresses which have been shown by Hsu [35] to exist in concrete which is undergoing volume changes. These volume changes were discussed in Appendix B.

Surface Cracks

Cracks can appear on the surface of a member when it is subjected to a compressive load. This is a very susceptible area since there is no external restraint to prevent their formation.

Pavement and slab surfaces are designed to carry all types of indirect compressive loads. Because of this, the aggregates used are of considerable importance. Since most natural aggregates such as quartz, quartzite, and granite are hard, brittle materials, they are unable to withstand the abuse, abrasion, and impact to which such pavements containing these materials are exposed to in service. The aggregates at the surface crack and shatter causing surface cracks. In addition, since hardened cement mortar has very little abrasion resistance, it soon pulverizes causing cracks.

Internal Matrix Cracks

Hsu et al. [31] found that internal matrix cracks or mortar cracks almost always bridge between nearby bond cracks, and usually where the distance between coarse aggregate particles is relatively small. In addition, the mortar cracks tend to bridge between bond cracks on large aggregates in preference to those on small aggregates.

Mortar cracks are negligible before the concrete is subjected to any external load. However, as the peak strength of the concrete is approached during loading, mortar cracks develop within the concrete

matrix. These mortar cracks begin to increase noticeably at strains of 0.0012 to 0.0018 inches per inch [31]. As the stress level continues to rise, mortar cracks increase rapidly in length and in number. Failure and disintegration of plain concrete loaded in uniaxial compression takes place when the bond and mortar cracks join to form a single or a number of rupture surfaces throughout the concrete.

Cracking Through Aggregate Particles

Only a small number of cracks go through aggregate particles when the ends of the loading device are free from creating a triaxial state of stress. However, when this state of stress exists on the ends, there is a large amount of failure through the aggregate. Compression loading with restrained ends may force final shear failure through some of the coarse aggregate, after an extensive network of other cracks have been formed prior to the final disruptive failure [31].

Creep Cracks

Bond cracking and mortar cracking can also be caused by creep. The slow crack growth anywhere throughout the concrete under sustained loading is probably associated with creep. Stress concentrations around the tip of a crack must invariably cause creep in the cement paste. The crack will continue to grow until it reaches an equilibrium position where the stress concentrations are insufficient to propagate the crack [4].

Compressive Microcracking Mechanism

This is the first of two crack formation and propagation mechanisms associated with concrete. Experimental evidence in recent years has

suggested that the shape of the stress-strain curve of a plain concrete specimen loaded in compression is related to the internal development of microcracks. Progressive development of microcracks with increasing external load has been indirectly detected by sonic and ultrasonic methods, by the measurement of changes of Poisson's ratio, by surface cracking, and by radiographic and microscopic examination. This existence of microcracks has already been discussed. Now the cracks will be related to the stress-strain curve and the inelastic behavior of concrete.

Typical Stress-Strain Curve

Performance of a structure under load depends to a large degree on the stress-strain relationship of the material from which it is made. Since concrete is used mostly in compression, its compressive stress-strain curve is of primary interest. Figure C.1 shows a typical stress-strain curve for plain concrete.

The relationship between stress and strain of hardened concrete subjected to short time uniaxial compression can be divided into three performance ranges. The typical stress-strain diagram consists of an initial relatively straight (linear), elastic portion in which stress and strain are closely proportional. This linear portion stretches to about 30 percent of the ultimate load. Several authors call this point the "proportional limit" of concrete. Beyond this point, the curve deviates gradually from a straight line (becomes non-linear), with strain increasing more rapidly than stress. Above 70 percent of ultimate, the strains become excessive, and the curve climbs toward the horizontal up to a certain stress which is called the maximum stress or the "critical

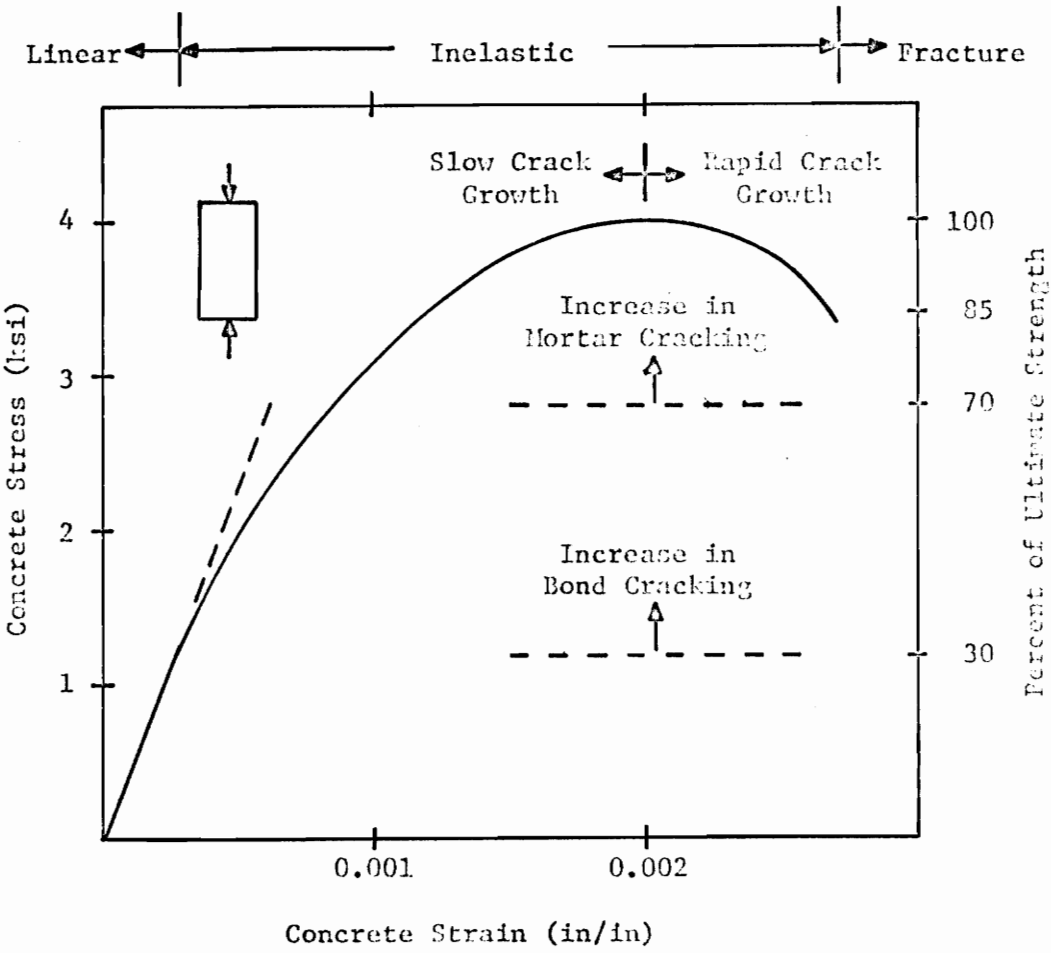

FIGURE C.1 TYPICAL STRESS-STRAIN CURVE OF PLAIN CONCRETE LOADED IN UNIAXIAL COMPRESSION

load" (this is the ultimate compressive strength of the concrete at a strain of approximately 0.002 inches per inch). Having reached a peak, the stress-strain curve begins to bend away from the horizontal with decreasing stress corresponding to increasing strain. The curve finally ends in a descending tail where failure eventually occurs. Failure is assumed to occur at 0.85 of the ultimate compressive stress.

It will be noted that the strain occurring near maximum stress is nearly the same for all strengths of concrete, being roughly 0.002 inches per inch as mentioned.

It has been proven conclusively that the stress-strain curve for the compression face of a beam is essentially identical with that for a standard compression test cylinder.

Cracking Related to the Stress-Strain Curve

In order to understand the nature, origin, and effects of the microcracking phenomenon, Hsu, Slate, Sturman, and Winter [31] investigated the case of plain concrete in concentric (uniaxial) compression. They studied the response of concrete from zero load through the elastic, inelastic, and descending ranges of the stress-strain curve to fracture. Cylinders were strained to various preselected strain values, then unloaded and prepared for microcrack observation. This observation was performed by radiographic and microscopic examinations of thin sections of concrete. The information was then used to relate the shape of the stress-strain curve of concrete in compression to the type and extent of microcracking. Progressive cracking with increasing strain had been indirectly observed by measurements of changes in Poisson's ratio, by

surface cracks, and by sonic methods. However, no investigators had directly examined a cross section of concrete to identify the nature of cracking until Hsu et al. did in 1963.

The results drawn by Hsu et al. for the shape of the stress-strain curve by microcrack development are as follows [31]:

1. Bond cracks exist even before the concrete is subjected to any load while mortar cracks remain negligible until a later loading stage.

2. Above about 30 percent of the ultimate load, the bond cracks begin to increase appreciably in length, width, and number. At this load, the stress-strain curve begins to deviate noticeably from a straight line.

3. In general, bond cracks occur first around the larger aggregate particles. Thus, the larger the aggregate, the weaker the bond strength. Cracks rarely penetrate through the aggregates. However, it is possible that for less strong aggregates, cracks would penetrate rather than detour around them.

4. At about 70 to 90 percent of the ultimate load (or at strains of 0.0012 to 0.0018 inches per inch), the number of cracks through the mortar begins to increase noticeably. By bridging between bond cracks, a continuous crack pattern begins to form. The formation of continuous crack patterns at about 70 to 90 percent correlates well with the fact that at this load the volume of concrete under increasing compressive load begins to expand rather than continue to contract. The load at which this change occurs is called the "critical load." At about 70 percent of the ultimate load the stress-strain curve begins to curve more sharply to the horizontal, indicating the beginning of the breakdown of the internal structure.

5. The total extent of mortar cracking is considerably less than that of bond cracking at all stages of straining. Thus, the size and proportion of coarse aggregate should have an effect on the strength of concrete. The curvature of the stress-strain curve increases with an increasing amount of coarse aggregate in the concrete.

6. The peak of the stress-strain curve occurs when microcracks are sufficiently interconnected by mortar cracks so that the remaining load paths are inadequate to carry the increasing load.

7. On the descending branch of the stress-strain curve, the concrete

> is extensively cracked. The amount of cracking is greater when the slope of the stress-strain curve is steeper. The descending branch of the curve of uniformly compressed, plain concrete represents a disintegration of internal structure, as is shown by the extensive interconnecting of mortar and bond cracks.

These facts can be summarized as follows: in the initial or linear range there is no appreciable increase in the observed microcracks. In the second range, at about 30 percent of ultimate strength, interfacial cracks begin to increase substantially in length, width, and number. Slow mortar crack growth does not increase noticeably until 70 to 90 percent of the ultimate strength. Beyond the critical load, extensive, rapid crack growth is associated with descending stress and leads to ultimate failure of the concrete. Figure C.1 also shows the three ranges of the stress-strain curve.

Inelastic Behavior

Inelastic behavior of concrete can be defined as that behavior in which the response of concrete to an externally applied load is non-linear and irreversible. Deformations due to creep are very small in comparison to those caused by the load.

Origin of inelastic deformations

The inelastic behavior of concrete in uniaxial compression can be seen in Figure C.2 where the typical longitudinal, lateral, and volumetric strain distributions are shown. It can be seen that these strains all obey the laws of classical elasticity up to a certain proportion of the uniaxial compressive strength. Beyond the load level (or stress level) designated X, the longitudinal strain begins to increase faster with stress than before. Also, the lateral strain begins to increase

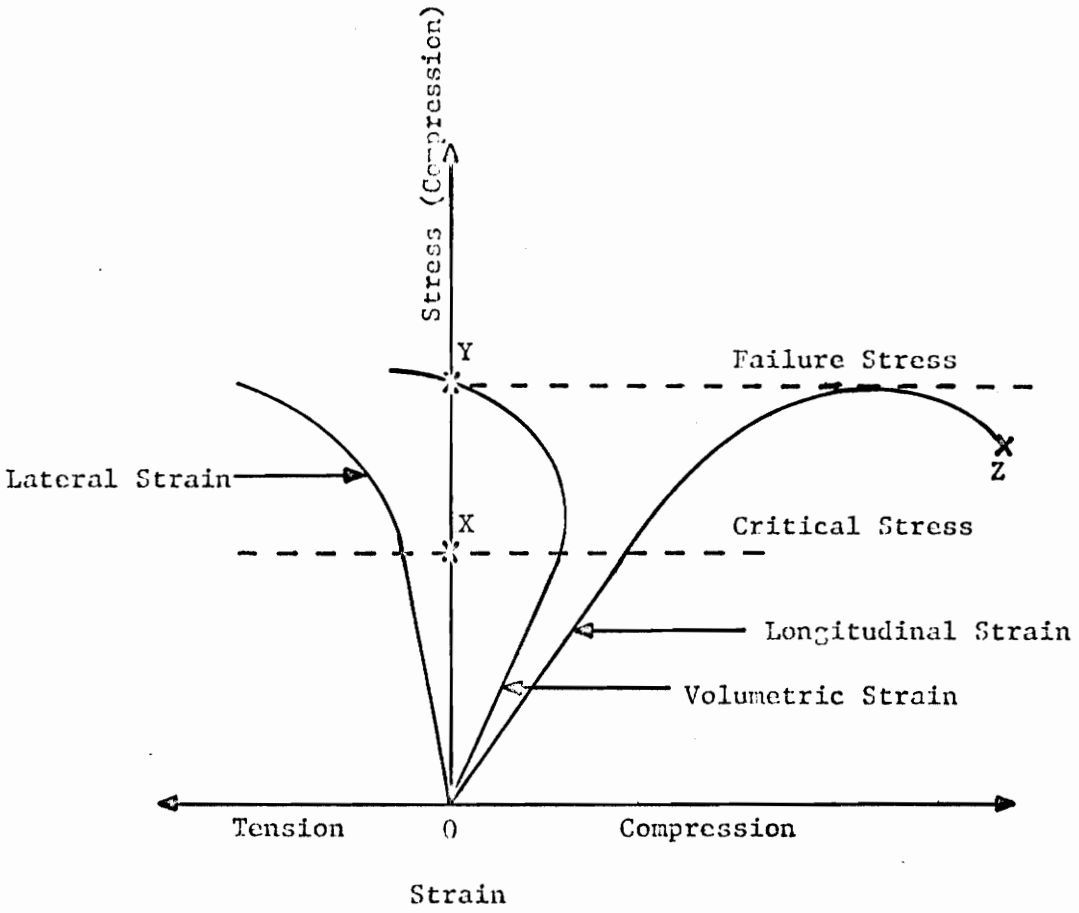

FIGURE C.2 DEVELOPMENT OF STRAIN IN CONCRETE UNDER UNIAXIAL COMPRESSION

rapidly, while the volumetric strain decreases and may eventually reverse itself. At the load level designated as Y, the specimen approaches its maximum strength, and the appearance of cracks parallel to the direction of the compressive load can be seen. At point Z, there is failure of the material. The inelasticity and non-linear stress-strain behavior are due to irreversible microcracking.

Poisson's ratio and volume changes have been related to compressive microcracking. For short-term static loading, Poisson's ratio remains constant up to a certain stress level, after which it starts to continuously and significantly increase. At a somewhat higher short-term static stress (critical stress) the volume of the concrete starts to increase rather than decrease. Similar behavior is not exhibited by either paste or aggregate; therefore, this inelastic behavior must be related to the composite nature of concrete.

To understand the response of concrete when it is loaded, Shah and Winter [42,4] studied the behavior of each of its components. They determined the stress-strain relations of hardened cement paste, aggregate, mortar, and concrete subjected to uniform compression up to failure. Figure C.3 shows typical stress-strain curves of hardened cement paste, aggregate, mortar, and concrete up to failure of each material.

From these curves the following conclusions can be drawn [42]:

1. The aggregate and hardened cement paste are almost wholly elastic materials.

2. Under load, concrete behaves inelastically, even though its constituents above are elastic.

3. The stress-strain curves for aggregate and hardened cement paste in compression are almost linear up to fracture.

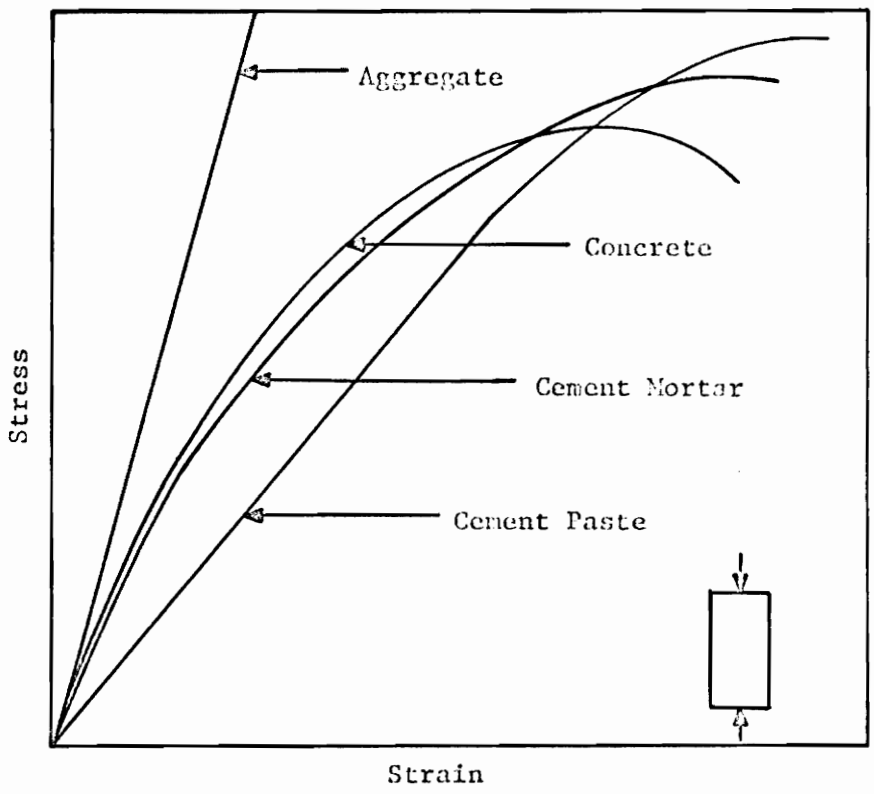

FIGURE C.3 TYPICAL STRESS-STRAIN CURVES FOR AGGREGATE, PASTE, MORTAR, AND CONCRETE

4. The stress-strain curve for mortar exhibits a shape similar to that of concrete. However, it does not bend as sharply to the horizontal as the curve for concrete. Also, for mortar, the stress-strain curve is more curved and the compressive strength is smaller than for paste of the same water-cement ratio.

5. In turn, the stress-strain curve for concrete is more curved and the compressive strength is smaller than for mortar of the same water-cement ratio.

From this it follows that since the material of most aggregate particles and cement paste exhibits a reasonably linear stress-strain relation, the departure of the stress-strain diagram of concrete from a linear curve (or in other words, its inelastic behavior) can be attributed chiefly to the presence of aggregates and the interfaces between the cement paste and these aggregates. Or, more specifically, it can be attributed to the development of internal microcracks at these interfaces. However, some creep probably also takes place producing a few additional microcracks.

The relationship between inelasticity and the presence of aggregates in concrete is also indicated by Kaplan's [43] observation that the higher the percentage of aggregates (with the same water-cement ratio), the lower the value of strain at which the stress-strain curve departs from a straight line.

Since mortar is weaker than either aggregate or cement paste alone, and since concrete is weaker than mortar, the bond between cement mortar and aggregate is likely to be a weak link in the heterogeneous concrete system. Consequently, one might suspect that the presence of aggregates produces inelasticity in concrete as a result of a relative weakness in the aggregate-matrix interfaces. This idea has been presented in the previous section by the investigations of Hsu et al. [31] (the section

entitled Cracking Related to the Stress-Strain Curve). Many other investigations have also determined that cracking arises from the spread of microcracks along the boundaries of the coarse aggregate. All this evidence strongly suggests that the bond between mortar and aggregate is the weak link in the concrete system, and that this interfacial bond is mainly responsible for the inelastic behavior of concrete under short-time loading. Therefore, in order to better understand the cause and mechanism of microcracking, it is desirable to study the behavior of the mortar-aggregate interface.

Stress-Strain Behavior of a Confined Interface

Since the behavior of concrete under an external short-time load seems to be significantly influenced by the interfacial bond, a study of stress-strain behavior at the interface between mortar and aggregate was undertaken by Shah and Winter [42,4]. The specimens prepared consisted of an inclined stone slab with mortar surrounding it. Three different inclinations of the stone slab were selected: 23, 42, and 50 degrees. The specimens can be structurally divided into two zones: the central zone containing the stone slab which represents the influence of the interface and the exterior zone of mortar surrounding the slab which simulates the effect of confinement to which an interface is subjected to in a real concrete mass.

The following observations were made for the specimens with the stone inclined at 23 degrees [42]:

1. When compressive loading is applied to the specimen, strains are uniform until the unconfined bond strength of the interface is reached.

2. When the unconfined bond strength is exceeded, a bond crack is formed at the interface.

3. With increasing load on the specimen, the cracked interface behaves essentially plastically. That is, after the appearance of the bond crack, the interface continues to carry more or less the same load at which the bond crack was formed.

4. When cohesion is lost by bond crack formation, there would have been sliding at the interface had it not been confined by the mortar in the exterior zones. This prevention of sliding produces tensile stresses and, hence, local vertical cracks in the mortar at the top and bottom ends of the stone. The formation of these cracks allows minute sliding to occur at the interface.

5. After the appearance of a bond crack, the increase in load on the specimen is carried entirely by the exterior zones. The specimen fails when the compressive strength of mortar in the exterior zones is reached, resulting in the crushing of the cement mortar.

Strength of an Unconfined Interface

It has just been shown that crack propagation and slip along an interface of an aggregate particle in concrete is affected by the confinement provided by the surrounding mass of mortar. An understanding of this complex behavior is facilitated if the behavior of an interface is studied in the unconfined state.

Taylor and Broms [44] investigated the strength of the unconfined interface of several specimens with different values of inclination of the interface. Shear and normal stress along the interface at failure were calculated from known inclinations and measured failure loads. For different interface inclinations they gave straight line plots. These results show that the bond strength in an unconfined interface obeys the Coulomb-Mohr failure theory. If the cohesion and friction angle are known, the unconfined strength of the interface can be reasonably pre-

dicted. Thus, the cohesion and friction angle are basic material properties. They depend on the mineralogical and surface characteristics of the aggregate and the composition of cement paste or mortar.

The results obtained by Taylor and Broms from their investigation are as follows [44]:

1. The cohesion increases with decreasing water-cement ratio. However, the water-cement ratio has less effect on cohesion than on mortar compressive strength.

2. For a given aggregate material, the coefficient of interfacial friction was found to be practically independent of the cement-sand and water-cement ratios of the paste or mortars.

Implications of Aggregate-Mortar Interface Behavior

The previous discussion of interface behavior is helpful in understanding the behavior of real aggregate-mortar interfaces in concrete under compressive loading. The major implications of this study can be summarized as follows [4,44]:

1. Secondary stresses caused by volume changes have been discussed previously. It was shown that large tensile, compressive, and shear stresses develop in a concrete mass which undergoes volume changes. These stresses are probably large enough to cause tensile or shear bond cracks at the interfaces between the aggregates and the mortar. These shrinkage cracks will affect the subsequent formation and propagation of shear bond cracks under load.

2. In concrete, the interfaces are located at various angles, and, therefore, bond cracks will form at different loads at these interfaces. Since bond cracks behave plastically and since there is a consequent redistribution of the internal stresses, a gradual curving of the stress-strain curve of concrete results. This provided an explicit explanation of the fact that aggregates in the mixture make the stress-strain curve deviate from a straight line.

3. The sliding of the interface is accomplished by widening of local vertical mortar cracks at the ends of the interface. This phenomenon probably accounts for the expansion in volume which is observed near the ultimate load.

4. The pseudo-plastic behavior of pre-existing no-load bond cracks explains the moderate non-linearity of the stress-strain curve of concrete even at very low loads.

5. The Coulomb-Mohr theory applied to the behavior of the interface, combined with the maximum normal stress theory applied to both tension and compression failure of the mortar, satisfactorily predicts the strength and behavior of the confined interface.

Influence of Aggregate and Voids on Young's Modulus

Hansen [29] has shown that the modulus of elasticity can be calculated for concrete, cement mortar, and cement paste when the modulus is known for the component materials. In this formulation of general theories for two-phase materials, concrete is defined as a two-phase material with aggregate particles embedded in a matrix of cement mortar. Cement mortar is defined as a two-phase material with aggregate particles embedded in a matrix of cement paste. Although rather crude models of the real materials are used, the formulas proposed by Hansen give results which are sufficiently accurate for most practical purposes.

For the first case of a two-phase material consisting of elastic particles embedded in an elastic matrix, Hansen has developed the equation

$$E = \frac{1}{\frac{V_1}{E_1} + \frac{V_2}{E_2}} \qquad \text{(C.1)}$$

where E = modulus of elasticity of the two-phase material (concrete)

E_1 = modulus of elasticity of the matrix (cement mortar)

E_2 = modulus of elasticity of the particles (aggregate)

V_1 = fractional volume of the matrix (cement mortar)

V_2 = fractional volume of the particles (aggregate)

The model used to develop this formula is based on the assumption

that the average stress due to an applied load is the same in both the matrix and the particles. Equation C.1 applies to real materials when the matrix has a lower modulus of elasticity than the particles.

This formula can also be applied to concrete for aggregate particles embedded in cement mortar. Hansen has shown that, provided the modulus of elasticity of the aggregate, E_2, is greater than that of the cement mortar, E_1, which is usually the case, concrete can be considered as a combined soft material. Assuming then that the stress is the same over the whole section of a specimen, the modulus of elasticity of concrete, E, is given by Equation C.1.

For the second case of a two-phase material consisting of voids embedded in an elastic matrix, Hansen has developed a formula which can be applied to the cement paste. For this case, the condition is for air-entrained pores in a cement paste. It is assumed that the modulus of elasticity, E_2, for the voids is zero. Thus, the practical formula determined for this case is Equation C.2 as follows:

$$E = \frac{1 - V_2}{1 + 2V_2} E_1 \qquad (C.2)$$

where E = modulus of elasticity of the plain cement paste

E_1 = modulus of elasticity of the cement paste matrix component

$E_2 = 0$ = modulus of elasticity of the air-entrained pores

V_2 = fractional volume of the air-entrained pores

For the third case of a two-phase material, Hansen has developed a formula for the cement mortar. For this case, the condition is for elastic fine aggregate (sand) or coarse aggregate particles embedded in

an elastic cement paste. Thus, the semiempirical equation obtained by Hansen is Equation C.3 as follows:

$$E = \frac{1}{0.5\left[\frac{V_1}{E_1} + \frac{V_2}{E_2}\right] + 0.5\left[\frac{1}{V_1E_1 + V_2E_2}\right]} \qquad (C.3)$$

where E = modulus of elasticity of the cement mortar

E_1 = modulus of elasticity of the cement paste

E_2 = modulus of elasticity of the sand or aggregate

V_1 = fractional volume of the cement paste

V_2 = fractional volume of the sand or aggregate

Stress Distribution Around A Single Elastic Particle

The following discussion is taken from an article by Torben and Hansen in Reference 4. In order to explain why bond cracks are formed in concrete under compressive load, it is necessary to consider the stress distribution around a single elastic particle located in a continuous elastic matrix of infinite extension and subjected to a uniaxial compressive stress. According to Goodier [45], the stresses in the elastic matrix surrounding an elastic inclusion or particle can be determined from Equations C.4, C.5, and C.6. Thus,

$$\sigma_{rr} = 2E_1\left(\frac{2A}{r^3} - \frac{2\nu_1}{1-2\nu_1}\frac{C}{r^3} + \frac{12B}{r^5} + \left[-\frac{2(5-\nu_1)}{(1-2\nu_1)}\frac{C}{r^3} + \frac{36B}{r^5}\right]\cos 2\theta\right) \qquad (C.4)$$

$$\sigma_{\theta\theta} = 2E_1\left(-\frac{A}{r^3} - \frac{2\nu_1}{1-2\nu_1}\frac{C}{r^3} - \frac{3B}{r^5} + \left[\frac{C}{r^3} - \frac{21B}{r^5}\right]\cos 2\theta\right) \qquad (C.5)$$

$$\sigma_{\psi\psi} = 2E_1 \left(-\frac{A}{r^3} - \frac{2(1 - \nu_1)}{(1 - 2\nu_1)} \frac{C}{r^3} - \frac{9B}{r^5} + \left[\frac{3C}{r^3} - \frac{15B}{r^5} \right] \cos 2\theta \right) \quad (C.6)$$

where E_1 = modulus of elasticity of the matrix material

r = distance from center of particle

ν_1 = Poisson's ratio of the matrix material

σ_{rr}, $\sigma_{\theta\theta}$, and $\sigma_{\psi\psi}$ = stresses in the matrix material defined by Figure C.4

ψ and θ = angles defined by Figure C.4

A, B, and C are constants and depend upon the shape and properties of aggregate particles. The values of the constants can be determined from the following equations:

$$\frac{A}{a^3} = -\frac{T}{8E_1} \frac{E_1 - E_2}{(7 - 5\nu_1)E_1 + (8 - 10\nu_1)E_2} \times \frac{(1 - 2\nu_2)(6 - 5\nu_1)2E_1 + (3 + 19\nu_2 - 2\nu_1\nu_2)E_2}{(1 - 2\nu_2)2E_1 + (1 + \nu_2)E_2} + \frac{T}{4E_1} \frac{\left[(1 - \nu_1) \frac{1 + \nu_2}{1 + \nu_1} - \nu_2 \right] E_2 - (1 - 2\nu_2)E_1}{(1 - 2\nu_2)2E_1 + (1 + \nu_2)E_2} \quad (C.7)$$

$$\frac{B}{a^5} = \frac{T}{8E_1} \frac{E_1 - E_2}{(7 - 5\nu_1)E_1 + (8 - 10\nu_1)E_2} \quad (C.8)$$

$$\frac{C}{a^3} = \frac{T}{8E_1} \frac{5(1 - 2\nu_1)(E_1 - E_2)}{(7 - 5\nu_1)E_1 + (8 - 10\nu_1)E_2} \quad (C.9)$$

where T = applied external tensile stress, positive for tension

ν_2 = Poisson's ratio of particle material

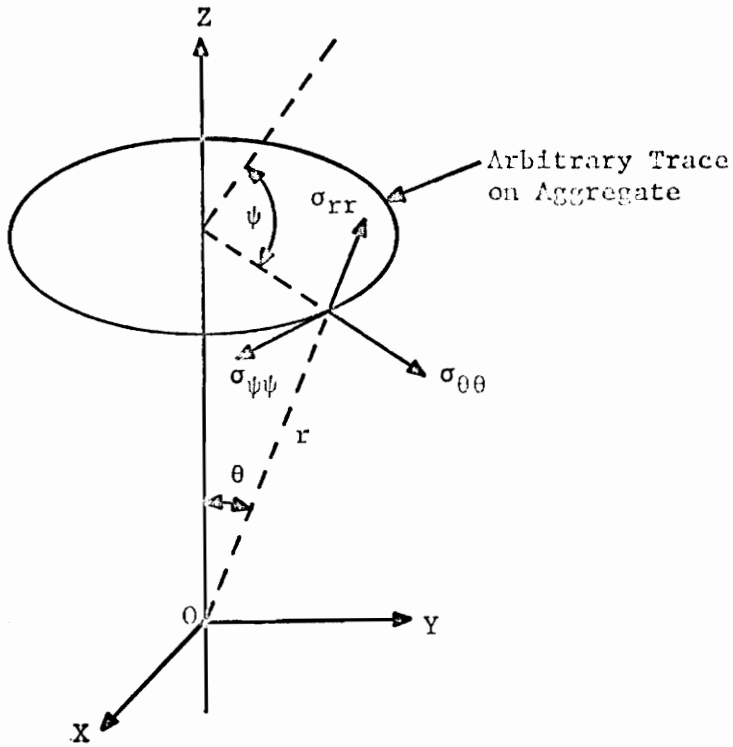

FIGURE C.4 NOTATION USED IN ANALYSIS OF STRESSES AROUND A SPHERICAL INCLUSION IN A MATRIX OF INFINITE EXTENSION

E_2 = modulus of elasticity of particle

a = radius of particle

A spherical cavity and a spherical rigid inclusion are the limiting cases. Thus, for a spherical cavity ($E_2 = 0$) we obtain

$$\frac{A}{a^3} = -\frac{T}{8E_1}\frac{13 - 10\nu_1}{7 - 5\nu_1} \tag{C.10}$$

$$\frac{B}{a^5} = \frac{T}{8E_1}\frac{1}{7 - 5\nu_1} \tag{C.11}$$

$$\frac{C}{a^3} = \frac{T}{8E_1}\frac{5(1 - 2\nu_1)}{7 - 5\nu_1} \tag{C.12}$$

For a spherical rigid inclusion ($E_2 = \infty$) we obtain for the constants the following equations:

$$\frac{A}{a^3} = \frac{T}{4E_1}\left[\frac{1 - \nu_1}{1 + \nu_1} + \frac{3}{16 - 20\nu_1}\right] \tag{C.13}$$

$$\frac{B}{a^5} = -\frac{T}{8E_1}\frac{1}{8 - 10\nu_1} \tag{C.14}$$

$$\frac{C}{a^3} = -\frac{T}{8E_1}\frac{5(1 - 2\nu_1)}{8 - 10\nu_1} \tag{C.15}$$

Torben and Hansen [4] pointed out in their article that the question arises whether it is valid to draw any conclusions concerning the stress distribution around particles in a closely packed concrete system, on the basis of an analysis of the stress distribution around an isolated particle in a matrix of infinite extension. The single particle model has been shown to give reasonable results when used in the analysis of elas-

ticity and shrinkage of concrete. This is an indication that it may also be applicable in the analysis of internal stresses. Nielsen [46] has measured the stresses on cylindrical stress gages embedded in concrete under uniaxial compressive load. The stiffness of the gages was equivalent to the stiffness of the various types of aggregate material used. Hast [47] has shown that the compressive stress on one isolated, elastic, cylindrical particle embedded in an elastic matrix of infinite extension, with the axis parallel to the direction of the applied load can be calculated according to the equation:

$$\sigma_2 = \left[\frac{E_2[1.125(1 - \nu_1^2)\pi R + h]}{1.125(1 - \nu_1^2)\pi R E_2 + h E_1} \right] \sigma_1 \qquad (C.16)$$

where σ_2 = axial compressive stress on cylindrical particle

σ_1 = applied compressive stress

E_2 = modulus of elasticity of particle

E_1 = modulus of elasticity of matrix

ν_1 = Poisson's ratio of matrix

R = radius of particle

h = height of particle

There is a reasonably good agreement between particle stresses in concrete measured by Nielsen and the stresses calculated by Hast according to Equation C.16 for a single particle model. It may therefore be assumed that Equations C.4 through C.15 apply to concrete. (The author also assumes that these equations can be applied to his concrete (prestressed) for calculating the stresses around certain aggregate particles.)

In the bond phase between an infinitely rigid particle and the mortar

matrix, the stress perpendicular to an applied compressive load of magnitude -T can be determined from Equation C.4 when inserting Equations C.13, C.14, and C.15, r = a, and $\theta = 90^{o}$. Therefore, Equation C.4 becomes the following:

$$\sigma_{rr} = -\left(\frac{1 - \nu_1}{1 + \nu_1} - \frac{5 - 5\nu_1}{8 - 10\nu_1}\right) T \qquad (C.17)$$

For real materials, the numerical values of σ_{rr} depends on the modulus of elasticity and Poisson's ratio of the component materials. When the modulus of elasticity of an inclusion (an aggregate particle in the author's case) is a few times higher than the modulus of elasticity of the matrix material, it can be shown that the stresses around the inclusion approximate the stresses around a particle.

The magnitude and sign for σ_{rr} can be estimated provided certain assumptions are made. By assuming that the modulus of elasticity of an inclusion is a few times higher than the modulus of elasticity of the matrix material, representative values of σ_{rr} can be determined. It can be shown that a tensile stress acts at the bond phase perpendicular to the direction of the applied load. The tensile strength of the bond phase is determined by the chemical composition and texture of the aggregate surface, by the water-cement ratio, and by the conditions under which the concrete is cured and stored.

The particle size does not affect the magnitude of the stress in the bond phase. However, according to Hsu et al. [31], the strength of the bond between cement mortar and large aggregate particles is somewhat less than the strength of the bond between cement paste and sand grains.

Therefore, it can be expected that cracks first appear along the boundaries of the larger aggregate particles.

Formation of bond and mortar cracks in concrete does not take place at random. Once the first crack has formed along an aggregate particle, the tensile stresses in the matrix material at this area are relieved. Subsequent cracks seldom develop parallel to the first crack. In addition, it is apparent from energy considerations, that it is easier to extend an already existing crack than it is to form a new crack. The number of cracks formed in a specimen is determined by the size of the specimen, and the distance between the individual cracks is probably determined by the maximum size of aggregate particles.

From experimental results, it can be concluded that compressive failure of concrete under loading only takes place in two stages. At a comparatively low stress, bond cracks develop parallel to the direction of applied load. Provided there is no friction between the specimen and the platens of the testing device, these cracks continue to grow until the specimen is split into a number of structurally independent columns. When there is considerable friction between the platens and the specimen, the cracks that form never extend all the way to the platens before the specimen fails in shear, producing the well-known "hour-glass" shaped failure pattern.

Although the mechanisms of initial cracking and ultimate failure are different, they are not completely independent. If the bond between cement mortar and aggregate is weak, the compressive strength of the concrete is also.

Now, using Goodier's equations, the stress distribution around a void embedded in a cement paste or mortar matrix will be considered. By insert-

ing Equations C.10, C.11, and C.12, $r = a$, and $\theta = 0^{o}$ into Equation C.5, and assuming that the material is submitted to an externally applied compressive load, it is found that a tensile stress exists above and below the void and perpendicular to the direction of applied load, of magnitude:

$$\sigma_{\theta\theta} = \left(\frac{3 + 15\nu_1}{14 - 10\nu_1} \right) T \qquad (C.18)$$

Making the same assumptions as before, concerning the properties of the cement mortar, it can be shown that the tensile strength of the mortar is exceeded above and below the void.

Creep

Creep is defined as the increase in strain under a sustained stress. For prestressed concrete, displacements and stresses change due to creep which weakens the structure. Elastic deformations occur immediately when concrete is loaded. Nonelastic deformations (creep) increase with time when the concrete is subjected to a sustained load. Creep increases at a decreasing rate during the period of loading. Energy dissipation also occurs in concrete due to creep and the time dependent characteristics when it is loaded in compression. This can contribute significantly to the measured deformations. Creep in concrete near an internal crack tip not only increases the crack length but also reduces the stress concentration in this region [48].

There are many theories which explain the cause of creep. The most important cause is thought to be due to the flow of the absorbed water out of the cement gel caused by external pressure in the form of external load and drying [19]. The author believes, however, that creep is caused

by a two stage phenomenon. The first stage is due to Poisson's elastic shortening after the application of load, and the second stage to the slow formation and propagation of internal microcracks caused by an external load. These microcracks cause an increase in strain in the structure even though the stress is sustained. This theory is true for concrete which undergoes both wetting and drying conditions. The author also believes the theory is true for concrete undergoing freezing and thawing conditions.

Also under uniaxial compression, creep not only occurs in the axial direction, but also in the transverse directions. This is referred to as lateral creep.

Further discussion of creep is too involved to be considered here. An extensive treatment of the subject of creep can be found in works by Adam M. Neville [22].

Compressive Fracture Mechanism

This is the second of two crack formation and propagation mechanisms associated with concrete.

Linear-Elastic Fracture Mechanics

Introduction

Linear-elastic fracture mechanics is a study of stress and displacement fields near the tip of a flaw or crack in an ideal, homogeneous, elastic material under stress. It is also concerned with the forces associated with the propagation of a crack and fracture of the material. Its concepts are most applicable to brittle materials in which the inelastic region near the crack tip is small compared to the specimen and flaw dimensions. Thus, the elastic stress field equations provide a good

approximation [49]. Unfortunately, the fracture of most homogeneous materials is a very complex process; and the fracture of concrete (being a polyphase, non-homogeneous material) is a more complex process than an ideally brittle material. Several applications of fracture mechanics have been made to mortars and concretes; however, in each instant, the material was assumed to be homogeneous. It appears that for different types of stress and loading conditions, concrete has different types of fracture. Fracture can occur by fracture of the cement paste, fracture of the aggregate, failure of the bond between cement paste and aggregate, or any combination of these mechanisms.

The complete fracturing process in concrete is a progressive failure that usually occurs in three stages: crack initiation, slow crack growth, and rapid crack growth. Fracture occurs by extension of a pre-existing crack or flaw in a material. The importance of a specific size flaw depends on the nominal stress normal to the crack and the fracture toughness of the material.

In a previous section it was shown that fine cracks exist at the interface between the coarse aggregate and cement paste prior to the application of any load. There may also be other flaws and cracks in the cement paste matrix. These cracks remain stable up to around 30 percent or more of the ultimate load or strength and then begin to increase in length, width, and number. This is the stage of slow crack propagation. At 70 to 90 percent of the ultimate strength, the cracks propagate through the cement paste and fine aggregate (the mortar) and bridge nearby bond cracks producing a continuous crack pattern. This is the stage of rapid crack propagation which will lead to the final failure of the material if

the load is sustained.

Many people have investigated microcracking and crack propagation in plain concrete under various conditions. Such people include: Kaplan [43,50], Glucklich [51,52,53], Sturman [34], and Lott [54].

Plane stress and plane strain

In the theory of elasticity there exists a special class of two-dimensional problems known as "plane problems." These can be solved more easily than the general three-dimensional problem since certain simplifying assumptions can be made. The geometry of the body and the nature of the loading on the boundaries permit a problem to be classified as a plane problem.

The thickness of the body must be uniform, and it need not be limited. It may be very thick or very thin; in fact, these two extremes represent the most desirable cases for the two plane problem conditions.

For the condition of plane stress, it is assumed throughout the thickness of the body that

$$\sigma_{zz} = \tau_{yz} = \tau_{zx} = 0 \qquad \text{(C.19)}$$

A plate of uniform thickness can be subjected to body forces or stresses that are applied in directions normal to the direction of uniform plate thickness and are independent of location in the direction of plate thickness. If the thickness is very small, all of the stress in the direction of the thickness may be assumed to vanish. This is given by Equation C.19 above, and the stresses normal to the direction of thickness are independent of location in that direction. Thus, the plane stress approach is employed when the body thickness is relatively thin in relation to its

lateral dimensions.

For the condition of plane strain, it is assumed throughout the thickness of the body that

$$\varepsilon_{zz} = \gamma_{yz} = \gamma_{zx} = 0 \qquad (C.20)$$

If the thickness of the plate is very large, strains will be independent of location in the direction of thickness. There may be a possible exception to this in the neighborhood of the plate surfaces where the lateral restraint vanishes. Thus, the plane strain approach is limited to the central regions of bodies which are very long or very thick in relation to their lateral dimensions.

Lott [54] explains that a thin plate offers no lateral restraint to the body. Thus, when a crack propagates under the plane stress condition, some lateral shearing displacement occurs between the crack surfaces. The displacements of the crack surface are normal to and parallel to the plane of crack extension. For cracks to propagate in a thin plate, the energy requirement for propagation is a combination of the requirements for the lateral shearing displacement and the normal opening displacement.

On the other hand, a thick plate provides a lateral restraint that prevents the lateral shearing displacements during crack propagation. Thus, under the plane strain condition, crack propagation is only due to the normal opening displacement requirement. The displacements of the crack surface are normal to the plane of crack extension. Some lateral shearing may occur near the free surfaces of the plate since no lateral restraint is developed here. It should also be noted that the energy requirement for crack propagation in the plane strain condition is less than the requirement for the plane stress condition.

Bonds in concrete

It appears that the strength of concrete made with aggregates of adequate strength is governed by the strength of either the cement paste or of the bond between the paste and the aggregate particles.

Cement-gel bonds

The cement-gel is composed of very fine sheet-like particles which are products of the hydration reaction. The bonds between these gel particles in the cement paste are physical in nature and are due to van der Waal's forces. They arise from the large amount of energy available in the surface of the gel particles, the surface forces being larger in comparison with the body forces. Since the physical bonds act over a very large area (the specific surface area of cement gel being almost 2 million cm^2/g), these bonds between the particles are strong enough to resist unlimited thixotropic expansion. Thus, the cement paste is composed of a gel which is a limited swelling material. This indicates that cohesive forces other than the physical bonds also act between the gel particles.

Conversely, the bonds inside the gel particles are chemical in nature and are of the ionic and covalent types. The chemical bonds are of a higher order of magnitude than the physical ones. The chemical bonds are also assumed to act where the particles make contact with one another.

Flaws in concrete may be present in the bond phase between unhydrated cement grains and hydrated cement paste, or in the form of air voids, but hardly in the form of capillary or gel pores which are usually much smaller. Cement grains larger than about 50 microns never completely hydrate; and, therefore, remain embedded as hard particles in the soft hydrated paste.

Powers [55] suggested that there is no direct contact between the cement gel and the unhydrated cement grains. He suggested that any adhesion is due to van der Waal's forces acting across a small distance between the gel and the anhydrous material. This zone may be occupied by water molecules and calcium or silicate ions. If this is true, the bond phase between hydrated cement gel and anhydrous cement grains could be a weak zone for the initiation of a possible microcrack.

Paste-aggregate bonds

The bonds at the cement paste and aggregate particle interface are thought to be largely of the physical type. The bonding here is affected by both the paste and aggregate properties. There is a possible mechanical interlock at this interface so that the bonds vary with the type of aggregate and the surface texture. The bonds may also be affected by chemical reactions at the surface of the aggregates. Research on microcracking at Cornell [36] indicates that the paste-aggregate bond strength is about one-half of the tensile strength of the paste.

Pore bonds

The gel pores do not affect the strength of cement paste because the physical bonds are effective across the width or diameter of the gel pores. However, the larger capillary pores reduce the cohesive force of the physical bonds and tend to lower the cement paste strength [54].

Tensile fracture of elastic materials (The Griffith Theory)

In 1920, Griffith [56] made the first attempt at investigating the propagation of cracks in a brittle material under stress by developing

an energy concept of fracture mechanics for an ideally elastic material. He suggested that the fracture strength of glass, a brittle material, was affected by initial cracks or flaws in the material or by cracks formed due to the application of a load. Griffith said that this effect was due to stress concentrations caused by these cracks. He also proposed a theory of fracture strength based on changes in strain energy and surface energy as the largest of these cracks extends. That is, the energy released by a small extension of a crack furnished the energy requirements of the crack extension. Since glass exhibited little ductile behavior, the only energy requirement considered was the surface tension.

Griffith assumed an elliptical shape for a crack and developed his energy concept in the following steps [34]:

1. The equilibrium condition of an elastic body, deformed by specified surface forces is such that the potential energy of the whole system (including the potential energy of the applied forces) is a minimum.

2. The criterion of rupture is obtained by further adding to Step 1 that the equilibrium position, if equilibrium is possible, can be one in which rupture of the material has occurred. This is true only if the system can pass from the unfractured to the fractured condition by a process involving a continuous decrease in potential energy.

3. In an elastic, solid body deformed by specified forces applied at its surface, the sum of the potential energy of the applied forces and the strain energy of deformation of the body is either reduced or unchanged by the introduction of a crack whose surfaces are stress-free.

4. If a body having linear stress-strain relations is deformed from the unstrained condition to a condition of equilibrium by constant forces, the potential energy of the body in the equilibrium condition is reduced by an amount equal to twice the strain energy of deformation.

5. The total decrease in potential energy due to the formation of a crack is equal to the decrease in strain energy minus the increase in surface energy. Thus, Statement 3 shows that the

total decrease in potential energy due to the formation of a crack must be positive. If U is the strain energy released due to the formation of the crack and W is the potential surface energy due to the formation of new surface area, the total reduction of the potential energy of the system is

$$U - W \tag{C.21}$$

and the condition under which the crack will start to propagate is simply

$$\frac{d}{dc}(U - W) = 0 \tag{C.22}$$

where c is the length of the major axis of an elliptical crack. Thus, from the requirement of minimum potential energy in equilibrium, a crack will propagate when the rate of energy release due to the crack extension reaches the rate of energy requirement of surfaces created by the virtual crack extension.

In the formation of a crack in a body composed of molecules which attract one another, work must be done against the cohesive forces of the molecules which attract one another on either side of the crack. This work appears as the potential surface energy. If the width of the crack is greater than the radius of molecular action, the surface energy per unit area is a constant for the material and is defined as the surface tension, T.

Since a crack may be thought of as a straight line, Griffith chose an ellipse as a convenient geometric approximation to this shape. The major axis being equal to 2c and the minor axis being equal to 2b. If the semi-minor axis, b, of the ellipse is reduced to zero, the ellipse reduces to a line with the semi-major axis, c, as its length. It should be noted that Griffith developed his theory for the propagation of an elliptical crack through an infinite plate of unit thickness, so loaded that in regions remote from the crack it has a uniform tensile stress perpendicular to the major axis of the crack. This model is shown in Figure C.5a for concrete under a uniform tension field.

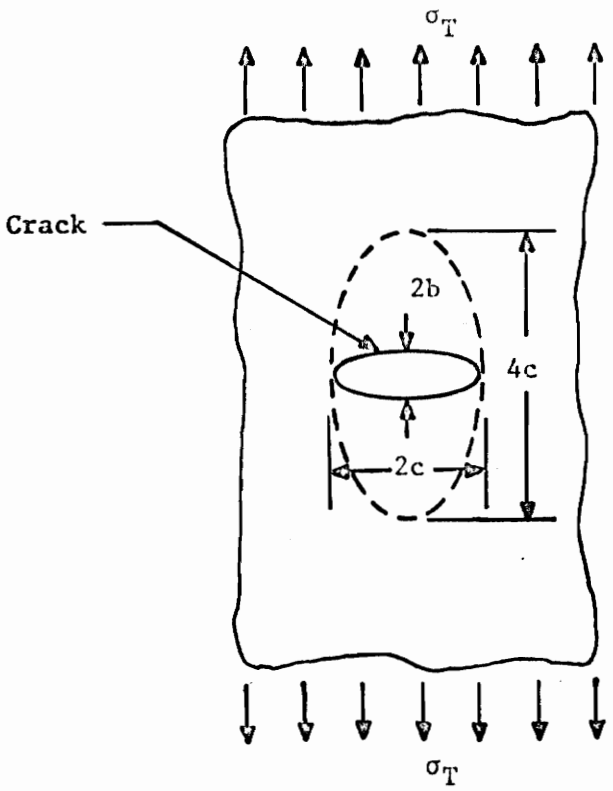

FIGURE C.5a EXTENSION OF A GRIFFITH CRACK IN A UNIFORM TENSION FIELD (FROM GLUCKLICH)

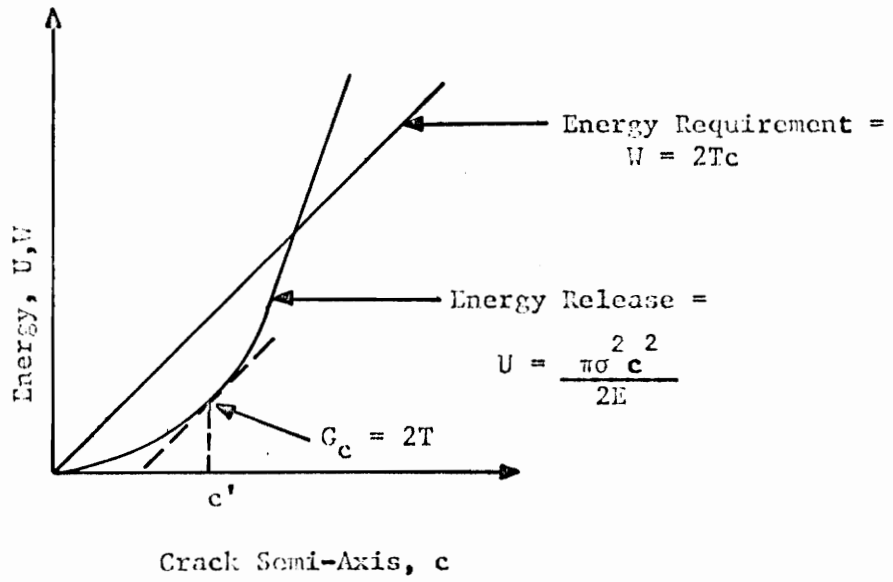

FIGURE C.5b DETERMINATION OF CRITICAL CRACK SIZE FROM ENERGIES BALANCE IN THE CASE OF A UNIFORM TENSION FIELD (FROM GLUCKLICH)

For the elliptic crack of semiaxis c, Griffith has shown that the decrease of strain energy is given by the function

$$U = \frac{\pi\sigma^2 c^2}{2E} \tag{C.23}$$

and the increase of surface energy by

$$W = 2Tc \tag{C.24}$$

Thus, the rate of decrease of strain energy is

$$\frac{dU}{dA} = \frac{d}{dc}\left(\frac{\pi\sigma^2 c^2}{2E}\right) = \frac{\pi\sigma^2 c}{E} \tag{C.25}$$

and for a surface tension of T, the rate of increase of new surface energy is

$$\frac{dW}{dA} = \frac{d}{dc}(2Tc) = 2T \tag{C.26}$$

where σ = the uniform tensile stress

E = the modulus of elasticity of the material

A = the fracture area

$\frac{d}{dc}$ = rate of change operator

Thus, applying the Griffith criterion that for an elliptically shaped crack of length c to propagate along a straight line in a homogeneous, brittle material, the rate of reduction of strain energy in the material must equal the rate of increase in free surface energy due to the formation of new surface area, i.e., $dU/dA = dW/dA$. Therefore, from Equations C.25 and C.26 we have

$$\frac{\pi\sigma^2 c}{E} = 2T \tag{C.27}$$

Thus, for a crack of semi-major axis c, the stress for propagation is

$$\sigma = \sqrt{\frac{2ET}{\pi c}} \tag{C.28}$$

which is the well-known Griffith equation.

The two functions given in Equations C.23 and C.24 are shown graphed in Figure C.5b. From this it becomes apparent that the critical crack size c' for a given stress σ is where the slopes of the two curves are equal, or in Equation C.27 where c becomes c'. Therefore,

$$c' = \frac{2ET}{\pi\sigma^2} \tag{C.29}$$

In the case of a thick plate the problem becomes one of plane strain, and Equation C.28 becomes

$$\sigma = \sqrt{\frac{2ET}{\pi c(1 - \nu^2)}} \tag{C.30}$$

where ν is Poisson's ratio.

Fracture of ductile materials (Modified Griffith Theory)

The basic theory of crack propagation developed by Griffith has been modified and extended to materials which are less brittle than glass. Irwin [57] and Orowan [58] have extended the theory to materials that exhibit ductile behavior. In essence this extension consisted of incorporating other types of energies in the energy balance. These included energies, other than the surface tension T, such as energy dissipated in plastic flow and in viscous damping. They recognized that for materials in which plastic flow precedes failure, unstable crack growth can occur if the plastic strains tend to localize near the boundaries of the

crack. In a stressed plate, the largest portion of the energy formed goes into the production of plastic strains at the tip of a sharp crack. Thus, the creation of new surface energy, which is considerably less than the energy required for plastic deformation near the crack tip, has less influence on the propagation of cracks in ductile than in brittle materials.

Irwin and Orowan pointed out that the Griffith theory must be modified so as to take into account the dissipation of strain energy in plastic flow. The formation of a plastic region near the crack modifies the elastic fields and, therefore, the strain energy stored in the body. The modification of the elastic fields away from the region of the crack is similar for a crack extension and for the formation of a plastic zone near the crack. It is now viewed that Griffith's theory in modified form may be applied to a wide range of materials if the surface energy term in Griffith's formula is replaced by the total work involved, or energy absorbed, in the process of fracture. In addition, Irwin has introduced the concept of strain-energy-release rate. Thus, the basic idea of the modified Griffith theory is that at the start of fast, unstable fracturing, the fracture work per unit crack extension may be equated to the rate of disappearance of strain energy from the surrounding elastically strained material. Irwin has shown that the strain-energy-release rate associated with extension of the fracture is the driving force motivating crack propagation. It may also be less than that required to cause unstable crack propagation.

Fracture toughness

Fracture toughness is defined as a material's resistance to propaga-

tion of an existing flaw. The fracture toughness of a material can be defined by either of two conditions, the strain-energy-release rate or the stress intensity factor.

Strain-energy-release rate

The strain energy supplied by a virtual crack extension must furnish the energy requirements of the crack surface. The strain energy is a function of the crack extension, and it is convenient to define this energy in terms of the rate of release of energy with respect to the crack extension as this extension approaches zero. Thus, the strain-energy-release rate which Irwin designates as G, may be expressed by

$$G = \lim_{\Delta c \to 0} \frac{\Delta U}{\Delta c} = \frac{dU}{dc} \text{ or } \frac{dU}{d\Lambda} \tag{C.31}$$

It was shown in a previous section for a thin, brittle plate containing an elliptical crack and subjected to a tensile load normal to the plane of the crack, that the strain-energy-release rate is given by Equation C.25.

For plane strain conditions, E is replaced by $E/(1 - \nu^2)$. Thus, the equation for the strain-energy-release rate becomes

$$G = \frac{(1 - \nu^2)\pi\sigma^2 c}{E} \tag{C.32}$$

The strain-energy-release rate at onset of unstable crack propagation is referred to as the critical strain-energy-release rate, denoted by G_c. The value of G_c is assumed to be a material property for given environmental conditions, and it is independent of the applied loads and body geometry. Also, it is a measure of the resistance of a material to

the propagation of a crack, that is, it is a measure of the fracture toughness of a material. The critical strain-energy-release rate may be considered as being a fundamental property of a material in the same way as the modulus of elasticity is regarded.

Stress intensity factor

The strain-energy-release rate G can be shown to be related to the elastic stress and displacement fields in the region of the crack tip in a homogeneous material. This relationship is known as the stress intensity factor and is designated as K. The stress intensity factor for plane strain is denoted by

$$K = \sqrt{\frac{EG}{1 - \nu^2}} \qquad (C.33)$$

The value corresponding to the onset of rapid, unstable crack propagation is called the critical stress intensity factor and is designated as K_c. It also is a measure of the material's resistance to crack propagation, known as the fracture toughness. The stress intensity factor is a function of load and geometry only. When concrete is analyzed as a homogeneous material, an effective fracture toughness is obtained. The critical stress intensity factor for plane strain is denoted by

$$K_c = \sqrt{\frac{EG}{1 - \nu^2}} \qquad (C.34)$$

For plain concrete, the critical stress intensity factor is derived from two sources: the fracture resistance of the mortar and the crack arresting mechanism due to the coarse aggregate. The fracture toughness increases with increasing volume of coarse aggregates. For the same

volume of aggregates, the larger their size, the greater the toughness. It also seems that the fracture toughness of concrete is independent of the water-cement ratio. However, for a paste or mortar, the toughness decreases with increasing water-cement ratio. A thorough explanation of the variation of fracture toughness can be found in Reference 49.

It is convenient to work with the stress intensity factor rather than the strain-energy-release rate since various elastic fields may be superimposed to determine the stress intensity factor under complex loading conditions.

Typical load-deflection curves for cement paste, mortar, and concrete are shown in Figure C.6. The area under the load-deflection curve for each case can be considered as a measure of the work required to fracture the specimen. This area is also termed the fracture toughness and is related through the two conditions, G_c and K_c.

Compressive fracture of a material

Jones [59] has shown that for a material under a uniaxial compressive stress field, the orientation of cracks is parallel to the direction of the applied axial stress since in all the other directions there is a normal compressive stress component. It is assumed that these cracks originate from holes or flaws present in the material in a manner similar to that in the case of a tensile stress field. It is known that the state of stress around a hole in a compressive field causes tension near the two vertices that form the axis which is parallel with the stress field. The severity of the stress concentration at the periphery of the hole is thought to initiate its extension. For propagation of such a hole, the

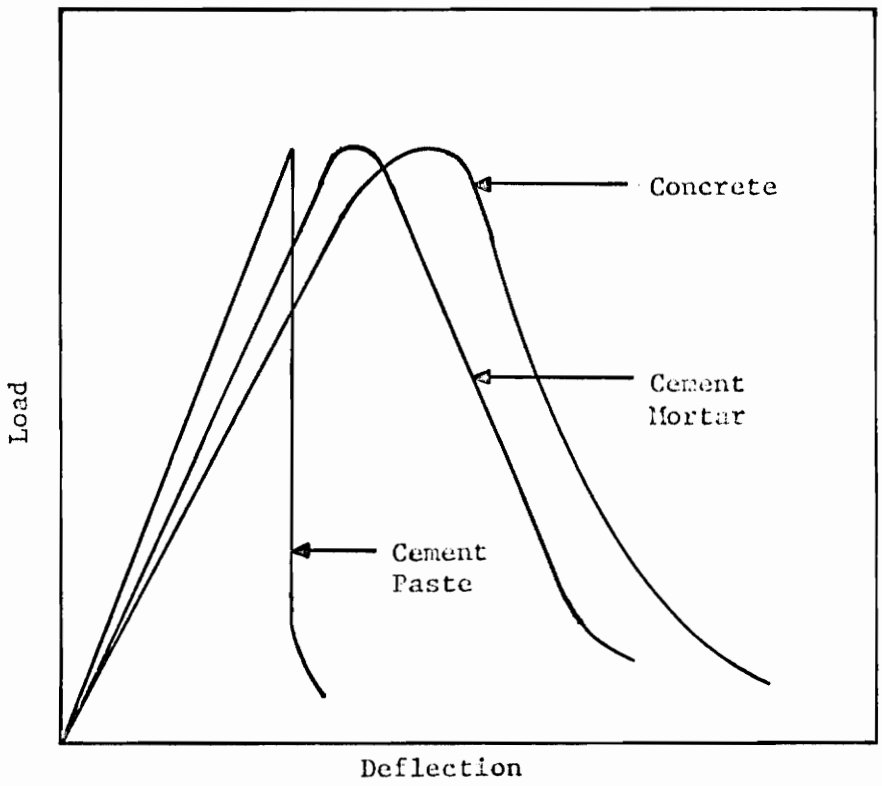

FIGURE C.6 TYPICAL LOAD-DEFLECTION CURVES FOR PASTE, MORTAR, AND CONCRETE

following two conditions should be fulfilled [52]:

1. There should be a high enough tensile stress to break the bonds in the material.

2. There should be a strain-energy-release rate at least equal to the rate of non-recoverable work done in forming the new surfaces when crack propagation takes place.

Glucklich [52] has shown that Condition 1 above can be satisfied by considering Figures C.7b and C.7c. A plane stress case for a circular hole in an infinitely wide plate subjected to a pure compressive stress is used. It can be seen in Figure C.7a that a circular hole in the material will cause a redistribution of stresses and create tension near its top and bottom vertices, shown at points A and B. If, in addition, there is a tiny flaw in the tension zone, the tension will be magnified in accordance with the stress concentration factor associated with the flaw. The stress concentration factor may be high enough to break the bonds between material particles. This is shown in Figure C.7b for a tiny satellite hole and in Figure C.7c for a small notch. Glucklich [52] also pointed out that the holes need not necessarily be circular. Any hole which has a considerable width so that it creates zones of tension will produce similar results. Such holes are not stress raisers but rather stress convertors (from compression to tension). The stress raisers are the smaller satellite holes or notches within the tension zones.

Condition 2 can be shown to be true also. Glucklich explains in his report [52] that when holes such as those in Figure C.7 are present, part of the body's capacity to resist compression is contributed by its tensile strength at zones A and B. Therefore, if the hole extends upwards and downwards through these zones, the body will become more compressible;

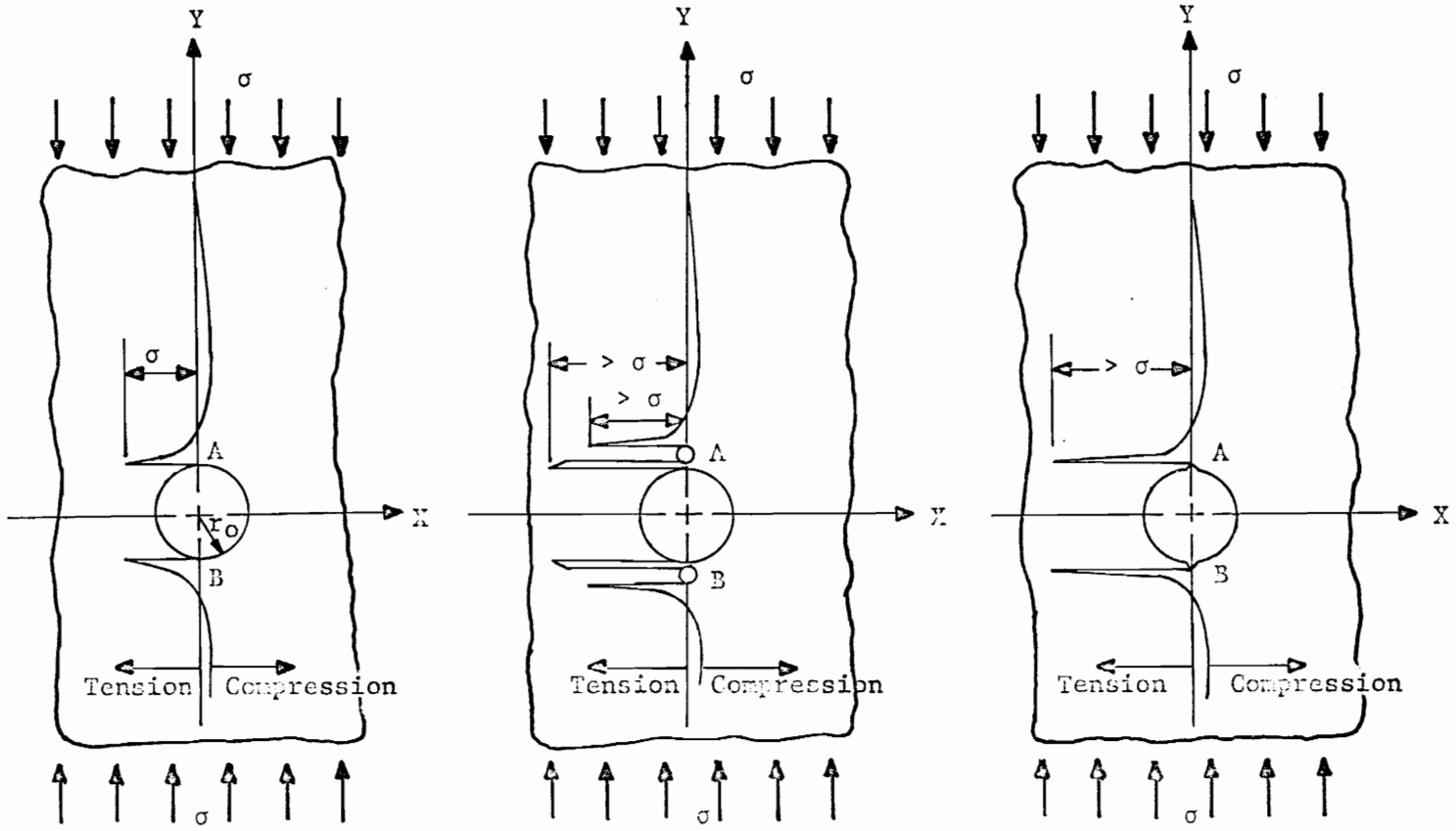

FIGURE C.7 DISTRIBUTION OF STRESS ALONG AN AXIS OF SYMETRY THROUGH A CIRCULAR HOLE IN AN INFINITELY WIDE PLATE SUBJECTED TO PURE COMPRESSION (FROM GLUCKLICH)

and its elastic energy content will diminish for a constant length. This release of energy will favor the extension of such holes but only within the tension zones. Thus, cracking should be checked close to the hole since the disturbance to the original uniform stress field caused by the hole does not extend very far upwards or downwards. The distribution of the tensile stress along the vertical axis will in this case be given by the equation

$$q = \frac{\sigma}{2}\left(\frac{r_o^2}{y^2} - \frac{3r_o^4}{y^4}\right) \qquad (C.35)$$

where σ = the applied uniform compressive stress

r_o = the original radius of the hole

From this equation it can be shown that at a distance $y = r_o$, there is the value $q = -\sigma$ (tension). This tension zone will extend only to a distance $y = r_o\sqrt{3}$ from the center of the hole. Beyond this distance a very low compressive stress will prevail and will tend to check further growth. However, the newly formed crack will open up, as in Figure C.8b, rather than remain closed, as in Figure C.8a, so that the restricted tension zone will be carried forward by the crack tip. This will favor a further expansion of the body provided the rate of strain energy released is equal to the rate of work done in forming the new surfaces.

The facts thus far presented in this section are helpful in applying the Griffith theory to a compressive field. Griffith originally based his theory on an elliptical crack normal to the applied tensile field. However, for the case of compression, the critical elliptical cracks are those parallel with the compressive stress field.

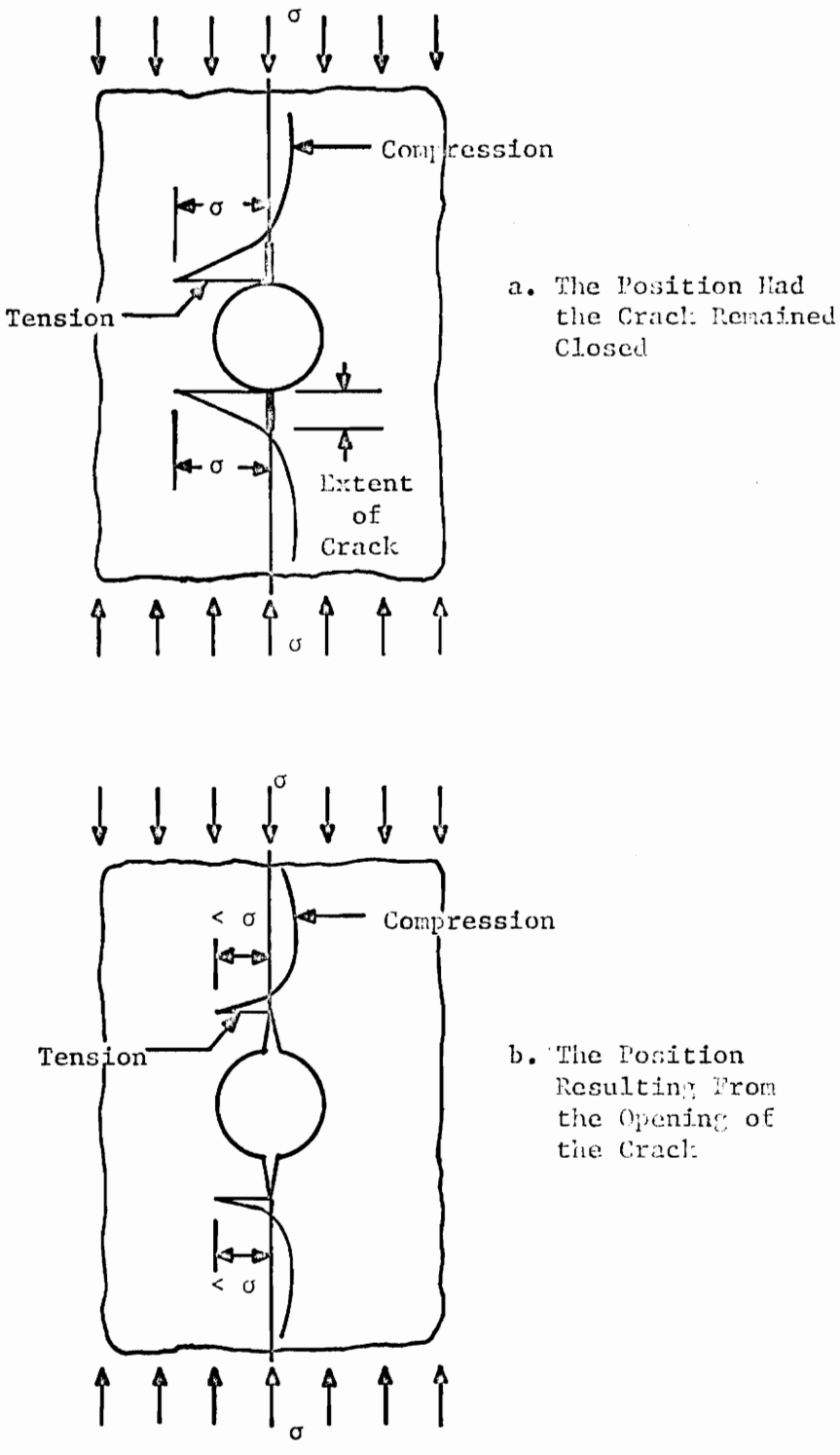

FIGURE C.8 THE TENSION ZONE CARRIED FORWARD BY THE TIPS OF AN EXPANDING CRACK (FROM GLUCKLICH)

In following a similar procedure as for the case of tension, Glucklich [52] developed an equation for crack propagation for the case of an elliptical crack in a compressive field. In the next section it will be shown that this development can be extended to crack propagation in concrete under a compressive load. Thus, for the compression analogy, Equation C.23 can be written as

$$U = \frac{\pi 2c^2\sigma^2}{2E} \tag{C.36}$$

This suggests that the lost strain energy in the case of tension may be regarded as that energy contained in an imaginary ellipse with axes 2c and 4c as shown by the dashed line in Figure C.5a. In analogy for the case of compression, Figure C.9a, the strain energy lost will be assumed to be that contained in the real ellipse of axes 2b and 2c. Glucklich wanted to show that U was proportional to c rather than to c^2 (as was in Griffith's case). Thus, Equation C.36 becomes

$$U = \frac{\pi bc\sigma^2}{2E} \tag{C.37}$$

and the increase of surface energy

$$W = 4Tc \tag{C.38}$$

These two functions are shown in Figure C.9b. Since both are linear, it is clear that no critical size of the crack exists in this case. Thus, applying the Griffith criterion, dU/dA = dW/dA, Glucklich obtained

$$\frac{\pi b\sigma^2}{2E} = 4T \tag{C.39}$$

and the stress for propagation is

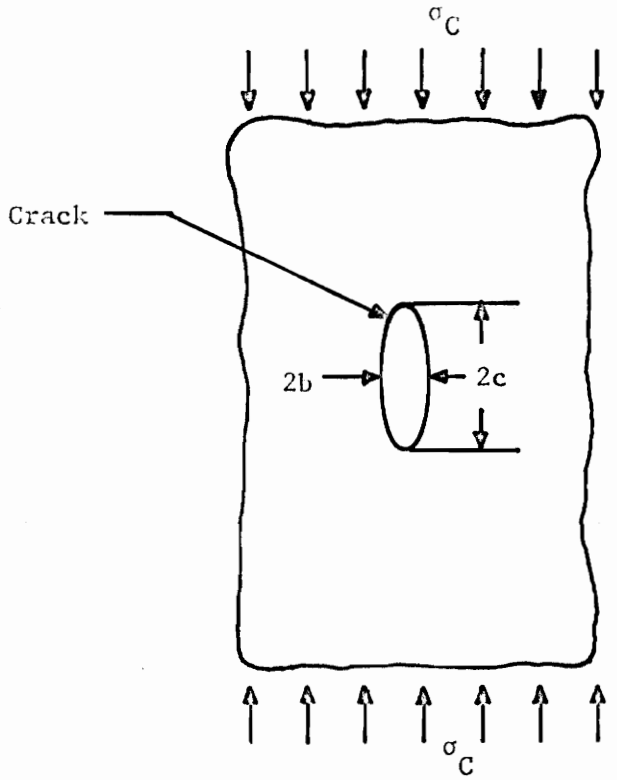

FIGURE C.9a EXTENSION OF A GRIFFITH CRACK IN A UNIFORM COMPRESSION FIELD (FROM GLUCKLICH)

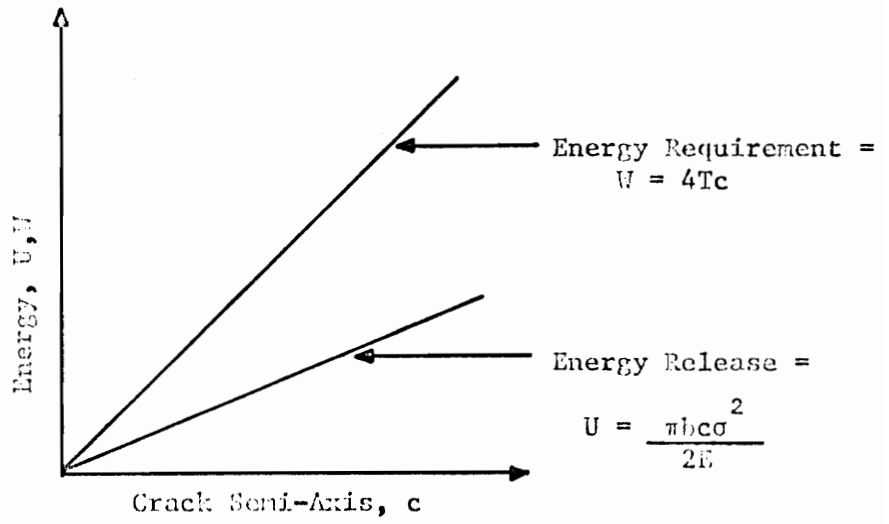

FIGURE C.9b DETERMINATION OF CRITICAL CRACK SIZE FROM ENERGIES BALANCE IN THE CASE OF A UNIFORM COMPRESSION FIELD (FROM GLUCKLICH)

$$\sigma = \sqrt{\frac{8ET}{\pi b}} \tag{C.40}$$

Equation C.40 is the approximate compression analogy of Griffith's equation, Equation C.28. For Condition 2, which was mentioned previously in this section, the growth of a crack in compression will be fulfilled when the nominal compressive stress has reached the value given by Equation C.40. Then the strain-energy-release rate will be equal to the rate of work done in forming the new surfaces.

In the case of a thick plate, the problem becomes one of plane strain, and Equation C.40 becomes

$$\sigma = \sqrt{\frac{8ET}{\pi b(1 - \nu^2)}} \tag{C.41}$$

where ν is Poisson's ratio.

Using the two formulas developed from the tension and compression analogy, it can be shown why a material such as concrete is stronger in compression than in tension. By assuming a random orientation of elliptical cracks with a given axes ratio c/b within the material, one can determine the ratio of compressive/tensile strengths for that material from Equations C.28 and C.40. Thus,

$$\frac{\sigma \text{ compression}}{\sigma \text{ tension}} = \sqrt{\frac{8ET}{\pi b}} \Big/ \sqrt{\frac{2ET}{\pi c}} = 2\sqrt{c/b} \tag{C.42}$$

Assuming c/b = 36, the ratio of strengths becomes 12. Therefore, for this ratio, the strength of the material in compression is 12 times greater than that in tension. Thus, by this formulation, it can be shown why concrete is stronger in compression than in tension.

Extension of compressive fracture to concrete

Introduction

Concrete and cement paste both behave as brittle materials and their tensile and compressive properties depend on fracture mechanisms. It is known that concrete is weaker in tension than it is in compression, and that concrete in tension fails by crack propagation. However, concrete is designed mainly to resist compressive loads, and, in most cases, no tensile strength is attributed to it at all. It is, therefore, necessary to study the compressive strength and compressive mechanisms of fracture in order to learn how concrete behaves under a compressive load. Since portland cement concrete is assumed to be a brittle material, various authors and investigators have tried to apply the Griffith theory to concrete. However, an objection that has been raised to this is that the theory of elasticity for uniform, homogeneous bodies could not be applied to concrete since the cracks were of microscopic dimensions and since both the grain size of the material and their orientation would violate the basic assumptions.

Model of concrete fracture

It has been shown by various authors that the propagation of an initial crack in a concrete body can be analyzed by an energy concept of fracture mechanics. Plane strain conditions can be assumed for structural concrete members because the members found in practice have cross sections that are relatively thick when compared to the size of the microcrack region that forms near a crack tip.

It is known that concrete is a heterogeneous material composed of a

matrix of hydrated portland cement paste and both fine and coarse aggregate. Thus, the properties of the whole concrete model are closely related to the properties of the cement paste matrix.

Cracks in plain concrete propagate mostly through the cement paste matrix, of which the cement-gel component is similar to glass. Crack development will depend on the relative magnitudes of the stress intensity factors associated with the energy requirements for crack growth, and of the stress intensity factors associated with the elastic fields near the crack tip in the paste. These latter stress intensity factors are a function of the applied loads and body geometry.

Kaplan's development

The first application of fracture mechanics to concrete was reported in 1961 by Kaplan [50]. Kaplan made an initial step towards a possible extension of the Griffith theory to concrete. He applied the energy concept of fracture mechanics to various concretes, and he showed experimentally that in flexure (and presumably in tension) concrete fails in accordance with the theory developed by Griffith in 1920 for brittle materials and later extended by Irwin, Orowan, and others to less brittle materials. Kaplan assumed that the concretes were elastic and homogeneous and then determined their fracture toughness (the critical strain-energy-release rate G_c). However, he neglected the idea of slow crack growth prior to fracture.

Sturman [34] and Glucklich [52] have pointed out that there are many limitations in Kaplan's analysis in that two important factors were ignored. First, he has not included in his analysis the presence of pre-

load cracks and cracks other than the main fracture crack. These cracks will contribute to the strain energy dissipated if they propagate during loading. Thus, by applying the Griffith criterion to the main fracture crack alone, Kaplan has ignored other energy dissipations which will give inconsistent results in his analysis.

Second, and perhaps more significant, Kaplan fails to account for the two phase character of concrete. As discussed previously in this appendix, crack propagation is sensitive to the effects of the inelasticity and the heterogeneity of concrete. Thus, a theory designed to predict crack propagation in a homogeneous material cannot be used for such predictions in a non-homogeneous material without considerable modification. It should also be noted that Kaplan assumed that no bond failure occurs, and that the fracture surface is smooth.

Obviously, a further modification of the Griffith theory, other than Kaplan's is necessary before it can be applied to concrete in compression. It is realized that further research is necessary; however, the results of the investigation by Kaplan nevertheless indicate that the Griffith concept of a critical strain-energy-release rate, being a condition for rapid crack propagation and consequent fracture, is applicable to concrete.

Glucklich's development

As described in the beginning of this appendix, there is ample evidence to support the fact that in concrete under compression, internal cracking starts at a load far below the ultimate load. Further evidence is given by Glucklich [53] who has demonstrated the presence of internal cracking even under a small load of 360 psi. Though this may be an

extreme, there is no doubt that cracking takes place fairly early in the course of loading.

In 1962, Glucklich [52] made an attempt to extend Griffith's theory to the case of concrete in compression. He modified Griffith's theory even further to account for the multi-phase character of concrete. It has already been shown how Glucklich considered the stress redistribution in a uniaxial compressive field containing a circular hole with a notch or a satellite hole and how he applied Griffith's theory to a compression field. Now, Glucklich's development of the variability of the strain-energy-release rate (G_c) will be considered. It is believed that this fact is responsible for the phenomenon of the fracture of concrete involving the slow growth of several microcracks.

For a material which is not ideally brittle, G_c is no longer equal to 2T, but is equal to a much higher value due to the presence of new, additional energies (plastic, kinetic, and viscous). The straight lines in Figures C.5b and C.9b, representing the energy requirements, should therefore make a much steeper angle with the c-axis (Kaplan [50] estimates the general requirement of energy to be about 10 times greater than that required by surface tension alone). Moreover, these lines should no longer be straight because the dependence between the new energies and c is no longer linear. Since investigating the requirement per unit of new surface of each of the energies involved is almost impossible, the rate of release of strain energy at the onset of crack growth was determined. This value, G_c, is the energy released for the formation of a unit area of new surface.

In a heterogeneous, multi-phase material such as concrete, there

are numerous values of G_c involved within its mass. The several G_c values are due to differences in T values within the material, such as exist between those of the cement gel, the sand aggregate, and the coarse aggregate. Considering the case of uniaxial compression for two values of G_c instead of one, the picture for a heterogeneous material such as concrete will not be as that shown in Figure C.9b, but will be as shown in Figure C.10a. This figure was developed by Glucklich [52] and shows that the energy requirement curve, which was a straight line in Figure C.9b, is now a stepped line with two slopes corresponding to the two different G_c values.

Glucklich explains that if an existing crack of half length c_o is assumed, the stress will have to be σ_o before the crack starts growing, where $\pi bc\sigma_o^2/2E$ is a line parallel with the energy requirement curve at c_o. The crack will then grow spontaneously up to c, where it will be checked due to the sudden increase in the slope of the energy requirement curve. For the crack to start growing again, the stress must now be raised to σ_1, where $\pi bc\sigma_1^2/2E$ is a line parallel with the energy requirement curve beyond c_1. The crack will now propagate unchecked since the slope of the strain-energy-release curve is now equal to the steepest slope of the energy requirement curve.

For numerous values of G_c, Figure C.10a becomes Figure C.10b. For this condition the stress will have to be increased gradually from σ_o to σ_6 for the crack to increase from c_o to c_6. Beyond c_6, the crack will grow unchecked to failure because the slope of the strain-energy-release curve is higher than any slope present in the energy requirement curve.

Since concrete does not exhibit ductile behavior, Glucklich [51,52]

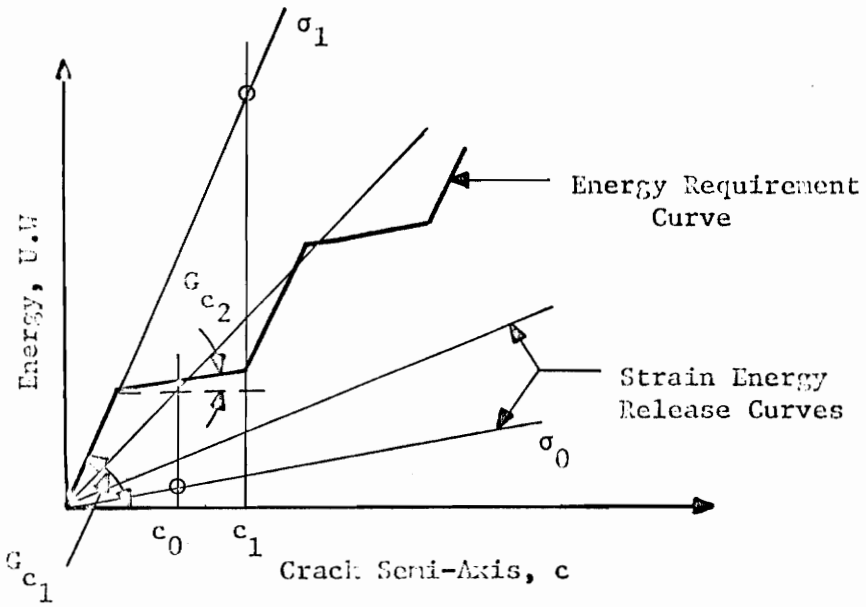

FIGURE C.10a THE FORCED GROWTH OF A CRACK IN A MATERIAL IN COMPRESSION WITH TWO G_c VALUES (FROM GLUCKLICH)

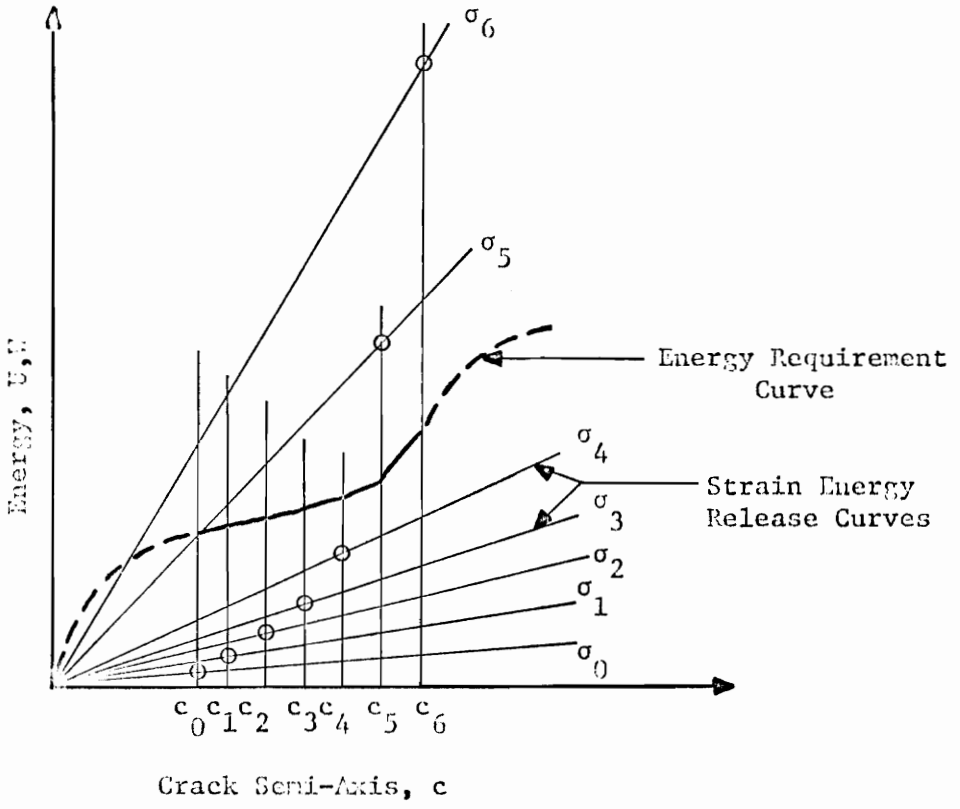

FIGURE C.10b THE FORCED GROWTH OF A CRACK IN A MATERIAL IN COMPRESSION WITH SEVERAL G_c VALUES (FROM GLUCKLICH)

has suggested that the increased energy requirement for crack propagation in cement paste is caused by the formation of a microcracking region near the crack tip. This region is a highly stressed zone with many microcracks, and it increases with the size of the crack. Since most of the microcracks are generally not incorporated into the main crack propagation, the total crack surface exceeds the area of the main (effective) crack surface. Thus, the total surface energy is greater than the energy required to form only the main crack, and the rate of energy requirement increases with the crack size. The microcracks form as the stresses near the crack tip reach some limiting stress level.

The heterogeneity of concrete provides crack arresters that are beneficial in as much as they prevent the premature occurrence of a running crack. For example, the path taken by a bond crack may be slightly deviated since both the aggregate particles and the paste act as crack arresters. This is because the propagation of a crack into a zone of higher strength demands an increase in the rate of energy requirement. However, if the crack avoids this zone of higher energy demand and detours it, the demand will increase anyway since a larger surface area of crack is formed than the surface area of the main crack. Thus, it is clear that the crack arresters prevent a premature occurrence of a running crack. Three specific crack arresting mechanisms are present in concrete. Microcracks can be arrested by encountering debonding areas, encountering air voids, or encountering a local low stress region such as between two debonded aggregate particles.

Glucklich [51] has also pointed out that in tension, the rate of strain energy release (the driving force) increases with the crack length

so that the first crack to grow is the fatal crack. Conversely, in compression, the rate of strain energy released is independent of the crack length and is therefore a constant value. Under a uniaxial compressive stress, cracks that start growing become stabilized when they encounter an obstruction or an increase in energy demand. After this, other cracks begin to grow and also become stabilized. Thus, there is progressive cracking with an increasing applied external load. This behavior explains the progressive nature of compression fracture, the considerable curvature of the stress-strain curve, and the higher strength of concrete in compression than in tension, all these having been explained in a former part of this appendix.

G_c and the surface energy of concrete

Brunauer, Kantro, and Weise [60] found that the surface energy of tobermorite (a component of the cement gel), which constitutes about 75 percent of hydrated portland cement by weight, to be approximately 390 ergs per square centimeter. It has also been found that the surface energy of quartz is approximately 980 ergs per square centimeter. Using these results, Kaplan [50] found that the average G_c value for his data was about 12 times greater than that predicted by the Griffith theory. The Griffith theory for brittle materials suggests that fracture will occur when the strain-energy-release rate just exceeds twice the surface energy of the material. Thus, it is interesting to note that Griffith himself found the experimental G_c value of glass to be approximately 10 times greater than twice its solid state surface energy.

Mechanisms of Failure In Concrete

Glucklich [52] has proposed three mechanisms of cracking fracture in concrete under compression. The first, which is called "the progressive-cracking type," is the most common. It occurs whenever the testing conditions favor the arrest of growing cracks so that others start growing in their place. Thus, there is a process of progressive cracking which ultimately leads to failure. This mechanism is a good indication of the quality of the material. The second, called "the first-crack type," occurs whenever the testing conditions favor the fast growing of an early crack, which is not necessarily the first. Such a crack is considered a premature fracture, and it traverses the entire cross section. The third mechanism of compression fracture is called "the shear failure." These three types of mechanisms are discussed in detail in Glucklich's report [52] and, therefore, will not be considered here.

APPENDIX D

CRACKING AND DETERIORATION IN PLAIN CONCRETE DUE TO FREEZING AND THAWING

Types and Causes

The deterioration of concrete due to freezing and thawing is usually conspicuous and easily detectable. Despite air entrainment, deterioration at the surface and inside concrete from alternating freeze-thaw cycles still exists. Even though cracking, crumbling of the cement paste, and scaling may produce an unsightly, uneven surface, the structure still has structural integrity, stability, and usefulness. This type of deterioration can be caused by such factors as lack of air entrainment, improper amount or type of entrained air, high water-cement ratios, excessive water content, excessive bleeding, improper finishing procedures, or lack of curing. The major classifications of freezing and thawing deterioration that may occur in concrete will now be discussed.

D-Line Cracking

An indication of freeze-thaw deterioration is the first appearance of fine cracks which run approximately parallel to transverse joints, cracks, or the free edges of a concrete surface [6,61]. Such surfaces include sidewalks, highway pavements, driveways, and other structural slabs. As deterioration progresses, the parallel cracks become larger and occur further away from the joint. Cracks also eventually occur along longitudinal joints. This type of cracking has been defined as D-line (deterioration line) cracking.

Several theories have been proposed to explain the cause of D-line cracking. One theory holds that cracking of the concrete is caused by the change in volume of coarse aggregate particles breaking the bond with the surrounding matrix. When water freezes in the voids of a paste or aggregate, forces are produced which become sufficiently great. This causes the tensile strength of the portland cement paste to be exceeded, and D-line cracks develop along lines of equal saturation, parallel to the joint. Disintegration is aided by the entrance of available water through cracks to feed the capillaries further from the edge of the slab. Continuing development of parallel cracks from the edge or joint results. Since moisture is available from moisture-holding materials in the joint (a material such as dirt) and from the base material, concrete next to a joint or a corner is exposed to more moisture than the inside portion of the slab and thus has a higher degree of saturation during freezing weather [6].

A second theory of why concrete deteriorates near a joint in a concrete slab is that as concrete is deposited and worked during construction, the fines and mortar are pushed toward the joint and a weaker, more susceptible concrete is placed near the edge [6]. This theory is not supported in some instances in that D-line cracking develops along a crack in the surface of a slab in much the same manner as it normally develops along the joint or the edge of a concrete surface.

A third theory involves the shape of the concrete structure. D-line cracking develops at vertical as well as horizontal corners and edges of rectangular slabs. Thus, it has been suggested that stress concentrations occur at the corners and the edges due to changes in temperature. This

theory has been supported by spheres made from an average concrete mixture undergoing rather little deterioration from 20 years of exposure to various weathering actions [6].

Map Cracking

Map cracking is a form of disintegration in which random cracks develop well-distributed over an entire surface instead of concentrated along joints or free edges as in D-line cracking [61].

Map cracking is caused mainly by the expansive properties of the aggregates used, and it may also be caused by alkali reactions, by freezing and thawing, by excessive heat, or by all of these [61]. It may or may not be associated with abnormal growth of the concrete.

Pattern Cracking

Pattern cracking, which is fine openings or cracks on concrete surfaces in the form of a pattern, usually occurs in concrete surfaces which experience either a reduced volume of material at the surface or an increased volume of material below the surface, or both [6].

Expansion of freezable water caused by freezing and thawing, either in the voids of the matrix or in the aggregate pores, produces pattern cracking.

Reduction of gel water where there is an abundance of air voids suggests the possibility of shrinkage in the paste under freezing conditions. Continuous cold weather will cause diffusion of water from the gel pores to the air voids and a consequent reduction of the gel pore water [6]. This will tend to cause fine cracks in the surface of the concrete.

Pitting and Popouts

Pitting is the disintegration of weak, friable pieces of aggregate due to frost action. Popouts are small, conical fragments of concrete split from the surface. Since pitting and popouts are localized in nature, considerable quantities of deleterious particles are necessary to affect the performance of a structure. Even though their appearance may be affected, many structures remain sound because of the small quantity of particles causing pitting and popouts. However, this type of deterioration can cause structural damage by allowing water to enter the structure through damaged areas [61].

Pitting is usually caused by the gradual deterioration of unsound particles near the surface of the concrete. Popouts are caused by rapid disruption of harder but saturated pieces of aggregate. That is, expanding aggregate particles are a source of internal pressure which produces a popout that leaves a shallow, conical-shaped depression whose apex is at the aggregate particle [61].

Scaling

Slabs of the highest quality concrete may undergo scaling. Concrete mortar at the surface will crumble or peel away in flakes with repeated cycles of freezing and thawing, gradually exposing the coarse aggregate particles. Scaling may be continuous, which is a progressive deterioration with time of the exposed surface until complete disintegration of the structure occurs; or it may be discontinuous, which is the deterioration of the original surface only.

Cordon [6] has gathered several theories from various authors which

can be advanced to explain scaling. These may also contribute partially to the explanation of the ultimate failure of concrete surfaces. These theories are as follows:

1. Pressure developed by expulsion of water from saturated aggregate particles.
2. Hydraulic pressure developed in more numerous capillary cavities just below the concrete surface.
3. Growth of moisture to ice crystals in capillary voids below the surface.
4. Osmotic pressures caused by a concentration of salt in capillaries immediately beneath a concrete surface.
5. Finishing operations which may create a finished surface dissimilar to the underlying concrete. Improper finishing may also densify the surface and destroy the effectiveness of air entrainment.
6. Compaction of the surface by the capillary force of receding water in the surface capillaries of drying plastic concrete and the subsequent formation of a plane of weakness.
7. Improper drying procedure. Drying reduces the water in the voids of the concrete below the critical saturation point and limits the moisture available for other deterioration mechanisms.
8. Additional freezing of subsurface ice crystals caused by melting snow and ice with de-icing salts.
9. Replenishment of surface moisture during freezing by melting snow and ice with de-icing salts.
10. Cracking and crazing (fine cracks) which provide channels for moisture to reach underlying capillary ice.

Paste Deterioration

A common type of freeze-thaw deterioration is the disintegration of the portland cement paste and subsequent exposure of the aggregate particles. Disintegration of the mortar on the surface progresses into the interior of the member. This type of deterioration can be found at

the water line of many structures.

This type of deterioration is caused by the concrete being saturated above the critical saturation point and then exposed to alternate cycles of freezing and thawing [6].

Contraction Cracks

Contraction cracks occur most frequently after the concrete hardens. They are large and fairly wide cracks occurring when contraction of the concrete takes place. Such cracks can be avoided by the proper spacing of contraction joints and by making sure that all exterior slabs are sectioned off in reasonable lengths.

Temperature variations which produce non-uniform stress distributions in a particular region are largely responsible for these cracks.

Structures Affected

Many concrete structures are affected by freezing and thawing action. Varying conditions of exposure have significant influences on the severity of deterioration that can be anticipated. The maximum vulnerability to damage by freezing action exists when the moisture in the concrete reaches the critical saturation point. Some of these structures are listed below [6].

Concrete Highway Pavements

Severe scaling may occur in concrete used in highway pavements. Pavement slabs are subjected to severe freezing and thawing exposure in cold climates. They lie flat on the ground and are exposed to precipitation and alternating cycles of freezing and thawing. These slabs may

also be exposed to salts used for snow and ice removal. Therefore, highway pavements must be protected against all the mechanisms which produce freeze-thaw deterioration. Techniques to do this include air entrainment of about 5 or 6 percent of the volume of concrete and low water-cement ratios. Except for bridge decks, deterioration of pavements due to freezing and thawing action has been essentially eliminated since air entrainment has been introduced.

Concrete Bridges and Bridge Decks

The problem of scaling on bridge decks is widespread even though air entrainment has been provided.

Other parts of bridges also present serious problems when exposed to freezing and thawing. Since most bridges span bodies of water, the abutments and piers are located in areas of fluctuating water levels. This presents the same problem as in hydraulic structures, which is the saturation of concrete at the water line. Deterioration is also prevalent on curbs, sills, cornices, and ledges because of their exposure to weathering action.

Hydraulic Structures

The use of hydraulic structures for the storage and transportation of water makes then particularly vulnerable to freeze-thaw action because there is ample opportunity for portions of these structures to become saturated. Concrete is particularly vulnerable in the region of fluctuating water levels or spray. Such concrete includes parts of dams, spillways, wasteways, tunnel inlets and outlets, valve houses, and canal structures. Exposure is also severe in such areas as the tops of walls,

piers, corners, and cornices.

Sidewalks, Driveways, Curbs, and Gutters

Concrete which can become saturated during freezing weather receives the most severe exposure to freezing and thawing. Such concrete includes gutters, tops of curbs, sidewalks, and driveways. These concrete structures have the same deterioration problem as highway pavements. The concrete can absorb water and may reach critical saturation during freezing weather.

Concrete in Buildings

Concrete in most buildings is not subjected to extreme exposure conditions except for that which is exposed to the external environment. The water to which it is then exposed comes from the rain and snow which falls on or is blown against it. However, there is usually little opportunity for the structure to reach a critical saturation level.

Foundation concrete has little opportunity to become saturated unless the concrete is below the ground water table or there is poor drainage around the concrete. When the concrete is below the ground water table, it is generally protected from freezing temperatures, and deterioration is not a problem.

The Mechanism of Frost Action in Hardened Concrete

Porosity of Concrete

The porosity of concrete is the ratio of the volume of voids (pores) to the over-all volume of the concrete specimen. Most of the important properties of hardened concrete are related to the quantity and the

characteristics of the various types of pores in the paste and aggregate components of the concrete [30]. The engineering properties of concrete, such as strength, permeability, shrinkage, and durability, are directly influenced by the pores in the concrete and the quantities of the different types and sizes of these pores.

The pores affect the properties of concrete in various ways. The strength and elasticity of the concrete are influenced by the total volume of pores, not their size or continuity. The permeability is influenced by the volume, size, and continuity of the pores. Shrinkage depends upon the nature of the solid surface and the total surface area of the pore system. The durability of concrete to freezing and thawing is controlled by the volume and the characteristics of entrained air voids.

In order to understand the significance of the various types of pores and their characteristic effects and relationships in connection with the frost action in concrete, it is important to understand the manner in which these pores originate, the factors that affect them, and the limits within which their sizes may vary.

Concrete may be visualized as a polyphase material consisting of a heterogeneous mixture of components, each component having its own characteristic pores. These components are the cement paste, the aggregate particles, and, in addition, a void component. This void component is composed of air voids, "under-aggregate" fissures, and "honeycomb" pockets [30].

"Honeycomb" pockets in concrete structures are considered to be abnormal and undesirable and can be avoided by use of proper mixture

proportions and placing practice. Therefore, these are not considered to be involved in the frost action phenomena in hardened concrete.

Fissures or zones of weakness occur under aggregate particles during the period of bleeding. The frequency with which they occur and their numbers are still unknown. It is thought that their occurrence is a function of the water content of the concrete, the bleeding properties of the cement, the amount of fine material in the mixture, and the bridging of coarse aggregate particles. Since only a weakened zone of high water-cement ratio may be produced under the aggregate, these "under-aggregate" fissures are sometimes difficult to detect.

Concrete normally contains air voids, accidentally entrapped or purposely entrained, dispersed throughout the cement mortar. The voids formed in the original plastic concrete are either water- or gas-filled. After the concrete has hardened, the water voids may tend to dry and become air voids. In terms of the other pores in the concrete, the air voids, usually the coarsest of all, may constitute from less than 1 to more than 10 percent of the total volume of the concrete.

The aggregate component in concrete occupies approximately 75 percent of the total volume. It has an internal pore volume varying from almost 0 to 20 percent or more (most commonly about 1 to 5 percent). These pores range in size from relatively fine to coarse.

The cement paste component usually contains both extremely fine gel pores and coarser capillary pores or spaces. The gel pores are considered to occupy about 28 percent of the paste volume, and the capillary pores an almost negligible volume for an essentially fully hydrated paste. Incomplete hydration would decrease the volume of gel pores and increase

the volume of capillary pores proportionately.

Thus, the total combined porosity of concrete contributed by each of its components is represented by the total capacity for evaporable water between the stages of complete saturation and dryness.

Permeability of Concrete

Permeability is defined as the ability of a liquid or gas to pass through the irregular passageways of a substance. The coefficient of permeability (having the dimensions of velocity) expresses the ease with which this movement occurs. In concrete, the liquid is in the form of water, and the irregular passageways are in the form of pores in the aggregate and pores or capillaries in the cement paste matrix. For portland cement concrete used as a highway material, a typical coefficient of permeability value is approximately less than 0.0001 ft/day [62].

Movement of water through concrete can be produced by temperature differentials, solutions of different concentrations (osmotic effects), various combinations of air or water pressure differentials, and humidity differentials. It is known that the rate of movement is dependent upon the characteristics of the membrane and of the material itself.

An increase in water permeability with rising water-cement ratio is observed with water-cement ratios higher than about 0.4 [63]. Because no capillary space is present in a fully hydrated cement paste prepared at water-cement ratios up to about 0.4, the water permeability of hardened cement paste begins to be affected only by water-cement ratios rising above this value.

The chemical composition of portland cement has little effect on the

water permeability of hardened cement paste. Also, the fineness of cement has no effect on the water permeability, provided that all other conditions remain the same. Thus, at identical water-cement ratios and degrees of hydration, there is no difference in permeability whether the cement is a fine or coarse grained [63]. However, a finely ground cement should be selected in order to minimize concrete bleeding. Extensive bleeding is an obvious source of permeability in concrete.

The permeability to water of hardened cement paste following an extensive hydration increases drastically if it is allowed to dry out. This drastic increase, produced even by mild drying, recalls the "irreversible shrinkage" which results in the extension of capillary pores. Therefore, to obtain a concrete of high impermeability, it should be protected against drying out for as long as possible.

Air voids purposely entrained in significant quantities in the concrete should increase the permeability of saturated concrete in proportion to their quantity, provided all other factors remain constant. This is because the air voids are much larger than the capillary and gel pores and do not obstruct the movement of water. However, all other factors usually do not remain constant when air entrainment is used. Air entrainment will usually reduce segregation and bleeding and permit reductions in the water-cement ratio. Consequently, the resulting concrete may actually be more impermeable despite the presence of air voids [30].

The cement-gel component of concrete has a porosity of 28 percent and a permeability of only about 2.3×10^{-15} ft/sec [22].

Absorption of Concrete

Absorption is defined as the process by which a liquid or a gas penetrates a material which increases in weight due to this penetration. With partially dried concrete, there is a weight gain upon contact with or immersion in water. In practice, there is a long period of time required to establish an equilibrium moisture condition.

The absorption of concrete will depend obviously upon the initial state and uniformity of dryness. Absorption occurs very quickly if there is complete immersion of the concrete, but the rate decreases rapidly with time. Considerable time is needed in order to reach the apparent saturation equilibrium. Identification of this equilibrium condition is very hard to determine since normal water gain of concrete by continued hydration, osmotic effects, and leaching must be considered.

Other factors significantly influencing absorption are the permeability and porosity of the concrete. These are directly influenced by factors such as the curing history, water-cement ratio, aggregate characteristics, air content, cement type and fineness, specimen size and shape, method of surface preparation, and surface carbonation, if any [30].

During absorption the larger paste capillary spaces are the first to become wetted. Next, perhaps, the finer gel pores acquire water, their rate of absorption being slow because of their low water permeability. Only after a relatively high degree of saturation (and water vapor pressure) is established in the paste surrounding the aggregate can the coarse pores in the aggregate itself become nearly filled with water. If the paste is ever below saturation, any water inside the aggregate particle can easily be removed. This is due to the much finer pore structure of the paste. It should be noted that when concrete is

immersed in water, it does not absorb as much water as its porosity permits. During immersion, a part of the air in the specimen is "entrapped" by the water and cannot find an exit. Thus, water is prevented from filling a certain percentage of pores [20].

Upon very long-continued exposure to water, the air voids, especially the smaller ones, may become filled with water. Such a process requires that the air in the void, compressed by the absorption process, be dissolved in the capillary water and slowly diffused out of the concrete to permit filling of the void with liquid [30].

Introduction to Frost Action in Concrete

When concrete is frozen, some type of action, presumably destructive, takes place within the material. Freezing of a liquid in submicroscopic spaces is a complicated phenomenon. Such is the case with the many pores and capillaries in concrete aggregates and the cement paste. The deterioration of concrete due to freezing and thawing is caused by the expansion and movement of freezing water in the pore systems of the components of concrete. Freezing may damage the paste, leaving the aggregate undamaged; or, conversely, freezing may damage the aggregate particles while the paste is only indirectly harmed.

There is more than one kind of frost action in concrete. One of the kinds produced in the freezing of fresh concrete has crystals of ice formed in the soft matrix leaving their imprints at the paste-aggregate interfaces. Sometimes when conditions are right, lenses of ice will form, producing frost heave as in solids.

However, the action of frost in hardened concrete is concerned here.

By general observations of structures throughout the land, the effects of freezing of water in concrete may range from practically no effect to total destruction.

Powers [17] explains that when damage occurs, it is due to the dilation of the cement paste, or to the dilation of some of the particles of rock, or to the dilation of both. In any case, the dilation of one component requires dilation of the structure as a whole.

Dilation is produced by pressure in the pores which may be hydraulic, osmotic, or a combination of both. Thus, if one or more of the pieces of aggregate in a concrete structure were caused to enlarge, or if the cement matrix was caused to expand, then the whole structure would have to enlarge. (However, the author does not agree totally with this. Expansion will occur when fracture occurs. Then the expansion will only be the width of the crack.)

The mechanism by which freezing causes the paste to dilate is somewhat more complicated than that which causes a rock to dilate. The difference is due to the difference in the texture or porosity of the two materials. A typical aggregate is much less porous than cement paste, and the pores it contains are usually extremely larger than those in cement paste. As a consequence of this structural difference, the osmotic pressure in a rock, if it is present at all, is a minor factor in the mechanism of frost action. In the cement paste, this pressure may be the dominant mechanism. Other mechanisms and properties are also different between these two components of concrete. Thus, it is advisable to discuss the two separately. Aggregates will be discussed first since their influence is less complicated than that of the cement paste.

Influence of Coarse Aggregate

Aggregate pores and pore characteristics

Most porous solids have a pore structure that is complicated in detail. The voids twist and turn, get larger and smaller, go in arbitrary directions, or stop altogether. The pore walls are usually crystal faces of widely varying size and orientation. The "size" of such pores is difficult to define. The most common model of porous solids is one in which the pore space is made up of a group of capillary tubes, perhaps of different sizes.

The porosity of a concrete aggregate affects the behavior of the concrete for either of two reasons--because the pore space system decreases the volume of solids in bulk volume of the aggregate, or because the pore space system permits the acquisition and retention of water or aggressive solutions and controls the movement of these liquids through the material. Chief among such effects is the great influence the aggregate pore system has on the frost durability of concrete.

Verbeck [30] has stated that aggregate constitutes about 75 percent of the total volume of concrete. Consequently, the properties of the concrete are significantly influenced by the characteristics of the aggregates and their pores. The porosity of common aggregates used in concrete ranges from nearly 0 to 20 percent or more by solid volume (most commonly about 1 to 5 percent). For lightweight aggregates the porosity may be in the range of 30 to 50 percent. The size of the pores also varies greatly among different aggregates. In very dense aggregates, such as granite and marble, the size of the pores are in the range of paste capillary spaces of intermediate size, and frequently are at least

the size of the largest paste capillaries. Other aggregates, such as various lightweight aggregates and sandstones, have a very coarse pore system.

The techniques used to determine the distribution of pore sizes include microscopic techniques, mercury porosimeter, and nitrogen or water vapor absorption methods.

The total volume and the size distribution of the pores in aggregates have an important influence on the volume stability, chemical and physical stability, bond with cement, and particularly the frost resistance of the aggregates and the concrete. They significantly affect the strength of any material, and also determine the properties of absorption, permeability, and capillary potential.

It seems that pore characteristics are the dominant factor in determining the durability of aggregates. Pore characteristics have an effect on the physical properties of a material. Larger void volumes mean a reduced specific gravity, and higher porosity results in lower strength. Both the roughness and the pore characteristics of the surface zone affect the surface texture and the quality of bond between an aggregate particle and the hardened cement paste. It has been stated that the harmful pore size is that which is large enough to permit water to readily enter much of the pore space but not large enough to permit easy drainage [6]. A rock with larger pores will have a higher absorptivity, a higher permeability, and a lower capillary potential than one with smaller pores [30]. This means that a rock with smaller pores will acquire water more slowly but will retain the water longer than will a rock with larger pores.

Basic material properties can be considerably changed when the pores of an aggregate particle are entirely or partially saturated with water. The differences between the thermal properties of plain water and dry aggregates are sufficiently important. Thus, the values of heat capacity, thermal diffusivity, thermal conductivity, and expansion coefficient of an aggregate change considerably with the absorption of relatively small amounts of water. It is believed that the thermal properties of various aggregates are of minor importance to concrete durability [30].

It is known that a few aggregates undergo excessive volume change when subjected to wetting and drying and, therefore, can contribute greatly to the shrinkage of concrete. This is basically because by shrinking the aggregate fails to restrain the shrinkage of the paste [30]. The materials which show large wetting and drying volume change usually have a large surface area and a fine pore structure.

Mechansims of frost action in aggregates

Concrete may deteriorate when exposed to freezing and thawing because of mechanisms within the aggregate particles as well as in the portland cement paste. The behavior of aggregate particles when exposed to freezing and thawing depends primarily upon the pore structure, pore size distribution, permeability, and the degree of saturation of the aggregate particle. The total porosity is of secondary importance.

Water expands slightly as its temperature falls from 39°F towards its freezing point of 32°F. It then expands much more when freezing occurs. If the expansion and escape of water is forcibly prevented,

freezing will not occur. The force required to prevent expansion and freezing is that which will sufficiently raise the hydrostatic pressure (the pressure exerted by freezing water when this water is at rest). For example, at 30°F, only a little below the normal freezing point, the hydrostatic pressure in a capillary would have to be about 2000 psi to prevent expansion and freezing. At 20°F, the hydrostatic pressure would have to be about 11,000 psi, and at 0°F, about 26,000 psi. At -7.6°F, the maximum possible pressure is reached at approximately 30,000 psi [17]. Pressures in this range may develop in aggregate particles when the saturation is critical.

It should be noted that the material strength of most aggregate is exceeded (the aggregate fractures) far in advance of most of these pressures. It is no wonder that a rock can easily be fractured by freezing. To avoid development of pressures in excess of the tensile strength of either the aggregate particles or the surrounding mortar, the water inside of the pores must be able to flow into unfilled pores or escape from the particle. The rate at which water must escape from the freezing zone and the pressure required to cause such flow depend on the rate of freezing and the permeability of the material [6]. Escape from the particle may be blocked by a frozen zone around the outside. Due to this zone, the water cannot escape and high pressures in the interior of the aggregate will then develop. Even when the flow of water is away from the freezing front or zone, hydraulic pressure (the pressure exerted by water in motion) is necessary to cause movement through small voids and may be so high as to cause fracture of the material. It is the hydraulic pressure which is the principal force developed when a rock freezes. However, stresses due to freezing

are not always due to hydraulic pressure. It is estimated that pores less than four microns in diameter will drain effectively only at pressures high enough to cause some rocks or concretes to fail [6].

It is possible for the concrete to suffer damage from freezing and thawing without the aggregate particle itself failing. Aggregates may have enough strength and elasticity to withstand the stresses without failure, but the surrounding cement paste matrix may be damaged by the expansion of the aggregate particle.

A number of mechansims explain deterioration of concrete aggregates and deterioration of the concrete containing questionable aggregates. The details of the process and the quantitative evaluation of the various mechanisms still have not been made clear, and only recently has the matter been reasonably well-understood. These various mechanisms are as follows:

Degree of saturation mechanism

Water, when it freezes at 32°F, increases in volume or expands by approximately 9.07 percent [17]. Therefore, the volume change associated with freezing water implies that a degree of saturation in the pores of the aggregate particle larger than about 91 percent (critical saturation) should be harmful to the structural integrity of the aggregate. In some cases, lower saturations are harmful because of non-uniform distribution of water in porous bodies with a variety of pore sizes. A liquid will remain preferentially in the smaller pores because of their larger capillary potential.

This so-called degree of saturation or milk-bottle-in-the winter hypothesis was the earliest and most obvious one for the deterioration of

aggregates due to frost action. If the water inside the voids cannot get out and the saturation of an aggregate particle is greater than the critical saturation, disruption of the material must occur because the pressures developed on freezing will be far larger than the material can withstand. If the degree of saturation of an aggregate particle is in the region of 90 percent or below, such that it can accommodate expansion of water when it freezes, the particle is not fractured and does not expand.

It should be pointed out that for any porous body there is a porosity value small enough so that even if the pores are completely saturated and the water freezes, the volume change will be accommodated by expansion of the solid. Verbeck and Landgren [18], in a recent analysis of the whole question of frost resistance of aggregates, gave the name of elastic accommodation to this effect.

Most aggregate particles have a greater tensile strength than portland cement paste. It is possible that some aggregates may be able to withstand relatively high pressures within the aggregate particle without fracturing; that is, the elastic strain within the rock structure itself may accommodate the expansion as water freezes to ice. As the pressures increase, the aggregate particle may expand elastically and accommodate the increased volume of ice. The surrounding concrete paste may not be able to withstand such expansion, and thus the aggregate can cause destruction of the paste even though it is not fractured. This phenomenon depends upon the size and number of pores within the aggregate particle and the strength and modulus of elasticity of the aggregate [6].

The degree of saturation hypothesis has limitations. A necessary condition is that the water has no escape from the region in question. However,

this condition is hardly ever met in concrete. There is almost always somewhere for the excess water to go. Both external boundaries of the aggregate and any internal pores within the aggregate particle may act in the same manner as entrained air bubbles and provide "escape boundaries" for the increase in pressure within the pore structure of the aggregate particle.

Hydraulic pressure mechanism

After the development of the degree of saturation hypothesis for cement paste and aggregates, Powers [17] proposed his hydraulic pressure hypothesis of frost action. This hypothesis is of major importance in understanding the mechanism of deterioration in the freezing of hardened portland cement paste, and it will be discussed in more detail in that section. The hypothesis is no less true for the aggregate component of concrete than for the paste. The only difference is quantitative.

A brief summary of the hydraulic pressure theory is that water forced out of a critically saturated region by the expansion due to freezing will move through a permeable porous solid. If the combination of speed of water movement, which is related to the speed of freezing, and distance the water must travel to an "escape boundary" is too great, the hydraulic pressure generated by this movement will be large enough to fracture the matrix material [30].

The principal function of entrained air in concrete is to give a paste that has voids spaced closely enough so that this critical distance is not exceeded. In an aggregate particle, some pores are not spaced as close and thus the critical distance is exceeded and large hydraulic pressures can

be generated to fracture the particle.

Critical size of the aggregate mechanism

The critical size theory is well-established, as much for aggregates as for paste. A rock able to absorb water contains a system of interconnected capillaries or pores, and when freezing takes place in these capillaries, the water will be forced to the outside surface. Resistance to the expulsion of excess water develops in these capillaries, and it is not localized. Other rocks have pore space within the material similar to entrained air bubbles. If one assumes that water which is forced from the void as freezing takes place must find its way to the outside surface of the rock, the size of the rock itself becomes critical [18]. Water forced for short distances would develop low hydraulic pressures which would increase as the distance increases. The critical size of an aggregate therefore depends on [6]:

1. Rate of freezing
2. Degree of saturation
3. Permeability

Powers [17] visualized the freezing of a saturated piece of rock with the aid of the sketch shown in Figure D.1. Heat is supposed to be flowing downward, and the dotted area has already become frozen. The lines with arrows represent general directions of the flow of water displaced during freezing. Freezing is supposed to be progressing at a steady rate at the inside of the frozen zone.

Powers [17] explains that during the freezing process, hydraulic pressure along any flow line is highest at the point of freezing, and is

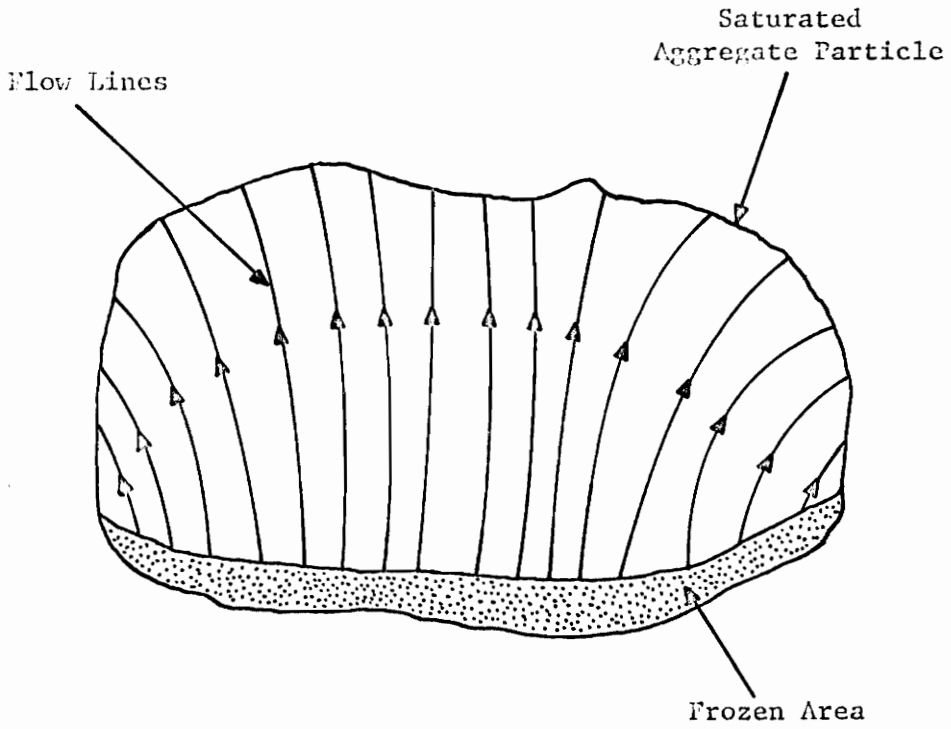

FIGURE D.1 SKETCH ILLUSTRATING FLOW LINES OF WATER DISPLACED DURING FREEZING OF A PARTICLE OF SATURATED ROCK

practically zero at the point of escape from the particle of rock. At a given rate of freezing, or given rate of water-flow, the maximum pressure is higher for the longer path of flow through an unfrozen boundary. For a given distance and rate of outward flow, the maximum pressure is proportional to the resistance to viscous flow. This resistance can best be expressed in terms of the coefficient of permeability of the material.

The highest hydraulic pressure that can be generated inside the aggregate particle is limited by the material strength of the particle. Thus, if at a given rate of freezing, the flow lines are long enough to develop stresses exceeding the strength of the rock, freezing causes fracture and destruction of the rock. It follows that a given kind of rock frozen at a particular rate in the saturated state will have a critical particle size, or critical thickness, above which the force developed from hydraulic pressure is able to fracture the particle, and below which the particle is not fractured. In practice, differentiating between sizes that will become fractured and those that will not is a difficult task, especially when dealing with irregular shaped particles.

An aspect that should be noted is that if the particle in Figure D.1, which is somewhat an elongated particle, were rotated 90 degrees with respect to the direction of the freezing front, it would develop a different pattern of flow lines, and a different stress in the rock at a given rate of freezing [17]. Thus, under given conditions, the rate of freezing inside the aggregate particle would depend on the orientation of the particle embedded in the cement paste matrix.

The permeability of most rock used as aggregate is much greater than that of hardened paste. High permeability allows more water to be absorbed

in a given period of time. On the other hand, it permits the water to be expelled from the particle more rapidly without developing high pressures. With rocks subject to the critical size failure, the permeability and hence the pore size is a factor of highest importance because it determines whether the size of the aggregates exceeds the critical distance or not. For any given capacity for freezable water (i.e., the quantity of water in a unit volume of rock that will become frozen at a specific subfreezing temperature), and for any given length of flow path, maximum pressure will be higher the lower the coefficient of permeability of the rock. At a given porosity, the smaller the mean size of the capillaries, the lower the coefficient of permeability and the higher the resistance to flow. In rocks the capillaries are intergrain spaces; thus the capillaries are considered very small which is one characteristic of an unfavorable capillary system.

Very porous rocks do not deteriorate when exposed to freezing because they allow the ingress and egress of water rapidly enough so that internal pressures do not develop. Rocks with relatively fine pores, on the other hand, are more susceptible to fracturing unless the rock particles are small enough that their size is not critical.

Rocks which cause typical popouts such as cherts, shales and some limestones are susceptible to fracturing when frozen in a saturated condition. Verbeck and Landgren [18] demonstrated the principle of critical size by direct freezing experiments carried out on three different size-groups of saturated chert. They calculated a critical distance of 1/2 inch for a typical chert particle. If the aggregate particle is larger than this (and critically saturated), it should fracture internally on freezing in a "critical size"

type of failure.

This is just the sort of behavior that is observed with popouts. Under each popout a fractured rock of comparatively high absorption and fine pores will be found. Typically a flake of mortar comes out and retains part of the aggregate piece. This behavior shows that the rock fractured internally just as the hydraulic pressure mechanism predicts. Furthermore, if this mechansim is valid, there should be more trouble with a larger coarse aggregate than with a smaller one which may be smaller than the critical distance. Accordingly, it has been proven that larger aggregate particles give much more difficulty from popouts than do smaller ones.

Expulsion of water from the aggregate into the paste mechanism

When a piece of aggregate is critically saturated and a freezing front passes across it, the increase in the volume during the formation of ice must be accommodated either within the aggregate particle itself or within the surrounding cement paste. Any excess water within the aggregate will be expelled. If, in the course of this process, the critical distance is exceeded, the aggregate will fracture internally. Even if the aggregate is not so affected, the excess water will be expelled into a paste of a very low permeability and small critical distance. This excess water will then be available for possible freeze-thaw destruction to the cement paste.

Verbeck and Landgren [18] presented this mechanism to account for the non-durability of large-critical-size aggregates. Analysis of this expulsion-into-the-paste mechanism shows that trouble will occur around the periphery

of the aggregate particle. Therefore, there must be sufficient entrained air bubbles in the paste not only to accommodate the expulsion of water from the capillaries of the paste, but also to accommodate the water which is expelled from the aggregate particle. A completely non-air-entrained paste would fail disastrously from the expulsion of water from an aggregate because since the particle is critically saturated, the paste is sure to be also. The degree of saturation of the aggregate has to be in the critical range since water will not be forced from the aggregate particle unless saturation is greater than 91 percent. It is usually considered that entrained air cannot be depended on adequately to correct a non-durable aggregate and result in sound concrete.

This expulsion-into-the-paste mechanism also implies that, as with the critical-size theory, a larger piece of aggregate will produce more destruction because it will contain more water to be expelled into the paste. One can determine a certain size where the destruction begins. The value depends on the porosity and degree of saturation of the aggregate particle and the air content, capillary porosity, and critical distance in the cement paste. The size that separates the harmful from the harmless is roughly the maximum size of coarse aggregates commonly used in concrete.

Rocks which contain a large number of pores, such as porous sandstones and reef rock, have pore sizes so large that there is no danger of deterioration from freezing and thawing. Water is easily absorbed by these rocks, and the permeability is sufficient that pressure is not built up within the rock during freezing. All excess water is expelled from the aggregate particle.

Rocks which have medium fine pores absorb water quite rapidly, and the permeability is also sufficient that water can be forced from the aggregate particle before building up any large pressures. Rocks of this type can cause more trouble by expulsion of the excess water into the surrounding paste and may cause popouts or expansion cracks to occur in the concrete.

Rocks of very fine pores do not saturate rapidly, but they do gradually become highly saturated by absorbing large amounts of water. Claystones, siltstones, cherts, and shales are very susceptible to popouts. Upon freezing, excessive pressures are built up within the rock particle causing it to expand and fracture the concrete.

Gel water diffusion mechanism

Powers and Helmuth adapted to cement paste an older theory of frost action in soils that leads to lens formation and frost heave [30]. This theory has been amplified by others for soils and has recently been considered in a general thermodynamic treatment for all porous solids. Powers and Helmuth called this the gel water diffusion mechanism which does not depend on a volume increase during freezing. There is no reason why this mechanism should not be applicable for ice in aggregate pores at the paste-aggregate interface as it would for the cement paste. Gel water can diffuse to such bodies of ice as well as to any other.

The principle is that some rocks have the property of attracting unfrozen water from an outside source to ice as ice crystals start to grow at a subfreezing temperature. This is similar to the growth of ice in the capillaries of portland cement paste. For the cement paste, the ice is in

the capillary pores, and the unfrozen water is in the gel pores. This process will generate distending pressures that will cause heave in soils and cracking in concrete [30].

However, the mechanism is considered to be of relatively minor importance. This is because the differential of free energy between the gel water in cement paste and the ice crystals within the aggregate particle would undoubtedly be limited to that portion of the surface of the rock immediately adjacent to the cement gel. Any aggregate particles which have a strong affinity for water would readily absorb the available water [6]. It is believed that the previous mechanisms discussed play more important roles in deterioration of aggregates than the possible effect of growth of ice crystals within the aggregate particle itself.

Influence of Cement Paste

Structure of portland cement paste

In order to understand the mechanisms of freezing and thawing action within the portland cement paste, a thorough understanding of the structure of the paste itself is essential.

Portland cement is composed of a mixture of several compounds, among which the two most important ones are tricalcium silicate, Ca_3SiO_2; and beta-dicalcium silicate, $B\text{-}Ca_2SiO_2$. These silicates constitute about 75 percent of the portland cement by weight [6]. During the hydration reaction these two silicates produce similar calcium silicate hydrates and different amounts of calcium hydroxide. Chemically heterogeneous hydrated cement, produced from the hydration reaction, is the name given collectively to the several products of reaction between the components of anhydrous cement

and water. The water-filled space in a freshly mixed cement paste represents space which was available for the formation of these cement hydration products. The volume of this space was initially determined by the water-cement ratio of the paste.

The calcium silicate hydrate, because of its similarity to the natural mineral tobermorite, has been called tobermorite gel. It has a bulk volume larger than the original unhydrated cement itself. The gel is an impure colloidal and is the most important constituent of hardened portland cement paste and, consequently, of the concrete. It is impure in the sense that it contains small amounts of components not usually stated in its chemical formula. Tobermorite gel plays a vital role in the setting and hardening of the paste and in determining the strength and dimensional stability of hardened paste and concrete.

The hydrates of the compounds containing iron and alumina are also colloidal. There is also an important non-colloidal component which occurs mostly as thin crystals intergrown with colloidal materials called crystalline calcium hydroxide.

Thus the structure of cement paste can be described as being composed of cement-gel, a residue of unhydrated cement, if any, and spaces not filled with cement-gel (i.e., voids). These components are described as follows:

Cement-gel

Cement-gel is composed of very fine particles which are products of the hydrated cement. The predominant component of cement-gel is calcium silicate hydrate which is called tobermorite gel. This may constitute about 50 percent of the cement-gel. The tobermorite gel is a poorly crystalline material,

consisting of extremely thin sheet-like particles that may be crumpled or rolled as foil. Another product of the hydration of the calcium silicates is calcium hydroxide, which may form crystals large enough to be seen by an electron microscope and which may constitute 22 to 25 percent of the cement-gel by weight. These two hydration components are collectively referred to as gel particles. Recent studies with the electron microscope indicate that gel particles are so aggregated as to form semi-discrete bodies having more or less laminar structure. The space apparently occupied by such a body is approximately 72 percent solid and 28 percent space accessible to evaporable water [17]. This means that the porosity of the cement-gel itself is approximately 28 percent.

Powers [17] described gel particles as being so small that they can be seen only with the aid of an electron microscope. They are approximately 30 or 40 angstroms thick, which is about 10 or 13 water molecule diameters. It is because of this dimension that they have such a high specific surface area and are classified as colloidal material. The average specific surface area of the solid part of cement-gel is about 175 to 200 m^2/g, which is almost one million square feet per pound.

It is known that two physical properties of hardened cement paste--surface area and porosity--are decisive in determining the two most important engineering properties of strength and dimensional stability. Thus, Powers applied the term cement-gel to the part of hardened paste that is responsible for surface area and porosity.

Residue of unhydrated cement

Some particles of dry cement which have not reacted with water are

sometimes contained in the cement paste. This is due to inadequate mixing procedures or insufficient water used in mixing.

Spaces not filled with cement-gel

The spaces not filled with cement-gel are the voids or pores within the portland cement paste. Freezing and thawing deterioration mechanisms occur in the pore structure of the cement paste as well as in aggregate particles. Knowledge of the submicroscopic pore system of hardened portland cement paste is necessary in understanding the mechanisms of freeze-thaw deterioration. Therefore, voids and pores in portland cement paste are classified and described as follows:

Gel pores: These are interstitial pores or cavities of molecular dimensions between the particles of tobermorite gel and other calcium silicate hydrates (or between the gel particles in general). It has been determined that the gel pores in the tobermorite structure constitute about 28 percent of the over-all volume of an essentially fully hydrated paste. Gel pores are extremely small and are believed to average approximately 15 to 20 A^{o} in diameter, 18 A^{o} being a reasonable average. Since a water molecule has a diameter of about 3.6 A^{o}, the gel pores are about 5 times the size of a water molecule [17]. From recent studies, it appears that there is no unique single size for these gel pores not are the gel pores totally different in size than some of the capillary pores. It is now considered that the typical shape of gel pores is slit-shaped or plate-like. The assumption of a cylindrical pore shape for some pores is also valid here. These pores are too small to be visible with an ordinary light microscope. The volume of the gel pores in the paste increases with continued hydration of

the cement.

Capillary pores or cavities: These are the larger unfilled spaces or pores between aggregations of gel particles. At any time, that part of the original water space which has not become occupied with hydration products constitutes the "capillary" cavities or system of the paste. These too are submicroscopic and cannot be seen with an ordinary light microscope. They are formed by uncombined water in excess of that required for hydration of the portland cement; or, in other words, when the cement-gel does not completely fill the originally water-filled space. Capillary cavities occur in a wide variety of shapes and sizes and are estimated to average approximately 5000 A^{o} in diameter [6]. Such an estimate of the size of capillary cavities is based on the assumption of a generally cylindrical pore shape and on calculations of the hydraulic radius of the pore system, this being the volume of the system divided by its surface area. For cylindrical pores the hydraulic radius is one fourth of the diameter, and for slit-shaped or plate-like pores the hydraulic radius is one half of the width [30]. At early ages, when a considerable amount of cement is still unhydrated, or in older pastes having a high water-cement ratio, these capillary cavities constitute an inter-connected system of capillaries; otherwise, these spaces occur as cavities isolated by cement-gel [17]. The volume of the capillary cavities depends on the water-cement ratio. The capillaries are more numerous and larger when the original water-cement ratio is higher and the period of curing is shorter. Verbeck [30] explains for an essentially fully hydrated paste having an initial water-cement ratio in the range of 0.35 to 0.38 by weight, the capillary spaces occupy an almost negligible volume of cement paste. This is because the bulk volume of the

gel is sufficient to fill the empty water space and thus, produce a paste free from capillary pores. A fully hydrated paste at a higher water-cement ratio of approximately 0.70 would contain about 20 percent gel pores and 30 percent capillary pores by volume [30]. This is because the gel volume is not sufficient to completely fill all the original water space in the paste. Thus, pastes having relatively large volumes of capillaries may be produced. Incomplete hydration would decrease the volume of gel pores and increase the volume of capillary pores proportionately.

Bubbles of entrained air (air voids): These are extremely large as compared with the capillary cavities and gel pores in the paste. They vary from a few microns to a few millimeters in diameter. Many of the accidentally entrapped voids can be seen with the unaided eye and may range in size up to about 2 mm in diameter. The purposely entrained voids which help reduce freeze-thaw destruction and de-icer scaling in the paste may range in size from 0.025 to 0.050 mm in diameter. For an average size bubble, the curvature of the boundary would hardly be discernible when compared with a gel pore or capillary cavity. The air voids may constitute from less than 1 to more than 10 percent of the total volume of the concrete. The number and size of these voids depend upon several factors including amount of air-entraining agent used, duration of mixing, concrete consistency, type of vibration, and size distribution and maximum size of aggregate.

Recalling that cement paste contains air voids, capillary pores, and cement-gel, and now noting that cement-gel contains gel pores, we understand that the total porosity of cement paste comprises gel pores, capillary pores and bubbles of entrained air, if any.

The volume of pore space occupied in a cement paste depends on the

initial amount of water mixed with the cement. When paste sets, it acquires a volume which is approximately equal to the volume of water plus the volume of cement used. If two pastes were prepared from the same cement, using the same amount of cement but different amounts of water, then after setting, the paste with the greater amount of water will have the greatest volume. After hydration the two pastes will contain the same amounts of solid material, because the same amounts of cement will produce the same amounts of hydration products. Therefore, the paste with the larger volume will contain a larger number of pores or larger pore space.

This effect has an important influence on the strength of the hardened paste and thus on the strength of the concrete. Paste which contains the fewest pores will produce the strongest concrete since the strength is in the solid part of the paste, primarily in the tobermorite. Pores which are filled with water and air have no strength. Therefore, in the mixing of concrete, no more water should be used than is absolutely necessary.

Lott [54] explained that the strength of cement paste is derived from physical and chemical bonds between the gel particles. Van der Waal forces are effective over the distance between gel particles in cement paste. These physical bonds are important because of the high specific surface area of the gel particles. Cohesive forces other than the physical bonds also act between the gel particles. Chemical bonds are assumed to act where the particles make contact with one another.

Water in gel pores will have characteristics, such as vapor pressure, freezing characteristics, and mobility, notably different from those of

free water in bulk. This water does not behave as normal free water. This is also true, but to a lesser degree, for water in the larger capillary spaces. The gel pores retain significant quantities of surface adsorbed water and hydrated water or both, even at relatively low humidities. Capillary water is more volatile than is gel water. The water in the capillary spaces is almost completely evaporable at humidities below 40 percent. Above 40 percent relative humidity, "capillary condensation" occurs, that is, the capillaries become filled with water by precipitation from the vapor phase [30].

The permeability of paste and concrete is more closely associated with the capillary pores because water in these pores can move much more freely under hydrostatic pressure than can water in gel pores.

Mechanisms of frost action in cement paste

It is safe to say that if the various aggregate particles in a concrete mixture become critically saturated, then the paste will definitely become saturated also. When this occurs, the paste will quickly become destroyed by freezing, regardless of the kind of cement used or the extent of the curing period.

When saturated cement paste becomes frozen, it has a critical thickness just as with aggregate particles. Whereas the initial thickness of aggregates is expressed in tenths of an inch, or in inches, that of cement paste is expressed in thousandths. The average critical thickness in pastes is probably around 3 thousandths of an inch [17]. That is why, if paste is to be frozen while saturated, it is necessary to incorporate large quantities of air bubbles so that the shells of paste around the bubbles have less than

the critical thickness.

Pastes are considered highly porous and have an extremely fine texture. Its relatively high capacity for freezable water and extremely low coefficient of permeability account for the extreme smallness of its critical thickness. In saturated pastes it is only that water which is evaporated at about 80 percent relative humidity that will freeze at normal winter temperatures [30].

It shall be noted that in this research, air entrainment was used to reduce or eliminate the destruction due to frost action. Thus, all destruction to the concrete was initially influenced by the aggregate particles and not the cement paste.

There are several mechanisms which have been advanced to explain deterioration of cement paste. Some mechanisms develop pressures in the pores of the paste. These pressures, as with aggregates, can either be positive (liquid in compression) or negative (liquid in tension). The positive pressures are of greatest importance since they are usually associated with freezing stresses, alkali-silica reactions, and strength reductions in the concrete. The various mechanisms are described as follows:

Critical saturation mechanism

As with aggregates, the degree of saturation and its relation to deterioration is very important in pastes. The mechanism is basically the same for the two components of concrete.

The theory of critical saturation is accepted without question. Any void or pore in the cement paste which is more than 91 percent full of

water will be subjected to pressures when freezing water turns to ice, unless the excess water can be forced from the void during freezing. Only when saturation is carried beyond 91 percent does the ice have insufficient room in expanding and thus produces cracks.

It seems obvious that a completely water-soaked aggregate will yield to frost action no matter what its strength while an incompletely water-soaked aggregate resists this action even when its strength is low. An aggregate saturated below or up to 91 percent of complete saturation is designated as incompletely saturated while above 91 percent is designated as critically saturated.

Hydraulic pressure mechanism

As already mentioned, the hydraulic pressure mechanism is of major importance in understanding the mechanism of deterioration in the freezing of hardened cement paste. It is equally true for the deterioration in aggregate particles. The phenomenon in cement paste alone will now be discussed.

Gel pores are generally filled with water in portland cement paste. In a water-soaked or saturated paste, the capillary cavities will also be filled. When the temperature falls to the point where freezing should begin, ice crystals appear in the largest capillary cavities. Ice can exist within the boundaries of the paste only in capillary or air-void cavities. This is because capillary cavities are sufficiently large to accommodate ice crystals. Bubbles of entrained air are not generally filled with water unless the concrete becomes saturated by means of vacuum or pressure. When the water in the larger cavities begins to change to

ice, the volume of water plus ice will exceed the original capacity of the cavity. Therefore, the cavity must dilate or the excess water must be expelled from it during the time when the water in the capillaries is changing to ice.

In the capillary cavities a very small amount of water freezes near the normal freezing point, but a significant amount of freezing occurs after the temperature falls below the normal freezing point [6]. This behavior indicates that most of the capillary cavities are extremely small. The surface tension of the bodies of water in capillary cavities puts them under pressure that is higher for the smaller bodies. Therefore, the smaller the void, the higher the pressure and the lower the freezing point.

Gel pores are so small that it is impossible for water to freeze unless the temperature drops far below the normal freezing point. It is believed that freezing cannot occur at any temperature above $-78^{\circ}C$. Since no more than probably a dozen or so water molecules can occupy a gel pore, ice crystals cannot form. Hence, in normal frozen concrete, water in the gel pores is supercooled but not frozen.

As already mentioned, freezing, when it occurs, is accompanied by the expansion of the water-ice system. If the concrete is at or above critical saturation, there is a tendency that the excess water will be expelled from the capillary spaces during the process of freezing. There is also a strong possibility for the excess water in the capillaries to escape to the nearest air void in the cement paste. The growing ice bodies in the capillary spaces can be considered as pumps forcing water through the paste toward the air void boundary (the escape boundary). The pore pressures produce triaxial dilation of the concrete. The factors which affect the pore pressures that

are developed during this process depend upon [30]:

1. The amount of freezable water.
2. The rate of freezing.
3. The distance from the capillary to the void boundary.
4. The coefficient of permeability of the surrounding material through which the water is forced.

In general, during the process of freezing, hydraulic pressure will exist throughout the paste. When water freezes in a capillary close to an escape boundary, the excess water can escape from this capillary more easily than from one farther away since the resistance to flow is less. For points farther away from an escape boundary, the escape of water will be harder since the hydraulic pressure will be higher. If a point in the paste is sufficiently remote from an escape boundary, the hydraulic pressure will be high enough to exceed the strength (exceed the elastic limit or tensile strength) of the surrounding gel, and thus will produce permanent damage known as frost deterioration.

Generation of destructively high hydraulic pressures during the freezing of water in the capillary pores can be prevented by the presence of air voids of proper number and size. These serve as escape boundaries for the expulsion of excess liquid and should be very close to the freezing site. Thus, it is assumed, that every air void in the cement paste is bordered by a zone in which the hydraulic pressure cannot become high enough to cause damage. Theoretically, pressure increases approximately in proportion to the square of the distance from the air void [6]. In pastes without air entrainment, the critical distance is in the range of approximately 0.12 to 0.25 mm [30]. Thus, by reducing the distance between

voids to the point where the protected zones overlap, disruptive pressures in the paste are prevented.

Diffusion and freezing of gel water in capillaries

Cordon [6] explains that ice in the capillary cavities of frozen cement paste is surrounded by unfrozen, supercooled water in the gel pores. If the cement-gel is saturated, the gel water will have the same free energy as that of ordinary water in bulk. At $0^{o}C$, the temperature at which the water in the capillary is assumed to begin freezing, there is thermodynamic equilibrium between the gel water and the ice in the capillary. This is true if the capillary is so large as to have negligible surface energy and if both the ice and gel water are under a pressure of one atmosphere. If the temperature drops below $0^{o}C$, the gel water is no longer in thermodynamic equilibrium with the ice because its free energy is higher than that of the ice. The gel water thus acquires an energy potential enabling it to move into the capillary cavity where it freezes and makes the ice crystals already present in the capillary space to grow and enlarge.

The cement-gel has a tendency to shrink as water is diffused from it. Conversely, the growth of ice bodies expands the capillary spaces and places the ice and the film around the ice under pressure. This swelling pressure in the ice film produces expansion of the paste. For example, [6], if the gel were saturated and the capillary cavities contained ice at $-5^{o}C$, pressure in the film between the ice and the solid gel could be as much as 1200 psi. This much pressure would surely cause the paste to dilate appreciably and the concrete specimen, as a whole, to expand.

It has been concluded that entrained air voids protect the concrete from ice pressures built up in the capillary voids. From thermodynamic considerations it can be seen that gel water will not only diffuse to the capillary cavities, but will also diffuse to ice previously forced into the air voids by hydraulic pressure. The period of diffusion to the capillary cavities is relatively brief for a paste containing air voids. Volume increase of the air-void ice results in very little expansive force at all. The ice in the air void grows, but it may be under no significant pressure.

It should be noted that an outside source of moisture, through cracks or fractures in the concrete, may replenish the gel water during a thawing cycle. This outside source will theoretically provide moisture for unlimited growth of the ice crystals.

Osmotic pressures

When concrete is setting and hardening, hydration of the cement takes place and alkalies (oxides of sodium and potash) are released. All silicate and silica minerals are attacked by these alkalies. Concrete prepared with cement of high-alkali content and reactive siliceous aggregates can produce an alkali-silicate type of reaction product (alkali-silica gels and fluids) which may cause expansion and cracking of the concrete. If the alkali-silicate product is gel-like, swelling pressures can be induced in the pores; or if the product is fluid-like, osmotic pressures can be induced.

Osmotic action occurs when solutions of different concentrations of soluble particles are separated by a semi-permeable membrane or barrier.

The particles will try to pass through the barrier into the solution where its concentration is lower, thus producing a differential head between the two solutions. The formation of the fluid- and gel-like products to which the gel particles in the concrete are relatively impermeable tends to absorb water and dilate, producing osmotic pressures that apply destructive pressure to the walls of the pores. This pressure may ultimately rupture the pore and the surrounding paste area. The alkali-silica products may then fill the fractures. The fissures gradually extend until they reach the surface of the concrete, and the cracks commonly expel gel.

A similar phenomenon occurs when water in the capillary cavities of cement paste contains a concentration of salts. Cordon [6] explains that this concentration increases as the water begins to freeze. The water that is being forced from the capillaries will have a higher concentration of salt than the surrounding gel pore water. This osmotic action increases the hydraulic pressure in the cement paste as the water is forced from the capillaries into the gel pores. A pressure differential develops in the direction toward the capillary pore and opposite to the flow of water. The pressure required to overcome osmotic pressure in the capillary pore is a combination of the hydraulic pressure required to force capillary water into the gel pore plus the osmotic pressure which resists this flow.

The mechanism just described has been suggested as a possible cause of scaling of concrete slabs or pavements where salt is used. Using salt on pavements to remove ice and snow will increase the concentration of salt in the capillary cavities near the surface of the pavement. The concentration of this salt increases as the salt solution begins to freeze;

and, thus, osmotic pressures are built up in the capillary cavities. This increase in pressure may be sufficient to cause rupture of the cement-gel near the surface of the pavement, and consequently cause scaling.

Scaling mechanisms

The surface of a concrete slab is artificially compacted by finishing. Such a finish on a slab exposed to freezing and thawing may lead to surface scaling.

The mechanism involved in this can be illustrated by a natural compacting phenomenon in concrete. When concrete is in its plastic state, the greater density of the aggregate and cement particles will cause them to settle and the lighter water will tend to rise, creating a film of water on the surface of the plastic concrete. This phenomenon has already been discussed and is known as "bleeding." As long as this film of water is on the surface, covering the aggregate and cement particles, the only natural compacting force is the force of gravity. Continued evaporation of the surface water may lower the water level so that the particles of aggregate and cement are exposed. Further lowering of the water surface is resisted by capillary forces in the surface voids among the particles of solids. The size of the capillary and the length of the tube govern the magnitude of these capillary forces. It has been determined that these forces can result in a compacting force ranging from 500 to 1400 psf [6]. This compacting force creates a dense surface layer of concrete with a less dense layer immediately beneath it. If sufficient moisture is present to permit the growth of capillary ice in the porous layer during freezing weather, the compacted surface will separate from the rest of the

concrete mass.

Concrete beneath the surface is not subjected to these capillary forces and is, therefore, not compacted. If this scaling mechanism develops before the concrete has set, bleeding water will continue to rise but will be trapped beneath the compacted surface layer. This trapped water will then be available for growth into ice crystals.

APPENDIX E

PAYNE'S STRESS CALCULATIONS

The stress calculations developed by Payne [13] for Figures 3.1a and 3.1b will now be shown here. The following equations and discussion are taken directly from his work, Reference 13. These equations and conclusions are pertinent in the author's work and in developing his rate of deterioration theory in Chapter III.

Stresses Due to a Fluid Pressure

To determine a relative value of the critical tensile stress created in a capillary by fluid pressure, the following assumptions were made:

1. The problem was analogous to the thick-wall cylinder problem.
2. The external pressure (p_o) was zero.
3. That "b" was large in comparison to "a" (see Figure 3.2a).
4. That p_o = external pressure and p_i = internal pressure.
5. A positive value for σ indicates tension.

Therefore, from Timoshenko [64] we obtain for the normal radial stress

$$\sigma_r = \frac{a^2 p_i}{b^2 - a^2}\left(1 - \frac{b^2}{r^2}\right)$$

and at r = a, which is at the capillary boundary

$$\sigma_r = -p_i \qquad \text{(E.1)}$$

Also from Timoshenko, the normal hoop stress is

$$\sigma_t = \frac{a^2 p_i}{b^2 - a^2}\left(1 + \frac{b^2}{r^2}\right)$$

and at r = a

$$\sigma_t = \frac{a^2 p_i}{b^2 - a^2}\left(\frac{a^2 + b^2}{a^2}\right) = \frac{a^2 + b^2}{b^2 - a^2} p_i$$

Dividing both numerator and denominator by b^2 we obtain

$$\sigma_t = \frac{\frac{a^2}{b^2} + 1}{1 - \frac{a^2}{b^2}} p_i$$

If b is assumed to be large in comparison to a, then

$$\sigma_t \simeq p_i \qquad \text{(E.2)}$$

It should be noted that if p_o is not zero, then σ_t decreases in absolute value as p_o increases, and if b is not relatively large in comparison to a, then σ_t increases in absolute value as b decreases.

This analysis indicates what could occur as the transient fluid pressure increases, and it indicates the direction of change in σ_t as p_o and b are varied.

The values of σ_r and σ_t, Equations E.1 and E.2, for the above assumptions are shown in Figure 3.1a of the first part of Chapter III. In that figure p_i, σ_r, and σ_t are changed to p.

Stresses Due to Uniaxial Prestressing

To determine a relative value of the critical stresses created at the surface of a capillary by a linear uniaxially applied prestressing stress (in the Z-direction), the following assumptions and notations were made (see Figure 3.2b):

1. A positive value for σ indicates tension.
2. The formulas are in terms of polar coordinates.

3. That a = radius of the hole

r = radius of the point in question

σ = prestressing stress

σ_r = radial stress

σ_θ = tangential stress

$\tau_{r\theta}$ = shearing stress

4. That "a" is small in comparison to the plate width.

5. Working with a unit depth into the paper.

6. The relationship between θ in Figure 3.2b and the infinitesimal element on Figure 3.1b is as follows:

Angle θ	Infinitesimal Element
0^o	3
45^o	2
90^o	1

Therefore, from Wang [65] we obtain

$$\sigma_r = -\frac{\sigma}{2}\left(1 - \frac{a^2}{r^2}\right) - \frac{\sigma}{2}\left(1 + \frac{3a^4}{r^4} - \frac{4a^2}{r^2}\right) \text{COS } 2\theta$$

$$\sigma_\theta = -\frac{\sigma}{2}\left(1 + \frac{a^2}{r^2}\right) + \frac{\sigma}{2}\left(1 + \frac{3a^4}{r^4}\right) \text{COS } 2\theta$$

$$\tau_{r\theta} = \frac{\sigma}{2}\left(1 - \frac{3a^4}{r^4} + \frac{2a^2}{r^2}\right) \text{SIN } 2\theta$$

At $\theta = 0^o$, and $r = a$

$$\sigma_r = -\frac{\sigma}{2}\left(1 - \frac{a^2}{a^2}\right) - \frac{\sigma}{2}\left(1 + \frac{3a^4}{a^4} - \frac{4a^2}{a^2}\right) \text{COS } 0$$

$$\sigma_r = 0$$

$$\sigma_\theta = -\frac{\sigma}{2}\left(1+\frac{a^2}{a^2}\right)+\frac{\sigma}{2}\left(1+\frac{3a^4}{a^4}\right)\text{COS } 0$$

$$\sigma_\theta = +\sigma \quad \text{(tensile stress at element 3)} \qquad \text{(E.3)}$$

$$\tau_{r\theta} = \frac{\sigma}{2}\left(1-\frac{3a^4}{a^4}+\frac{2a^2}{a^2}\right)\text{SIN } 0$$

$$\tau_{r\theta} = 0$$

At $\theta = 45^\circ$, $r = a$

$$\sigma_r = -\frac{\sigma}{2}\left(1-\frac{a^2}{a^2}\right)-\frac{\sigma}{2}\left(1+\frac{3a^4}{a^4}-\frac{4a^2}{a^2}\right)\text{COS } 90$$

$$\sigma_r = 0$$

$$\sigma_\theta = -\frac{\sigma}{2}\left(1+\frac{a^2}{a^2}\right)+\frac{\sigma}{2}\left(1+\frac{3a^4}{a^4}\right)\text{COS } 90$$

$$\sigma_\theta = -\sigma \quad \text{(compressive stress at element 2)} \qquad \text{(E.4)}$$

$$\tau_{r\theta} = \frac{\sigma}{2}\left(1-\frac{3a^4}{a^4}+\frac{2a^2}{a^2}\right)\text{SIN } 90$$

$$\tau_{r\theta} = 0$$

At $\theta = 90^\circ$, and $r = a$

$$\sigma_r = -\frac{\sigma}{2}\left(1-\frac{a^2}{a^2}\right)-\frac{\sigma}{2}\left(1+\frac{3a^4}{a^4}-\frac{4a^2}{a^2}\right)\text{COS } 180$$

$$\sigma_r = 0$$

$$\sigma_\theta = -\frac{\sigma}{2}\left(1+\frac{a^2}{a^2}\right)+\frac{\sigma}{2}\left(1+\frac{3a^4}{a^4}\right)\text{COS } 180$$

$$\sigma_\theta = -3\sigma \quad \text{(compressive stress at element 1)} \qquad \text{(E.5)}$$

$$\tau_{r\theta} = \frac{\sigma}{2}\left(1 - \frac{3a^4}{a^4} + \frac{2a^2}{a^2}\right) \text{ SIN } 180$$

$$\tau_{r\theta} = 0$$

The value of σ_θ at element 3 is hypothesized to have an initial effect, i.e., to assist in originating the initial microcrack. The value of σ_θ decreases in value rapidly as r increases in value.

The values of σ_θ from Equations E.3, E.4, and E.5 for the above assumptions are shown in Figure 3.1b on elements 3, 2, and 1 respectively, in the beginning of Chapter III. In that figure, σ is changed to σ_p.

APPENDIX F

ORIGINAL BEAM DATA

This section contains the original beam data arranged in tabular form. For Z_1, X_i, and Y_i (i = 1, 2, 3) in the following tables, a value in the column is the actual distance, in inches, between gage points measured by the Whittemore strain gages. The 2" Whittemore gage measured the gage lengths in the X and Y-directions, and the 10" gage measured the Z-direction. These values are the average of two actual gage length measurements made to the nearest 0.0001 of an inch. For the weight, a value in the column is the actual weight of the beam in grams.

This data can now be processed for each individual beam by the following steps:

1. To obtain the total change in length (ΔZ_1, ΔX_i, or ΔY_i) or weight (ΔW) per freeze-thaw cycle, subtract the zero cycle value from its respective cycle value in each row. For ΔZ_1, ΔX_i, and ΔY_i, a positive sign indicates expansion; for the weight, a positive sign indicates a gain in weight.

2. To obtain the total change in length for one inch (in inches/inch) per freeze-thaw cycle, divide each value obtained in Step 1 by its gage length, i.e., $\Delta Z_1/10$, $\Delta X_i/2$, and $\Delta Y_i/2$, or in general, $\Delta L/L$.

3. To obtain a statistical average for the change in length per inch in the X and Y-directions respectively per beam, average similar rows. These values represent directional disintegration vs. freeze-thaw cycle per beam. Thus, each final value for the X and Y-directions has been obtained by averaging over six inches. Since only one reading was

taken for the Z-direction, the values given in Step 2 above represent the total change in length per inch in the Z-direction for each beam. These values also represent directional disintegration vs. freeze-thaw cycles and are averaged over 10 inches per beam.

The original beam data for each beam is given in the following tables:

TABLE F.1 ORIGINAL BEAM DATA

Beam # D1 Prestress Level 500 psi

Cycle	Z_1	X_1	X_2	X_3	Y_1	Y_2	Y_3	Weight
0	10.0301	2.0568	2.0667	2.0591	2.0639	2.0639	2.0659	6214
1	297	584	680	604	647	646	669	6218
2	295	593	693	612	651	652	674	6214
3	298	595	700	619	654	655	676	6217
4	298	598	708	629	653	656	677	6221
5	296	605	715	638	656	659	681	6218
9	298	622	743	667	658	662	684	6222
10	297	628	750	676	658	663	685	6227
11	296	635	756	684	659	663	688	6225
15	299	650	781	710	660	667	693	6226
16	295	659	789	719	663	670	699	6226
20	296	676	812	741	671	680	707	6228
25	301	692	831	758	676	688	715	6230
30	299	700	842	765	681	692	723	6235

TABLE F.2 ORIGINAL BEAM DATA

Beam # B2 Prestress Level 500 psi

Cycle	Z_1	X_1	X_2	X_3	Y_1	Y_2	Y_3	Weight
0	10.0445	2.0846	2.0723	2.0747	2.0708	2.0648	2.0718	6349
1	447	857	731	757	718	652	727	6354
2	451	866	743	768	727	659	735	6355
3	452	874	751	776	731	661	735	6357
4	453	881	759	784	736	663	737	6360
5	455	892	769	795	741	666	741	6360
9	457	920	800	829	750	674	748	6364
10	458	931	812	840	756	680	752	6365
11	459	939	820	850	759	681	754	6366
15	460	961	846	880	769	684	764	6368
16	461	972	858	893	778	692	770	6368
20	461	1001	889	926	796	709	783	6369
25	463	1014	903	938	810	721	793	6370
30	464	1021	912	947	817	728	799	6373

TABLE F.3 ORIGINAL BEAM DATA

Beam # B3 Prestress Level 500 psi

Cycle	Z_1	X_1	X_2	X_3	Y_1	Y_2	Y_3	Weight
0	10.0323	2.0599	2.0583	2.0618	2.0688	2.0641	2.0603	6251
1	320	614	604	635	693	648	609	6247
2	322	630	617	652	700	655	618	6245
3	323	637	626	664	704	656	623	6245
4	325	647	639	676	704	657	623	6246
5	324	657	648	687	708	661	623	6253
9	327	689	682	724	713	667	625	6256
10	328	698	692	734	715	669	626	6251
11	329	702	696	738	713	669	630	6258
15	331	730	728	772	721	673	632	6259
16	331	738	736	782	728	679	635	6260
20	330	763	764	809	733	683	641	6265
25	331	789	789	839	743	693	646	6268
30	333	807	809	846	751	696	649	6267

TABLE F.4 ORIGINAL BEAM DATA

Beam # B4 Prestress Level 1000 psi

Cycle	Z_1	X_1	X_2	X_3	Y_1	Y_2	Y_3	Weight
0	10.0381	2.0590	2.0641	2.0581	2.0687	2.0742	2.0799	6209
1	372	603	649	600	696	752	814	6212
2	365	613	657	612	703	759	825	6213
3	364	623	665	623	704	764	829	6214
4	364	630	673	635	712	769	835	6216
5	360	635	678	644	716	773	839	6218
9	356	655	699	672	721	773	841	6219
10	355	662	706	678	723	777	845	6220
11	353	669	717	686	725	779	846	6220
15	353	685	730	704	731	784	852	6222
16	350	694	738	714	736	790	856	6223
20	349	719	760	736	750	801	869	6226
25	350	741	781	752	765	816	881	6227
30	349	756	795	763	777	825	889	6229

TABLE F.5 ORIGINAL BEAM DATA

Beam # B6 Prestress Level 1000 psi

Cycle	Z_1	X_1	X_2	X_3	Y_1	Y_2	Y_3	Weight
0	10.0427	2.0712	2.0647	2.0603	2.0668	2.0532	2.0723	6218
1	419	728	662	625	672	541	729	6223
2	419	748	683	641	678	549	736	6224
3	418	762	693	650	678	551	737	6229
4	418	779	707	662	680	549	740	6230
5	417	792	719	673	682	551	741	6232
9	412	825	756	709	683	552	746	6235
10	413	841	772	722	686	554	747	6236
11	410	853	786	731	687	555	748	6239
15	408	879	819	766	695	554	753	6238
16	409	898	840	782	701	559	758	6240
20	406	953	900	834	713	565	763	6244
25	402	1020	971	893	731	574	770	6246
30	401	1031	1034	953	742	581	773	6252

TABLE F.6 ORIGINAL BEAM DATA

Beam # B7 Prestress Level 1500 psi

Cycle	Z_1	X_1	X_2	X_3	Y_1	Y_2	Y_3	Weight
0	10.0136	2.0636	2.0584	2.0648	2.0820	2.0641	2.0648	6278
1	129	649	608	663	832	649	654	6282
2	126	660	615	681	843	655	663	6284
3	124	667	625	693	845	658	663	6284
4	121	677	636	703	849	659	657	6286
5	121	686	647	714	853	661	661	6286
9	116	725	686	754	860	667	674	6289
10	114	736	698	765	864	671	677	6290
11	112	742	707	773	863	671	678	6292
15	111	776	741	807	872	680	698	6293
16	109	786	751	817	875	683	700	6294
20	106	809	774	842	882	693	719	6295
25	106	825	792	858	890	700	729	6298
30	108	834	800	865	894	704	731	6299

TABLE F.7 ORIGINAL BEAM DATA

Beam # D8 Prestress Level 1500 psi

Cycle	Z_1	X_1	X_2	X_3	Y_1	Y_2	Y_3	Weight
0	10.0196	2.0607	2.0542	2.0692	2.0722	2.0679	2.0633	6249
1	186	632	557	714	731	689	645	6253
2	184	651	572	731	739	697	655	6255
3	181	663	584	740	742	699	658	6257
4	182	678	594	753	746	705	663	6256
5	176	693	609	764	749	709	667	6257
9	172	741	645	806	754	717	681	6260
10	172	754	658	818	757	723	685	6261
11	170	766	667	829	759	725	688	6262
15	165	805	706	867	766	733	701	6264
16	165	821	722	881	771	739	706	6264
20	160	864	761	922	782	751	719	6267
25	158	909	804	962	792	762	730	6271
30	156	946	841	994	798	772	736	6273

TABLE F.3 ORIGINAL BEAM DATA

Beam # B9 Prestress Level 1500 psi

Cycle	Z_1	X_1	X_2	X_3	Y_1	Y_2	Y_3	Weight
0	10.0162	2.0627	2.0639	2.0578	2.0678	2.0599	2.0629	6231
1	156	637	655	589	684	610	639	6233
2	154	647	666	608	689	619	651	6240
3	152	653	674	628	693	626	659	6240
4	152	657	680	646	693	635	666	6240
5	152	663	688	663	694	638	672	6236
9	150	675	707	709	697	650	684	6236
10	151	681	715	724	704	657	692	6240
11	150	685	719	732	707	662	697	6242
15	151	692	731	760	722	681	711	6239
16	152	699	739	772	734	693	721	6241
20	154	718	763	808	781	744	761	6244
25	158	731	779	823	861	822	826	6247
30	165	739	739	832	934	893	887	6250

VITA

Lemuel Bembry Battle, Jr. was born in Franklin, Virginia, on August 7, 1951. He attended Franklin Elementary School and graduated from Franklin High School in 1969.

He entered Virginia Polytechnic Institute and State University in September 1969 and was graduated with a Bachelor of Science Degree in Civil Engineering in June 1973. After graduation he entered the graduate school at Virginia Polytechnic Institute and State University in September 1973 with the Structures option. While in graduate school he was a Graduate Teaching Assistant for the 1973-1974 and 1974-1975 academic year, teaching surveying and construction materials laboratories and grading papers for various professors.

He is a member of the American Society of Civil Engineers and Chi Epsilon, the Civil Engineering Honor Fraternity; and he is certified as an Engineer In Training in the state of Virginia.

Lemuel B. Battle, Jr.

Lemuel B. Battle, Jr.

THE EFFECTS OF VARIOUS LEVELS OF COMPRESSIVE STRESS FIELDS ON THE DETERIORATION RATE AND MICROCRACKING OF PLAIN CONCRETE SUBJECTED TO FREEZING AND THAWING

by

Lemuel Bembry Battle, Jr.

(ABSTRACT)

The effects of various levels of compressive stress fields on the deterioration rate and microcracking of plain concrete subjected to freezing and thawing were investigated. Three levels of compressive stress (prestress), 500, 1000, and 1500 psi, were applied by the post-tensioning method to beams 3" x 3" x 14". The deep-seated (aggregate generated) type of frost damage was investigated since the cement mortar matrix was protected by entrained air.

It was found that the deterioration rate in the lateral direction of the members increased as the level of the compressive stress field increased. The compressive stress directionalized the disintegration in planes parallel to the direction of the applied stress.

A five step theory is presented which explains the involved physical phenomena. The theory is based on tensile stresses existing at the crack tip and around the aggregate particles.